# A METHODOLOGY FOR THE OPTIMIZATION OF ROBUST UNMANNED VEHICLE COMMUNICATIONS IN MARITIME ENVIRONMENTS

A Thesis
Presented to
The Academic Faculty

by

Pierre Emmanuel Valdez

In Partial Fulfillment
of the Requirements for the Degree
Doctor of Philosophy in the
School of Aerospace Engineering

Georgia Institute of Technology
May 2017

# A METHODOLOGY FOR THE OPTIMIZATION OF ROBUST UNMANNED VEHICLE COMMUNICATIONS IN MARITIME ENVIRONMENTS

Approved by:


Professor Dimitri Mavris, Advisor
School of Aerospace Engineering
*Georgia Institute of Technology*

Dr. Kelly Griendling, Research Engineer
School of Aerospace Engineering
*Georgia Institute of Technology*

Professor Eric Feron
School of Aerospace Engineering
*Georgia Institute of Technology*

Dr. Ayodeji Coker
Command and Control
*Space and Naval Warfare Systems Center, Pacific (SPAWAR), San Diego CA*

Professor Daniel P. Schrage
School of Aerospace Engineering
*Georgia Institute of Technology*

Dr. Matthew Bays
Autonomous Systems
*Naval Surface Warfare Center (NSWC), Panama City FL*



Date Approved: March 23, 2017

*This thesis is dedicated to my parents, my sister, and my three angels Abuelitos Agustina Medina and Vicente González, and Tio Parin*

**Acknowledgements**

The author would like to thank Professor Mavris for his advise and guidance throughout the doctorate program. Thanks to Dr. Kelly Griendling for her hep and guidance in research and academic work. Thanks to the team led by Dr. Coker in Space and Naval Warfare Systems Center, Pacific (SPAWAR) in San Diego CA who helped me understand the concepts and guided me through my research. Also thanks to Logan Straatemeier from SPAWAR for his help during my internships. Thanks to the team led by Dr. Matthew Bays in Naval Surface Warfare Center (NSWC) in Panama City FL for their help and guidance through my research as well. Thanks to the Adaptive Design Prototyping and Testing Lab (ADEPT) team at the Aerospace Systems Design Laboratory (ASDL) for working with me through my research. Thanks to Professor Feron for his input and counseling in my thesis. And finally, thanks to Professor Schrage for his guidance and help with my thesis.

# TABLE OF CONTENTS

# LIST OF TABLES

# LIST OF FIGURES

## 0.1 List of symbols

$\mathbf{X}$ vector of design variables

$F(\mathbf{X})$ objective function

$g(\mathbf{X})$ inequality constraint

$h(\mathbf{X})$ equality constraint

$RCS$ radar cross section

$P(RCS)$ probability distribution of RCS

$v_t$ velocity at time $t$

$P_m$ motor propulsion power

$(x, y, z)$ UxV location with respect to base ship

$E_m$ motion energy required

$P_c$ communications power required

$E_c$ communications energy required

$P_s$ sensors power required

$E_s$ sensors energy required

$N$ number of UxVs

$EC$ total energy cost

$E$ maximum endurance

$B_{hr}$ battery hour rating

$\tau$ battery discharge parameter

$\mu$ total propulsion system efficiency

$\nu$ batter voltage

$C$ battery capacity

$\rho$ atmospheric density

$U$ UAS speed

$C_{D_0}$ zero-lift drag coefficient

$w$ weight

$k_{C_L}$ coefficient of lift-dependent drag

$S$ reference planform area

$h$ altitude from earth's surface

$R_E$ earth's radius

$\beta$ index of refraction

$M$ modified index of refraction

$F$ propagation factor

$E_p$ electric field at point $p$

$E_0$ electric field at free-space conditions

$r$ range

$\lambda$ radio frequency wavelength

$L_{APM}$ propagation loss calculated by Advanced Propagation Model (APM)

$\omega$ average signal-to-noise (SNR) ratio

$\sigma$ square root of fading power gain

$E_{sy}$ energy per transmitted symbol

$N_0$ additive white Gaussian noise (AWGN) variance

$m$ Nakagami probability function shape parameter

$\chi$ envelope of radio frequency signal

$\Gamma$ Gamma function

$P_{Nak}$ Nakagami probability distribution function

$P_{Ray}$ Rayleigh probability distribution function

$P_o$ outage probability

$\omega_T$ threshold SNR

$P_R$ received power

$P_N$ AWGN power

$P_T$ transmitter power

$G_T$ transmitter antenna gain

$G_R$ receiver antenna gain

$L_{sys}$ system losses

$L_{rs}$ receiver sensitivity

$L_{cp}$ cross-polarization losses

$x_t$ map occupancy state at time $t$

$z_t$ measurement at time $t$

$u_t$ control action at time $t$

$bel$ belief of a state

$\zeta$ static logic

$\vartheta$ communication network state

$\varphi, \psi$ Linear Temporal Logic (LTL) formulas

$\xi$ infinite sequence of communication network states

$\eta$ formula of static logic $\zeta$

$\xi^k$ infinite sequence of communication network states starting at $\vartheta_k$

$A$ target area (TA)

$\theta$ TA orientation with respect to base ship x-coordinate

$S_p$ surface point

$(x_p, y_p)$ pixel resolution in the $x$ and $y$ TA directions

$N_p$ number of pixels in a TA

$b_p$ number of bits per pixel

$N_b$ number of bits of information available in a TA

$L$ length of TA

$W$ width of TA

$d_{ss}$ lateral range of side scan sonar

$d_{dz}$ dead zone distance of side scan sonar

$d_{sc}$ lateral coverage of side scan sonar

$d_t$ unmanned underwater vehicle (UUV) sweep distance at time $t$

$N_{pc}$ total number of pixels measured

$N_{bc}$ total number of bites measured

$X$ finite static state random variable of the occupancy of pixels in a TA)

$P_M$ probability that a pixel is occupied

$P_{NM}$ probability that a pixel is not occupied

$P_d$ probability of detection

$P_{ag}$ aggregate sweep detection probability

$d_A$ characteristic search width

$B$ average probability of successful detection

$P_d(d_{ss})$ probability of detection within $d_{ss}$

$H$ information entropy

$\Delta I$ information gain

$IGR$ information gain rate

$t_a$ time of acoustic communication updates

$t_{rf}$ time of radio frequency communication updates

# SUMMARY

As the military moves towards using more unmanned vehicles in the operational environment, accounting for communications during the mission planning phases is critical to meet the mission objectives. The quality of radio frequency (RF) and acoustic communications in maritime environments are highly dependent on the environmental conditions. Maritime atmospheric and underwater environments provide a complex medium for RF and acoustic communications that need to be accounted for to meet the robust and reliable communication requirements for unmanned vehicles.

This thesis proposes a methodology for predicting communications network between unmanned vehicles (UxVs) by using the Advanced Propagation Model (APM) to model the physics of RF electromagnetic (EM) wave propagation and probabilistic approaches to make the transmission channel robust to environmental conditions. In particular, a Nakagami-m transmission channel model is suggested for its ability to model a wide range of fluctuation intensities caused by environmental conditions. Communications network reliability methods are also proposed to help maintain communications in case of communication link failures. The methodology follows the Navy Planning Process (NPP) closely to provide communications-based course of actions (COAs) and schedules that lead to optimal measures of performance (MOPs) and measures of effectiveness (MOEs) of the mission. The proposed methodology is demonstrated using the mine survey mission scenario.

# CHAPTER I

# MOTIVATION AND INTRODUCTION

The use of unmanned and autonomous vehicles for commercial, military, and day-to-day applications has increased significantly over the last few years. Whether they operate on the ground, on the air, underwater, or over the water surface, they provide unique capabilities and benefits over manned vehicles. In military applications for example, they are able to fulfill dangerous tasks without putting a person at risk. There are however many challenges and problems that need to be solved for these unmanned vehicles to complete their tasks to successfully achieve a given mission. One of these challenges is communications between unmanned/autonomous vehicles. Whether it is sensor data, vehicle position and state, or navigation data, these sources of information need to be communicated successfully and in a timely manner. Therefore, there is a need to account for communications during the mission planning processes to better allocate unmanned vehicles and plan their paths.

One military branch interested in such benefits and advantages of using unmanned vehicles in the operational environment is the United States (U.S.) Navy. Over the years, the Navy has been facing new changing threats, such as mines, piracy, and submarine attacks. Since the end of World War II, mines have damaged or sunk four times more U.S. Navy ships than all other means of attack [150]. Following the collapse of the Soviet Union, U.S. Navy has shifted its focus from waging blue-water combat to anti-piracy, visit, board, search and seizure (VBSS) techniques [178]. Today's naval missions require regional contingency operations where friendly forces must be capable of projecting power ashore, and develop the capability to insert marines and materiel from sea to shore where shallow water and beaches are defended [155]. Navy

operations in the future will be centered on dominating littoral combat, and rapidly achieving area control despite high traffic density, high technology enemies, and asymmetric challenges. Advantage will lie in sea-basing that employs sea shield and sea strike capabilities to ensure sea supremacy.

## *1.1 Paradigm Shift Towards Network Centric Operations*

In order to meet these new threats, the Navy's Concept of Operations (CONOPS) provides guidelines and requirements using three benchmark sea-base missions [220]: (1) Mine Countermeasures (MCM), (2) Surface Warfare (SUW), and (3) Anti-submarine Warfare (ASW). The goal of MCM mission is to defeat the mine threat in domestic and away waters by improving mine detection capability, decrease sensor false alarm rate, reduce/eliminate post-mission analysis detect and classify time, automize the target recognition, improve neutralization time, and improve network communications [162]. The goal of SUW is to defend against asymmetric threats such as swarming of fast-attack crafts, pirate ships, and provide area patrol services by leveraging advances in gun systems, counter-boat missile systems, radar and detection systems, and communications. The goal of ASW is to maximize undersea advantage anywhere in the world by leveraging advances in active variable depth sonar detection, torpedo detection, and submarine hunting [203]. To meet these goals, the Navy is moving towards mission packages for each of these missions on board the Littoral Combat Ship (LCS). The LCS is expected to be optimized for warfighting in the littorals due to its fast, maneuverable shallow draft, reconfigurable single-mission focus, flexibility for dynamic dynamic battlespace, and onboard sensors, weapons, command, controls, communications and computers (C4).

A paradigm shift towards a network-centric warfare is taking place at the Navy which involves using more unmanned vehicles (UxVs) in the operational environment [154]. UxVs are viewed as a key component towards transforming the U.S. Navy

and other military forces to meet the new threats. Compared to manned systems, UxVs advantages include: reduced risk to U.S. personnel, low observability, ability to operate in inaccessible places, and lower procurement and operating costs. Major roles envisaged for UxVs include: intelligence, surveillance and reconnaissance (ISR), communications relays, detection and neutralization of hazards, targeting and strike operations. As a vision for the future employing more UxVs in the operational environment, the UV Sentry Team at the Space and Naval Warfare Systems Center, Pacific (SPAWAR) and the Naval Surface Warfare Center (NSWC) Panama City FL are developing a CONOPS for a system of UxVs, called the UV Sentry Missions [141]. UV Sentry missions are expected to provide Sea Shield as sentries to sense and identify current and projected surface and subsurface threats to sea base assets. An exemplary sea base UV Sentry mission description for SUW, ASW and MCM missions is shown in Fig. 1, with corresponding representative sea base dimensions in Table 1.

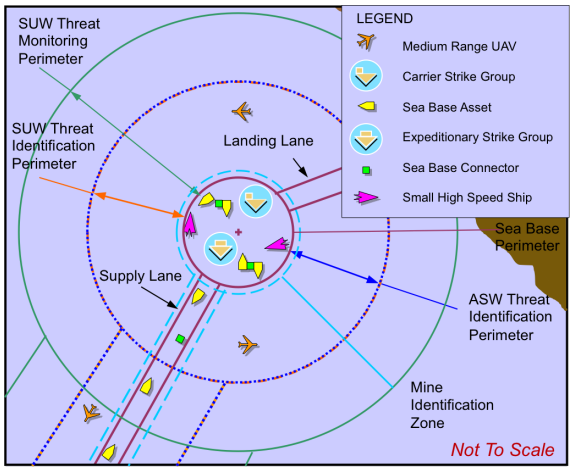


**Figure 1:** UV Sentry sea base exemplary description [141].

Key enabling capabilities and technologies towards meeting these UV Sentry missions have been identified to include C4, autonomous collaboration, heterogeneous vehicles, unmanned surface vehicles (USVs) hosting unmanned underwater vehicles (UUVs) and unmanned aerial vehicles (UAVs), autonomous launch and recovery of

**Table 1:** Representative sea base dimensions [141]

| | |
|---|---|
| Area ($nm^2$) | 1000 |
| Diameter (nm) | 36 |
| Supply Lane (nm) | 200x0.5 |
| Landing Lane (nm) | 15x0.5 |

UxVs, onboard data processing, alternative energy sources, modularity, sensor capability, secure wireless networks, network-centric architecture, automated data fusion, autonomous mission planning and task allocation. In order for these vehicles to perform in the operational environment, and use their projected capabilities and technologies, they need to be in communication with other unmanned and manned vehicle assets. Their ability to meet the mission objectives and specific tasks may be highly dependent on being able to communicate under certain environmental conditions, and while different vehicles are changing their location and speed relative to each other. These key enablers and UV Sentry requirements for communication lead to the first observation:

**Observation 1**: *Robust and reliable UxV communications above and below water are key for meeting mission level objectives in UV Sentry missions.*

## *1.2 Maritime Communications Environment*

UxV communications in UV sentry missions require radio frequency (RF) and acoustic underwater communications. The quality of RF and acoustic communications are very dependent on the medium of propagation. Maritime atmospheric and underwater environments provide a complex medium for RF and acoustic communications that need to be accounted for to meet the robust and reliable communication requirements for UV Sentry missions.

As RF electromagnetic (EM) waves propagate through the atmosphere, they are

attenuated by absorption and scattering effects. Absorption and scattering is manly due to water vapor, $CO_2$, ozone, $O_2$, liquids and solids in the atmosphere [34]. Changes in temperature, moisture, and pressure cause a change in density, which affects EM, and lead to change in propagation direction or bending: refraction, reflection, diffraction. RF signals experience phase interference from signals reflected off the sea surface, ships, land, refracted down from the atmosphere, etc. leading to constructive or destructive interference at the receiving antenna. Attenuation can be decomposed as the result of multi-path fading due to refraction and reflection, and the transient fading due to absorption and scattering [181]. If great enough, this attenuation can reduce a communication signal to the point where it can no longer be received and/or interpreted, leading to a loss in communications.

Similarly, as acoustic sound waves propagate through the water, they are attenuated by absorption and scattering effects. Absorption and scattering in this case is manly due to salinity, temperature, pressure, acidity, season, sea state, and depth, all described by poor sound velocity profiles (SVP) [194]. Multi-path interference due to reflections and refractions from ocean surface, ocean floor, ships and other obstacles also lead to constructive and destructive interference at the receiver. Noise is also added to the signal from multiple sources, including transient, shipping, wind, and thermal noise. To make matters worse for acoustic communications, signal at the receiver has low energy due to high absorption by water, and therefore lower bandwidth compared to RF communications [193].

These maritime atmospheric and underwater complex effects on RF and acoustic communications, respectively, lead to the second observation:

**Observation 2**: *Maritime communications are challenging because of poor SVPs, complex atmospheric environments, limited resources, distributed assets, etc. Therefore, there exists a need for a way to account for communications during mission*

*planning.*

## *1.3 Planning Process*

Before going into details about how Navy mission planning is performed today, it is important for the reader to become acquainted with some terminology and concepts regarding mission planning for military applications.

Mission (military) planning definitions in the literature include the following:
*1) The art and science of envisioning a desired future and laying out effective ways of bringing it about (Marine Corps Doctrinal Publication, 2010)* [64]

*2) A comprehensive process that enables commanders and staffs at all levels to make informed decisions, solve complex problems, and ultimately accomplish assigned missions (Navy Planning, 2013)* [151]

*3) A process to develop and provide an effective team composition and tasking mechanism and an optimal team dynamics and tactics algorithm to destroy the opposing force combat capabilities (D. Shen, 2007)* [55]
From these definitions, a compiled version for the definition of mission planning is given as:

*Mission Planning: the art and science of envisioning a desired future and laying out effective ways of bringing it about through effective team composition, tasking mechanisms and optimal team dynamics and tactics by following a comprehensible process to make informed decisions*

According to Boukhtouta et. al., attributes of good mission planning involve [40]:

- Structure: information, knowledge, and decision structure relationships exist.
- Organization: functional, personnel, and task relationships contribute to mission planning performance.
- Management: mission planning operates as a C2 function, providing internal/external synchronization and managing planning functions.
- Feedback: feedback information of different kinds and levels are available.
- Optimization: battle-space situational awareness and asset planning are merged to produce an optimized plan.

The output of the planning process are formal and or informal directives, plans and orders that are either oral or written. The complexity of these directives, plans and orders are highly dependent on the situation and on the time available to perform the mission planning process.

Also important is the hierarchy within the staff who is involved in the mission planning and making decisions. In the Navy, the Superior Chief Commander's high level vision and orders serve as guidelines to other Commanders, staff, and planning teams during the mission planning [151]. Planning teams and Commander's staff help Commanders make better decisions to meet the Chief Commander's vision. Communication of pertinent information and possible solutions among all levels of the hierarchy is critical to meet the mission requirements.

The U.S. Navy's heritage has inculcated an expectation of commanders to operate independently while following their superior commander's intent; to act when an opportunity presents itself and to feel comfortable in conditions of ambiguity [151]. These are attributes honed by mutual trust and confidence and years of experience at sea. This description of disciplined initiative is also known as mission command in joint doctrine. To ensure that planning does not stifle mission command, the

superior Navy commander and staff focus more on the purpose of operations rather than the details of how subordinates will execute the tasks and avoid overly restrictive command and control concepts. The commander's intent cannot be a staff product; rather it must be a true embodiment of the commander's vision and the centerpiece of the commander's discussions with subordinate commanders.

The iterative process for planning naval operations is referred as to as the Navy Planning Process (NPP) [151], and is shown in Fig. 2. Through the NPP, Commanders and their staff can plan for, prepare, and execute operations from operational to tactical levels of war. The first half of the NPP involves the commander and their staff analyzing the situation, generating and analyzing various friendly and hostile courses of action, and selecting a friendly course of action to execute. The last two steps of NPP involve disseminating orders to subordinates, executing the plan, and using feedback from the execution to inform future plans. The NPP can assists in analyzing the operational environment, distilling the multitude of planning information, and determine what, why, how, and with what available means to perform a Course of Action (COA). Interactions among the Commander and staff during the NPP steps ensure complete, concurrent, coordinated effort. The NPP also ensures flexibility, makes efficient use of available time, and facilitates continuous information sharing. The result of NPP is a set of military decisions, in forms of COAs, that can be translated into an operational plan.

The NPP process is a well established doctrine within the Navy and other U.S. military forces that can be used to generate communication-based COAs during the mission planning phases. This leads to the third observation.

**Observation 3**: *There exists a need for a mission planning framework and methodology that assists in generating communications-based COAs while following the NPP doctrine.*

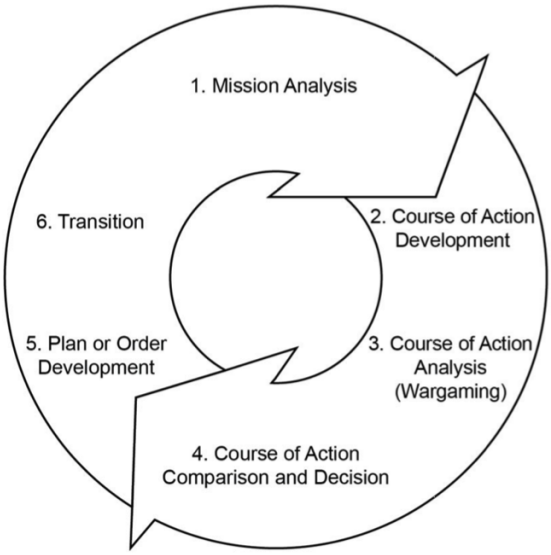


**Figure 2:** Navy Planning Process (NPP) [151].

## *1.4 Research Objective*

In light of the the three observations in the previous sections inspired by the need to account for communications between UxVs during the mission planning phases, the research objective of this thesis proposal is the following:

Research Objective (RO): ***Develop a methodology and a mission planning framework to find optimal communication COAs during the mission planning phase, which lead to high probability of mission success, and are robust to uncertainties in the environmental conditions and reliable to network failures.***

# CHAPTER II

# NAVY PLANNING PROCESS AND PROPOSED METHODOLOGY

The proposed approach to meet the RO is a multi-step methodology that is consistent with the Navy Planning Process (NPP) doctrine for predicting communications in UV Sentry mission environments which generates optimal communications-based COAs. It is a multi-step iterative process that is mapped to the first four steps of the NPP. The proposed methodology considers robustness of communications channels from uncertainty in environmental conditions and network reliability from loss of communications. Optimal communication COAs and their schedule are identified in the process, while also assessing the quality and quantity of communicated information. This chapter focuses on presenting each of the first four steps of the NPP, and how the proposed methodology can be used to adhere to these steps. In the process, research questions are identified and the proposed experimental plan that is conducted to answer these research questions is presented. Hypotheses to the research questions are also formulated.

## *2.1 Navy Planning Process*

Military planning, done by the NPP, is the process by which a Commander visualizes an end state as well as the arrangement of potential actions in time and space that will allow the realization of that future [151]. Planning is a way of figuring our how to move from the current state to a more desirable future state. It is essential to a military Commander because it aids in handling the complexities in the operational

environment (OE) and the numerous uncertainties inherent in warfare, involving projecting thoughts forward in time and space to influence events before they occur rather than merely responding to events as they occur.

The U.S. Navy's heritage has included an expectation of Commanders to operate independently while following their superior Commander's intent; to act when an opportunity presents itself and to feel comfortable in conditions of ambiguity [151]. These are attributes honed by mutual trust, confidence, and years of experience at sea. The NPP is used by the Commander to plan for, prepare, and execute operations through the tactical levels of war.

The NPP is the process that assists commanders and their staffs in analyzing the operational environment (OE) and distilling a multitude of planning information in order to provide the commander with a coherent framework for determining the what and why (ends) as well as developing the method for execution (ways), given the forces and resources available (means) and the level of risk of the mission and forces (wargaming) [151]. It is an iterative process and is designed to gain decisions from the Commander as how to proceed toward a solution. The process is through and helps apply clarity, sound judgement, logic, and professional expertise to identifying problems, developing solutions, and communicating directions.

In the next sections, the first four steps of the NPP process, which deal with planning, developing and analyzing course of actions (COAs), will be described in detail. For each step, the inputs, the process, and the outputs will be highlighted to determine the structure and analysis needed for the proposed methodology. Research questions will be posed for those areas and analyses that need further investigation. The research questions formulation will aid in steering this thesis focus and scope. After this is done, the following sections provide an overall map of the proposed methodology, with inputs and outputs clearly stated. Hypotheses to each of the posed research questions will be formulated as well, along with experimental plans to

test the validity of each hypothesis.

### 2.1.1 NPP Step 1: Mission Analysis

This is the first step of the NPP, where Chief commander's vision is interpreted into mission goals and requirements in the form of a mission statement [151]. These requirements are high level mission objectives such as protect sea-base, provide ISR for SUW or anti-piracy missions, detect, identify and clear mine threats, etc. How well these mission objectives are performed can be quantified by Measures of Performance (MOP) and Measures of Effectiveness (MOE). The planning team aids the commander to frame the mission statement more accurately by reviewing and analyzing orders, translating mission goals and requirements into mission objectives, and creating MOEs and MOPs that help quantify how well these mission objectives are performed. The inputs, tasks, and outputs of the mission analysis step are shown in Fig. 3.

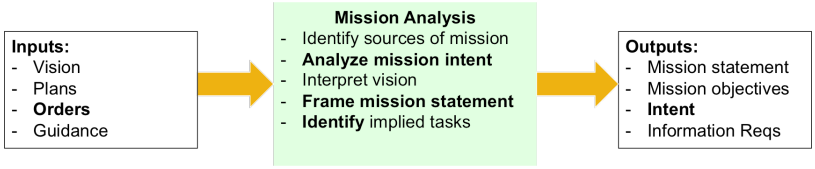


**Figure 3:** Mission analysis NPP step

UV Sentry missions can be interpreted as Chief's commander's vision to meet the new asymmetric and changing threats. A sea base with given dimensions, as represented in Table 1, and high level requirements such as providing sea shield to sense and identify surface and subsurface threats, anti-piracy patrolling, and area ISR coverage can be mission requirements resulting from interpreting Chief's Commander's vision.

By incorporating feedback from the COA analysis (NPP step 3) and COA comparison and decision (NPP step 4) back into the mission analysis NPP step 1, the

mission requirements can be re-interpreted and MOPs and MOEs can be redefined if needed such that resulting COAs have higher probability of success.

### 2.1.2 NPP Step 2: COA Development

Based on mission objectives and intent in the mission statement generated from the Mission Analysis step, the next step of the NPP mission planning process is to perform asset allocation and distribute mission tasks [151]. The goal is to generate COA options that meet the mission goals based on environment conditions and available assets. Based on required information, also determine what sensor data is critical for mission success. Enemy reaction to a given COA, also known as counter-COA, also needs to be anticipated and accounted for to some extent. The inputs, process, and outputs of the COA development step are shown in Fig. 4.

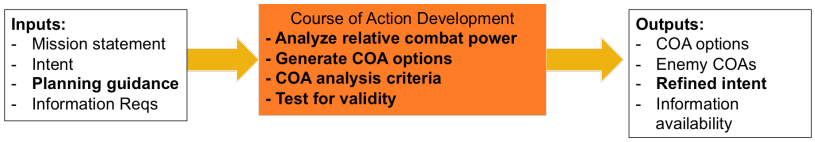


**Figure 4:** COA development NPP step [151]

COA Development should consider all maritime force capabilities and those joint capabilities necessary to achieve the maritime objectives and achieve the Commander's vision. For each COA, the Commander and planning staff should visualize the employment of forces as a whole, taking into account externally imposed limitations, the factual situation of the operational environment, and the conclusions perviously reached during Mission Analysis [151]. COA Development is a deliberate attempt to design at least two (and often more) valid and distinguishable COAs for the Commander, each of which will accomplish the mission. Finally, a good COA provides flexibility to meet unforeseen events during execution [151].

With these guidelines in mind, a multi-step COA Development process is proposed for the methodology which generate COAs in the form of UxVs, their capability

and performance, the sensor information that they provide, their communications capability, and their allocation in the OE. UxVs capability and performance will be driven by their ability to operate underwater, on the sea surface, and in the air. It is important to know how many assets are available, and their performance in terms of maximum range, endurance, speeds, etc. This level of detail is essential for determining if our available assets can perform the tasks needed to meet the mission objectives. If this step is not performed, it can lead to serious consequences, such as vehicles not having enough power to complete the mission, or not able to reach a certain target because it is out of range, or not being able to complete the mission in a timely manner because it does not have the thrust necessary to reach certain speeds, etc.

In terms of communications, it is important to know what communications hardware each UxV asset can carry, and the means by which they can communicate. Whether they can communicate above water via RF or underwater by acoustic communications, it is important to know the hardware limitations. These limitations include minimum receiver power, maximum power losses, acceptable signal-to-noise (SNR) ratios, acceptable bit-error rates (BER), etc. If this step is not accounted for, it can lead to situations where the signal experience a level of power attenuation that the receiver cannot interpret the message or demodulate the message content. For example, vehicles can reach certain levels of attenuation in given environments which leads to low SNR, or high BER, which leads to loss of signal. This becomes important especially when performing asset allocation, for determining allowable ranges that these vehicles can be so that they can communicate.

Sensory information that needs to be communicated is also crucial. What sensory information, how fast to communicate this information, how much resolution is needed, and what are the sensor limitations are the questions that need to be addressed in this step. The right sensor needs to be selected which will provide the

levels of MOP and MOE needed to complete the mission objectives. The limitations on these sensors can be posed in terms of their range, resolution, probability of detection, false-alarm rate, and power required to run these sensors. If these sensor COAs are not considered, it can lead to instances where the sensor does not provide the resolution necessary to make further decisions or detect targets, or the sensor data is too dense to be communicated via a given means of communication. It should be noticed that this step should involve a sensor model for determining the quality of information that needs to be communicated. Tradeoffs on sensory type, resolution, range, data rates needed, and means of communicating this sensory information need to be performed in this crucial step.

Asset allocation based on target area locations, their domain, the operational environment, and required tasks, need to be considered. This step should go hand-in-hand with UxV asset selection to determine which kind of vehicle is assigned to what task. UxV asset performance and capability drives the selection of asset allocation and path planning to perform the tasks required to meet the mission objectives. Enhanced communications vehicle capability should be considered in this step as form of possible COAs, such as UxVs deploying from other UxVs, vehicles that can operate in multiple domains (underwater, surface, and in air), and multiple forms of communication (acoustic and RF). This step should also consider the environment and how it affects communications between the different assets. In maritime environments, certain environmental conditions can significanly attenuate the RF signal. For acoustic communications, certain noise levels can lead to critical SNR levels, and multipath can lead to significant destructive interference of the signal. Therefore, asset allocation needs to account for communications early in the COA Development process.

Within the asset allocation step, a network topology composed of all assets needs

to consider robustness of the communications to uncertainties in environmental conditions, reliability to possible communication link or vehicle failures, quality of communication for transmitting important sensory information, and stability of the communication links to vehicle relative motions. Therefore, this is an important step that needs its own iteration process with feedback from communication predictions. Based on the selection of UxVs, their sensor capability, communications hardware, and sensor information that needs to be communicated, the communications model predicts the state of the transmission channels, and this is used to determine if assets are too far in range from each other to communicate, or if the range can be extended. This involves a trade-off between available assets, their endurance, range, and communications capabilities, both RF and acoustic. Asset allocation can be described in terms of the communications network topology that results as vehicles are placed in their assigned locations and performing their required tasks. With this in mind, the first natural question is how can the UxVs be placed such that we meet the quality, reliability and stability requirements of the mission statement? This leads to the first research question:

**Research Question 1 (RQ1)**: *What communication network topology is reliable to communication link failures based on asset availability, which has the best network quality and is stable due to vehicle relative motions?*

Critical to predicting communications is the ability to characterize the environment. The environment needs to be characterized based on the expected allocation of these UxVs in the OE. Given the ranges that these vehicles are located within the UV Sentry mission, and their assigned tasks, we can extract the maximum ranges and possible paths to determine how far or deep do we need to characterize the environment to make better communications predictions. Not being able to characterize the

environment can lead to situations where the RF signals are attenuated more than expected due to multipath resulting from the refraction of RF signals. Evaporation ducts and surface based ducts for example can band the signals in certain way as to create a multipath that leads to serious attenuation. Vehicle relative motions can also affect the time variance of the signal due to Doppler effects and spreading of the signal. For underwater communications, the sea floor and temperature gradient profile can lead to multipath of the acoustic signals which also attenuates more than expected.

Once the environment has been characterized, the next critical step in the methodology should be to predict communications. These predictions should take into account antenna heights between the vehicles, system losses due to cross-polarization, or free-space losses, and other losses due to the time variation of the signal due to vehicle motions and spreading of the signal from back scattering. It should also consider the communications hardware, the signal specifications such as frequency, bandwidth, data rates, receiver limitations, etc. Sensory information should also be considered to make sure the communications are good enough to transmit that kind of sensor data at the rates necessary to meet the MOPs and MOEs. Depending on the environmental conditions, the communications may experience multipah fading, free space propagation losses, back scattering, and fluctuations of the signal intensity due to vehicle relative motions. Therefore, a good way to predicting the quality of communications from all these effects should be considered in this step. This leads to the next research question:

**Research Question 2 (RQ2)**: *How can the fading channel be modeled such that it captures the multipath effects and time-variant mechanisms due to relative vehicle motion, that is robust to environmental conditions uncertainty and fading fluctuations?*

Once the predictions of communications are made, with a channel model that allow us to assess the quality, robustness, and stability of the communications channel, the next step is to perform COA Analyses by determining how good is the given network topology based on the asset allocation and selected vehicle assets, their capability, performance, communications hardware, and sensory information quality. This is done by performing wargaming of our developed COAs against possible link failures and possible environmental conditions that can lead to failure to meet the mission objectives. This leads to the next step of the NPP process: COA Development and Wargaming.

### 2.1.3 NPP Step 3: COA Analysis and Wargaming

The next step in the NPP mission planning process is to conduct analysis on the selected COAs from the previous step. It involves a detailed assessment of each COA as it pertains to the adversary and the OE [151]. Each friendly COA is war-gamed against selected adversary COAs. This step assists planners in identifying strengths, weaknesses, and associated risks, and in assessing shortfalls for each prospective friendly COA. Wargaming also identifies branches and potential sequels that may require additional planning. Short of execution, COA wargaming provides the most reliable basis for understanding and improving each COA. This step also allows the staff to refine its initial estimates based on a more refined understanding of the COA that is gained through the war game. Fig. 5 shows the inputs, process, and outputs of the COA analysis step.

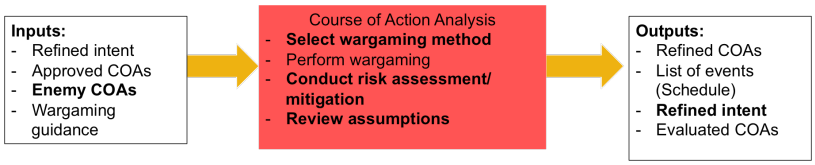


**Figure 5:** COA analysis NPP step.

In this step, the Commander and planning staff closely and critically examine potential COAs to reveal details that will enable them to identify their validity, benefits, limitations, and how they "react" to potential enemy tactics. Wargaming is the primary means of conducting this analysis. Wargaming is a conscious attempt to visualize the flow of the operation, given force strengths and dispositions, adversary capabilities and valid possible adversary COAs, and other aspects of the operational environment [151].

For our methodology, the COA Analysis should consider wargaming the asset allocation with our available UxV assets and their sensor and communications hardware, in the form of a communications network, against the environmental conditions, the channels stability, the network reliability, and the robustness of the channel to possible signal fluctuations and attenuations. Based on our communication predictions of the channel, and the UxVs capability and performance, we can consider network topologies that allow us to keep the network connected so that critical sensor information can reach its destination, and make sure the network is reliable and stable to possible link failures and signal attenuations and fluctuations. This wargaming analysis will result in a trade-off on its own, for some network topologies might meet the connectivity requirements, but not necessarily the reliability or stability requirements. Deploying more UxVs to help relay communications in the OE might need to be considered. Given the environmental conditions, UxVs that can operate above or below evaporation or elevated ducts might be needed to keep the communication network robust. But given UxVs range and endurance limitations, the relays might need to be deployed from other UxVs and re-charge their batteries for the next relay task. These are the kinds of wargaming analysis that are needed in this step for our methodology, and certain graph theory methods to model and quantify the quality of the communications network will be investigated.

The output of the network topology analysis will be a set of topology solutions

that meet all or part of the requirements and meet the mission level objectives. These network topology solutions should be fed back to the asset allocation in the COA Development step to make sure UxVs are assigned to target areas and perform tasks that still meet the network topology. As vehicles perform their tasks, they will move at certain speeds and change locations or even domain of operation, and they need to be accounted for to make sure the network topology is still connected, the resulting network is still stable and reliable. To do this, UxV asset re-allocation and path planning might be needed to keep the network connected.

When a network topology that meets all or most of the requirements has been found, the UxV paths during their assigned tasks should be investigated to make sure the quality and quantity of the sensory information communicate through the network meets the requirements and mission goals. The modeling of the effects of COAs on the quality and quantity of information depends on assigned tasks and vehicle capability. As the vehicle traverse its path taking measurements, the quality and the quantity of the information collected depends on the path itself. For example, during detection of objects of interest, sweeping over an area multiple times provides better detection and classification probability, but the entropy of the information decreases, due to the lower uncertainty in the state of the occupancy of the area. We need a way to track the progression of this uncertainty and how it affects the quality and quantity of information communicated, which leads to the next research question:

**Research Question 3 (RQ3)**: *How should the effects of COAs on the quality and quantity of information communicated through the communications network be modeled such that it captures sensor model, path planning, and uncertainty propagation?*

This analysis should study the effects of vehicle paths on the quality of the observations which are made by the sensor, and which are communicated through the

network. For example, some measurements might be better than others based on how these measurements are taken. During detection of objects, minimizing the uncertainty of object occupancy in a given map is a priority, not so much the certainty of what the object actually is. During classification of objects however, the minimizing the uncertainty of what the object is becomes the priority. Therefore, based on the mission objectives and requirements posed in the mission statement, vehicle paths need to be considered that will allow for the communication of the needed information. Therefore we need a method for accounting for these uncertainty propagation in our methodology and how it affects the quality and quantity of information.

Finally, given all possible COAs in the form of network topology solutions, limitations on available assets, their capability and performance, sensor and hardware limitations and capabilities, and the modeling of uncertainty propagation, an optimization procedure should be performed in this analysis to find the best COAs that leads to an optimum way of meeting the mission level objectives and requirements. As was described during the Mission Analysis step, the mission level objectives can be described and quantified in terms of MOPs and MOEs. Therefore, these MOPs and MOEs can be used as objective functions in the optimization analysis. Depending on the mission at hand and the Commander's vision, the objective function can be composed of multiple MOPs and MOEs, which can lead to a multi-objective function. The objective functions and requirements can also be non-linear, and discrete or continuous. Therefore, a general guideline for how to perform optimization and the different methods available and used in the literature should be investigated for the proposed methodology.

### 2.1.4 NPP Step 4: COA Comparison and Decision

The next step of the NPP mission planning process is to compare the different COAs and decide which COAs are the best, as shown in Fig. 6. This can be done by further

COA analysis through the simulation and visualization environment. COAs can be reviewed one last time, and final COAs validity can be tested.

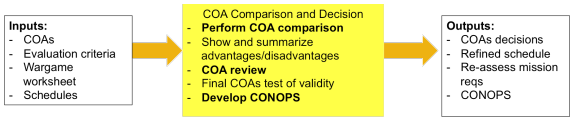


**Figure 6:** COA comparison and decision NPP step.

In this step, the Commander evaluates each friendly COA against established evaluation criteria, compares them with each other, and selects the COA the Commander believes will be the best to accomplish the mission [151]. The process should highlight the differences, advantages, and risks of each COA, and should be a clear evaluation based on most realistic scenario simulation possible. This can be accomplished with visualization and simulation environments that play out the mission and simulates the OE and mission with the selected COAs. High or low fidelity simulation, depending on the degree of accuracy needed to make the comparisons and evaluation of the COAs, should be considered to help visualize and better assess the validity of each COA.

### 2.1.5 NPP Steps 5: Plan and Order Development, and Step 6: Transition

Step 5 of the NPP process, Plan and Order Development, involves the staff using the commander's COA decision, mission statement, commander's intent, and guidance to develop plans or orders that direct subordinate actions. Plans and orders serve as the principal means by which the commander expresses the decision, intent, and guidance [151]. Step 6 of the NPP process, Transition, is the orderly handover of a plan or order to those tasked with execution of the operation. It provides staffs with the situational understanding and rationale for key decisions necessary to ensure that there is a coherent transition from planning to execution [151]. Since steps 5 and 6 deal with actually making orders and executing the COAs, it is beyond the scope of this study and is left for further consideration in future studies.

The process, however, does not end here. As depicted in Fig. 2, the process is iterative and continuous. Staffs maintain running estimates that allow for plans and orders refinement. The planning staff continues to examine branches and sequels to plans and orders. Key to this continuous process is the ongoing assessment of the operation's progress.

### 2.1.6 Proposed Methodology Scope and Validation

This thesis is intended to demonstrate how different tools, physics-based and probabilistic methods can be used at different levels of analysis in a methodology, to provide robust, reliable, and optimal communication solutions for high-level decisions that need to be made in matters of minutes or hours in the operational environment through the NPP process. The goal of this methodology is to demonstrate the benefits and limitations of our methodology during the planning phases in the operational environment, and emphasize the trade-offs that our methodology can provide in terms of communications with unmanned or autonomous vehicles. With this said, this thesis is not intended to provide a methodology to solve every communications problem or requirement, but it will be a procedure with step-by-step instructions of how to go about finding feasible and reliable communication solutions. This is not a final product, and the methodology may be modified if needed throughout the thesis timeline and as the experiments are performed while applying it to the demonstration study. With this in mind, the final research question is the following:

**Research Question 4 (RQ4)**: *Can the proposed methodology be demonstrated on a mine survey mission scenario, providing optimal COAs that maximize a given mission level objective, while also ensuring a reliable communications network?*

This research question can be answered by applying the resulting methodology to

a specific case study, and demonstrating the trade-offs within a structured analysis, with flow of information that allows the Commander and planning staff to develop and analyze COAs that consider communications between unmanned vehicles. The resulting COAs from the methodology can be compared to baseline procedures for performing that case study, and the benefits and limitations can be highlighted.

With these research questions in mind, and the different needs for each step of the NPP process for generating and analyzing communications-based COAs, the steps of the different processes of the proposed methodology will be described next. In each step, the inputs, outputs, and proposed analysis level and methods will be described. Hypotheses will be posed for each research question which will be tested in subsequent chapters through a series of experiments. After these steps are described, later chapters focus on those analysis steps that need further investigation and elaboration.

## *2.2 Proposed Methodology*

The observations made in the previous chapter identified the need of considering communications between UxVs early in the mission planning phases, and the necessity in modern mission planning with UxVs to consider communications and develop COAs that meet the mission level objectives that is consistent to existent planning doctrines such as the NPP. The needed methodology needs to explicitly handle communications and the required information to take communications into considerations during mission planning. For these UxVs, certain mission level objectives and requirements are highly dependent on how robust, reliable, and stable these communication links are, and they need to be assessed in a structured and formal way that a methodology can provide.

In the previous section, the NPP process was presented with description of the types of analysis needed to develop COAs, quantify them, and compared them to select the COAs that best meet the mission level objectives. With these needs and

observations, and the guidelines and structure provided by the NPP, a methodology that meets these needs in the observations and meets our research objective is proposed in this section. Each process of the proposed methodology is mapped to the first four steps of the NPP process. For each process, the different steps needed for our methodology that were identified in our previous discussion will be discussed further, with corresponding methods and modeling approaches at the level of fidelity needed. This discussion will help in steering our areas of focus and scope of analysis for this methodology for the subsequent chapters.

### 2.2.1 Mission Analysis Process

Shown in Fig. 7 is the first step of our methodology, which involves the translation of the vision, plans and orders from the Commander into quantifiable requirements and mission-level objectives.

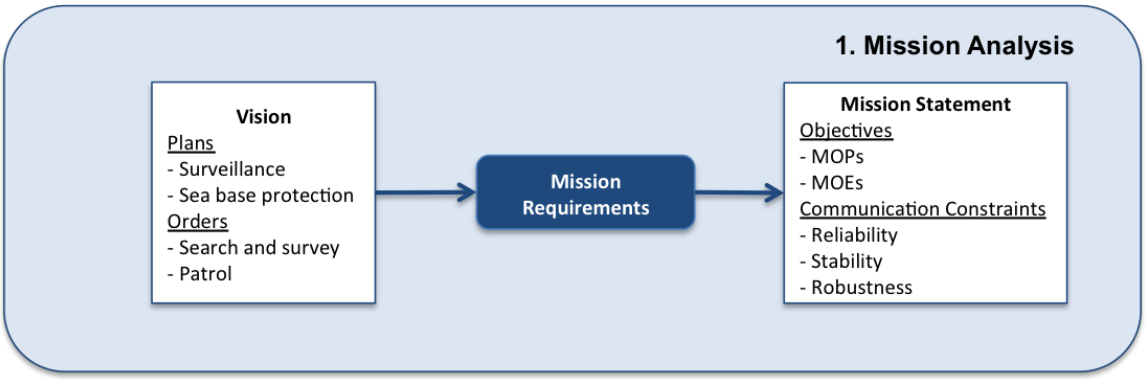


**Figure 7:** Mission requirements phase of the Mission Analysis step of Methodology

Interpreting the vision and guidance from the Commander can be a flexible process, normally consisting of several non-sequential activities tailored to the situation at hand, the time available, and how straightforward the plans and orders are. The process is neither rigid or static; it is continuous, evolving as the mission is taking place, iterative, and dynamic [151].

For the proposed methodology, focus is placed on interpreting the vision and

guidance from the Commander in terms of mission level objectives and constraints that are affected by communications. These interpretations can be either specified straight from the plans and orders, implied, or essential tasks and capability that must be assumed. For example, with the vision of providing sea base protection in littoral environments, the main order can be to provide search and survey tasks to areas around the sea base. The specified interpreted objectives are then to cover certain number of target areas and provide object detection procedures. The measure of performance can be the time it takes to provide sea base area protection. The measure of effectiveness can be measured by the total area coverage provided during the search and survey procedures. The implied and essential tasks involve having unmanned vehicles capable of performing the search and survey mission, having reliable communications with each vehicle to gather the sensor data, and being able to re-direct each vehicle as response to changes in the operational environment or enemy change of tactics. Whether they are specified or implied, communications-based objectives and constraints must be successfully interpreted during the Mission Analysis step.

### 2.2.2 COA Development Process

The next sub-subsections describe the proposed methodology steps and corresponding suggested methods to meet the COA Development step. Hypotheses corresponding to research questions will be posed for those steps that need further research investigation.

#### *2.2.2.1 Asset Allocation and Mission Tasks*

Based on the mission requirements, planning and guidance from the Chief Commander, and information requirements, the planning staff and commander in charge needs to make decisions on how and where to place available assets, and what mission tasks

do these assets need to perform. These are important decisions since it will determine what are the overall ranges and vehicle motion paths that need to be considered during the COA Development and the COA Analysis in the next step.

From the mission statement generated in the Mission Analysis step, requirements dealing with asset allocation and mission tasks can be extracted, as is shown in Fig. 8. These requirements are based on the MOEs and MOPs from the mission statement, translated into required tasks that can be quantified and tracked. These can be the amount of area coverage, number of threats detected, time to complete the search and survey tasks, etc. Also important in terms of communications, even thought it may not be specified but implied in the mission statement, are the communications network requirements. These affect asset allocation and tasks because the network is affected by where vehicles are with respect to each other when they try to communicate with one another. Network quality can be measured by how connected the network is, how reliable it is to asset or communication failures, and how stable it is to required vehicle motions.

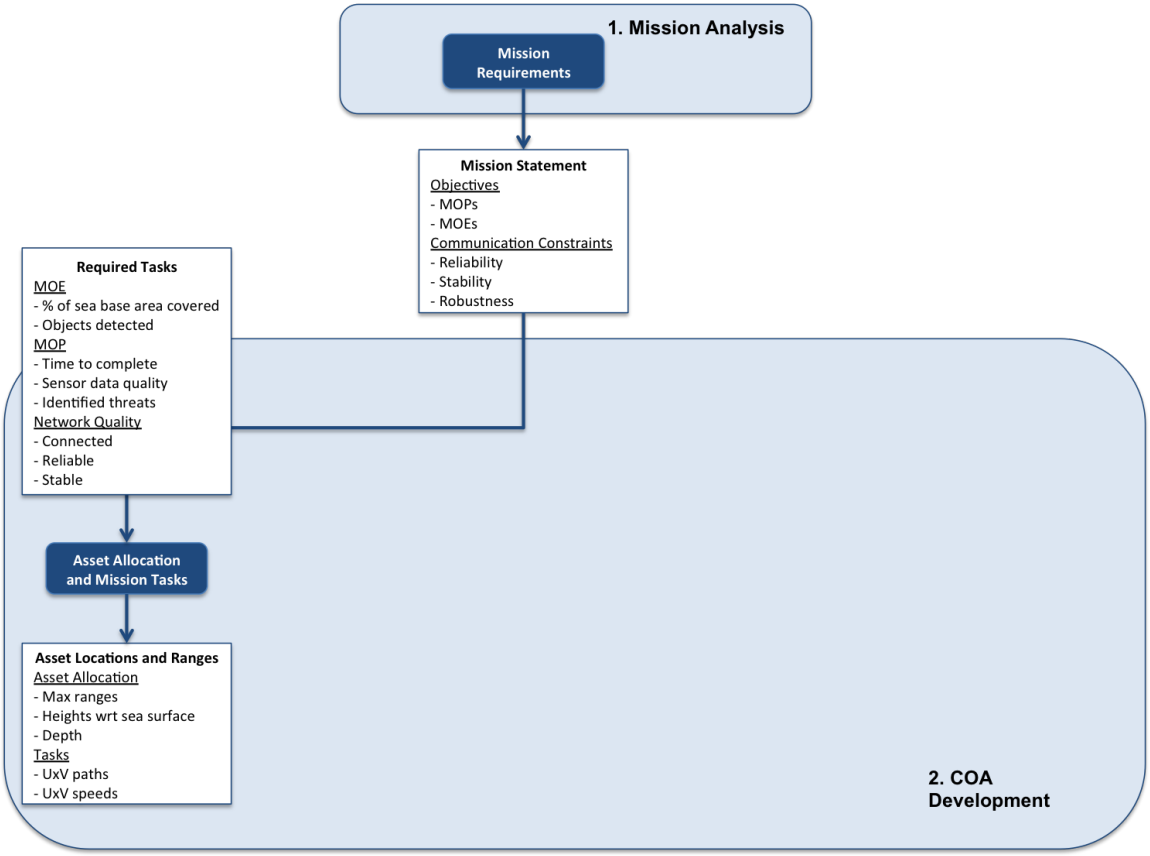


**Figure 8:** Asset allocation phase of the COA Development step in the methodology

The output of the asset allocation phase are UxV placement and paths which can be used to track their relative location and motions. Based on their required tasks, be it to map a target area, or provide communications relay, the UxV locations, paths and relative speeds are crucial when determining wether they can communicate with other assets or not. This information is crucial when making communications predictions as the mission takes place in the given environment.

The communications network is composed of communication link channels that are affected by the environment and the motions of the vehicles with respect to each other. Therefore, we need to asses the communication channels between each vehicle

transmitter and receiver and be able to predict the quality of the channel, the stability due to time variations of the signal amplitude intensity as the vehicles move, and the reliability to possible link or vehicle failures. This leads to the first hypothesis:

**Hypothesis 1 (HP1)**: *A network topology that takes into account acceptable probability of communications, require the time-varying fading amplitude of the signal to be within certain thresholds, and which requires each asset to have spatial redundancy, will result in a reliable communications network.*

To answer RQ1 and test HP1, a UV Sentry mission will be selected, and a limited number of assets and their assigned tasks will be defined. Based on the communication channel prediction for a given environmental condition, the allowable ranges between the vehicles will be determined, and the vehicles motion and schedule will be constrained such that they are always connected with another asset in the network, not necessarily with the main ship. This experiment is posed as follows:

**Experiment 1 (Exp1**: *For a given mission scenario, determine maximum ranges (UxV to main ship and UxV to UxV ranges) based on mission requirements, and characterize the maritime environment within those ranges (e.g. unique scenarios: surface/elevated evaporation ducts). Based on those environmental conditions, determine how the RF signal propagates and the time variations of the signal due to vehicle motions and spreading of the signal. Based on those predictions, limit vehicle locations and motion in the network such that they lay within good communication ranges.*

This experiment can result in different outcomes, which can be anticipated to some degree and prepare an alternative method if necessary. The following are possible outcomes of this experiment with corresponding following experimental plans:

- Some ranges fall within acceptable channel states , while other ranges do not. If this affects the requirement of having some UxVs at certain ranges specified during asset allocation, then a network topology that adds more assets (if they are available) to strategic relay locations may be needed. After adding more assets in the network, the network topology is considered static once again. However, if adding more assets is not an option, then consider deploying UAVs from USVs to relay the communications when needed. In this case, the network topology is no longer static, but it will change only for the duration of time necessary to relay the communications and maintain a connected network.

- All ranges fall within the standard deviation from the maximum probability of communications. In this case, no further actions are necessary.

- None of the ranges fall within the standard deviation from the maximum probability of communications. If this is the case, then consider adding more assets, or consider other possible network topology during asset allocation, where the vehicles are closer to each other and can communicate.

The expected results of the experiment will be a set of allowable ranges between vehicles and a minimum required number of available link paths for each asset such that the communication network is reliable to communication link failures. These ranges will then be considered as constraints during COA optimization of each vehicle during the mission while performing their corresponding tasks.

As an example of the importance of asset allocation and network topology configuration, initial proof of concept studies were conducted to capture robust and adaptive link capability on the communication network given changes in the simulation and vehicle parameters [214]. The variables included the following: vehicle asset allocation and path definition, sea-base radius, vehicle specifications, enemy specifications and appearance frequency. Measurements included the following: good and bad links,

successful and unsuccessful relays, area patrolled, detected and un-detected enemy, neutralized and non-neutralized enemy, and lost supply ships. The location and time were fixed to a 200x200 nm area near the southern California coast for which grib2 weather and digital terrain elevation data (DTED) was available. The weather data and resulting propagation loss profile from an emitter at the center of the target area considered, is shown in Fig. 9 in the ACF-UV visualization environment. Figure 1 can be used as a reference of the sea-base area considered.

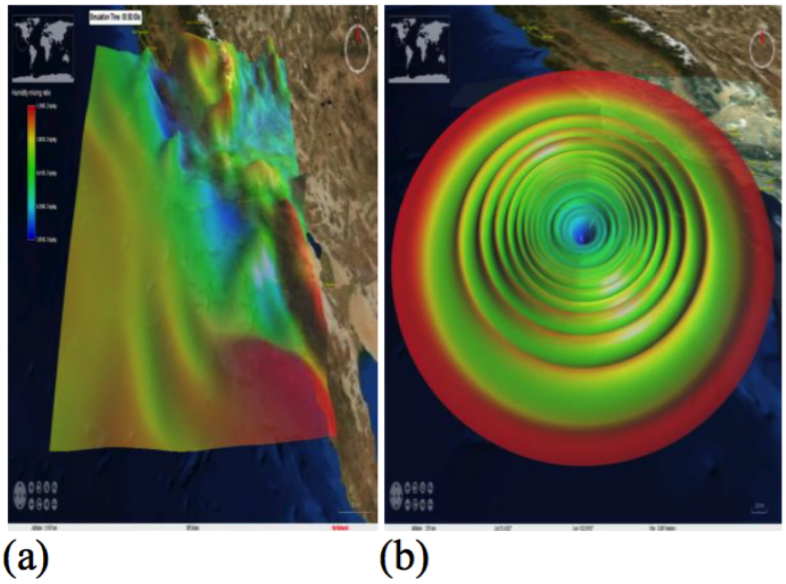


**Figure 9:** (a) Weather condition of Southern California, (b) Propagation loss profile [214]

Results from these proof of concept studies were the following. Increasing the threat identification perimeter beyond 20% leads to failure of communication between patrolling USVs and LCS near the edge of the threat identification perimeter, and relaying links to neighboring patrol USVs also fail. This leads to a need to add USVs with user defined paths between the patrolling USVs and the LCS. Figure 10 shows the resulting links using the following color code for the communication links and relays: green = good link, red = bad link, cyan = good relay, purple = bad relay.

Enemy penetration to sea base perimeter is highly dependent on number of threat

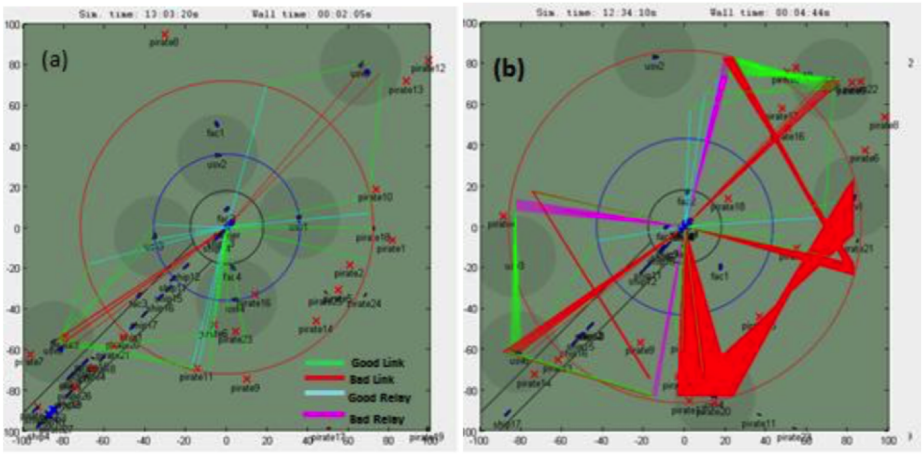


**Figure 10:** (a) Original configuration, (b) Threat identification perimeter increased by 20% [214]

identification radius patrolling USVs and their detection radius. As shown in Fig. 11, when only 4 USVs are patrolling the threat identification perimeter, pirates 18 and 19 are able to breach the perimeter undetected and reach for the sea base. But when the number of patrolling USVs is increased to 6, their detection radius overlap and makes it impossible for pirates to breach the threat identification perimeter.

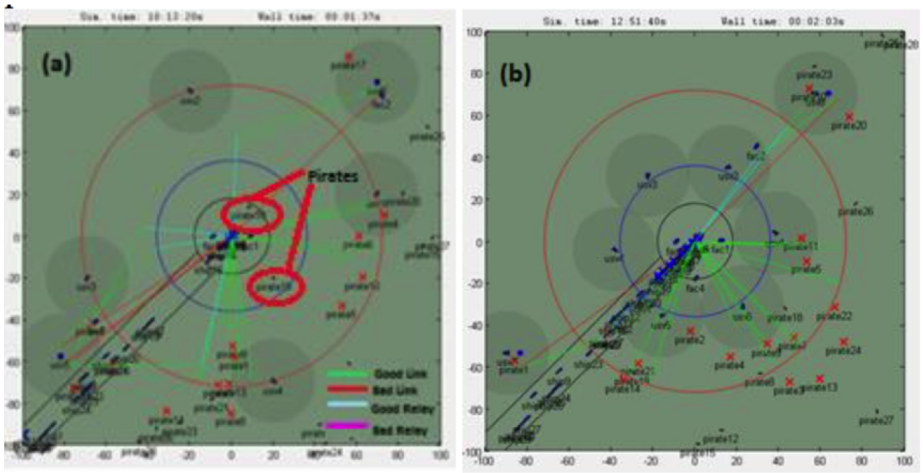


**Figure 11:** (a) 4 patrolling USVs, (b) 6 patrolling USVs [214]

These preliminary results show that threat identification perimeter radius and number of vehicles patrolling the sea base have a significant effect on the capability to maintain communications and detect enemy threats. This information is then

able to be used by mission planners to make key decisions about asset allocation and mission tasks from the prediction of communications given the environmental conditions.

#### *2.2.2.2 Vehicle Performance and Capability*

As part of the COA Development phase, vehicle performance and capability from both manned and unmanned assets need to be analyzed to determine the COAs that they can provide to the mission and unique capabilities that can be used to meet the communications requirements, as is shown in Fig. 12. From the MOPs and MOEs in the mission statement, required UxV performance and capability can be obtained. For example, the patrolling UxV must be able to get to the patrolling area, conduct patrolling tasks, and come back to base. This translates into required range and endurance for the vehicle. Depending on the tasks, the vehicle might be required to carry sensors and communications hardware, which translates into required payload capacity, which will also affect its range and endurance.

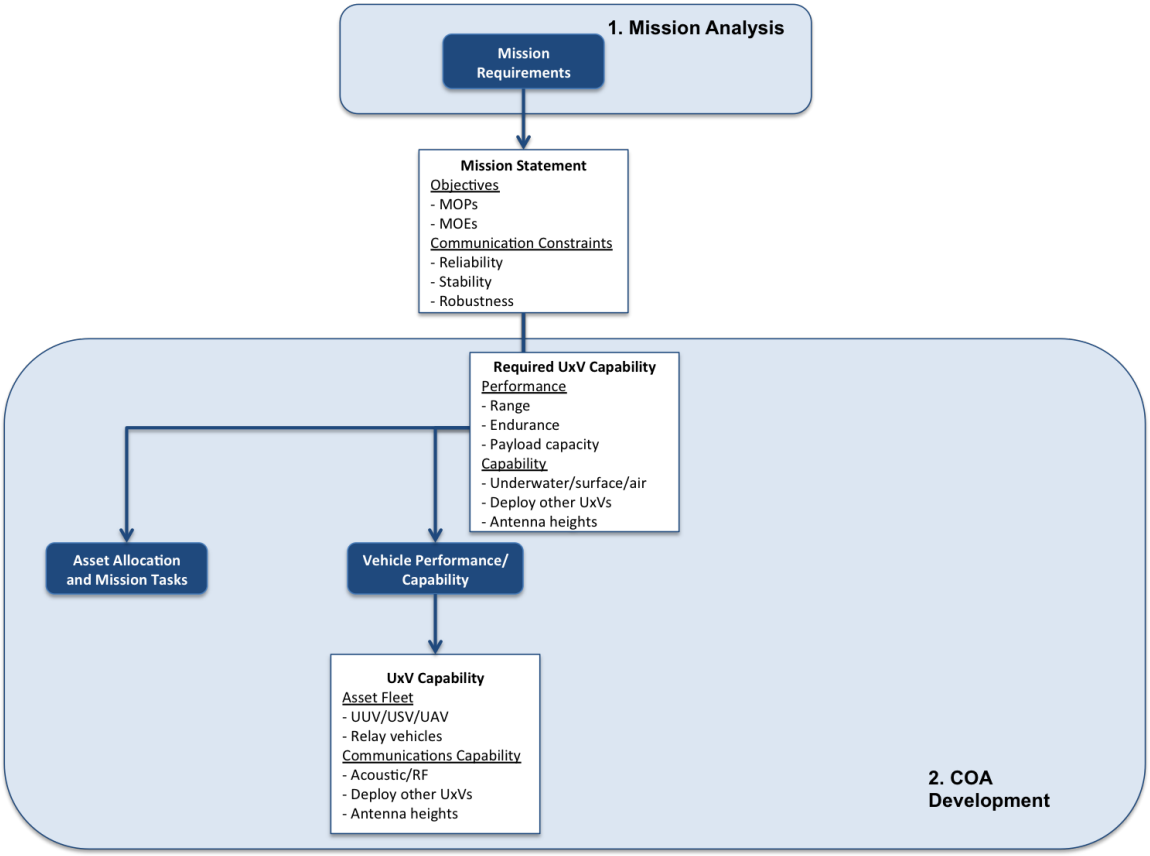


**Figure 12:** Vehicle performance and capability phase of the COA Development step

UxV required capability includes both capability to perform the mission tasks and to meet the communications requirements. For example, in order to provide underwater search and survey, the vehicle must be able to submerge and reach a depth to carry out the search and survey. This limits the option to certain vehicles, such as UUVs. For communications capabilities, vehicles can have the capability to communicate either by acoustic or RF, or communicate via both. For example, a UUV can communicate by acoustics communications while underwater, but its able to also communicate via RF by surfacing. Other types of capability involve having UxVs deploying other UxVs to help relay communications. For instance, a USV can be used to deploy a UAV to temporary provide better communications relay in a

given environmental condition, given that USV in general have more endurance than UAVs.

In keeping with the idea of a modular and data driven tool, UxVs and manned vehicles are initially modeled through the use of top level specifications. These specifications included range, endurance, speed, payload capacity, and overall dimensions (e.g. antenna height). These high level performance and capability specifications can be loaded from a library developed from open source reference, and combined with a model of the basic movement dynamics in the simulation environment to understand the behavior of UxVs. The vehicle classes include unmanned surface vehicles (USVs), unmanned underwater vehicles (UUVs), unmanned aerial vehicles (UAVs), manned vehicles (i.e., high speed vessels (HSVs)), base ships (i.e., LCS, carrier), friendly boats (cargo ships), helicopters, as well as enemy assets such as pirate ships and submarines.

#### *2.2.2.3 Communications Hardware*

Another important phase of the proposed methodology during COA Development is the Communications Hardware options development. This phase involves generating means of communication that meets the requirements from the mission statement. From the MOPs and MOEs, specified, implied, or essential requirements can be used to drive the selection of the communications hardware, as shown in Fig. 13. For example, as a measure of performance, during a mine survey mission the Commander might desire to have low quality imagery of certain areas around the sea base to determine if certain objects of interest can be detected, but this images might be desired as quick as possible. This translates into a required resolution of the data and the data rate needed for communicating this information. RF in general provide faster data rates than acoustic communications due to a higher bandwidth. But for a UUV gathering these images underwater, or being in an environmental condition

that prohibits RF communication, it might only be able to communicate via acoustics. These are the kind of tradeoffs that need to be anticipated when creating these communications hardware options.

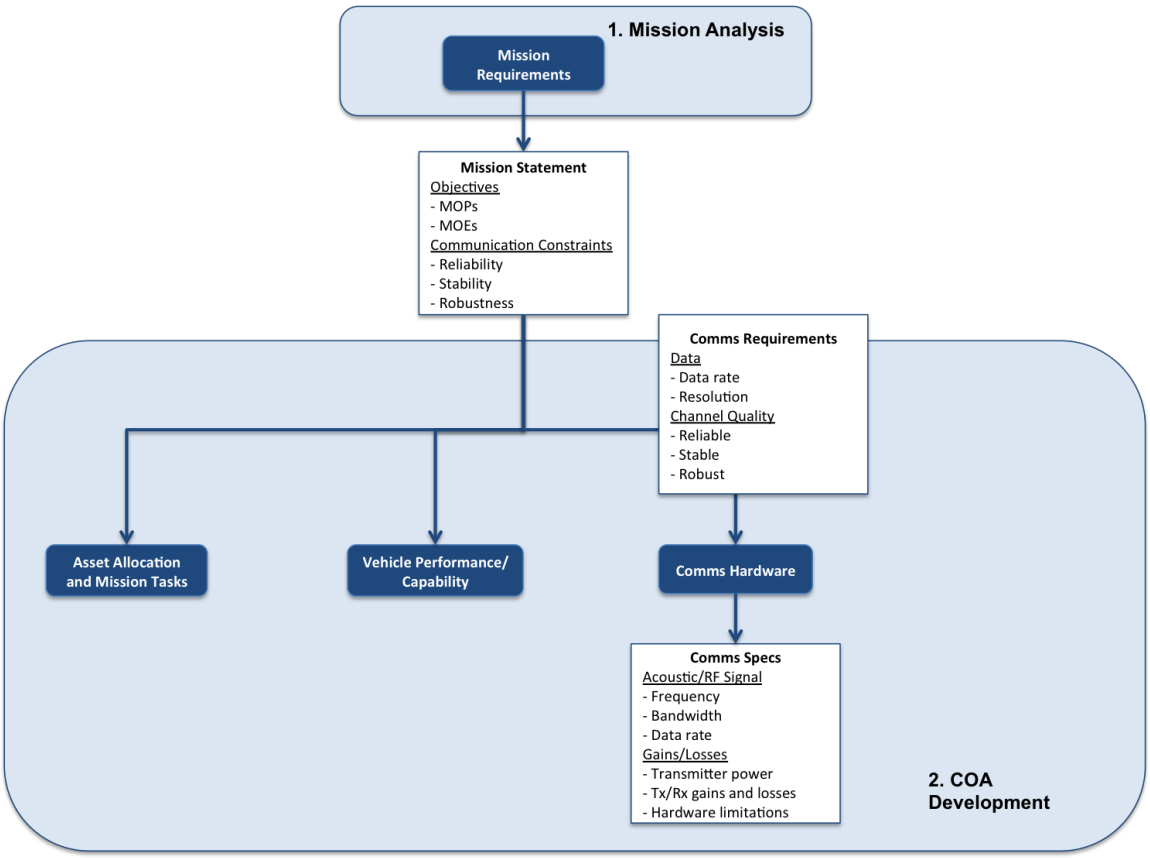


**Figure 13:** Communications hardware phase of the COA Development step

Other requirements that can be extracted from the mission statement that can drive the selection of communications hardware are channel reliability, stability and robustness. To deal with reliability, apart from asset location reliability for link failures and asset failure, there are mitigation techniques that can help increase channel reliability. Two examples of these mitigation techniques are multi-channel transmission and multiple-channel modulation techniques. These can help guide our selection for RF and acoustic communications hardware. Similarly for stability and robustness, certain RF and acoustic communications might be bore robust and stable than others

under certain environmental conditions.

The output of the Communications Hardware phase is a set of options for meeting the communications requirements in terms of communications specifications, as is shown in Fig. 13. These specifications include the frequency of the signal, bandwidth, and data rate. It also includes the specified gains and losses from both the transmitter and the receiver. The transmitter power for RF is also specified, which is an important parameter since this power attenuates as it propagates through space and time. Hardware limitations are also specified for the selected communications hardware. These limitations include receiver minimum power level to successfully translate the signal, the minimum SNR, or the maximum propagation loss the signal can withstand before dropping to certain data rate. These limitations become important to determine the quality of the channel in terms of meeting these limitations or threshold values.

For our studies, each vehicle is equipped with a communications hardware depending on the mission requirements, type of vehicle and its capability. The two only means of communication considered in this thesis are RF and acoustic underwater communications. USVs and UUVs, depending on their size and capability, can be equipped with both RF and acoustic communications hardware (UUVs can surface and communicate via RF), and aerial vehicles can be assumed to communicate via RF only. The user can specify the hardware based on communications needs, the frequency and frequency bandwidth required, and the expected range of operation.

The communications hardware selection can also be based on required communication network architectures and protocols. Well established communication architectures, such as the Joint Architecture for Unmanned Systems (JAUS) [171], and network protocols, such as link-16 [61], can be used as guidelines for selecting the communication hardware that meets these required architectures and network protocols.

#### *2.2.2.4 Sensor Hardware*

The next phase of the COA Development is to find sensor options that meet the mission statement's requirements. Based on the MOPs and MOEs, certain sensory capability and performance can be extracted, either from implicit or explicit (essential) requirements, as is shown in Fig. 14. For example, the MOE can be to locate enemy threats in a given area, and the objects of interest might be mines or enemy underwater vehicles. Based on where the areas are, how deep underwater the vehicles will provide the search, and the dimensions and physical shapes of these objects of interest, the selection of sensor options can be determined. For objects that are moored or are navigating above the sea floor, a forward-looking sonar might provide better searching capability. For objects on the sea floor, side-scan sonars might be more adequate.

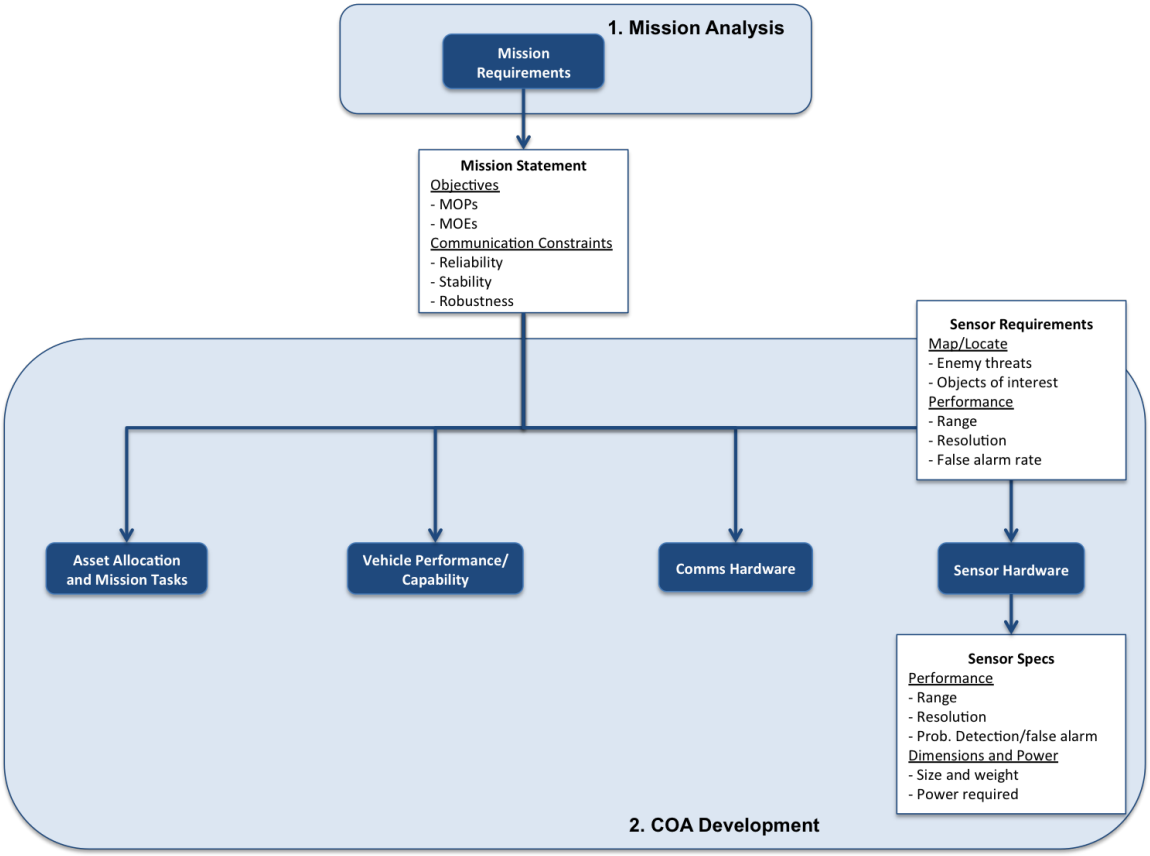


**Figure 14:** Sensor hardware phase of the COA Development step

In terms of required sensor performance, the MOPs might require the sensory data to be high resolution, or the data to be collected over large ranges. Resolution will be affected by the type of sensor, the environment, and how close/far is the vehicle from the object of interest in the time of measurement. Therefore, the selection of sensor requirements might also be tight in with the asset allocation, since sensory data depends on how the vehicles take the measurement. Another measure of performance is the detection probability and the false-alarm rate. The probability of detection and false-alarm rate are related to the signal power level and translating it to a probability that the target is an actual target or a false positive, given that it meets a certain threshold power level. These are important requirements when the sensory information is dependent on how the sonar signal or laser scanner propagates through

water or space, respectively, and when the target shape and size matter. These can be used in a sensor model to better determine the probability of detection or false-alarm rate.

The outputs will be sensor hardware options and their specifications, as is shown in Fig. 14. These specifications are performance metrics of the sensor, such as range, resolution, and probability of detection and false-alarm rate. Other specifications include size and weight of the sensor, and the power required to run the sensor. These are important specifications that are used to determine what vehicles can carry them, or to size new vehicle concepts that can be added to the fleet of assets to enhance communications capabilities.

For our study, certain UxVs are equipped with a sensors for navigation, detection, classification, and recording. Sensor selection is a critical part of the COA development process since it determines what type of sensor information will be communicated to other UxVs and to main ship, and the quality of the information. This information is critical for the situational awareness of the mission and for meeting the mission goals.

#### *2.2.2.5 Sensor Model*

Once the sensor hardware options have been specified, the outputs of the Sensor Hardware phase can be used to model the type and quality of the information data that is communicated through the communication channels in the network. The goal of this sensor modeling phase is to quantify the quality of the sensory information so that we can develop better COAs, as is shown in Fig. 15. For example, knowing that the probability of detection is a given number $P_d$ for a given range, we can search for better vehicle paths and locations that provide the best certainty of mapping of a given area. This will be useful when we do COA Analysis in terms of the progression of the measurements and mapping uncertainty as the vehicles perform their tasks.

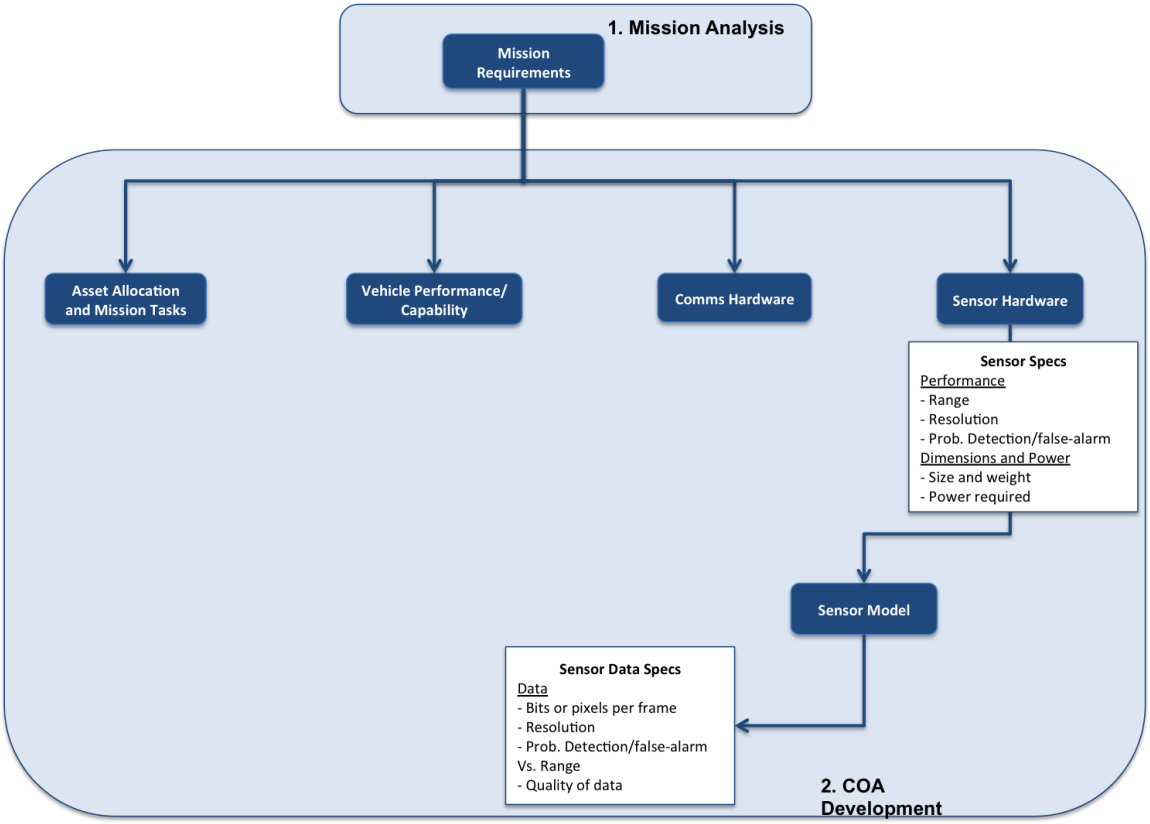


**Figure 15:** Sensor Model phase of the COA Development step

Another important output of the sensor modeling is the type of data and resolution of the data. This can be quantified differently for different sensors. For example, for images, we might care about the number of pixels per bit of information. This is useful when modeling the communications channel and making sure we have enough bandwidth and data rates from the communications hardware to send all that information, or part of that information, over the communication channel.

Different sensors can be modeled using different approaches and methods. Target detection sensors, for example, can be modeled as a stochastic process, where the probability distribution of detection is based on a post processing of the signal-to-noise ratio (SNR) (Fig. 16) [112] [42] [4]. False-alarm rate is used to determine the necessary level of accuracy in the detection. SNR is modeled physically based on the propagation loss based on the medium. The target energy return is modeled as based

on the sensor range and expected target geometry. Sensor system specific losses and noise are added for a more realistic model [42].

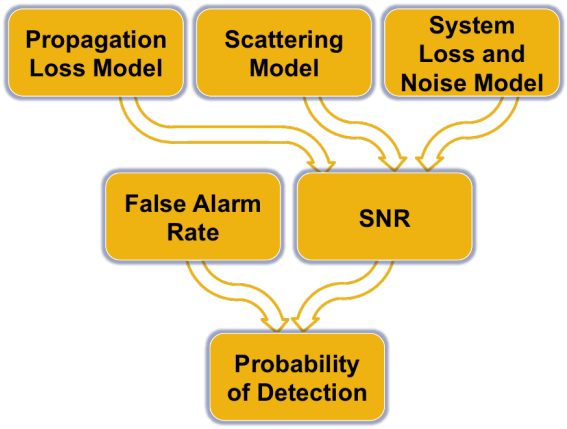


**Figure 16:** Stochastic sensor model process [112].

Sonars are used extensively to detect and classify underwater mines for MCM missions, and will be critical for UV Sentry missions. Different types of sonars are used for detection and classification. Side-looking Sonars (SLS) [112] and Forward Looking Sonars (FLS) [79] are generally used to detect and classify mines, depending on the type and location of the mines. Propagation loss of sonars can be calculated using methods such as the parabolic Helmholtz equation, ray-tracing algorithms, and simplified attenuation equations [120]. Each method takes into account the underwater conditions and the frequency. As is shown in Fig. 17, propagation loss per distance varies depending on the underwater conditions in different oceans around the world [120]. The method selection highly depends on the accuracy and fidelity needed of the model. Target backscattering cross section can be modeled with Swerling target models, where it is assumed that the probability of detection is constant within each scan, but varies independently between scans [184].

Another important sensor is Radar, which is used to detect and classify targets and objects in the atmosphere [67]. Similar to sonars, propagation loss is modeled using the parabolic approximation of the Helmholtz equation, where only forward

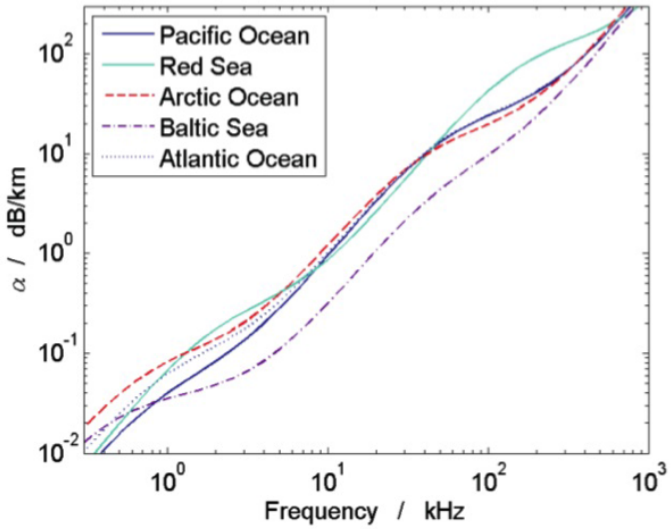


**Figure 17:** Propagation loss per distance as a function of frequency in different oceans [120].

propagation is assumed, and the model accounts for atmospheric and terrain induced refractivity, diffraction and reflection [42]. Target Radar Cross-Section (RCS) is also modeled as a Swerling target, assuming RCS is constant within each scan, but varies independently between scans [184]. The probability distribution of the RCS can be modeled using a Chi-squared distribution with $m = 1$ degrees of freedom, given by Eq. 1 [122]:

$$P(RCS) = \frac{1}{RCS_{avg}} \exp(-\frac{RCS}{RCS_{avg}}) \tag{1}$$

#### *2.2.2.6 Characterize the Environment*

The next phase in the COA Development step is to characterize the environment. The output from the asset allocation phase is used to determine overall ranges, heights, and depths underwater, that these UxVs are expected to be performing their mission requirement tasks. The goal in this phase is to characterize the environmental conditions that may affect communications within this distances, heights, and depths, as shown in Fig. 18. For atmospheric propagation of RF signals, the refractivity profile helps describe how electro-magnetic (EM) signals bend and propagate through space

due to the changes in density, temperature, and pressure as a function of altitude and range. Certain atmospheric conditions can lead to special conditions that can affect the EM wave propagation of the RF signal, such as evaporation ducts and surface or elevated ducts. These can also be described by the refractivity profile.

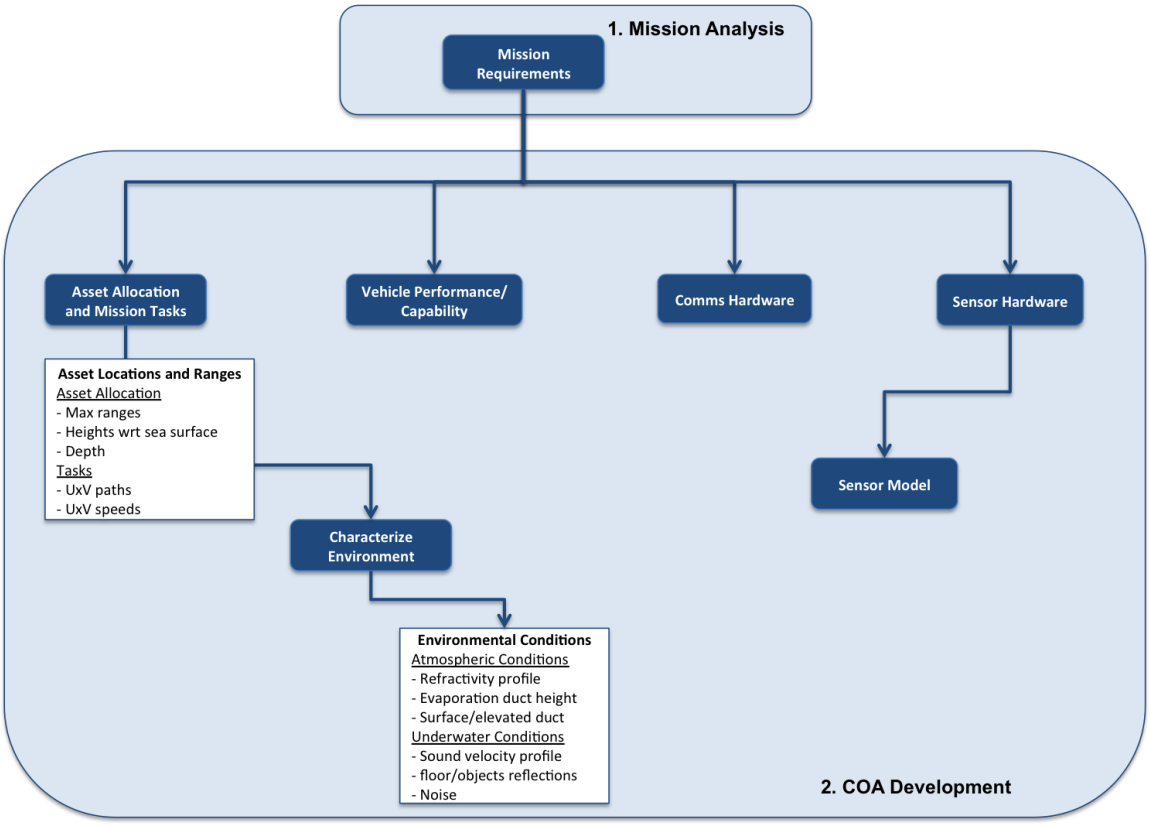


**Figure 18:** Characterize the Environment phase of the COA Development step

For underwater propagation of acoustic waves, the changes in temperature, pressure, and density of water also affect how the acoustic waves propagate in water. Similar to how atmospheric conditions can refract EM RF signals, the underwater conditions can lead to bending and refraction of the acoustic wave signals. These effects can be described by the sound velocity profile (SVP), which is similar to the index of refraction for EM waves. Other parameters of interest for sound wave propagation are reflections from the sea bottom, the sear surface, and other objects. There is also noise that can affect the SNR of the signal.

The outputs should be a set of parameters and profiles that can help us during the prediction of communications. For example to calculate how RF signals propagate, we can use the refractivity profiles to see how signals bend and how they create interference and therefore attenuation. For acoustic signals, the SVP can also be used to determine how different signals interfere with each other and how the signal can be attenuated.

#### *2.2.2.7 Predict Communications*

The final, and crucial phase of the COA Development step is to Predict Communications. These predictions are useful for generating COAs that take into account whether vehicles can communicate in the operational environment under the given environmental conditions. If communications are not accounted for early during the COA development of the planning process, it can lead to serious problems, such as the loss of unmanned/autonomous vehicles, lack of sensory information provided by vehicles to make important decisions, and not being able to give vehicles commands as the mission is taking place.

To make better predictions of communications, the outputs from the previous COA Development phases, which were driven by the mission statement, are used to make our predictions more in accordance with our available assets, the environment under which they are expected to perform their tasks, their expected positions and motions, their capability and performance, their communications hardware, and the sensory information that they need to communicate over the channels, as is shown in Fig. 19.

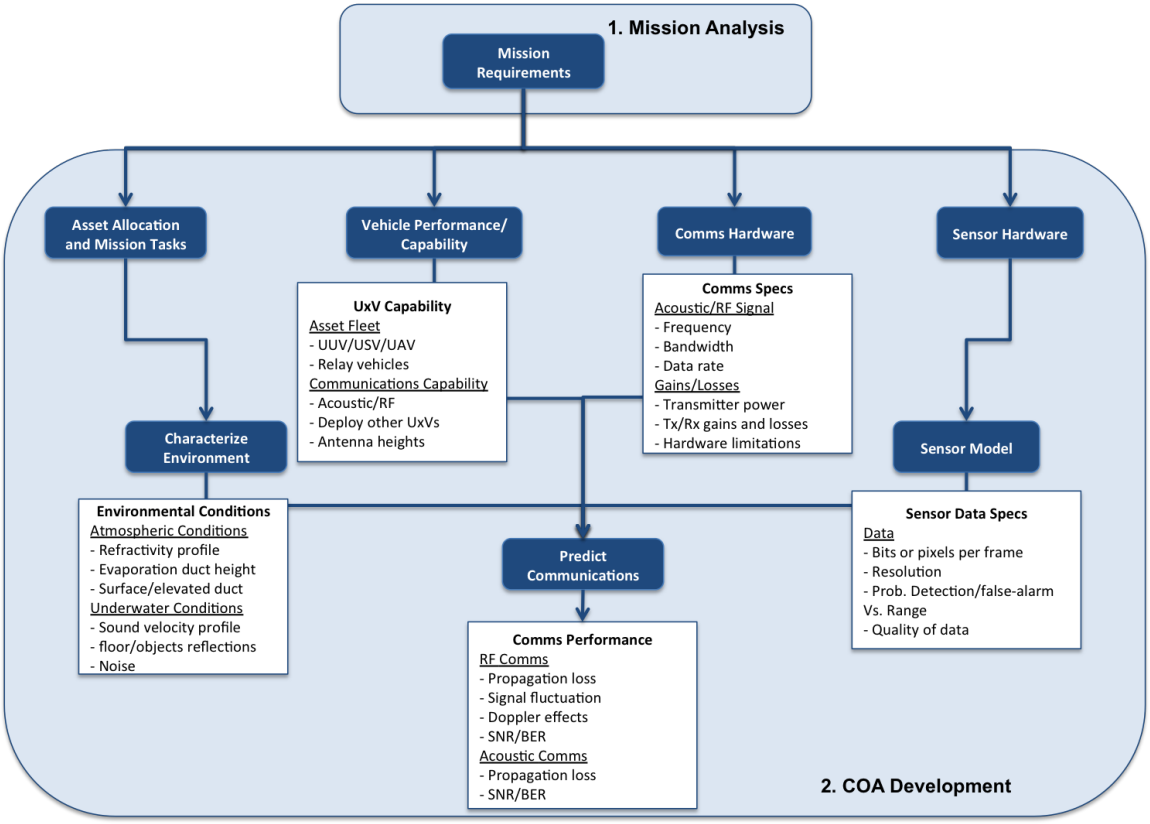


**Figure 19:** Predict Communications phase of the COA Development step

As RF signals propagate in space, they are attenuated significantly as a function of distance squared, according to the free-space propagation model [187]. The line-of-sight signal attenuation is highly dependent on the distance between transmitter and receiver. Therefore it is important to take into account the expected locations and motions of our assets as they perform their tasks, to make sure they can communicate back to the base station or relay communications with near-by unmanned vehicles.

As described in the Characterize the Environment phase, different refractivity conditions can lead to the refraction, diffraction, and reflection of EM waves as they propagate in the atmosphere. For maritime environments, important degrading conditions include evaporation ducts, surface and elevated ducts, and combination of these phenomena which can lead to complex attenuation of the EM waves as the multi-path signals interfere each other [167]. Therefore it is important to take these

environmental conditions into account while making our predictions.

As the vehicles move with respect to each other, the signal is also affected by Doppler effects in which different signals can interfere with each other at different times. This leads to time variation of the signal. As the signal propagates, it is also attenuated by scattering effects, diffraction by objects in the path of the channel, and other gases or liquids in the path, which leads to time-spreading of the signal [187]. These effects lead to further signal attenuation which is time and space dependent which can be complex to model and specific for a given operational environment condition.

Communications hardware can pose further limitations or enhancements to the quality of communications. Given the radio specifications form the output of the Communications Hardware phase, the transmitter power, and transmitter/receiver gains and losses can be used in a link budget equation to keep track of the expected received power at the receiver, and compare it to hardware limitations and thresholds to quantify the quality of the channel. Signal parameters such as the frequency and bandwidth also affect how the signal propagates through the atmosphere in maritime conditions. Therefore, it would be important to study the effects of frequency, narrow and wide band communications on the amount of attenuation from maritime environmental conditions.

Sensor data specifications from the output of the Sensor Model phase are also used to make sure we have enough bandwidth and data rate to transmit the sensory information over the channel. Based on the total attenuation of the signal due to propagation losses, interference, time variation of the signal, and scattering, it will result to certain amount signal-to-noise ratio of the signal, which, given a modulation scheme to code the sensor information, it can be translated to bit-error rates (BER) and symbol-error rates (SER) that can be used to determine how the sensory information is affected by the attenuation, and the ability of the transmitter to demodulate

the signal. If the attenuation leads to high BER or SER, then the resolution of the sensory information can be degraded, and can affect our MOP of the mission and fail to meet the requirements of the quality of the sensor information needed to make further decisions by the Commander.

Given that the time-variation and time-spreading or back-scattering of the signal is dependent of the given environmental conditions, vehicle relative motions, and dynamic complex environment, a probabilistic approach would provide a way to take into account our modeling uncertainty and uncertainty in environmental conditions. It would also allow for robust modeling of the transmission channel under these complex environments. This leads to the following corresponding hypothesis:

**Hypothesis 2 (HP2)**: *Given communication constraints that reflect communications hardware limitations, a probability model will provide a robust fading channel model that takes into account multi-path and Doppler effects.*

To answer RQ2 and test our hypothesis HP2, a series of experiments need to be conducted for studying the effect of maritime environmental conditions on the multipath fading of the signal, and how the time-variation and time-spreading of the signal can be modeled probabilistically under the given maritime environmental conditions. The first experiment will be a series of studies on the effect of propagation loss on narrowband and wideband signals, under different frequencies, and between unmanned vehicles that we expect to have in the available fleet of assets. The first experiment is the following:

**Experiment 2 Part A (Exp2)**: *Study the multi-path fading characteristics of the channel under different evaporation duct conditions representative of maritime environments for a sea-base operational environment. Study the effects of frequency,*

*frequency bandwidth, multipath attenuation, vehicle antenna heights with respect to the evaporation duct, and hardware limitations on the communications channels.*

To model the time-variation and spreading of the signal under the environmental conditions, a series of studies will also be performed to investigate stochastic and probabilistic methods to make the modeling more robust to environmental conditions uncertainty and different signal fluctuations due to spreading and vehicle motions. The next experiment is also part of Exp 2 for modeling the communications channel:

**Experiment 2 Parts B and C (Exp2)**: *Investigate ways to model the transmission channel probabilistically which captures the time-variation (Part C) of the signal and the time-spreading of the channel (Part B). Based on these probabilistic methods, search for ways to capture the signal intensities found in maritime environments which leads to a robust modeling of the fading channel, and simulate the channel under these conditions.*

The results of Exp2 will be general guidelines and recommendations on the modeling of fading multipath channels under maritime environments. The fading intensities corresponding to different atmospheric conditions found uniquely in maritime environments will be emphasized. Such atmospheric conditions include evaporation ducts, surface-based ducts, elevated ducts, and other special refractivity conditions.

### 2.2.3 COA Analysis and Wargaming Process

To meet these COA analysis and wargaming tasks, first the communications network will be assessed based on the quality of each transmission channel, to check whether vehicles are connected. This will be done using graph theory methods to quantify the connectivity of the networks. In the next step, communications-based COAs

will be identified and schedule of these COAs in the operational environment will be considered for the optimization of mission level MOPs and MOEs. A bayesian filter will be used to model the probabilistic nature of the evolution of vehicle state, situational awareness and measurements. Constraints in the optimization problem include the UxV performance and capabilities generated during the COA Development step, network reliability constraints, and robustness of communication channels. Design variables used for optimization are communications-based COAs and their schedule.

#### *2.2.3.1 Communications Network Analysis*

The first step of the COA Analysis step is to assess the communications network based on the communications predictions and the asset allocation done during the COA Development step, as is shown in Fig. 20. Communication networks can be represented as graphs, with nodes representing vehicles and edges representing communication links between them. These networks can be assessed in terms of connectivity, stability, robustness, and reliability by assigning weights to each transmission channel link in the network. This analysis is done to make sure our COAs developed in the previous step meet our communications requirements and MOPs and MOEs from the mission statement. In this phase, relay vehicles and their allocation can be considered to make sure we meet these mission objectives and constraints.

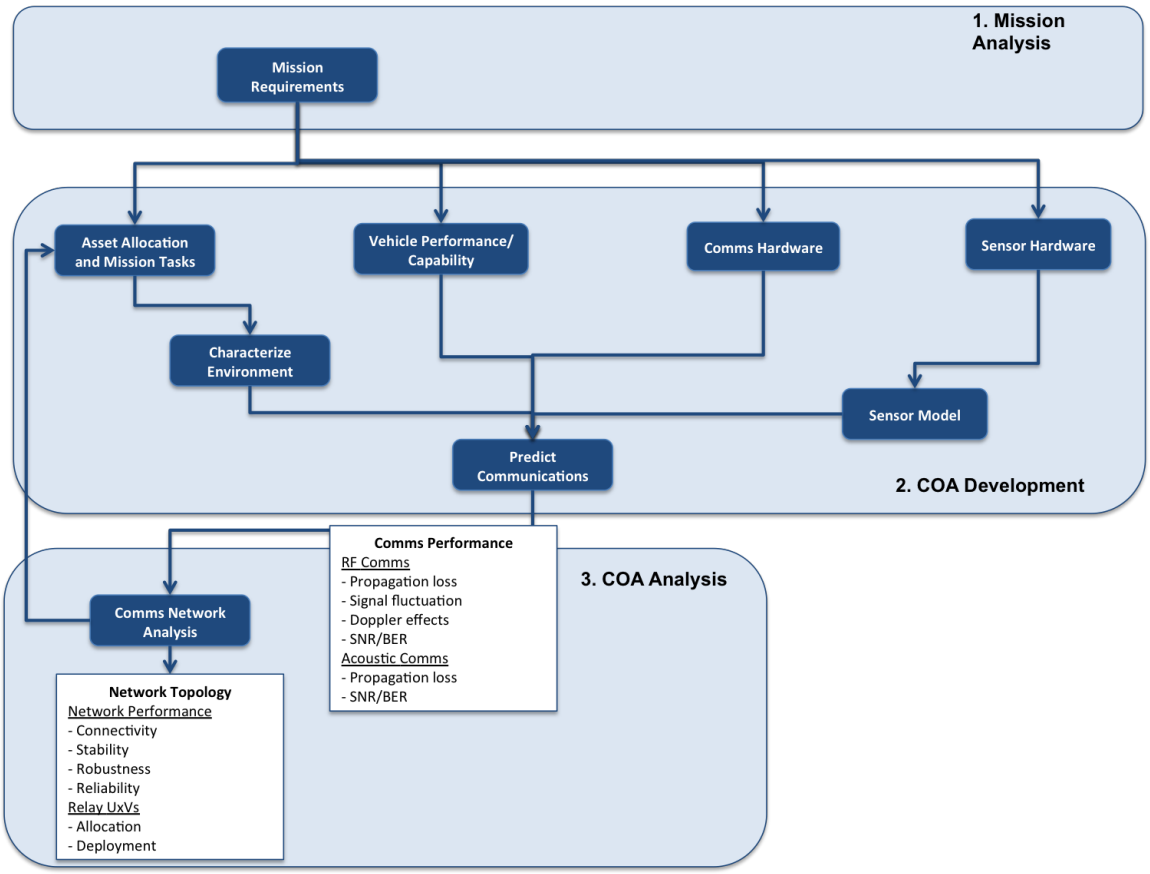


**Figure 20:** Communications Network Analysis phase of the COA Analysis step

The input to the network analysis are the communications performance metrics for each channel between any two vehicles. These were generated during the COA Development in the Predict Communications phase. Based on these predictions, and depending on our connectivity requirements, we can quantify how connected each UxV is with other vehicles in the network. We can also quantify how stable the network is due to time-variations and spreading of the signal from vehicle motions and scattering effects. By looking at the network topology, we can also play wargames by anticipating possible link failures and making sure that the resulting network is still connected. This can be translated to network reliability, where we make sure the network is configured in such a way that if a link fails, other vehicles can help relay communications with other vehicles.

Robustness of the network can be quantified by the probability of communications of each link in the network. The higher the probability of communications, the more robust it is to time-variations and spreading of the signal. This can be translated into quality of communications of each link in the network, and making sure vehicles are within good ranges of communications where higher probability of communications can be achieved.

The outputs of the Communications Network Analysis is a network topology composed of available assets and relay UxVs that is connected, stable, reliable, and robust. If the network topology does not meet any of these communications requirements, then an iterative process is done by feeding this analysis to the Asset Allocation and Mission Tasks phase of the COA Development step to re-assign tasks or add more vehicles to our fleet of assets that can help meet these requirements. The planning staff can also use the results of the network analysis to make better decisions on other phases of the COA Development. For example, better communications hardware can be chosen that provide better and more robust communications channels. UxV capability and performance can be driven based on the need of vehicles that can operate under certain environmental conditions. And finally, sensory information quality and quantity can be driven by use of better sensor hardware.

For Exp1, these wargaming analysis will be used in the Mine Survey mission to make sure we meet all of our communication constraints. The addition of relay vehicles, and relaxing certain communication constraints will be considered to come up with a network topology that meet most of our constraints and provides the best MOP and MOE of the mission level objectives.

#### *2.2.3.2 Bayesian Filter*

The next phase in the COA Analysis step is the Bayesian Filter, shown in Fig. 21, which provides analysis on the model integration and uncertainty propagation as

the vehicles perform their assigned tasks. This is an important phase since the way UxV perform their COAs to meet the MOPs and MOEs of the mission statement affects the quality and the amount of information that is communicate through the network. During mapping or localization tasks for example, where UxVs rely on their sensors to make observations and make decisions, active sensing is used to control sensor parameters such as position, orientation, and paths in order to obtain better information and reduce uncertainty [126] [91] [49]. The planning for search and exploration COAs depends on the sensor being used and the quantity of information that is being captured, such as during the target detection and identification of objects of interest in a Mine Survey mission. Therefore, the Bayesian Filter analysis provides a method for representing and updating the estimate and associated uncertainty, the belief state of the mapping or localization task, and a way of using the belief of the state to determine expected information that will be communicated through the network.

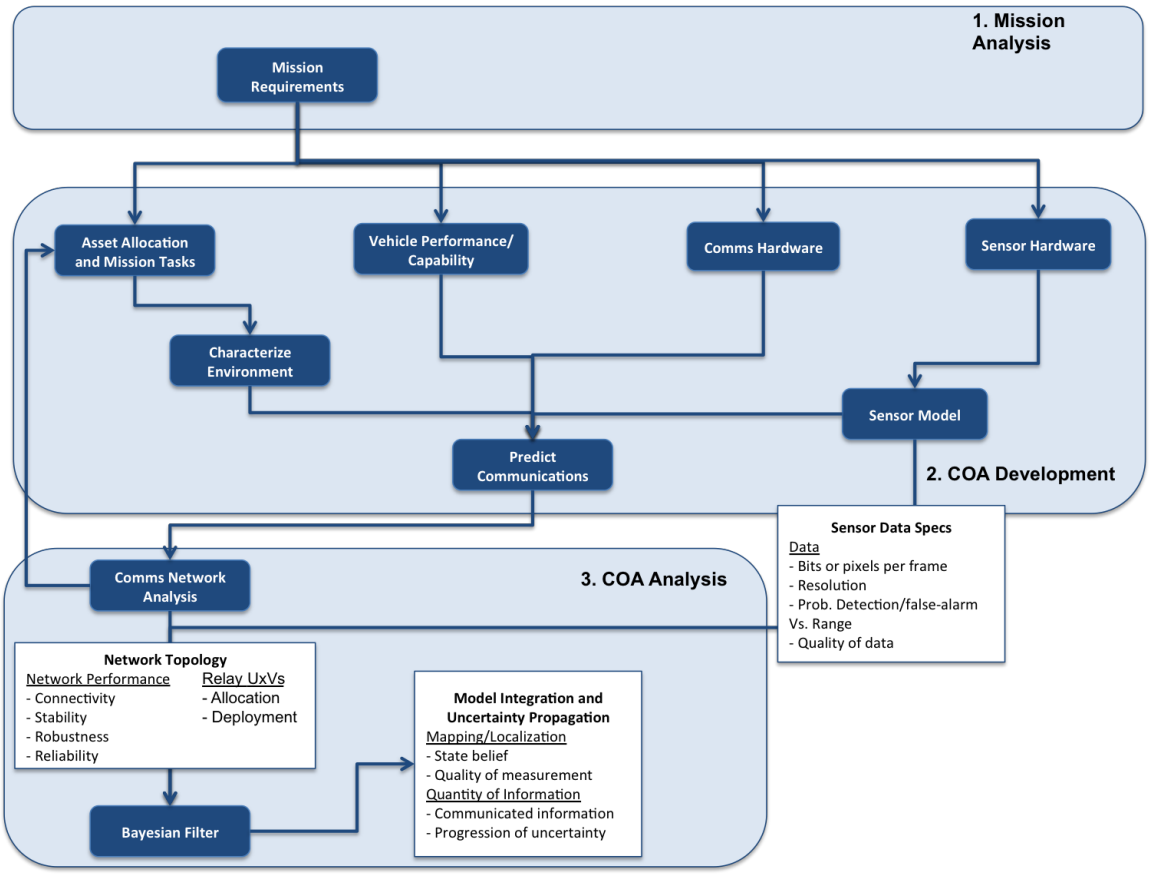


**Figure 21:** Bayesian Filter Analysis phase of the COA Analysis step

The Bayesian Filter provides the framework to keep track of uncertainty as measurements and control actions are taking place, but we need to find ways to model how information is represented and how it translates into quality and quantity of information. Since quality of information depends on the sensor model, it can be captured by the belief of the state as measurements are taking place. Quantity on the other hand, depends on how much uncertainty is communicated through the communications channel. This leads to the next hypothesis regarding RQ3:

**Hypothesis 3 (HP3)**: *A sensor model can model Quality of information, and quantity of information can be modeled as the amount of state uncertainty that is communicated through the network.*

The output of the Bayesian Filter analysis should be a method of integrating different models, such as the sensor model and vehicle motion model, and accounting for the uncertainty propagation as the vehicle is performing its tasks while collecting sensor measurements. This includes the belief of the state, be it occupancy for mapping tasks or location for localization tasks, the quality of the measurement due to the sensor model and how the vehicle collects the sensor data, and the quantity of uncertainty that is communicated as information over the channel. These outputs can be used to make further COA analysis by finding optimal ways to collect the most information and the best quality of information by selecting different paths or ways to communicate that information.

#### *2.2.3.3 Optimization*

The final phase of the COA Analysis in the proposed methodology is Optimization, where we search for optimum ways to meet the mission level objectives stated in the mission statement, while also abiding to all constraints, as sis shown in Fig. 22. The mission level objectives come from the mission statement in the form of quantifiable MOPs and MOEs, such as area protection or clearance, threat detection, and enemy asset neutralization. Other MOPs and MOEs can be directly linked to communication objectives, such as maximum information available, situational awareness, and robust communication network.

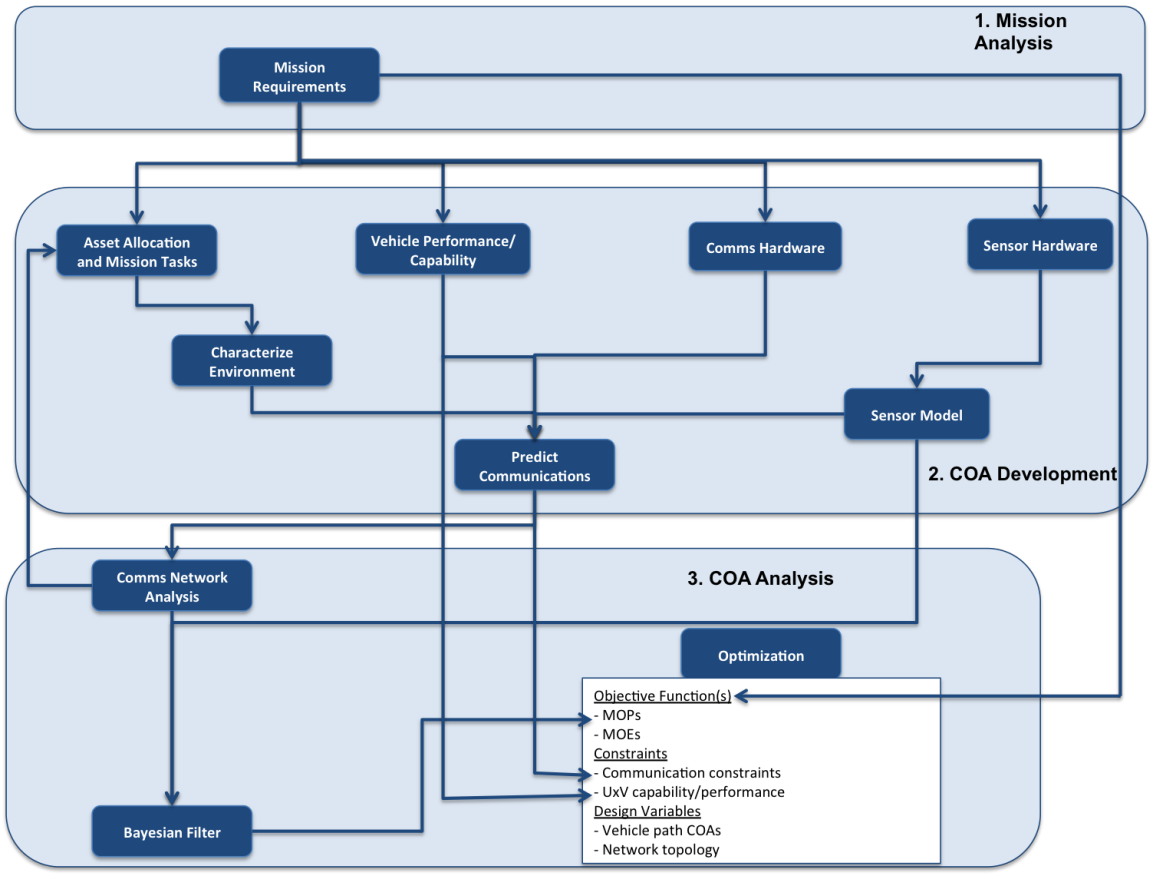


**Figure 22:** Optimization Analysis phase of the COA Analysis step

The constraints come from different parts of the COA Development or COA Analysis steps. For example, communication constraints can be posed in terms of meeting the hardware limitations from our communications predictions, or can be posed in the form of network requirements, such as reliability, stability, and connectivity. Other constraints include vehicle capability and performance, and sensor capability such as range and resolution.

Design variables are those parameters that are allowed to vary as we try to optimize the objective function or functions. They can be the vehicle paths and asset allocation in the operational environment. For example, the path a UUV takes to provide situational awareness can be found such that it maximizes the area coverage, while also meeting the communications constraints. The network topology can also

be changed by adding/deleting assets that can help meet the network requirements, while also helping to maximize/minimize a mission objective.

During our demonstration case study for the Mine Survey mission, we will demonstrate the optimization analysis by choosing communications based MOPs in terms of maximizing the information entropy communicated over the network, and will be compared to baseline methods for sweeping through a given target area. Benefits of our optimal solution will be compared to these baseline methods, and the benefits and limitations of our methodology, and trade-offs available will be identified.

### 2.2.4 COA Comparison and Decision Process

The next sub-subsections describe the proposed methodology steps and corresponding suggested methods to meet the COA Comparison and Decision Process.

#### *2.2.4.1 Simulation and Mission Planning Visualization*

In this Simulation and Mission Planning Visualization phase of the COA Comparison and Decision step, shown in Fig. 23, the COAs are validated to make sure they meet all mission level objectives and all requirements, which include mission level requirements, communications requirements, vehicle capability and performance requirements, communications network requirements, and sensor data requirements. In this phase, the mission is played out as would be expected in the operational environment, and the benefits and limitations of each selected COA are assessed through simulation results. Things to keep track is how each COA compare in terms of how good they meet the mission level objectives, the robustness of each solution to changes in enemy tactics, and how adaptable it is to uncertainty in environmental conditions.

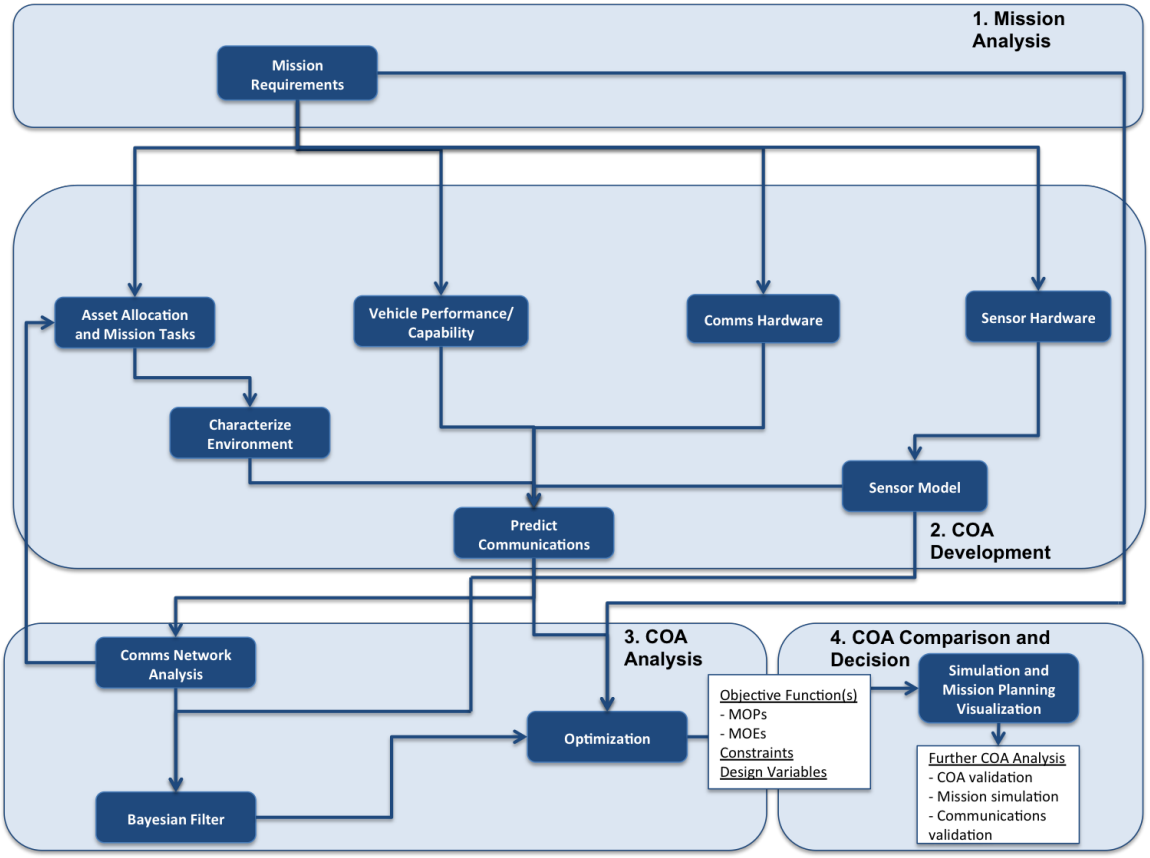


**Figure 23:** Simulation and Mission Planning Visualization phase of the COA Comparison and Decision step

#### *2.2.4.2 Adaptive Communications Framework for Unmanned Vehicles (ACF-UV)*

ACF-UV was developed by a team at the Space and Naval Warfare Systems Center (SPAWAR) in San Diego CA, led by principal investigator Dr. Ayodeji Coker. UV Sentry missions have been modeled within the ACF-UV, along with the integration of RF and acoustic communications models to predict the UxV communications network [66].

ACF-UV differs significantly in its purpose from the numerous communications frameworks which exist for handling unmanned communications. The established frameworks such as Robot Operating System (ROS), Mission Oriented Operating

Suite (MOOS), etc., focus on the structure and interoperability of the message being passed, while ACF-UV focuses on providing a predictive estimation of the future state of an intermittent communication link between two or more autonomous platforms as well as their respective command and control (C2) stations. This work focuses on the physics and prediction of intermittent transmission channels. The purpose of such a framework is to allow system designers, performance engineers and System of Systems (SoS) designers the ability to make improved design choices that lead to better connectivity between UxVs. A second purpose of ACF-UV is to allow mission planners, commanders, and onboard operators to make intelligent choices in the path planning and operational placement of assets to ensure network connectivity can be maintained [63]. ACF-UV accomplishes the goal of providing a predictive model of intermittent communication through the use of a modular framework that integrates a series of detailed models used to study the potentially detrimental effects of the physical and EM environment (Fig. 24).

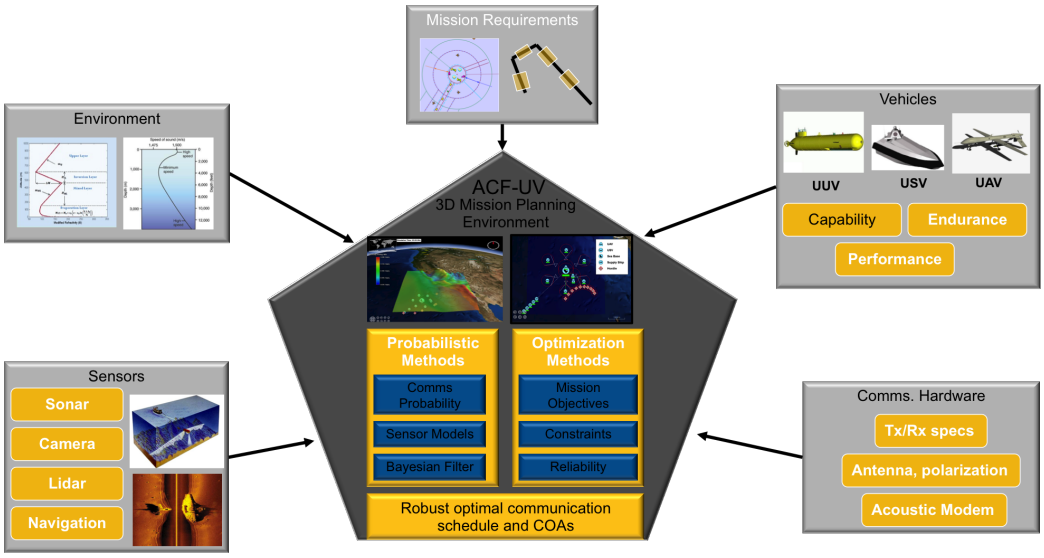


**Figure 24:** ACF-UV modules and models integration [63]

ACF-UV includes models to predict the state of transmission channels in maritime environments, as well as a simulation environment that is used as an operations

view of the signal links between UxVs. ACF-UV has evolved from a 2-D Matlab environment to a 3-D Java environment as a tablet application and a multi-user surface table application (Fig. 25). With these capabilities, the framework provides a high level common operational picture of expected communications network quality in an operational scenario and is used as a test-bed for demonstrating the methodology while following the NPP doctrine.

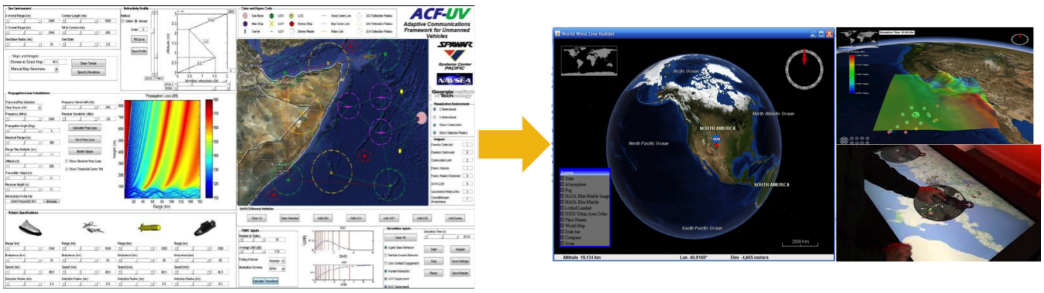


**Figure 25:** ACF-UV transition from 2D in Matlab to 3D environment in Java

An essential element of the ACF-UV is a data driven visual simulation environment which integrates the outputs of independent modules into a common operational picture that provides a representation of the quality of the network. The value in this data driven modular approach is that it allows for an estimation of connectivity such that the elements can be adapted to fit specific purposes. For an example use case, ACF-UV can be used as an analytical component within the autonomy package of the robotic platform, which allows it to maintain its own connectivity to the C2 station while plotting its own route through an environment. In this situation, the modules that provide a predicative estimation of the communication link based on the robotic system and C2 station, as a function of atmospheric conditions and emitter characteristics are left unchanged, while the modules within the ACF-UV framework concerning vehicle location and behavior are substituted for the AI control software. In this way, the ACF-UV provides a predictive estimation of the connectivity for that vehicle as it moves through the environment that can be used by the AI to optimize the route taken. An alternative set of substitutions can allow for the framework to be

applied to a different use case where a system designer executes the described analysis in setting requirements for a robotic system's emitter. If an operational perspective is desired, the ACF-UV can be used to refine the operational layout of a system of robotic systems which maintains connectivity.

Inputs for the simulation environment include: atmospheric environment characteristics (refractivity profile), radio signal specifications, UxV and LCS performance and capabilities, UxV and LCS initial locations, UxV and LCS paths and agent based behavior, and stopping criterion (time or a set goal). An Agent Based Modeling (ABM) and Emergent Behavior approach is also being developed to enable UxVs to autonomously position themselves to optimize area coverage while maintaining constant communication with all UxVs and LCS. Outputs of the simulation are measures of performance with emphasis on the communication network which include: enemies detected, enemy radars detected, mines detected, communication links lost, successful relay links, and overall mission awareness.

## *2.3 Methodology Demonstration and Scope*

The effectiveness of the methodology should not only be judged on its proficiency to provide communication solutions, but rather, and more importantly, on its capability to provide the user with the tools and methods to assess the communications problem more effectively during the NPP process, and to provide awareness of the possible feasible solutions. The demonstration study for Mine Survey Mission is a first-order analysis that should capture all these capabilities. This leads to the final hypothesis regarding the methodology and the demonstration study:

**Hypothesis 4 (HP4)**: *The proposed methodology provides a useful approach towards predicting communications between UxVs, generating optimal communications-based*

*COAs, and will be demonstrated in the mine survey mission, while ensuring communication channels are robust to environmental uncertainties, reliable to communication failures, and that optimize a given mission objective.*

To test this HP4 and answer RQ4, the Mine Survey mission will be posed having multiple TAs which are assigned to UUVs for MLO detection in a lawn-mower pattern. The methodology will be followed step-by-step, while at the same time performing the NPP process, within the ACF-UV framework environment to simulate realistic operational environment.

In the process of case study demonstration, the proposed methodology will be shown to provide communication solutions that are robust to environmental uncertainty and reliable to network failures that outperform baseline mission approaches. This proof-of-concept demonstration study provides a useful example to Commander and planning staff on how to use the methodology and make tradeoffs for better decisions.

# CHAPTER III

# COMMUNICATIONS PREDICTIONS

In this chapter, the characterization of mobile RF communication channels in maritime conditions are presented with methods and models for representing and predicting each phenomena. The proposed methodology is highly dependent on these communication predictions for the development and analysis of COAs. This is a crucial step in the COA Development process, shown here again in Fig. 26 that needs further investigation.

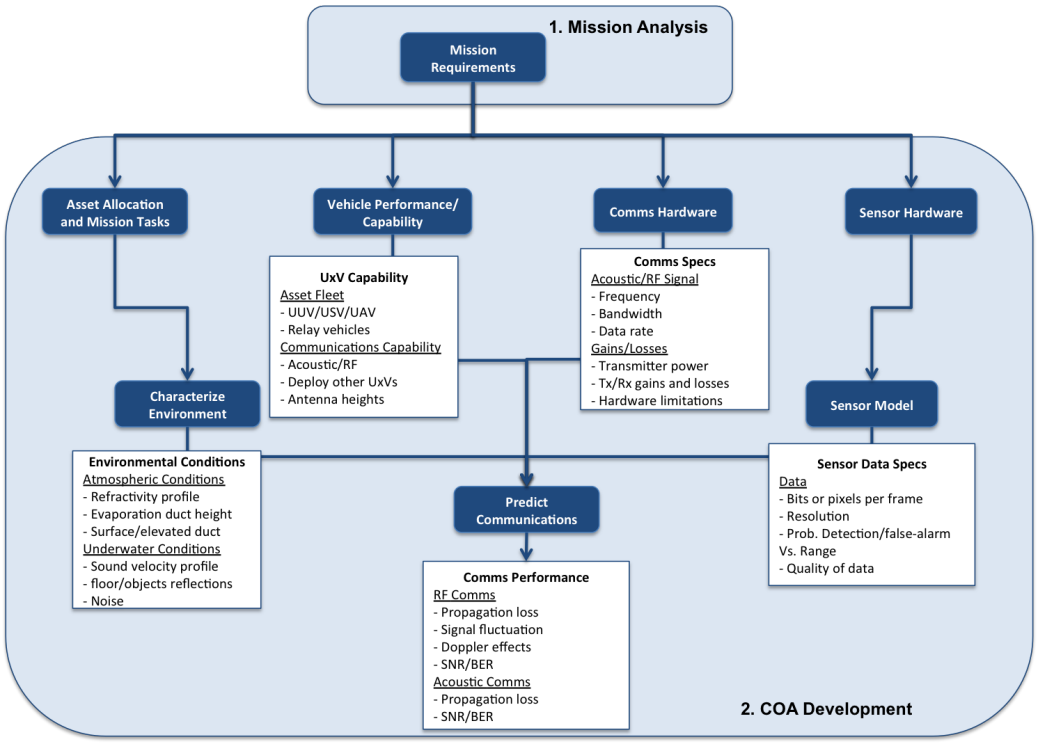


**Figure 26:** Predict comunications phase of the COA Development step

In this chapter we also focus on Experiment 2, which is divided into three parts,

Part A, Part B, and Part C, where each part provide case studies and detail investigation for answering RQ2 and testing corresponding hypothesis HP2.

## *3.1 Characterization of Fading Channels in Mobile Communications*

The transmission channel between a transmitter and a receiver can vary from simple line-of-sight to one that is obstructed by obstacles, refracted by pressure and temperature gradients, reflected by ground or water surface, and attenuated by signal interference [167]. The motion speed also impacts how rapidly the signal level fades as a mobile terminal moves in space. Therefore, radio channels are extremely random and do not offer easy analysis, and it is typically done in a statistical fashion, based on measurements made specifically for an intended communications system or spectrum allocation.

In a wireless mobile communication system, a signal can travel from transmitter to receiver over multiple reflective paths; this phenomenon is referred to as *multipath* propagation [187]. Multipath propagation can cause fluctuations in the received signal's amplitude, phase, and angle of arrival, giving rise to *multipath fading*. The modeling and design of systems that mitigate the effects of fading are usually more challenging than those whose sole source of performance degradation is additive white Gaussian noise (AWGN).

The different fading channel manifestations are shown in Fig. 27. They are generally broken down into large-scale and small-scale fading. Large-scale fading is represented by the average signal power attenuation or propagation loss due to motion over large areas, refractivity, and reflection. This phenomenon is affected by prominent terrain contours (hills, forests, clumps of buildings, other ships) sea surface between the transmitter and receiver, and atmospheric conditions. The statistics of large-scale fading provide a way of computing an estimate of propagation loss as a function of distance, which is described in terms of a mean-path loss ($n$th-power law)

and a log-normally distributed variation about the mean.

Small scale fading refers to the dramatic changes in signal amplitude and phase that can be experienced as a result of small changes (as small as half-wavelength) in the spatial separation between the transmitter and receiver [187]. As is shown in Fig. 27, small-scale fading manifests itself as the time-spreading of the signal (or signal dispersion) and the time-variant behavior of the channel. The channel is time-variant because motion between the transmitter and receiver results in propagation path changes. The rate of change of these propagation conditions accounts for the fading rapidity (rate of change of the fading impairments). A mobile radio roaming over a large area must process signals that experience both types of fading: small-scale fading superimposed over large-scale fading.

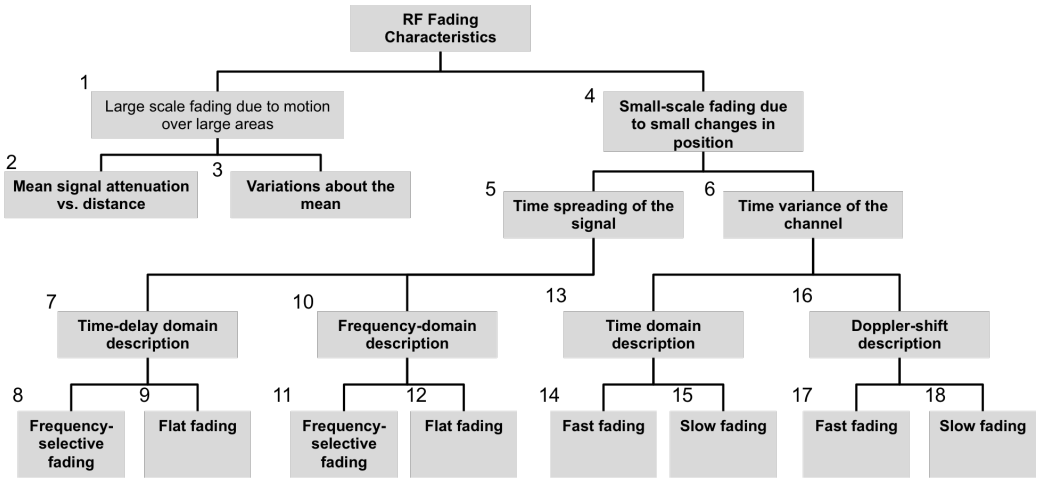


**Figure 27:** Fading channel manifestations [187]

There are three basic mechanisms that impact signal propagation in a mobile communication system. They are reflection, diffraction, and scattering [167]. Reflection occurs when a propagating electromagnetic (EM) wave impinges on a smooth surface with very large dimensions compared to the RF signal wavelength ($\lambda$). Diffraction occurs when the radio path between the transmitter and receiver is obstructed by a dense body with large dimensions compared to $\lambda$, causing secondary waves to form

behind the obstructing body. Diffraction is a phenomenon that accounts for RF energy traveling from transmitter to receiver without a line-of-sight path between the two. Finally, scattering occurs when a radio wave impinges on either a large rough surface or any surface whose dimensions are on the order of $\lambda$ or less, causing the reflected energy to spread out (scatter) in all directions.

In the subsections that follow, some of the details regarding the statistics and mechanisms of large-scale and small scale fading will be identified, along with the corresponding deterministic and probabilistic models to be used in this study.

### 3.1.1 Large-scale Fading: Mean Propagation Loss and Standard Deviation

Large-scale fading can be described by the mean propagation loss and standard deviation as a function of distance between the transmitter and receiver. Propagation loss can be defined as the amount of signal lost experienced by an EM wave, as a function of distance, during transmission between a transmitter and receiver. It can be decomposed into two terms, one due to free-space propagation $L_{fs}$ and the other due to the interference of multipath arriving at the receiver, $L_{mp}$, in units of dB, shown here:

$$L_{mean} = L_{fs} + L_{mp} \tag{2}$$

The free-space propagation assumes ideal free space, where the region between transmit and receive antennas are free of all objects that might absorb or reflec RF energy. It also assumes that the atmosphere behaves as a perfectly uniform and non-absorbing medium. Furthermore, the earth or water are treated as being infinitely far away from the propagating signal. When the antenna is assumed isotropic, the free-space propagation loss in dB is given as [188]:

$$L_{fs} = 10\log(\frac{4\pi r}{\lambda})^2 \tag{3}$$

where $r$ is the distance between transmitter and receiver, and $\lambda$ is the wavelength

of the propagating signal. The multipath portion of the propagation loss can be calculated using different methods, depending on the environment and conditions. It can be measured by experiment, as has been done by Okamura [152] for mobile land-based environments, it can be approximated using average distances between transmitter and receiver smaller than the assumed far-field of the free-space model [167] [187], or it can be directly calculated using deterministic approaches to solve Maxwell's equations for the propagation of EM waves under simple conditions for which solutions are available or approximations are good enough. Next, the mechanisms affecting RF wave propagation in maritime environments are described, and then the deterministic model used to calculate multipath propagation loss $L_{mp}$ is described in detailed.

#### *3.1.1.1 Maritime Atmospheric RF Communications*

Central to this proposed methodology is a predictive estimation of the quality of RF communications in maritime environments. The mechanisms that govern the propagation of radio wave signals in maritime environments are complex and depend on multiple atmospheric variables including temperature, moisture, and pressure. As the EM waves propagate through the atmosphere they undergo degradation and therefore attenuation due to the effects of gaseous and particulate absorption of energy, also described in the literature as molecular refraction. These effects alter the orientation of the EM wave fronts and causes convergence or divergence of EM energy.

Propagating RF signals experience phase interference from signals reflected off the sea surface, ships, land, etc., as well as from signals refracted down from the atmosphere. This leads to constructive or destructive interference at the receiving antenna. The phenomenon described is known as multipath propagation induced fading [181], which results in zones of communication loss between transmitters and receivers (skip-zones).

#### *3.1.1.2 Atmospheric Conditions*

Changes in temperature, moisture, and pressure in the atmosphere cause a change in atmospheric density, which in turn causes variations in the speed of EM waves in both the vertical and horizontal directions. These changes in speed lead to changes in the propagation direction, or bending, of the waves. RF signal propagation in the troposphere is affected by many parameters of which the index of refraction $n$ is the most influential [34]. A useful parameter known as the modified index of refraction $M$ (or modified refractivity) takes into account the curvature of the earth and the index of refraction $\beta$, and is given by [29]:

$$M(h) = (\beta - 1 + \frac{h}{R_E}) \times 10^6 \tag{4}$$

where $h$ is the altitude of the measurement point above the sea surface of the earth, and $R_E$ is the earth's radius. Different modified refractivity profiles can lead to normal, sub-refraction, super-refraction, or trapping layers. In maritime environments, ocean water evaporation results in the occurrence of atmospheric trapping layers. The modified refractivity profile of these trapping layers varies sharply, as is shown in Fig. 28 for surface-based trapping layers, elevated trapping layers, and evaporation ducts.

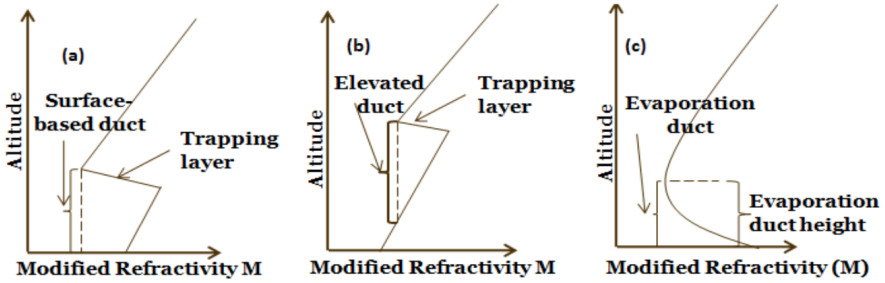


**Figure 28:** Representation of modified refractivity profiles for (a)surface-based ducts, (b) elevated ducts, and (c) evaporation ducts.

These evaporation ducts result in a wave-like conduction of EM waves, which not only has the potential to increase the range of transmitted RF signals by trapping the

signals and propagate EM waves over long distances, even surpassing the normal horizon range, but also generates signal skip-zones or blind spots where a signal cannot be received [101], as seen in Fig. 29 [191]. This can lead to situations where further ranges between transmitter and receiver are beneficial to maintain RF communications [42]. The evaporation duct height $h_{ed}$ changes on a scale of tens or minutes to hours in coastal regions and on a scale of hours in the open ocean.

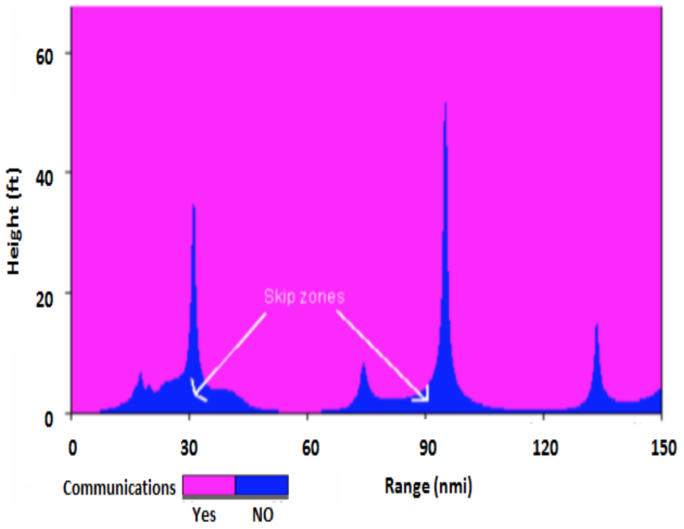


**Figure 29:** Resulting skip zones in RF communications under surface ducting conditions [191].

Only a limited frequency range within the radio wave spectrum is affected by these non-standard atmospheric conditions. In this study, we concentrate on those frequencies that are affected by refractive conditions in the troposphere in maritime conditions, which is the frequency range between 100 MHz and 20 GHz [30]. Below 100 MHz the dominant propagation mechanisms are the surface wave and sky wave dye to the ionosphere. Above 20 GHz scattering and gaseous absorption are dominant.

#### *3.1.1.3 Multipath Advanced Propagation Model (APM)*

These multipath effects on the propagating RF signal are modeled using the Advance Propagation Model (APM), a hybrid model built by integrating the Radio Physical Optics (RPO) model, and the Terrain Parabolic Equation Model (TPEM) [30]. RPO

is an over-water model capable of computing propagation loss coverage at all heights and ranges. TPEM is an integrated over-water and land model capable of computing propagation loss coverage at only low angles and heights. APM is then an EM propagation model that can compute propagation effects from the following environmental inputs and mechanisms: (1) range-dependent refractivity environments, (2) variable terrain elevation environments, (3) range varying dielectric ground constants for finite conductivity and vertical polarization calculations, and (4) troposcatter.

Communication links under maritime conditions can, in basic cases, be modeled as a two-way propagation channel with a direct line-of-sight path and a reflected path, effectively constituting a multipath model. In this case, APM can be used to perform calculations to compute the field resulting from coherent interference of both the direct and sea-reflected rays. The computation is based on the path length difference between the two rays, and accounts for the appropriate magnitude and phase of the reflection coefficient for the reflected ray.

The propagation factor $F$ is the fundamental quantity in the radio propagation model, and is defined as the ratio between the field strength $E_p$ at a point $p$, including antenna pattern effects but normalized to unity gain antennas, and the field strength $E_0$ which occurs at a point under free-space conditions, if loss-free isotropic antennas were used for both the transmitter and receiver [30], $F = |\frac{E_p}{E_0}|$. Propagation loss due to multipath in decibels (dB), calculated by APM model, as a function of the propagation factor $F$ is given by

$$L_{mp} = -20\log(F) \tag{5}$$

Note that $F$ contains all environmental effects on the emitted EM wave, which includes effects from the atmosphere and a variable reflecting surface, such as rough ocean or land [30]. The way APM solves for the propagation factor is by solving Maxwell's wave equations in the form of a parabolic equation (PE). The PE equation is derived from Maxwell's curl equations for the electric and magnetic fields, with the

assumption of azimuth independence on all variables [129]. The simplified equations are then transformed into the form of 2-dimensional Helmholtz equations. They are then transformed into a rectangular coordinate system in which x corresponds to the surface range on the earth with the origin directly below the source antenna, and z is the altitude [129]. Finally, by neglecting back scattering fields, and limiting accurate representation of the field to "nearly horizontal" propagation directions [202], the PE can be derived, which is given by

$$\frac{\partial^2 u(x,z)}{\partial z^2} + 2ik_0 \frac{\partial u(x,z)}{\partial x} + k_0^2(n^2 - 1 + \frac{2z}{R_E})u(x,z) = 0 \tag{6}$$

where $x$ and $z$ represent the cartesian range and height coordinates, respectively, $u$ is the scalar component of the electric field, $k_0$ is the free-space wave number ($\frac{2\pi}{\lambda}$), and $n$ is the index of refraction. The term $\frac{2z}{R_E}$ accounts for the spherical shape of the Earth; when it is neglected, (6) describes propagation over a flat Earth.

The PE equation (6), in conjunction with the proper boundary conditions, is an initial value problem that can be solved using numerical schemes that march out in $x$. The Fourier split-step algorithm has proven to be the most stable and efficient method for advancing the solution [77]. The solution, using the wide-angle propagator, is given by [30]

$$u(x + \Delta x, z) = e^{ik_0 \Delta x 10^{-6} M(z)} \mathcal{F}^{-1}[e^{i\Delta x \sqrt{k_0^2 - p^2} - k_0} \mathcal{F}[u(x,z)]] \tag{7}$$

where $\Delta x$ is the incremental range step over which the field solution is propagated, $M(z)$ is the height-varying modified refractivity profile, and $\mathcal{F}$ and $\mathcal{F}^{-1}$ represent the forward and inverse Fourier transforms, respectively. The transform variable $p$ is given by $p = k_0 sin(\theta_p)$, where $\theta_p$ is the propagation angle referenced from the horizontal. The quantity $u$ retains an explicit range dependence in the process of normalizing and converting from spherical to cartesian coordinates, where the propagation factor $F$ can be calculated as

$$F = |u(x,z)|\sqrt{x} \tag{8}$$

or in dB units:

$$20logF = 10log[(u_r^2 + u_i^2)x] \tag{9}$$

where $u_r$ and $u_i$ are the real and imaginary components of $u(x, z)$, respectively. The propagation factor $F$ given in (9) is then used in (5) to calculate $L_{mp}$, and finally this is then used in (2) to calculate the mean propagation loss $L_{mean}$.

APM is also capable of computing threshold propagation loss which is the maximum attenuation a signal can absorb without dropping the communications link. As an example, Fig. 30 shows the propagation loss of a signal with a given threshold value, computed as a function of range between transmitter and receiver.

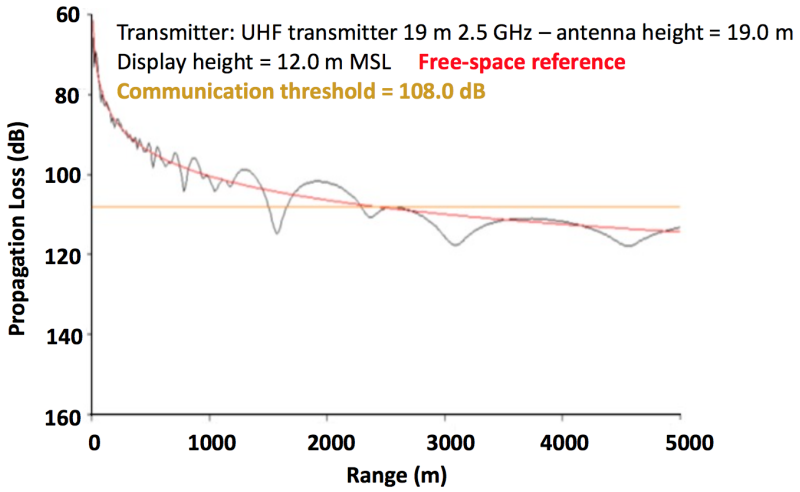


**Figure 30:** RF communications threshold propagation loss vs. range at a fixed radio transmitter and receiver height.

Note that APM does not include any meteorological models. APM models the effects from the medium but does not model the propagating medium itself. For upper air information the refractivity profile is obtained by direct measurement via radiosondes or rocketsondes. There are several bulk models that are commonly used to compute evaporation duct profiles from bulk meteorological measurements [170]. All environmental information needed to adequately compute propagation loss over sear or land are treated as inputs to the model. Terrain information is readily available

through various databases such as the Digital Terrain Elevation Database (DTED) and the United States Geological Survey (USGS).

The mean propagation loss profile as a function of range and altitude computed in (2) is an average, and therefore not adequate to describe a particular setting or signal path. The variations about the mean due to different environments from different locations may be quiet different for similar transmitter-receiver separations. Measurements have shown that for any given distance between transmitter and receiver, the propagation loss $L_{PL}$ is a random variable having a log-normal distribution about the mean distant-dependent value $L_{mean}$ [65]. Therefore, the propagation loss $L_{PL}$ can be expressed in terms of the mean propagation loss $L_{mean}$ plus a random variable $X_\sigma$ as [167]

$$L_{PL} = L_{fs} + L_{mp} + X_\sigma = 10log(\frac{4\pi r}{\lambda})^2 - 20log(F) + X_\sigma \tag{10}$$

where $X_\sigma$ denotes a zero-mean Gaussian random variable (in dB) with standard deviation $\sigma$ (in dB), and it is site and distance dependent. The value for $X_\sigma$ is often based on measurements for a given location and scenario. There are several good references dealing with the measurement and estimation of propagation path loss under different configurations and for many applications [167] [104] [183] [65] [179] [22].

### 3.1.2 Experiment 2, Part A: Multipath Fading Studies with APM

Once the environment has been characterized, communications are predicted in the next phase of the COA Development step based on propagation loss deterministic calculations and multi-path fading probabilistic models. The predicted propagation loss as a function of transmitter and receiver distance is compared to a minimum required value and good or bad communication ranges can be generated between each vehicle.

The first experiment to be considered is Exp2, which focuses on investigating

ways to predict communications in maritime environments. In this first part of the experiment, Part A, we focus on the large scale fading mechanisms and the multipath fading created by the environmental conditions. We will assume evaporation ducts of different heights and study their effect on narrowband and wideband signals in terms of propagation loss calculated by APM model.

#### *3.1.2.1 Channel Modeling and Simulation*

In this section we present an analytical channel model for the optimization of wideband communication systems with specific application to autonomous unmanned vehicles (UV) operating in maritime environments. In particular, we focus on the impact of maritime atmospheric conditions and phenomenon on the transmission of radio frequency signals. The Advanced Propagation Model (APM), developed at the Space and Naval Warfare Systems Center San Diego, is used to characterize the transmission channel in terms of evaporation duct induced signal propagation loss. APM uses a hybrid ray-optic and parabolic equations model which allows for the computation of electromagnetic (EM) wave propagation over various sea and/or terrain paths. The signals are then normalized to an APM computed communications threshold communications value, indicating the ability for a UV to communicate or not communicate. We then model the small scale fading using a Nakagami-m probability model to take into account the time spreading mechanisms of the fading signal.

The U.S. Navy concept-of-operations (CONOPS) for USVs includes having multiple USVs as sensor platforms controlled from a manned platform (e.g., a Littoral Combat Ship (LCS)) and providing payload sensor data back. The control platform(s) and USVs will ultimately share one or more communications resources for the ship-to-USV communications. The communications resources will include line-of-sight (LOS) systems and (potentially) satellite links for beyond-line-of-sight (BLOS).

The performance of the communications system is impacted by many factors,

as has been explained in the literature review. A key factor is the effect of the state of the transmission channel (or channels) between nodes. The channel is a function of both the mean propagation loss and statistics of the variation about the mean, also known as fading. The propagation loss and fading characteristics are a function of frequency, the atmospheric refractivity structure, that structure?s time dependence, the earth?s surface characteristics, as well as node positions and their time dependence. The mechanisms that govern the propagation of radio wave signals in maritime environments are complex and a factor of multiple atmospheric variables including temperature, moisture, and pressure. As the EM waves propagate through the atmosphere they undergo refraction and?particularly at C-band and higher, rain attenuation and gaseous absorption. These effects alter the orientation of the EM wave fronts and causes convergence or divergence of RF energy.

In this work we take these factors and mechanisms in consideration for assessing communication links between the unmanned platforms, focusing primarily on the S and C band center frequency range of a  16 MHz bandwidth (BW) wideband radio system.

#### *3.1.2.2 Communications Modeling Framework*

Results are generated using a framework we developed called ACF-UV (Adaptive Communications Framework for Unmanned Vehicles). ACF-UV is also used in the analysis of intermittent communications, which includes models to predict the state of transmission channels in maritime environments, as well as a simulation environment that is used as an operations view of the signal links between heterogeneous teams of unmanned vehicles (UxVs). The central propagation loss module implemented by ACF-UV is the APM model. ACF-UV utilizes APM to calculate maritime signal propagation loss using atmospheric and environmental conditions (temperature,

humidity, pressure, etc) and phenomena (evaporation ducts) to predict signal transmission channel quality. APM uses a hybrid ray-optic and parabolic equations model to compute electromagnetic (EM) propagation over various sea and/or terrain paths, and is the only EM propagation (applicable between 2 MHz to 57 GHz) model accredited for use in Navy systems by the Chief of Naval Operations. A commercial off the shelf (COTS) lightweight 48 MB/s multi-band network radio configured for maritime communications was used as the radio model in this study. The methodology for the experimental work presented is as follows:

- Compute propagation loss vs. range based on radio, environmental, and platform inputs using the APM model.
- Range and altitude partition is determined by model physics.
- For each range partition, propagation loss is classified as a function of above or below a threshold value.
- Signal time spreading due to small scale fading is modeled using Nakagami-m statistics.
- Assume azimuth-independence propagation and permanent refractivity structure.

#### *3.1.2.3 APM Propagation Loss*

Propagation loss can be defined as the amount of signal lost experienced by an EM wave, as a function of distance, during transmission between transmitter and receiver antenna nodes. The propagation factor $F$ is the fundamental quantity in the radio wave propagation model, and is defined as the ratio of the electric field $E$ at a point, to the ratio of the electric field strength $E_0$ which occurs at a point under free space conditions [30]; $F = E/E_0$. Propagation loss in decibels reference to mW power

(dBm) as a function of propagation factor $F$ computed by APM is given by:

$$L_{APM} = 20Log(\frac{4\pi r}{\lambda}) - 20Log(F) \tag{11}$$

Where $20log(4\pi r/\lambda)$ is the Free-space-loss parameter, $r$ is the range, and $\lambda$ is the RF signal's wavelength. APM is capable of computing threshold propagation loss which is the maximum attenuation a signal can absorb without dropping the communications link.

#### *3.1.2.4 Effects of Evaporation Ducts on Propagation Loss*

In this section the effects of evaporation ducts on signal frequency diversity is simulated and analyzed. The impact of evaporation ducts on wideband and narrowband frequency selection is analyzed as a function of the communications link platforms. We present another approach for specifically analyzing the communication link states of the vehicles, based on the propagation loss calculated by APM. These results represent a first order proof of concept study.

Two evaporation duct heights were considered: (1) 14 m (worldwide mean) evaporation duct (EVD)height, and (2) 24 m EVD height. A 25 m transmitter antenna height and a 3 m receiver antenna height were considered, which are consistent with Ship-to-USV links for a superset of of the range of center frequencies for which the COTS radio can be tuned to. The resulting propagation losses vs. range and wideband frequency range for the 14 m and 24 m EVDs for the Ship-to-USV link are shown in Fig. 31 and 32 , respectively. From Fig. 31 and Fig. 32 it can be seen that the lower the evaproration duct height, the higher the signal attenuation, over the same frequency range and distance from receiver. It can also be inferred that the antenna height relative to the duct elevation also affect transmission performance. Plotted in Fig. 33 and Fig. 34 are the resulting propagation losses vs. range and wideband frequency range for the 12 m and 24 m EVDs for the USV-to-USV link, respectively. These results indicate that better signal transmission occur for USV-

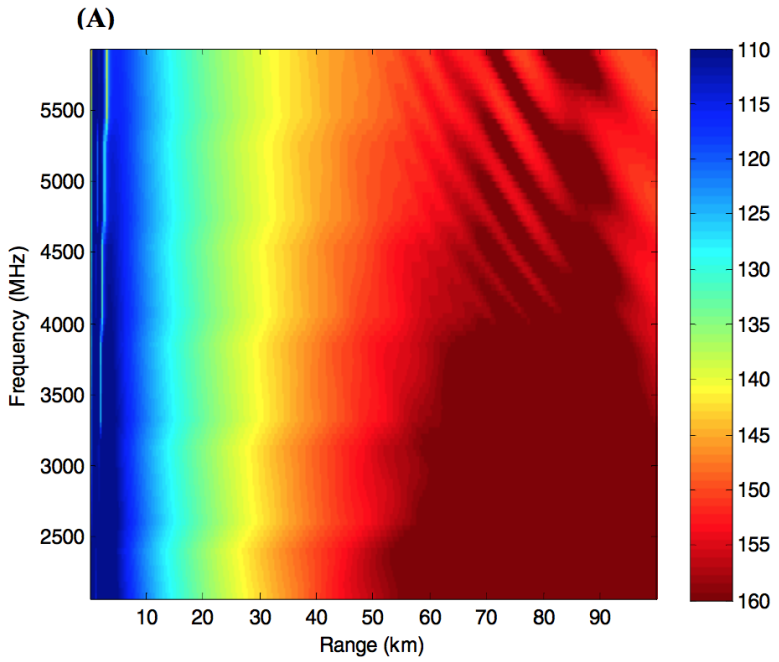


**Figure 31:** Propagation Loss vs. Range and Frequency in a 14m EVD for wideband signal of Ship-to-USV link.

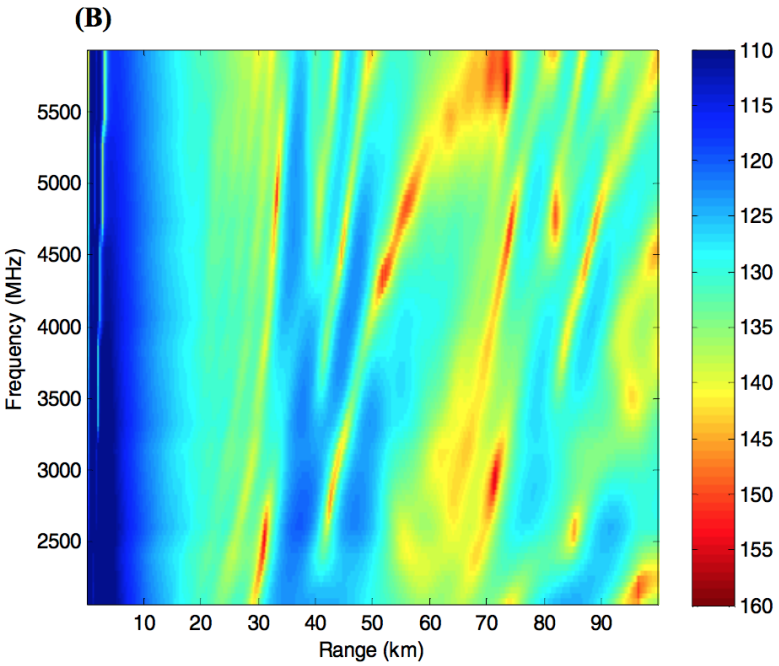


**Figure 32:** Propagation Loss vs. Range and Frequency in a 24m EVD for wideband signal of Ship-to-USV link.

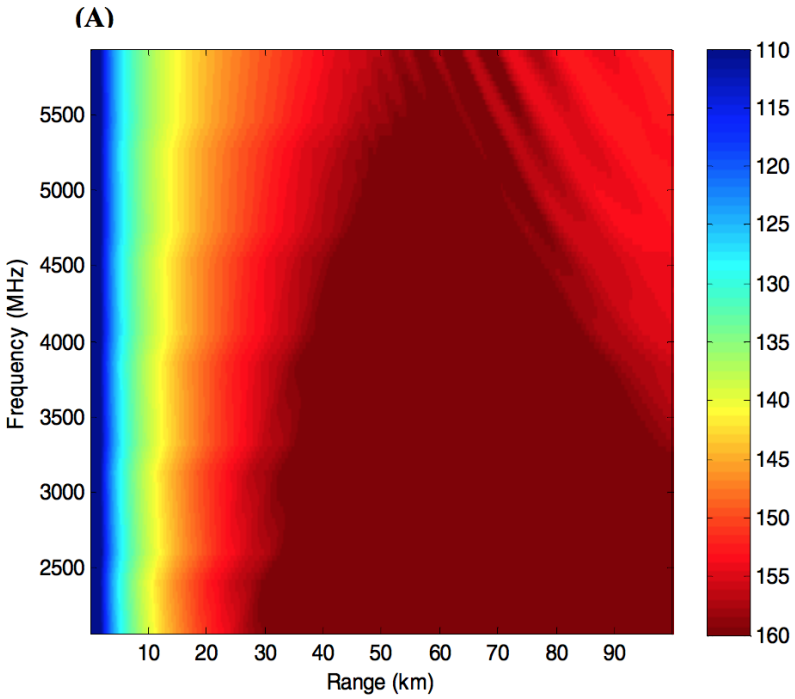


**Figure 33:** Propagation Loss vs. Range and Frequency in a 14m EVD for wideband signal of USV-to-USV link.

to-USV communications (Figs. 33 and 34), most likely due to the height of their transmitting antenna relative to the evaporation duct elevation. The 14m and 24m duct elevations allow the transmitting signals of the USVs 3m antennas to be better trapped within the confines of the waveguide-like ducts.

Extending these analyses further, the impact of frequency diversity on propagation loss can also be investigated. From the plot of Figs. 31 32, 33 and 34, it can be seen that over wide frequencies propagation loss differs greatly, even at the same range. On the other hand, when looking at a narrowband of 16 MHz, as simulated in Figs. 35 and 36 for the Ship-to-USV link, and Figs. 37 and 38 for the USV-to-USV link, it can be observed that the 16 MHz bandwidth of the cots radio will offer a substantial advantage over wideband transmissions.

To summarize, in this small study we analyzed the effects of evaporation duct

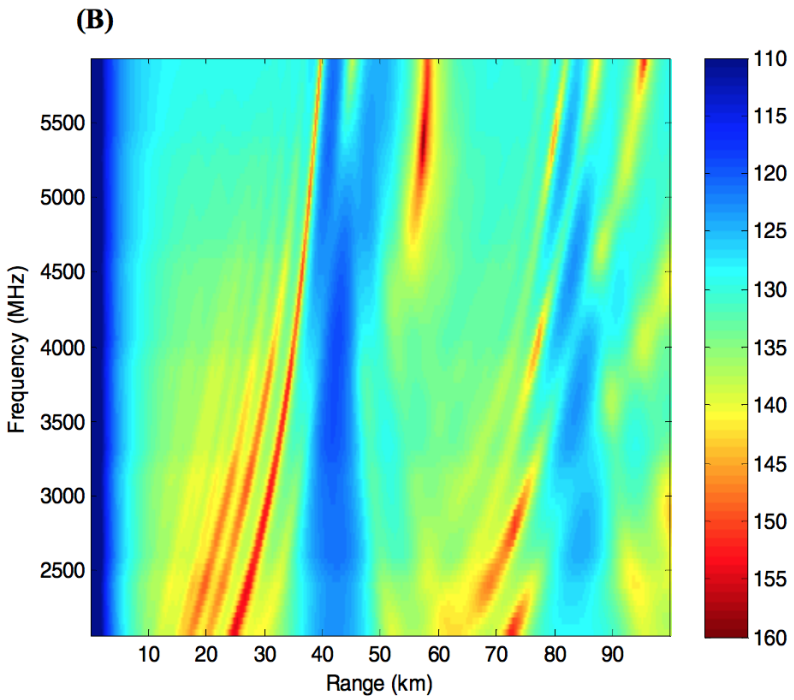


**Figure 34:** Propagation Loss vs. Range and Frequency in a 24m EVD for wideband signal of USV-to-USV link.

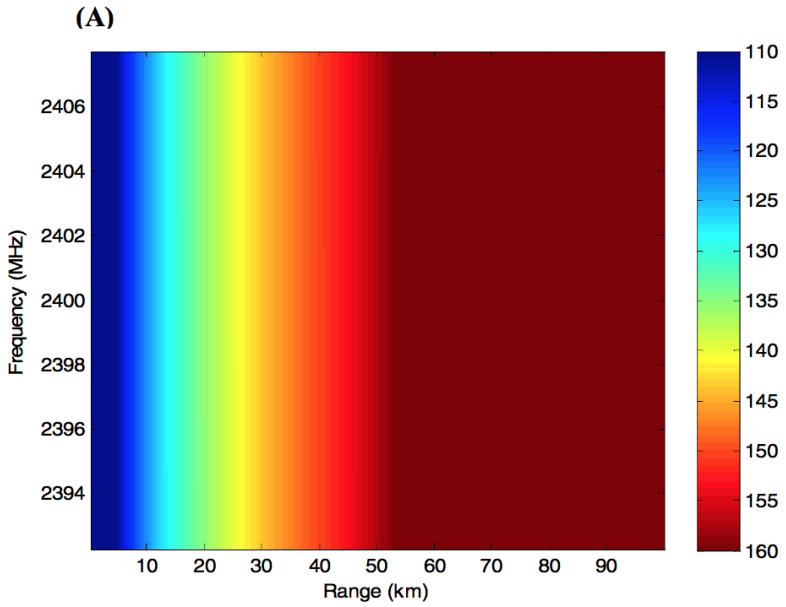


**Figure 35:** Propagation Loss vs. Range and Frequency in a 14m EVD for narrowband signal of Ship-to-USV link.

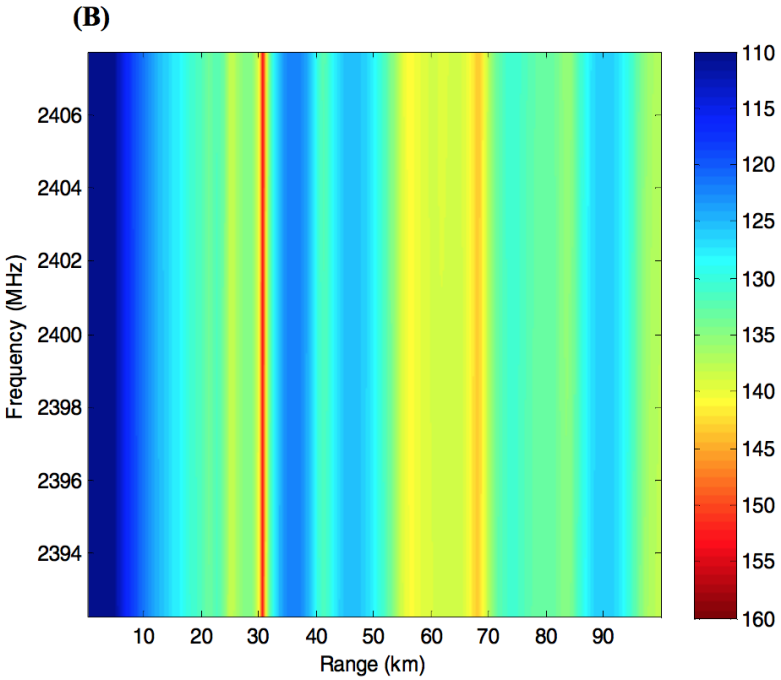


**Figure 36:** Propagation Loss vs. Range and Frequency in a 24m EVD for narrowband signal of Ship-to-USV link.

heights on the signal attenuation calculated by APM for Ship-to-USV and USV-to-USV links, in both wideband and narrowband channels. It was shown that the lower the evaporation duct, the higher is the attenuation for both Ship-to-USV and USV-to-USV links. This can be explained by the relative height between the transmitter and receiver relative to the duct height. In the Ship-to-USV link for the 14 m EVD, the ship transmitter antenna is above the duct height, and so the ducts acts as a refractive layer that bends the signal and does not allow it to reach the receiver below the duct. In the 24 m EVD, the ship antenna is still above the duct height, but much closer to the duct, and the refractive bending of the signal is less pronounced. For the USV-to-USV situation, both transmiter and receiver antennas are below the duct in both the 14 m and 24 m EVDs, but in the 14 m EVD, the attenuation is higher due to signals being more trapped and having multipath signals interfering with each other more often than in the higher EVD at 24 m. Another observation

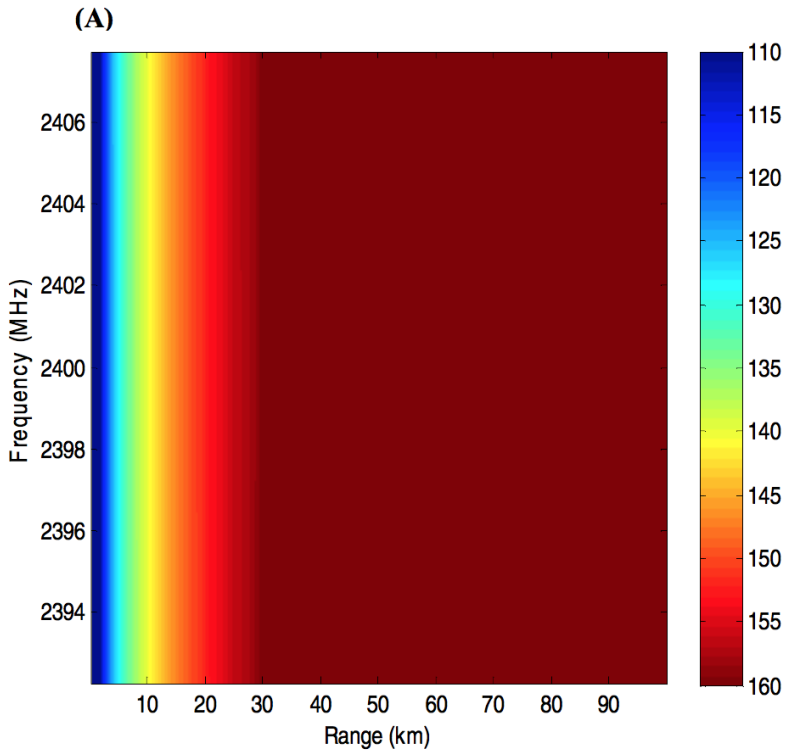


**Figure 37:** Propagation Loss vs. Range and Frequency in a 14m EVD for narrowband signal of USV-to-USV link.

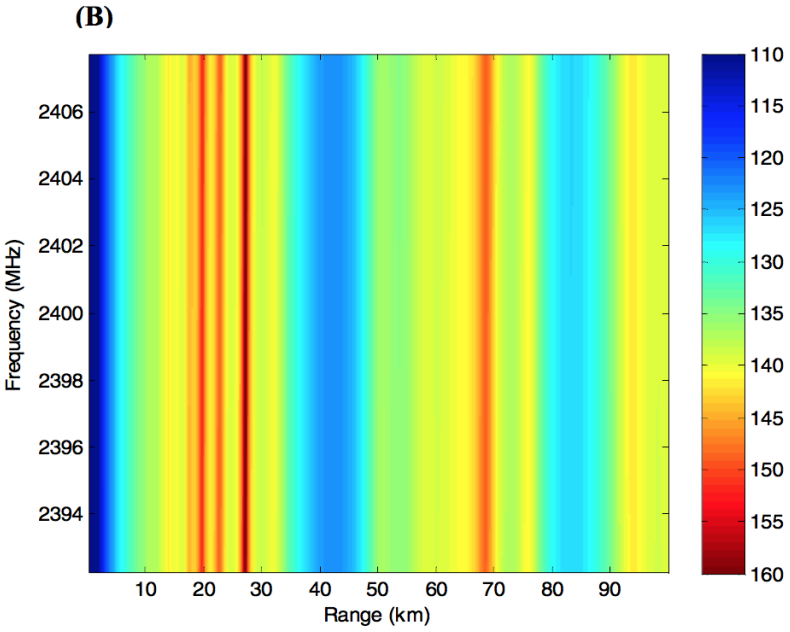


**Figure 38:** Propagation Loss vs. Range and Frequency in a 24m EVD for narrowband signal of USV-to-USV link.

was that a narrowband is more beneficial than a wideband because the propagation loss varies much more over the wider band, which makes it more difficult to determine if a threshold of communications can be reached. In other words, the narrowband offers more control over the range of frequencies for which the signal attenuation can be compared to a threshold value to determine if good or bad communications exist in a transmission channel.

#### *3.1.2.5 Propagation Loss for Narrowband Signal*

From the previous results, it was determined that a narrowband signal will be used throughout this demonstration case study. Shown in Fig. 39 and 40 are the propagation loss vs. range and height in a 14 m and 24 m EVDs, respectively, for the Ship-to-USV link in a narrowband signal. These plots help determine heights and

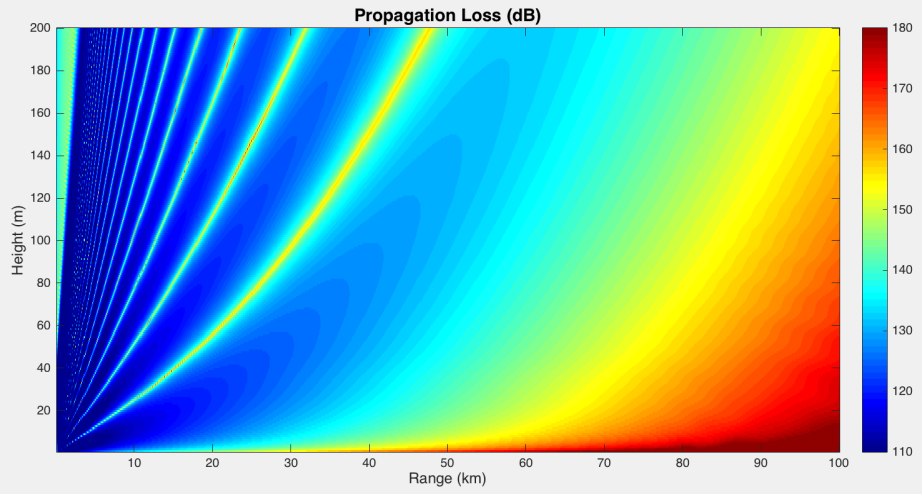


**Figure 39:** Propagation Loss vs. Range and Height in a 14m EVD for narrowband signal of Ship-to-USV link.

ranges where propagation losses are expected to be highest. They show the effects of the M-gradients on the bending of the signals, as it is transmitted from the origin at a given propagation angle. It can be seen that, depending on the angle at which it is transmitted with respect to the refractivity gradient, each ray will bend in different directions as it propagates in space. There are areas where the signal does not reach,

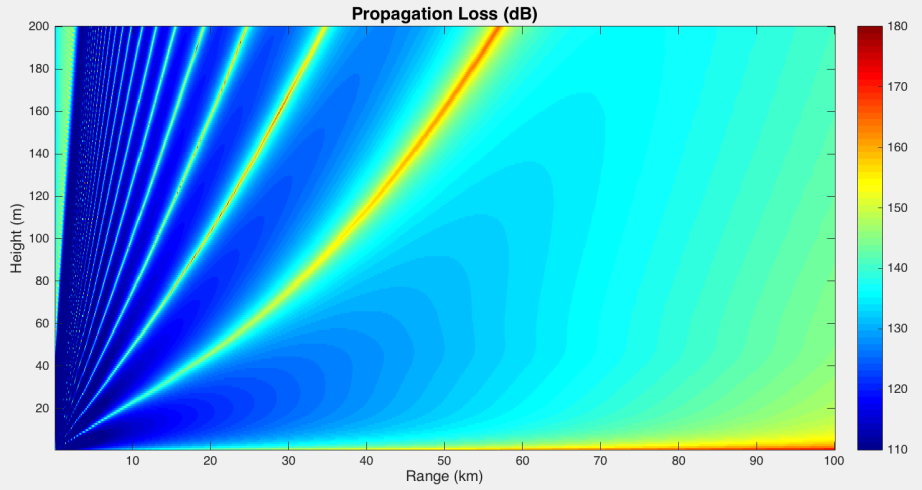


**Figure 40:** Propagation Loss vs. Range and Height in a 24m EVD for narrowband signal of Ship-to-USV link.

or it is attenuated by the multipath effects of the signal as it is interfered by other signals.

Comparing the 14 m EVD to the 24 m EVD, it can be seen clearly that both refractivity structures are about the same near the transmitter, but as the range and height increases, the 14 m EVD tends to have areas of higher propagation loss. In the 14 m EVD, the signals bend more upwards because the transmitter antenna is outside above the duct, and the duct acts as a refractive layer to the incoming signals. On the other hands, in the 24 m EVD, the transmitter antenna is closer to the EVD heigh (at 25 m), and the signal refracts less, and therefore the signals are bend much less.

The propagation loss vs. range and height in a 14 m and 24 m EVDs are shown in Figs. 41 and 42, respectively, for the USV-to-USV link in a narrowband signal. In this case, the transmitter and receiver antennas are inside each of the EVDs. However, in the 14 m EVD, the attenuation is higher due to signals being trapped in a layer that is smaller than in a 24 m EVD, which causes signals to refract more often and bend at higher angles, as is clearly shown in the plots. This also causes signals to interfere destructively more often which overall creates greater attenuation.

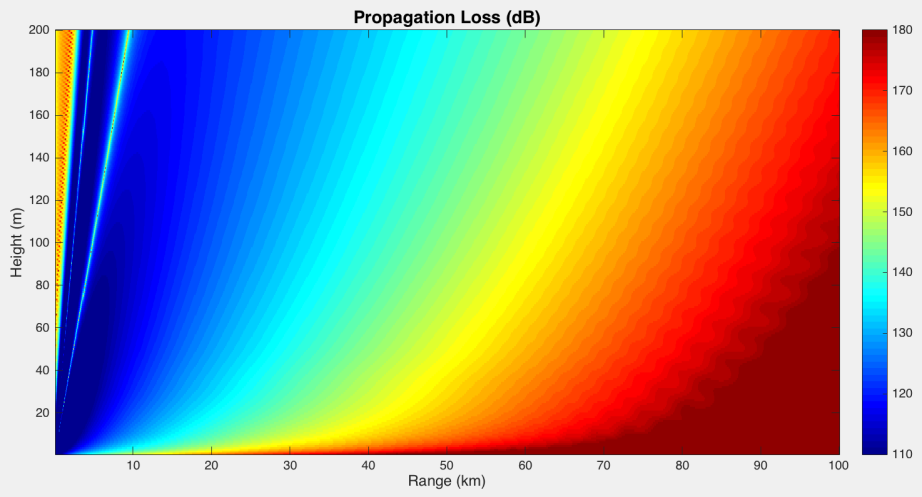


**Figure 41:** Propagation Loss vs. Range and Height in a 14m EVD for narrowband signal of USV-to-USV link.

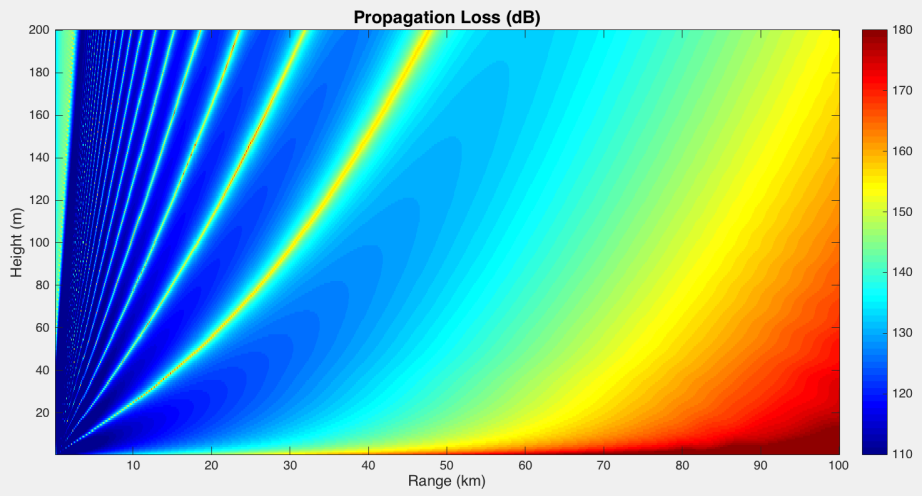


**Figure 42:** Propagation Loss vs. Range and Height in a 24m EVD for narrowband signal of USV-to-USV link.

Based on these results, propagation loss profiles created by APM can be very useful in determining placements of the transmitter and receiver antennas with respect to the duct heights and with respect to distance between each other that minimizes the attenuation. This is studied next by assuming a threshold of communications based on an assumed receiver sensitivity.

#### *3.1.2.6 Communications Awareness Approach*

A different approach towards determining communications awareness from the results of the APM models is through the use of threshold crossings. There are different ways of specifying a threshold of communications. It can be specified in many ways, including as the threshold of a minimum BER allowed, or an acceptable receiver SNR value, or minimum propagation loss, or minimum receiver power. For simplicity, lets assume that it is specified as the minimum propagation loss that a received signal can have. The specifications of the COTS radio under consideration indicate that data rates of 6 MB/s to 48 MB/s should occur over a range of $\approx$ 25 dB. Therefore, lets consider threshold crossings for propagation loss values from 120 dB to 140 dB. In Figs. 43 and 44 we show the threshold crossings for the Ship-to-USV link. Generally, the lower propagation loss values correspond to higher data rates. Ranges where the propagation loss goes from above threshold (+1) to below threshold (0), would correspond to a drop in data rate, or loss of communications. Due to the depth of the nulls (skip zones), it is evident that when either opening or closing range between the the Ship and the USV, the data links can transition through several thresholds.

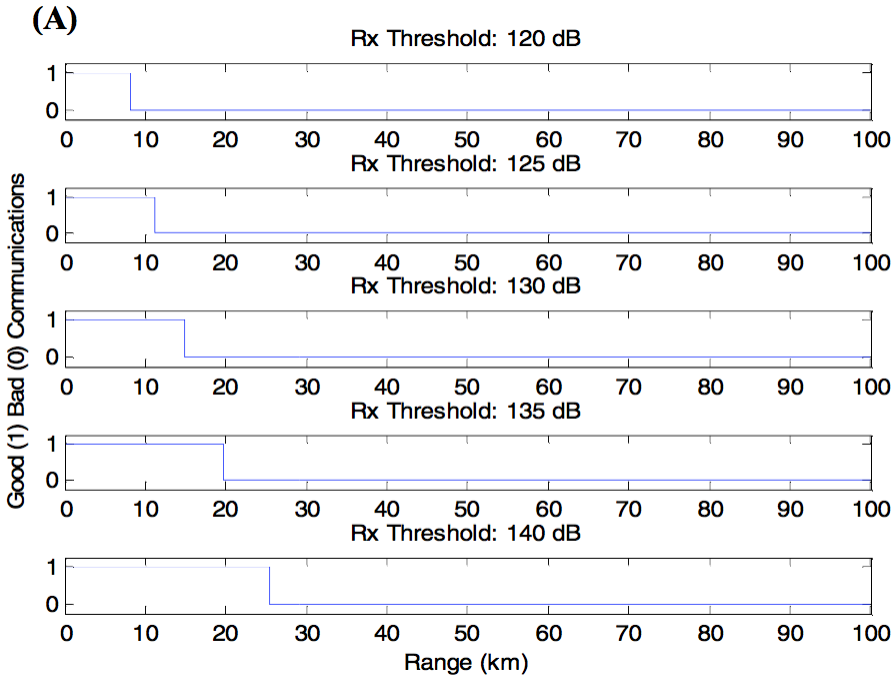


**Figure 43:** Threshold of communications vs. range in a 14m EVD for Ship-to-USV link.

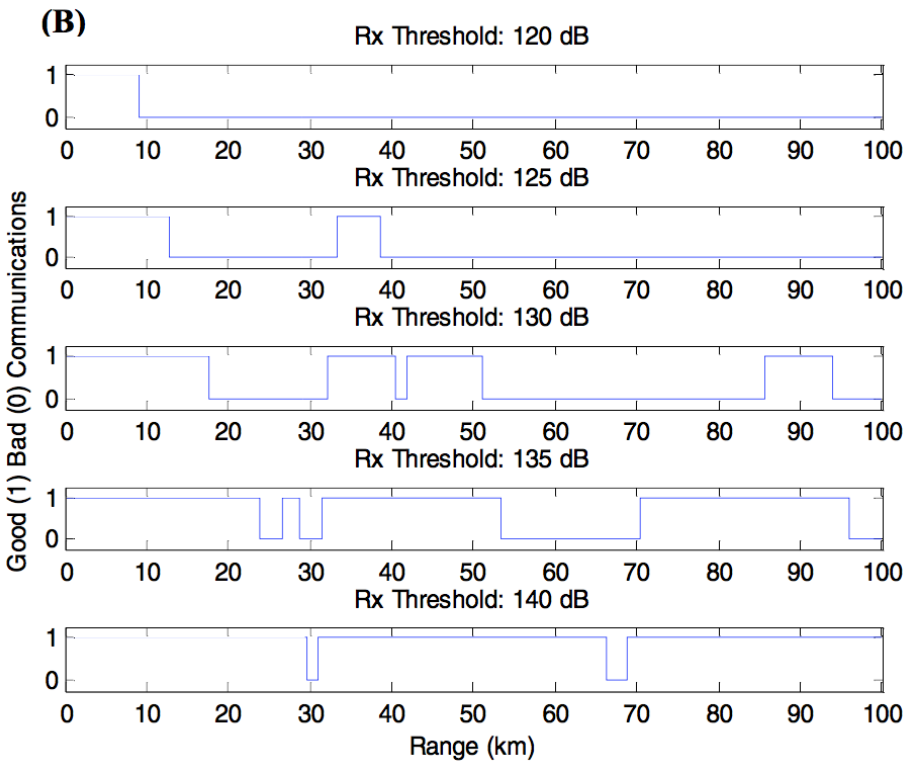


**Figure 44:** Threshold of communications vs. range in a 24m EVD for Ship-to-USV link.

The threshold crossings for hte USV-to-USV link in a 14 m and 24 m EVDs are shown in Figs. 45 and 46, respectively.

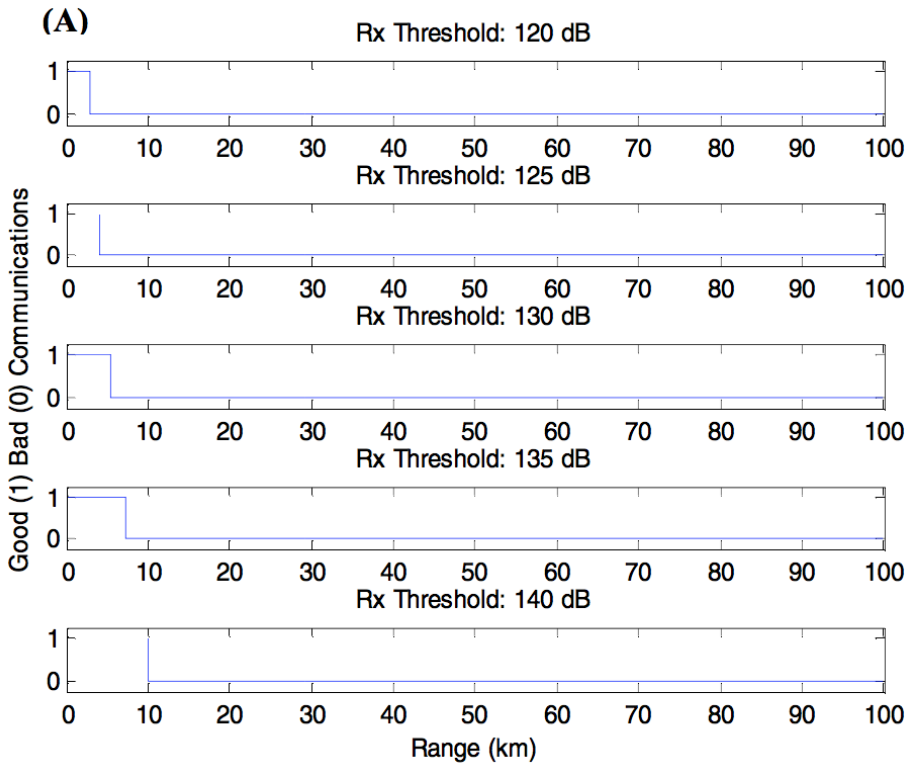


**Figure 45:** Threshold of communications vs. range in a 14m EVD for USV-to-USV link.

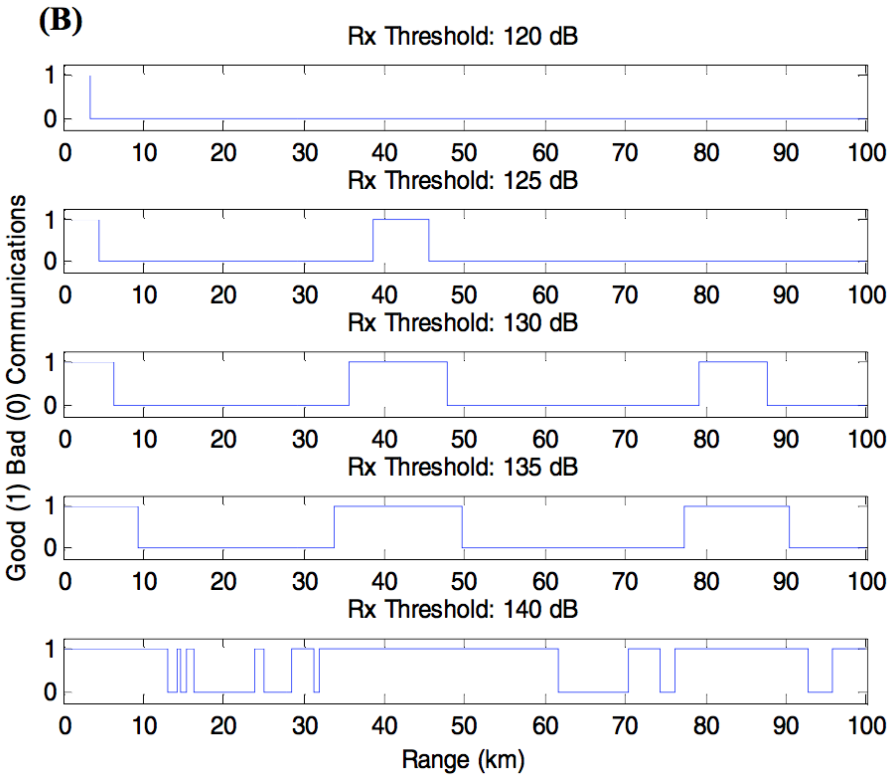


**Figure 46:** Threshold of communications vs. range in a 24m EVD for USV-to-USV link.

Comparisons of simulation results presented in Figs. 44 and 46 show that null crossings occur more frequently for the USV- to-USV link than they do for the Ship-to-USV links. This is due to antenna heights of the USVs being so close to the water that they become more susceptible to the attenuation inducing effects of evaporations ducts, sea roughness, ocean spray, sea reflection, etc. This threshold crossing analysis for communications awareness can be used to determine ranges of good and bad communications between different assets, which is used during asset allocation and network configuration to guaranteed assets are always within good communication ranges.

As a final note on large scale fading, the expected propagation loss profile as a function of range and altitude computed by the APM model is an average, and

therefore not adequate to describe a particular setting or signal path. The variations about the mean due to different environments from different locations may be quiet different for similar transmitter-receiver separations. Measurements have shown that for any given distance between transmitter and receiver, the propagation loss $L_{PL}$ is a random variable having a log-normal distribution about the mean distant-dependent value $L_{mean}$ [65]. Therefore, the propagation loss $L_{PL}$ can be expressed in terms of the mean propagation loss $L_{mean}$ plus a random variable $X_\sigma$ as [167]

$$L_{PL} = L_{fs} + L_{mp} + X_\sigma = 10log(\frac{4\pi r}{\lambda})^2 - 20log(F) + X_\sigma \tag{12}$$

where $X_\sigma$ denotes a zero-mean Gaussian random variable (in dB) with standard deviation $\sigma$ (in dB), and it is site and distance dependent. The value for $X_\sigma$ is often based on measurements for a given location and scenario. There are several good references dealing with the measurement and estimation of propagation path loss under different configurations and for many applications [167] [104] [183] [65] [179] [22].

### 3.1.3 Small-scale Fading: Statistics and Fading Channel Model

As is shown in Fig. 27, small-scale fading manifests in two forms: time-spreading (signal dispersion) of the underlying digital pulses within the signal, and the time-variant nature of the channel due to motion (e.g., a receiver antenna on a moving vehicle). Each manifestation can take place in time and frequency domains, as is shown in Fig. 27 in blocks 7, 10, 13, and 16. For signal dispersion, the fading degradation is categorized as frequency-selective fading and frequency-nonselective (flat) fading, as shown in blocks 8, 9, 11, and 12. For the time-variant form, the fading degradation is categorized as fast- or slow-fading, as is also listed in blocks 14, 15, 17, and 18. These two small-scale fading mechanisms, the domains used view them (time or time-delay and frequency or Doppler shift), and the degradation categories that each exhibit are shown in Fig. 47. Any mechanism can be characterized in the time domain or

the frequency domain. As is shown in Fig. 47, the time spreading mechanism will be can be characterized in the time-delay domain as a multipath delay spread, and in the frequency domain as a channel coherence bandwidth. In the same manner, the time-variant mechanism can be characterized in the time domain as a channel coherence time, and in the frequency (Doppler shift) domain as a channel fading rate or Doppler spread [187]. These mechanisms and categories will be explained in more detail in the following sections.

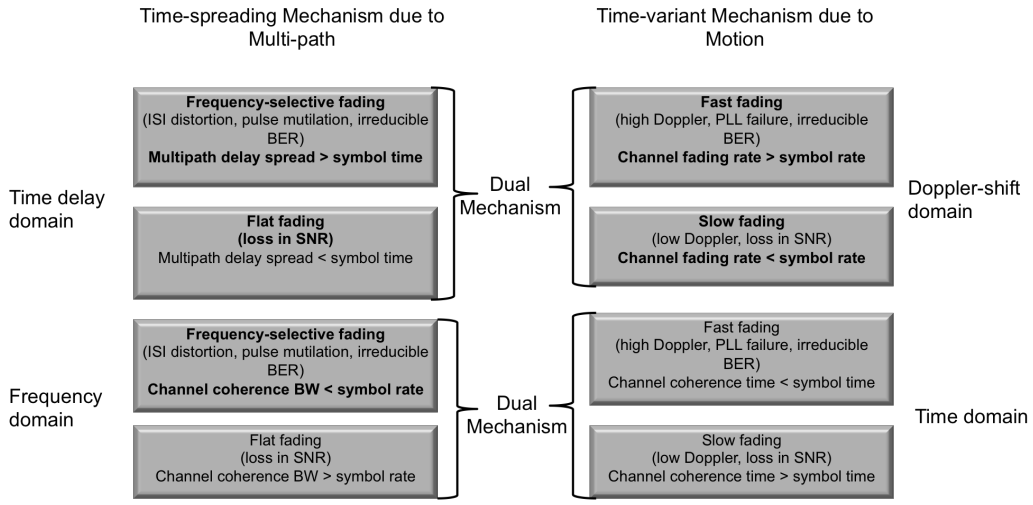


**Figure 47:** Small-scale fading mechanisms in the different domains, degradation categories, and effects [187].

#### *3.1.3.1 Signal Time-spreading Mechanism due to Multipath*

In order to characterize and measure the multipath intensity profile, wideband signals (impulse signals or spread spectrum) need to be used [157]. As an example, assume an impulse signal is sent from the transmitter, and the non-line-of-sight component of the received signal has the intensity profile shown in Fig. 48a. This intensity profile, denoted $S(\tau)$, versus time delay $\tau$, helps describe how the average received power vary as a function of time delay. The time delay $\tau$ is used to refer to the excess delay, which represents the signal's propagation delay after the arrival of the first signal at the receiver. The *maximum excess delay* $T_m$ is the time between the first and the last

received component, during which the multipath signal level falls to some threshold level below the that of the strongest component (usually the first one), as is shown in Fig. 48a.

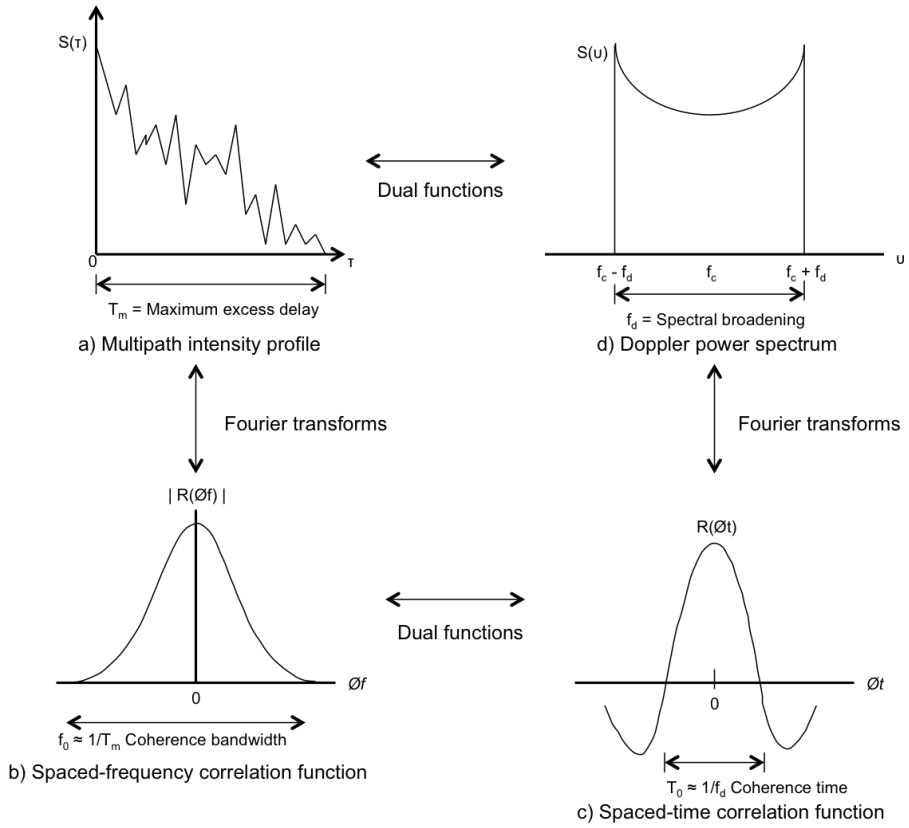


**Figure 48:** Relationships between the channel correlation functions and power density functions [187].

The symbol rate $f_s$, measured as symbols per second, or *baud* rate, represents the number of symbol changes, waveform changes, or signaling event changes across the channel per unit time. The symbol time $T_s$ is the time between symbol transitions, and can be calculated as

$$T_s = \frac{1}{f_s} \tag{13}$$

The relationship between maximum excess delay time $T_m$ and symbol time $T_s$ can be viewed in terms of two different degradation categories: *frequency-selective fading*

and *frequency-nonselective* or *flat fading*. A channel exhibits frequency-selective fading if $T_m > T_s$ where the received multipath components of a symbol extend beyond the symbol's time duration. This dispersion of the signal results in channel-induced inter-symbol interference (ISI). On the other hand, a channel exhibits flat fading if $T_m < T_s$, where all the received multipath components of a symbol arrive within the symbol time duration, and the components are not resolvable at the receiver. In this case there is no channel-induced ISI since the signal time spreading does not result in significant overlap among neighboring received symbols. But there is still degradation due to the unresolvable phasor components which can add up destructively to result in a substantial reduction in SNR. To mitigate this loss in SNR due to flat fading, a technique used is to improve the received SNR or reduce the required SNR, such as signal diversity and error-correction coding.

An analogous characterization of signal dispersion can be done in the frequency domain. The spaced-frequency correlation function, $|R(\Delta f)|$, is plotted as a function of frequency difference between two signals in Fig. 48b. $R(\Delta f)$ represents the Fourier transform of $S(\tau)$, and describes the correlation between the channel's response to two signals as a function of frequency difference between the two signals. In this case the time-spreading manifestation can be viewed as if it were the result of a filtering process, where a pari of sinusoids separated in frequency by $\Delta f$ can be transmitted, cross-correlating the two separated received signals, and repeating the process many times with larger separation $\Delta f$. The *coherence bandwidth* $f_0$ is a statistical measure of the range of frequencies over which the channel passes all spectral components with approximately equal gain and linear phase. That is, the coherence bandwidth represents a frequency range over which frequency components have a strong potential for amplitude correlation. A signal's spectral components in that range are affected by the channel in a similar manner as exhibiting fading or no fading. $f_0$ and $T_m$ are reciprocally related, and as a good approximation, and without loss of generality, it

is possible to say

$$f_0 \approx \frac{1}{T_m} \tag{14}$$

In the frequency domain, the channel is frequency-selective if $f_0 < \frac{1}{T_s} \approx W$, where $\frac{1}{T_s}$ represents the symbol rate and can be approximated by the signal bandwidth $W$. $W$ may be different from $\frac{1}{T_s}$ due to system filtering or data modulation type (e.g., quaternary phase shift keying, QPSK, etc.) [187]. Frequency-selective fading occurs whenever a signal's spectral components are not all affected equally by the channel. Some of the signal's spectral components, falling outside the coherence bandwidth $f_0$, will be affected differently compared to those components contained within $f_0$. This condition is illustrated in Fig. 49a.

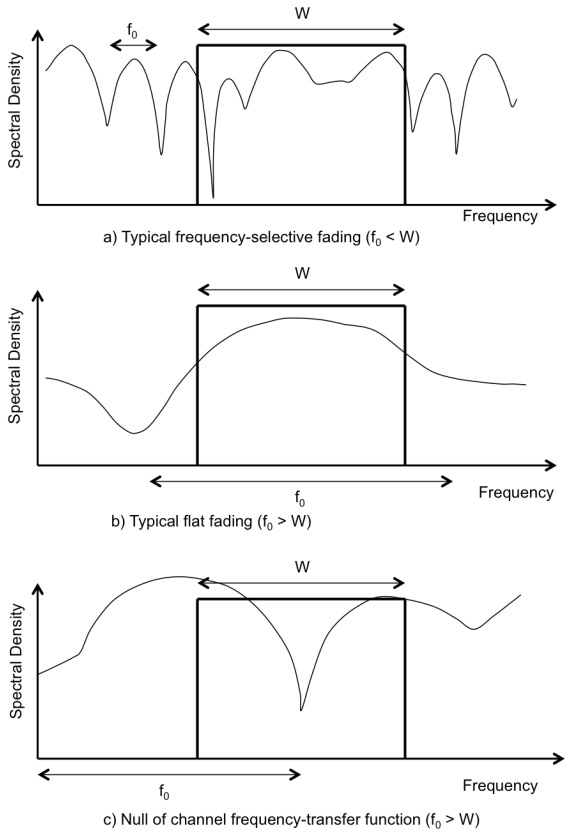


**Figure 49:** Relationships between channel frequency-transfer function and signal bandwidth W [187].

Frequency-nonselective or flat fading degradation can be represented in the frequency domain whenever $f_0 > \frac{1}{T_s} \approx W$. In this case, all of the signal's spectral components will be affected by the channel in a similar manner (fading or no fading), as illustrated in Fig. 49b. Flat fading does not lead to channel-induced ISI distortion, but performance degradation can still be expected due to loss in SNR when the signal is fading. Hence to avoid channel-induced ISI distortion due to frequency-selective fading, the channel coherence bandwidth $f_0$ sets an upper limit on the transmission rate that can be used without incorporating an equalizer in the receiver.

When the signal is experiencing flat-fading, where $f_0 > \frac{1}{T_s} \approx W$, as the mobile radio changes its position the received signal can experience frequency-selective distortion. This is due to possible nulls of the channel's frequency transfer function occurring at the center of the signal band, as shown in Fig. Fig. 49c. When this occurs, the baseband pulse will be especially mutilated by deprivation of its DC component. Therefore, a mobile radio channel classified as having flat fading degradation can exhibit frequency-selective fading at times.

#### *3.1.3.2 Time Variance of the Channel due to Motion*

So far we have described the parameters signal dispersion and coherence bandwidth which can be used to describe the channel's time-spreading properties in a local area. However, they do not offer information about the time-varying nature of the channel caused by the relative motion between a transmitter and receiver, or by movement of objects within the channel. For applications where the radios are on mobile platforms, the channel is time-variant because motion between the transmitter and receiver results in propagation path changes. Because of such motion, the receiver experiences variations in the signal's amplitude and phase in time. Because the channel characteristics are dependent on the positions of the transmitter and receiver, time variance in this case is equivalent to spatial variance.

The *spaced-time* correlation function $R(\Delta t)$, shown in Fig. 48c, is the autocorrelation function of the channel's response to a sinusoid. This function helps describe the extent to which there is correlation between the channel's response to a sinusoid sent at time $t_1$ and the response to a similar sinusoid sent at time $t_2$, where $\Delta t = t_2 - t_1$. The *coherence time* $T_0$ is a measure of the expected time duration over which the channel's response is essentially invariant. To study signal time-spreading due to multipath we made measurements of signal dispersion and coherence bandwidth by using wideband signals (impulses or spread spectrum). In this case, to measure the time-variant nature of the channel, we use a narrowband signal instead [157]. For example, a single sinusoid ($\Delta f$) can be transmitted to measure the autocorrelation function $R(\Delta t)$ of the received signal. The function $R(\Delta t)$ and the parameter $T_0$ provide knowledge about the fading rapidity of the channel. For an ideal *time-invariant* channel (no motion at all), the response of the channel would be highly correlated for all values of $\Delta t$, and $R(\Delta t)$ would be a constant function. If a dense-scatterer channel model is used, with constant velocity of motion and an unmodulated continuous wave signal, the normalized $R(\Delta t)$ is described as [60]

$$R(\Delta t) = J_0(kV\Delta t) \tag{15}$$

where $J_0(\cdot)$ is the zero-order Bessel function of the first kind, $V$ is the constant velocity, $V\Delta t$ is the distance traversed, and $k = \frac{2\pi}{\lambda}$ is the free-space phase constant. The coherence time $T_0$ can be measured in terms of either time or distance traversed (assuming constant velocity). In [21] Amoroso describes such measurement using a continuous wave signal and a dense-scatterer channel model. He measured the statistical correlation between the combination of received magnitude and phase sampled at a particular antenna location $x_0$, and the corresponding combination of receiver magnitude and phase sampled at some displaced location $x_0 + \zeta$, with displacement measured in units of wavelength. He found that for a displacement of $\zeta = 0.38\lambda$ between the transmitter and receiver antennas, the combined magnitudes and phases

of the received continuous wave are statistical uncorrelated. Assuming a constant velocity of motion, this displacement can be transformed into units of time, giving the coherence time.

As is shown in Fig. 47, the time-variant nature of the channel or fading rapidity mechanism can be characterized in terms of two degradation categories: *fast fading* or *slow fading*. Fast fading is represented by channels for which $T_0 < T_s$, where $T_0$ is the channel coherence time, and $T_s$ is the time duration of a transmission symbol. It describes a condition where the time duration in which the channel behaves in a correlated manner is short compared to the time duration of a symbol. In this case the fading character of the channel will change several times while a symbol is still propagating, leading to distortion of the baseband pulse shape. The resulting distortion is due to the receiver signal's components are not all highly correlated throughout time. Hence, fast fading can cause the baseband pulse to be distorted, resulting in a loss of SNR that often yields an irreducible error rate. Such distorted pulses cause synchronization problems (e.g., failure of phase-locked-loop receivers), in addition to difficulties in adequately defining a matched filter [187].

On the other hand, a channel is referred to as providing slow-fading if $T_0 > T_s$. In this case, the time duration that the channel behaves in a correlated manner is long compared to the time duration of a transmission symbol. Thus, the channel state is expected to virtually remain unchanged during the time in which the symbol is transmitted. However, like flat-fading mechanism, the primary degradation of slow-fading is loss in SNR.

The time variance of the channel can also be viewed in the frequency domain, in terms of the Doppler-shift. In Fig. 48d, a the *Doppler power spectral density* $S(v)$ is plotted as a function of the Doppler-frequency shift $v$. For the dense-scattered model, a vertical receive antenna with constant azimuthal gain, a uniform distribution of signals arriving at all angels throughout the range $(0, 2\pi)$, and an unmodulated

continuous wave signal, the signal spectrum at the receiver antenna is [60]

$$S(v) = \frac{1}{\pi f_d \sqrt{1 - (v/f_d)^2}} \tag{16}$$

where $f_d$ is the spectral broadening. The equality in 16 holds for frequency shifts of $v$ that are in the range $\pm f_d$ about the carrier frequency $f_c$, and would be zero outside that range. The shape of the RF Doppler spectrum described by Eq. 16 is classically bowl-shaped for mobile radio channels in dense-scatterer models, as seen in Fig. 48d.

In Fig. 48d, the sharpness and steepness of the boundaries of the Doppler spectrum are due to the sharp upper limit on the Doppler shift produced by a vehicular antenna traveling among the stationary scatterers of the dense scatterer model. The largest magnitude (infinite) of $S(v)$ occurs when the scatterer is directly ahead of the moving antenna platform or directly behind it. In this case, the magnitude of the frequency shift is given as

$$f_d = \frac{V}{\lambda} \tag{17}$$

where $V$ is the relative velocity, and $\lambda$ is the signal wavelength. $f_d$ is positive when the transmitter and receiver move toward each other, and negative when they move away from each other. For scatterers directly broadside of the moving platform, the magnitude of the frequency shift is zero. Doppler components arriving at exactly $0 and 180$ have an infinite power spectral density, and is not a problem since the angle of arrival is continuously distributed and the probability of components arriving at exactly these angles is zero [167].

$S(v)$ is the Fourier transform of $R(\Delta t)$. The Fourier transform of the autocorrelation function of a time series is the magnitude squared of the Fourier transform of the original time series [187]. Therefore, measurements can be made by transforming a sinusoid (narrowband signal) and using Fourier analysis to generate the power spectrum of the received amplitude [157]. This Doppler power spectrum of the channel provides knowledge of the spectral spreading of a transmitted sinusoid (impulse in

frequency) in the Doppler shift domain. As indicated in Fig. 48, $S(v)$ can be regarded as the dual of the multipath intensity profile $S(\tau)$, since the latter yields knowledge about the time spreading of a transmitted impulse in the time-delay domain.

Knowledge of $S(v)$ allows us to determine how much spectral broadening is imposed on the signal as a function of the rate of change in the channel state. The width of the Doppler power spectrum is referred to as the *spectral broadening* or *Doppler spread*, denoted by $f_d$, and also referred to as *fading bandwidth* of the channel. In a typical multipath environment, the received signal arrives from several reflected paths, with different path distances and different angle of arrival, and the Doppler shift of each arriving path is generally different from that of another path [187]. The effect on the received signal is seen as a Doppler spreading or spectral broadening of the transmitted signal frequency, rather than a single shift. The Doppler spread $f_d$ and the coherence time $T_0$ are reciprocally related, and we can approximate this relationship to be

$$T_0 \approx \frac{1}{f_d} \tag{18}$$

Therefore, the Doppler spread $f_d$ or $\frac{1}{T_0}$ are regarded as the typical *fading rate* of the channel.

In the Doppler-shift (frequency) domain, a channel is referred to as fast fading if the symbol rate $\frac{1}{T_s}$ (approximately equal to the signaling rate or bandwidth $\approx W$) is less than the fading rate $\frac{1}{T_0}$ (approximately equal to $\approx f_d$). That is, fast fading is characterized by

$$W < f_d \tag{19}$$

or

$$T_s > T_0 \tag{20}$$

On the other hand, a channel is referred to as slow fading if the signaling rate is greater than the fading rate. Therefore, to avoid signal distortion caused by fast

fading, the channel myst be made to exhibit slow fading by ensuring that the signaling rate must exceed the channel fading rate. In other words, ensure that

$$W > f_d \tag{21}$$

or

$$T_s < T_0 \tag{22}$$

If these conditions are not satisfied enough, the random frequency modulation due to varying Doppler shifts will limit the system performance significantly. The resulting Doppler effect yields an irreducible error rate that cannot be overcome by simply increasing the SNR [32].

### 3.1.4 Brief Overview of Mitigation Techniques for Degradations due to Multipath Fading

Over the years, the evolution of strategies for mitigating the degrading effects of multipath in dense scatterers amounts to a rather mature engineering activity [21]. Among the many techniques either proven or under development are the following:

- Antenna diversity (space diversity) [106].
- Frequency diversity (more than one simultaneous radio frequency carrier per link) [106].
- Polarization diversity [106].
- Error detection and forward error correction coding [43] [44] [45] [98] [78].
- Time division multiple access (TDMA) to increase the instantaneous bit rate on each of many multiple access channels [89].
- M-ary orthogonal signal sets consisting of multiple simultaneous narrowband orthogonal frequency tones multiplexed to lengthen symbols and thereby avoid intersymbol interference [147] [119].

- Decision feedback [156] [144].
- Embedded pilot tones for channel monitoring (transparent tone-in-band - TTIB) [53].
- Spread spectrum signaling with or without the use of orthogonal signal sets, whether by direct sequence spread spectrum (DS/SS) or by frequency hopping [117] [165] [98].

A through discussion of each of the above strategies would extent beyond the scope of this thesis. It should be pointed out that these strategies are not considered in the process of developing course of actions to enhance the quality of links between the vehicles. Rather, the large scale and small scale degradations will be taken into account for a given transmission protocol and modulation, and a channel model will be developed that can be used to determine asset allocation and path planning that provides good quality link in the communication network. However, these strategies should be kept in mind for further research into ways to increase the connectivity between vehicles and mitigate some of these large and small scale fading.

### 3.1.5 Probabilistic Modeling of the Fading Channel

Probabilistic models allow for a more realistic modeling of radio wave propagation. Typically the average reception power at a specified distance is calculated using a deterministic model, in our case the APM model, and the individual reception power of each arriving frame is determined using a probability distribution with the average reception power as one of the parameters. This results in a much more diverse (and realistic) distribution of successful receptions. A clear geometric partitioning is not visible anymore, instead, receptions in near distance might fail, as well as receptions in distances further than the classic reception range are also possible. The intensity of aforementioned effects depends on parametrization and the characteristics of the probabilistic models [128].

The RF propagation channel is modeled as a slow time-varying fading channel with none frequency-selective fading (flat-fading). In other words, we will assume that the vehicles move in relatively slow velocities with respect to each other that the channel fading rate due to doppler effects is much smaller than the symbol rate. The flat fading assumption is made to simplify our analysis by restricting ourselves to cases where the multipath delay spread is smaller than the symbol time, and therefore ignoring inter-symbol distortions, pulse mutilation, and irreducible bit-error-rates. Although this assumption rules out many realistic RF channels, it allows us to scope our problem to one that can be analyzed from the NPP point of view in the COA development phases, without any loss of generality.

The primary property of the fading channel is that it is a correlated and time varying random process. Specifically, the communications channel is dynamic and the fading channel gain fluctuation is a random process that varies with time in a correlated way [176]. The signal fluctuation is due to multi-path effects caused by reflection and the scattering of the radio waves as they propagate through the environment. The multi-path induced fluctuation of the transmitted signal results in a received signal envelope that can be modeled using a Nakagami-m distribution, where the model parameter $m$ describes the effect of the fading channel, and can be used to capture a wide range of fluctuation intensities to develop a more robust and practical framework of the fading channel. This model is particularly valuable because the $m$ parameter can be used to approximate other fading distributions such as Rician and Lognormal distributions [100]. The Nakagami model can hence be used in this work to model certain environmental conditions and their impact on the RF signal power [128]. It also offers greater flexibility for fitting empirical data, making it an ideal candidate for use while modeling intermittent communications under maritime conditions.

Let $\omega$ denote the average signal-to-noise ratio ($SNR$), given by

$$\omega = \sigma^2 \frac{E_s}{\frac{N_0}{2}} = 2\sigma^2 \frac{E_s}{N_0} \tag{23}$$

where $\sigma^2$ is the fading power gain, $E_s$ is the energy per transmitted symbol, and $(N_0/2)$ is the variance of the $AWGN$. Then, the Nakagami-m fading channel model probability function [149], which has been shown to provide the most general model for ionospheric and tropospheric modes of propagation, and which has been well confirmed by observations, is given by equation (24), as a function of $\chi$, which denotes the envelope of the RF signal, and parameter $m$:

$$P_{Nak}(\chi, m) = (\frac{2m^m \chi^{2m-1}}{\Gamma(m)\omega^m}) \exp(-\frac{m\chi^2}{\omega}), \chi \geq 0 \tag{24}$$

where $\Gamma(m)$ is the gamma function evaluated at parameter $m$. A value of $m = 1$ corresponds to Rayleigh fading, $m \leq 1$ correspond to deeper fading characteristics more sever than Rayleigh fading, and values of $m \geq 1$ correspond to shallower fading distributions trending towards free-space behaviors. For the special case of Rayleigh fading ($m = 1$), combined with $AWGN$, the received $SNR$ is proportional to the square of the signal envelope and is exponentially distributed:

$$P_{Ray}(\chi) = (\frac{1}{\omega}) \exp(-\frac{\chi}{\omega}), \chi \geq 0 \tag{25}$$

A standard performance criterion for evaluating communication systems operating over fading channels is the outage probability $P_o$, defined as the probability that the instantaneous $SNR$ falls below a specified communications threshold value [123]. $P_o$ is thus the cumulative distribution function (*cdf*) of the $SNR$ signal envelope $\chi$ evaluated at $\omega$:

$$P_o(\chi) = 1 - \exp(-\frac{\chi}{\omega}), \chi \geq 0 \tag{26}$$

The *cdf*, expressed by 26, by definition expresses the percentage of bit packets contained within the signal envelope $\chi$, that have a reception power less than the average

$SNR$, $\omega$. This is used to predict the probability that the signal $SNR$ will fall below a threshold value, and therefore the probability of communications.

From the results presented in [62], it can be seen that the Rayleigh fading channel model offers a more robust modeling of the communications channel in the face of fading intensities when compared to simply considering the threshold of communications for a given receiver sensitivity. In [128], the free-space deterministic model was used to calculate the average reception power as a function of distance and frequency (i.e. the Friis model), and the Nakagami-m probabilistic model was used to model the multi-path fading due to environmental conditions and reflections. This allowed for a more robust fading channel model, where the probabilistic model provided an interval of possible good and bad communication ranges based on the specified threshold value. Figure 50 shows the signal reception power as a function of distance between transmitter and receiver for both the deterministic and the probabilistic model. And Fig. 51 shows the corresponding probability of reception as a function of distance between transmitter and receiver, again for both the deterministic and the probabilistic model.

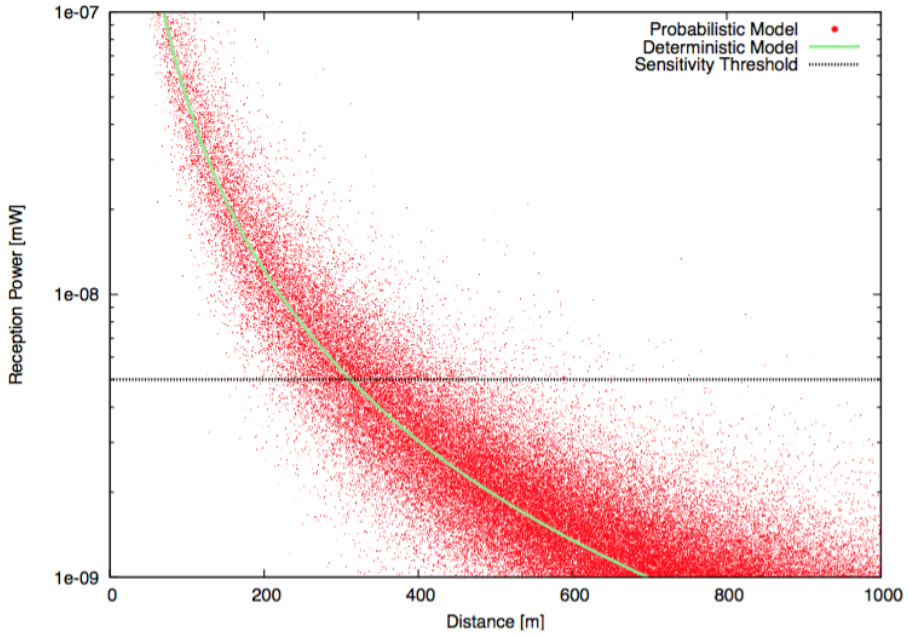


**Figure 50:** Signal Reception Power Vs. Distance between Sender and Receiver [128]

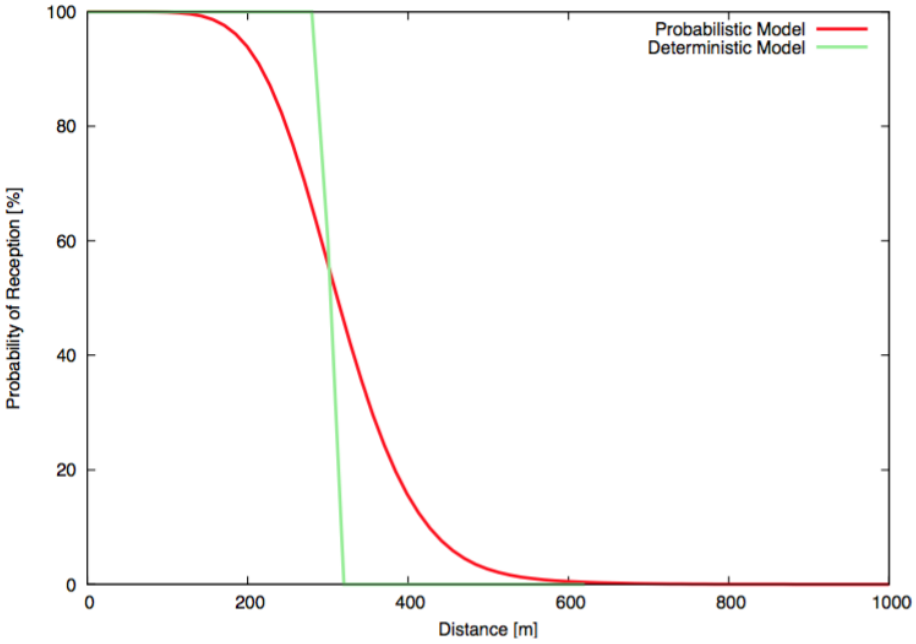


**Figure 51:** Probability of reception Vs. Distance [128]

These results show that once the average signal reception power has been calculated, either by the free-space model as was done in [128] or the APM model in our case, then the channel model can be made more robust by fitting a probabilistic model such as the general Nakagami-m distribution around this average signal reception. This new probabilistic model will take into account uncertainties in environmental conditions by providing a shape parameter $m$ that best fits empirical data for that given condition.

### 3.1.6 RF Link Budget

A link budget is used to account for all the power gains and losses from the transmitter, through the atmospheric medium, and the receiver for a given link. The instantaneous $SNR$ parameter is computed as follows:

$$SNR = P_R - P_N \tag{27}$$

where $P_R$ is the received power, and $P_N$ is the $AWGN$ power. The received power $P_R$ can be decomposed into the following contributions and losses:

$$P_R = P_T + G_T + G_R - L_{APM} - L_{sys} - L_{cp} \tag{28}$$

where $P_T$ is the transmitter power, $G_T$ is the transmitter antenna gain, $G_R$ is the receiver antenna gain, $L_{APM}$ is the propagation loss calculated by APM, $L_{sys}$ is assumed system loss, and $L_{cp}$ is cross polarization loss. This received power includes both the large and small scale fading described in previous sections. The instantaneous $SNR$ parameter is then compared a threshold $SNR$, denoted by $\omega_T$, which is given by

$$\omega_T = P_T + G_T + G_R + L_{rs} - L_{sys} - L_{cp} \tag{29}$$

where $L_{rs}$ is the receiver sensitivity.

### 3.1.7 Experiment 2 Part B: Nakagami-m Probability Studies and Channel Simulation

APM model results discussed simulate the RF propagation through space and captures the large scale fading mechanisms due to free-space losses and the effect of the atmospheric refractivity on the multipath fading of the signal intensity. As described in the *Characterization of Fading Channels in Mobile Communications*, the signal will also experience further attenuations due to the small-scale fading, which include the time spreading of the signal and the time variance of the channel.

In order to take into account these small scale fading, a probabilistic approach is proposed in this study. As previously described, we mode the RF propagation channel as a slow-time varying fading channel with non-frequency-selective fading (flat-fading). The signal fluctuations are due to multipath fading, spreading of the signal, and the time variations, and scattering of the radio waves as they propagate through the environment. In the literature, this multipath induced fluctuation of the transmitted signal results in a received signal envelope that can be modeled probabilistically. The *Nakagami-m* probability distribution captures a wide range of fluctuation intensities that can be experienced in different environments and provides a robust and practical framework for the fading channel.

Lets denote the envelope of the fading intensity by $\chi$, and the Nakagami parameter by $m$. Then the Nakagami-m probability distribution is given by

$$P_{Nak}(\chi, m) = \left(\frac{2m^m \chi^{2m-1}}{\Gamma(m)\Omega^m}\right) \exp\left(-\frac{m\chi^2}{\Omega}\right), \chi \geq 0 \tag{30}$$

where $\Gamma(m)$ is the gamma function evaluated at parameter $m$, and $\Omega$ is the expected fading intensity squared. A value of $m = 1$ corresponds to Rayleigh fading, $m \leq 1$ correspond to deeper fading characteristics more sever than Rayleigh fading, and values of $m \geq 1$ correspond to shallower fading distributions trending towards free-space behaviors. Therefore, the $m$ parameter can be used to describe a wide range of fluctuation intensities.

A study of the effect of the $m$ parameter representing different fluctuation intensities represented by the Nakagami-m model was performed next. First, the expected fading intensity squared was set to $\Omega = 1mW^2$, and the Nakagami parameter $m$ was varied from the lowest possible value, $m = 0.5$, to $m = 5$. The resulting Nakagami distributions are shown in Fig. 52. As can be seen from the plot, the lower the

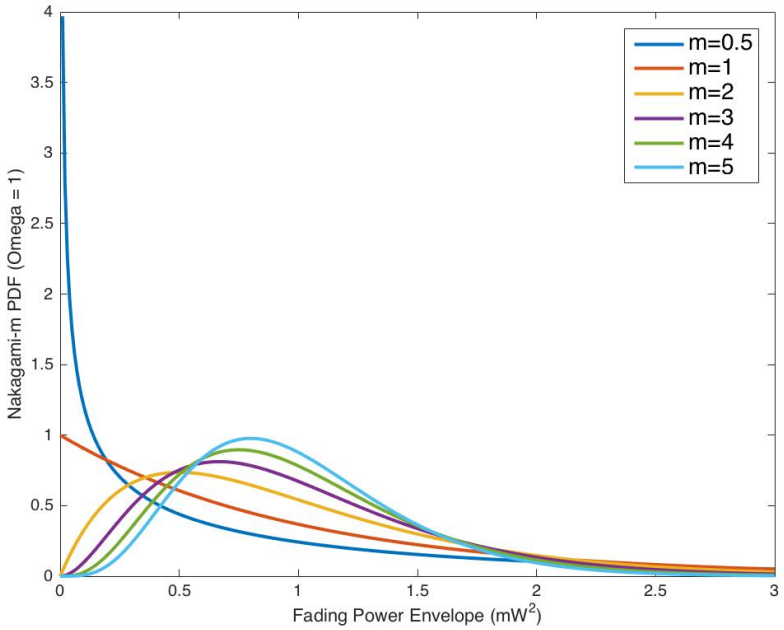


**Figure 52:** Nakagami probability distributions with $\Omega = 1mW^2$ and varying m-parameter.

$m$ value, the higher the probability of the fading intensity. The $m$ parameter also controls the shape of the Nakagami distribution. As the $m$ parameter increases, the shape of the distribution appears more like a Lognormal distribution. In general, as demonstrated in [39], as the parameter $m$ increases, the smaller the variance of the fading signal intensity and the larger the skewness of the Nakagami distribution.

Next, the $m$ parameter was set to 1, which corresponds to a Rayleigh fading distribution. This distribution is given by

$$P_{Rayl}(\chi) = (\frac{1}{\Omega}) \exp(-\frac{\chi}{\Omega}), \chi \geq 0 \tag{31}$$

The expected fading intensity $\Omega$ was varied from 0.5 to 5, similar to the variation of the m-parameter, and the corresponding Rayleigh distributions were calculated, and are shown in Fig. 53. As can be seen in the plot, the probability distribution

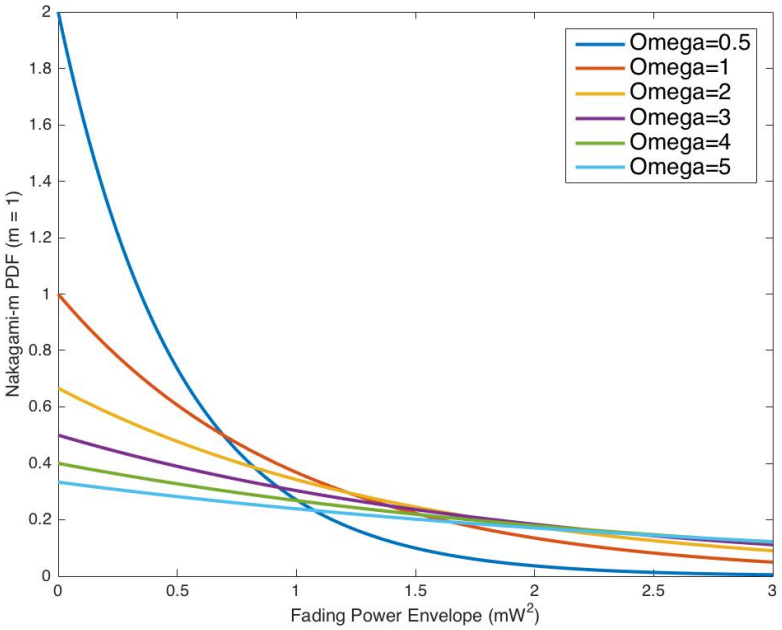


**Figure 53:** Rayleigh probability distributions (m = 1) with varying expected signal intensity $\Omega$.

tends to flatten-out as the expected signal intensity increases, which indicates that the signal intensity variation is more spread, and higher fading intensities have higher probabilities.

The selection of the $m$ parameter of the Nakagami probability model is not trivial and is usually done experimentally. The $m$ parameter is related to the expected fading signal intensity $E[\chi^2]$ and the variance of the fading signal intensity $Var[\chi^2]$ as [149]

$$m = \frac{E^2[\chi^2]}{Var[\chi^2]} \tag{32}$$

Note that, in a sense, the $m$ parameter is given by the inverse of the normalized variance of the fading signal amplitude.

A well accepted method of estimating the $m$ parameter from experimentation is by estimating the expected fading signal intensity $\Omega$ by

$$\Omega \approx \hat{\Omega} = \frac{1}{N} \sum_{i=1}^{N} \chi_i^2 \tag{33}$$

Where $N$ is the number of available samples $\chi_i$ of the fading signal intensity envelope. The variance can be calculated similarly, and the $m$ parameter can be estimated.

On the other hand, If empirical data is available from experiments, the $m$-parameter can be estimated to better fit the actual field conditions according to the literature. Two major statistical methods used in the literature to fit the Nakagami-m probability model to empirical data are the method of moments (MoM) and maximum likelihood (ML). Next we present some of these estimators.

Let us denote the $kth$ sample moment by $\mu_k$, given by:

$$\mu_k = \frac{1}{N} \sum_{i=1}^{N} \chi_i^k \tag{34}$$

Using this notation, then $\hat{\Omega} = \mu_2$. For the $kth$ order moment of the Nakagami random variable $\chi$, we have [149]

$$E[\chi^2] = \frac{\Gamma(m + k/2)}{\Gamma(m) m^{k/2}} \Omega^{k/2} \tag{35}$$

Therefore, a general moment-based estimator [135] for $m$, denoted $\hat{m}$, is given by

$$\frac{\Gamma(\hat{m}_k + k/2)}{\Gamma(\hat{m}_k) \hat{m}_k^{k/2}} = \frac{\mu_k}{\mu_2^{k/2}} \tag{36}$$

For odd values of $k$, this trascendental equation must be solved (involving the gamma function) to obtain $\hat{m}$. For even $k$ values, on the other hand, we have an algebraic equation which is generally preferred [14]. It is also noted in [14] that, since the process of modeling empirical data (which inevitably have finite range) using an infinite range probability density function, higher order sample moments will deviate from the theoretical moments significantly, i.e., $\mu_k$ differs from $E[\chi^k]$ significantly for large $k$ when $\chi$ is a random variable with infinite range. Therefore, it is better to use

the lowest possible even order sample moment. For $k = 2$, 36 reduces to the identity, while for $k = 4$, we obtain the inverse normalized variance (INV) estimator, denoted by $\hat{m}_{INV}$, given by

$$\hat{m}_{INV} = \frac{\mu_2^2}{\mu_4 - \mu_2^2} \tag{37}$$

Replacing the moments in the definition of $m$ in 32 with the sample moments, we arrive at $\hat{m}_{INV}$.

Another $m$ parameter estimator is the *Toparev-Polyakov* (TP) estimator, denoted by $\hat{m}_{TP}$ [209], given by

$$\hat{m}_{TP} = \frac{1 + \sqrt{1 + (4/3)ln(\mu_2/B)}}{4ln(\mu_2/B)} \tag{38}$$

where $B$ is given by

$$B = (\prod_{i=1}^{N} \chi_i^2)^{1/N} \tag{39}$$

A third estimator is the *Lorenz* estimator, denoted by $\hat{m}_L$ [136], given by

$$\hat{m}_L = \frac{4.4}{sqrt\mu_2^{dB} - (\mu_1^{dB})^2} + \frac{17.4}{[\mu_2^{dB} - (\mu_1^{dB})^2]^{1.29}} \tag{40}$$

where $\mu_k^{dB}$ is hte $kth$ sample moment in dB.

In [14], these three MoM-based methods were used to find the $m$ parameter that fit a given empirical data. Their results showed that the inverse normalized variance estimator resulted in a better fit, while the Tolparev-Polyakov estimator showed larger sample confidence regions, and the Lorenz estimator showed a positive increasing bias as $m$ was increased.

On the other hand, in [56] two ML estimators are compared to the normalized variance MoM estimator from [14] and are shown to have smaller variance. These methods can be used to estimate parameter $m$ and their goodness of fit to the APM deterministic calculation can be compared. Other more general methods may be applied as well, such as the Generalized Moment Estimators, as was used in [57], where real (integer and non-integer) sample moments were used for the derivation

of the parameter $m$. These moment calculations are generally more complicated to compute, but may be a possible solution to the parameter $m$ estimation.

#### *3.1.7.1 Modeling and Simulation of Small Scale Fading*

Given that the estimation of the $m$ parameter involves having experimental empirical data, we will limit our Nakagami-m model to a well studied case where $m = 1$, which is given by the Rayleigh fading. As was described earlier, the Nakagami-m probability model is particularly valuable since by varying the $m$ parameter, the Nakagami probability function can be made to approximate other fading distributions, such as the Rician and Lognormal distributions. When there is a line-of-sight (LOS) signal, the Rician model provides the best model for the fading of the signal intensity. The Rayleigh fading model is used to represent scenarios where there is no LOS signal, which means all fading is only due to the multipath and time-spreading mechanism of the signal.

Since the LOS signal large-scale fading due to multipath is already computed by APM, we cannot use the Rician model, since it will be "double-counting" the effects of LOS large-scale fading due to space propagation and multipath. If empirical data were available, instead the Nakagami-m probability model would be fitted to the data and the m-parameter be estimated. Therefore, the best approach to modeling the time-spreading mechanism of the fading signal will be to use the large-scale fading computed by APM as the average signal fading, and convolute it with the small scale fading due to time-spreading of the signal alone, which can be modeled using the Rayleigh model.

With this in mind, we modeled and simulated the signal intensity fluctuation due to the time-spreading mechanism in a Rayleigh fading channel. We use the radio specifications for the MPU5, shown in Table 11. We assume a link budget corresponding to the capabilities of the COTS RF radio, using the link budget equation

**Table 2:** Link Budget Components

| Component | Value (dBm) |
|---|---|
| $P_T$ | 33.01 |
| $G_T$ | 25 |
| $G_R$ | 3 |
| $L_{sys}$ | 3 |
| $L_{cp}$ | 3 |

41:

$$P_R = P_T + G_T + G_R - L_{APM} - L_{sys} - L_{cp} \tag{41}$$

The losses due to large scale fading are computed by APM and are given by the $L_{APM}$ expression in the link budget. The rest of the link budget components are given in Table 2. The minimum received power sensitivity for the COTS MPU5 radio is $P_{R_{min}} = -98dBm$, as is given in Table 11. Assuming the same 24m EVD, for the Ship-to-USV link, and extracting the propagation loss experienced by the receiver at the corresponding antenna heights from the propagation loss vs. range and height profiles generated by APM, then the received power $P_R$ from the assumed link budget given by 41 can be calculated and plotted as a function of range, and is shown in Fig. 54. Also shown in Fig. 54 is the MPU5's minimum received power sensitivity threshold value. As can be seen in Fig. 54, just looking at the large-scale fading, it can be determined that, since all received powers are above the minimum receiver threshold values, the two vehicles can communicate at any range within 100 km. This is the same method used in the *Communications Awareness Approach* subsection described above, except that now we are looking at the total received power from the link budget equation, and the threshold of communications is the minimum receiver power instead of the receiver propagation loss threshold value.

Using the Rayleigh probability model (Nakagami-m with $m = 1$) given by 31, the probability can be plotted as a function of the fading signal intensity $\chi^2$, and is shown in Fig. 55. Next, the Rayleigh channel is simulated through the use of MAT-

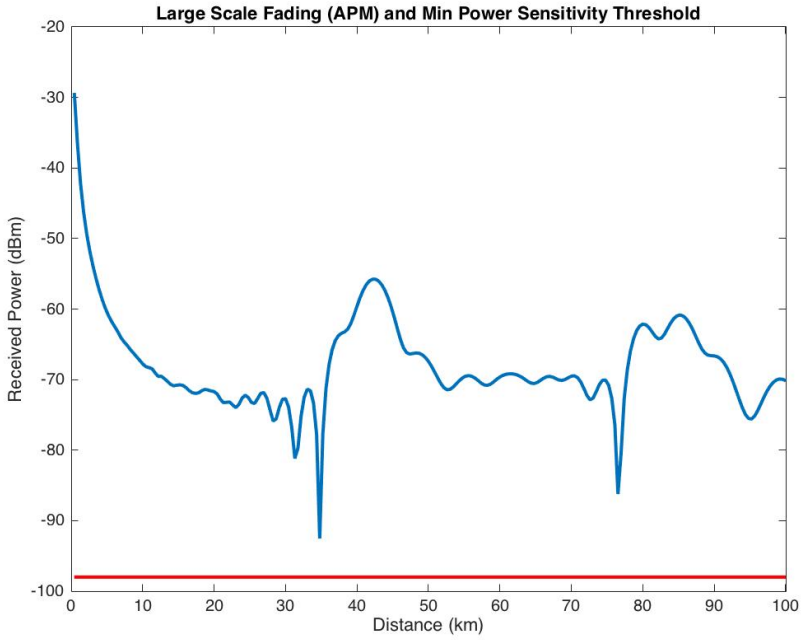


**Figure 54:** Received power vs. range assuming only large scale fading computed by APM at receiver location for Ship-to-USV link in a 24 m EVD.

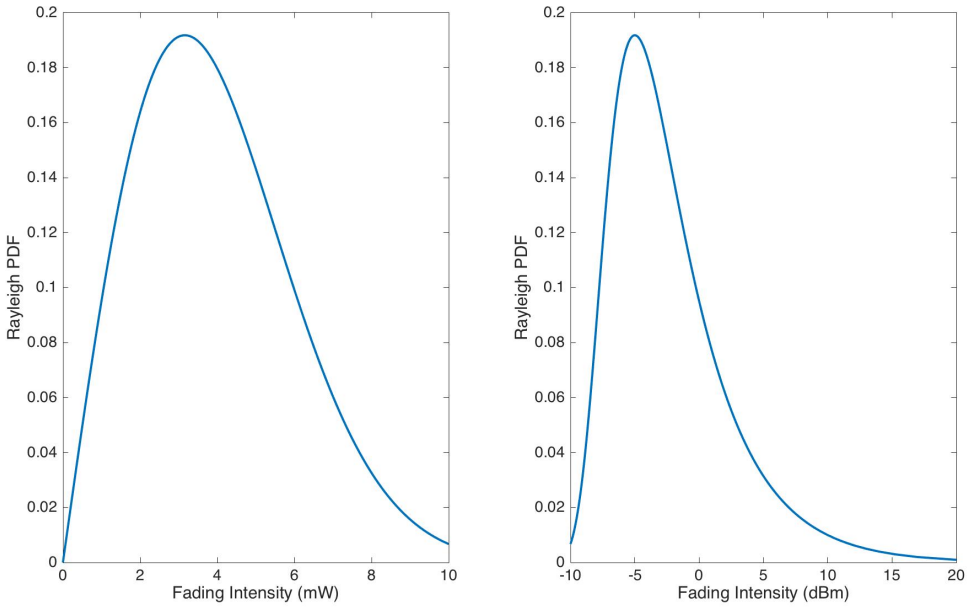


**Figure 55:** Rayleigh probability density functions vs. fading intensity in mW (left) and dBm (right).

LAB's communications systems toolbox [164]. The MPU5 modulates the transmitted signal using the BPSK modulation scheme, using the orthogonal frequency-division multiplexing (OFDM) method of encoding digital data n multiple carriers. For simplicity of modeling and simulation, we consider only one of those orthogonal carriers, which can be modulated using the BPSK scheme. Assuming a symbol sample rate of $f_s = 31.25$ kHz, corresponding to the sample frequency of a data package using the OFDM standard, this corresponds to a sample time of $T_s \approx \frac{1}{f_s} = 3.2 \times 10^{-5}$ seconds. Given that the MPU5 radio operates at the center frequency of $Freq = 2.4$ GHz, that the speed of light is $V_{light} \approx 3 \times 10^8$ m/s, and assuming that the maximum relative speed of the vehicles will be about $V = 7$ knots (or 3.6 m/s), the maximum doppler shift is given by

$$f_d = V(\frac{Freq}{V_{light}}) \approx 160Hz \tag{42}$$

Since we are assuming a frequency-non-selective or flat-fading channel, it is required that the coherence bandwidth $f_0$, which is given by $f_0 \approx \frac{1}{T_m}$, where $T_m$ is the maximum excess delay of the signal, be greater than the symbol rate $\frac{1}{T_s}$, $f_0 > \frac{1}{T_s}$. Therefore, given that the sample time for a standard OFDM subcarrier is $T_s = 3.2 \times 10^{-5}$ seconds, then we require that $f_0 > (\frac{1}{3.2 \times 10^{-5}}) \approx 66.67kHz$. Therefore, translating this to maximum excess delay of the signal, we have $\frac{1}{T_m} > 66.67kHz$, or equivalently $T_m < \frac{1}{66.67kHz} \approx 1.5 \times 10^{-5}$ sec. Choosing an arbitrary maximum path delay that meets this condition, given by $T_m = 1 \times 10^{-6}$, we can simulate the signal intensity variation to an impulse response to study the multipath intensity profile and the coherence bandwidth in the time domain, or simulate the signal intensity variation to a frequency response using the spectral density. Shown in Fig. 56 is the simulated input response of the signal at some instant in time over the Rayleigh channel, with the time delay between each signal. As can be seen in Fig. 56 for some instant in time, the time delay of consecutive signals is less than the required $T_m < 1.5 \times 10^{-5}$. Shown in Fig. 57 is the frequency response of the simulated signal over the Rayleigh

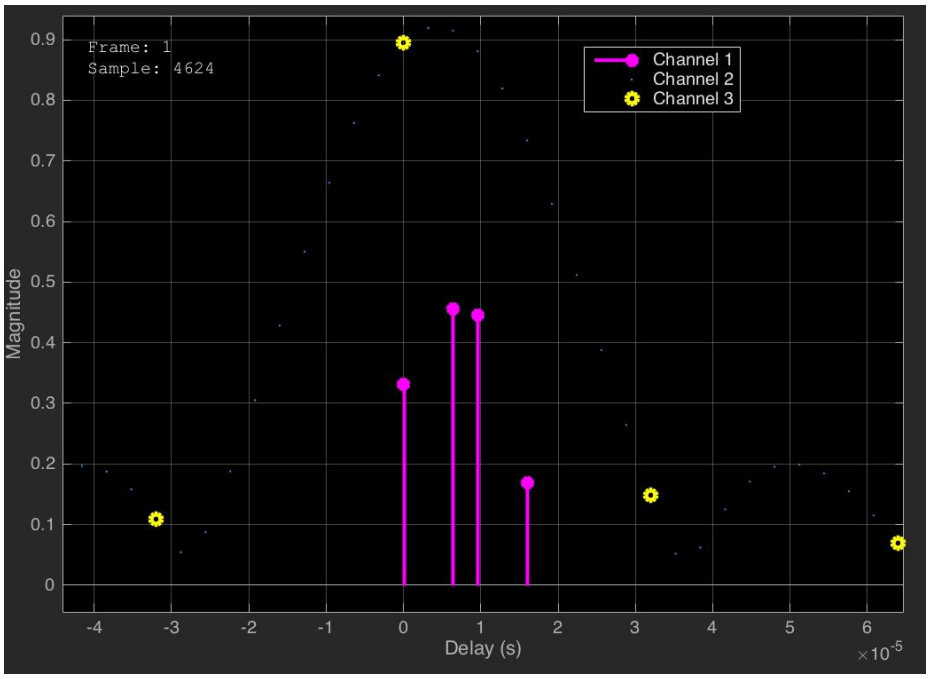


**Figure 56:** Impulse response of the generated signal at some instant in time over the Rayleigh channel.

channel at some instant in time. As can be seen in Fig. 57, the condition on the coherence bandwidth $f_0 \approx \frac{1}{T_m} > (\frac{1}{3.2\times10^{-5}}) \approx 66.67kHz$ for a flat-fading channel is met, since $f_0 \approx \frac{1}{1\times10^{-6}} = 1MHz$ which is much greater than 66.7 kHz (more than two times the bandwidth).

Now that the flat-fading assumption has been validated through our modeling and simulation, we assume a standard OFDM subcarrier which is modulated using the BPSK scheme, where the number of bits transmitter per frame (or data package) is $Bpf = 0.004624Mbpf$ (Mbpf stands for Megabits per frame). A transmitted signal was generated in the MATLAB toolbox by generating $Bpf$ binary symbols (0s and 1s) and then passing the generated symbols through a BPSK modulator with a phase offset of $\pi/4$. The Rayleigh channel in the MATLAB communications toolbox was created with the sample time $T_s$ and maximum doppler shift $f_d$ as inputs. The generated modulated signal was passed through the channel, and the response of the signal was calculated. Shown in Fig. 58 is the simulated small scale fading over the

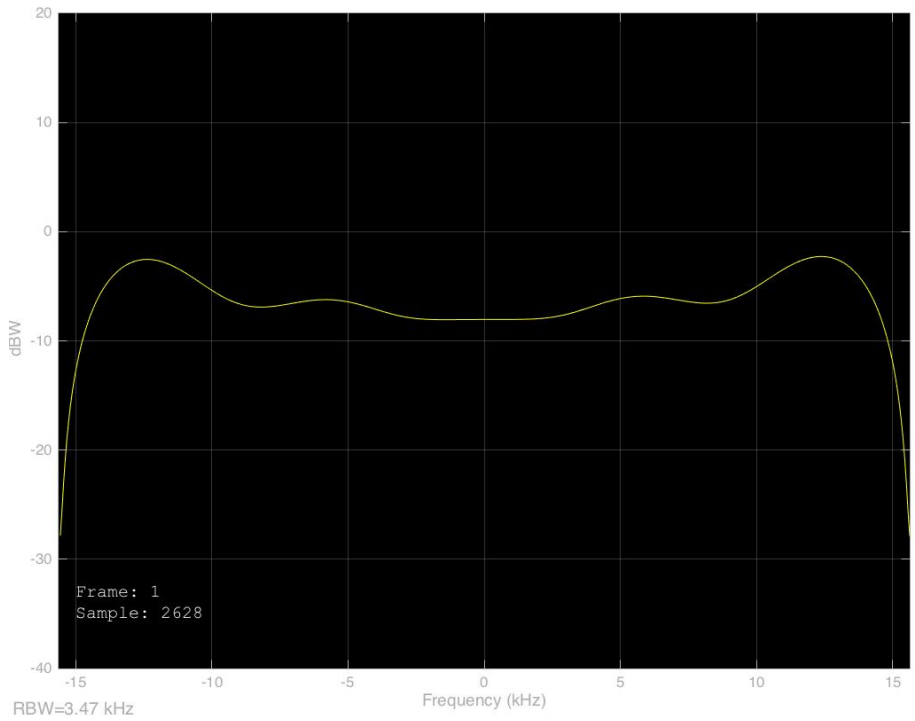


**Figure 57:** Frequency response of the generated signal at some instant in time over the Rayleigh Channel.

time of the simulation. Comparing this simulated signal intensity to the Rayleigh distribution given in right hand side of Fig. 55 for dBm values, it can be shown that the mean is about $E[\chi] \approx -4dBm$. As can be seen in the plot, the signal intensity can vary significantly over a very small time period due to the time-spreading mechanism and the time-variation due to the assume relative motions between the two vehicles.

The simulated fading signal intensity from small scale fading can be convoluted to the received power intensity to show the total received power at some time instant. This is shown in Fig. 59. Also shown in Fig. 59 is the minimum receiver power threshold value of the MPU5 radio. As can be seen in this plot, there are regions where the received power falls below the minimum threshold value, which correspond to skip zones or ranges where the two assets cannot communicate with each other. Comparing this received power with both large and small scale fading with the plot shown in Fig. 54, it can be seen that small scale fading can attenuate the transmitted

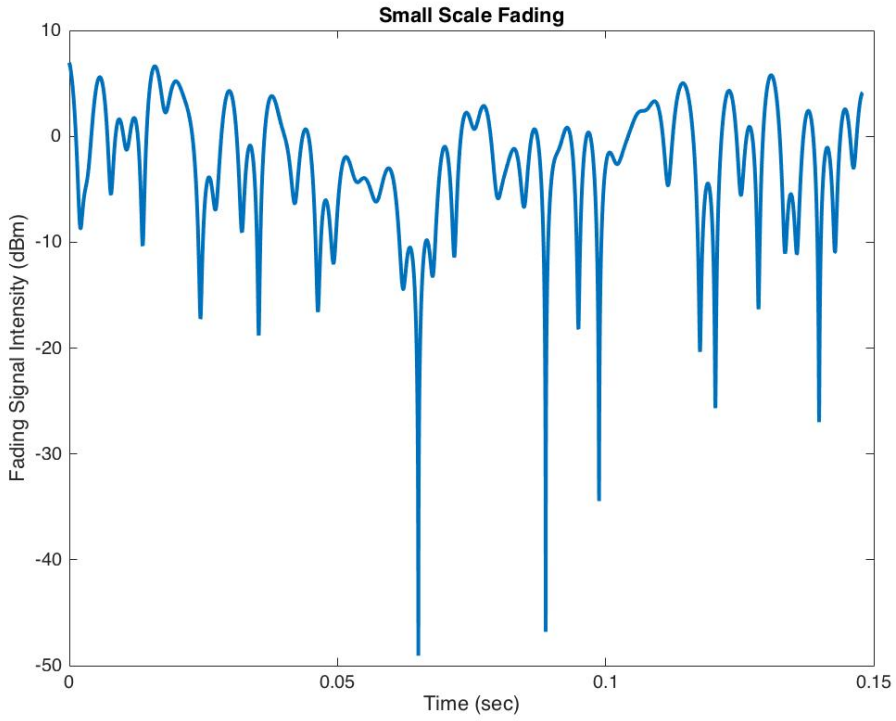


**Figure 58:** Simulated signal intensity fading due to small scale fading for the Rayleigh channel.

signal significantly to the point of falling below the threshold value. This helps to show the benefit of modeling the small scale fading mechanisms during the asset allocation phases of the COA development process.

#### *3.1.7.2 Probability of Communications*

A standard performance criterion for evaluating communications systems operating over fading channels is the outage probability $P_{out}$ [123]. In this work, the outage probability is defined as the probability that the instantaneous fading signal intensity $\chi$ falls below a specified communications threshold value. Given that we are constrained by the communications hardware capability of the MPU5, we use the threshold value specified by its minimum receiver power sensitivity threshold, denoted by $P_{rec_{min}}$.

Going back to the link budget equation, the received power at the receiver will be given by 41. In this link budget equation, the large-scale losses calculated by


**Figure 59:** Simulated received power with large scale and small scale fading at some instant in time using the Rayleigh fading model.

APM can extracted from the propagation loss profiles, and given the transmitter and receiver heights, the corresponding propagation loss as a function of distance between transmitter and receiver $r$. Therefore, we can create a link budget as s function of the distance $r$ between the transmitter and receiver as

$$P_R(r) = P_T + G_T + G_R - L_{APM}(r) - L_{sys} - L_{cp} \tag{43}$$

Given that the threshold of communications will be represented by the minimum receiver power sensitivity threshold, we can formulate this condition as the received power being greater than this minimum threshold value:

$$P_{rec_{min}} \leq P_R(r) = P_T + G_T + G_R - L_{APM}(r) - L_{sys} - L_{cp} \tag{44}$$

Solving for $L_{APM}(r)$ gives us an equation based on the condition for the large scale

fading propagation loss calculated by APM as

$$L_{APM}(r) \leq P_T + G_T + G_R - L_{sys} - L_{cp} - P_{rec_{min}} = L_{APM_{max}} \tag{45}$$

where $L_{APM_{max}}$ stands for the maximum allowable mean propagation loss from APM to meet the minimum power threshold sensitivity value. The outage probability then is given by the cumulative distribution function (CDF) of the Rayleigh fading distribution (or Nakagami-m distribution) of the random variable $\chi$ evaluated at the expected APM value $\Omega$. In other words, the probability of communications is the probability that the APM average expected value is above the threshold value, given by

$$Pr(comms, r) = Pr(L_{APM}(r) \leq L_{APM_{max}}) \tag{46}$$

$$= 1 - Pr(\chi \leq L_{APM_{max}}) \tag{47}$$

$$= 1 - \int_0^{L_{APM_{max}}} (\frac{2m^m \chi^{2m-1}}{\Gamma(m)\Omega^m}) \exp(-\frac{m\chi^2}{\Omega}) d\chi \tag{48}$$

Or, for the Rayleigh fading channel we have:

$$Pr(comms, r) = 1 - \int_0^{L_{APM_{max}}} (\frac{1}{\Omega}) \exp(-\frac{\chi}{\Omega}) d\chi \tag{49}$$

The probability of communications will be a function of the distance between the transmitter and receiver, and will be calculated at each APM deterministic large-scale fading average value. The probability of the signal intensity is calculated at each range $r$ given the average APM value, and the probability of the small scale fading adding to the average APM model which results in a value that falls above the minimum threshold received power will be computed.

Next we simulate the probability of communications for the Ship-to-USV and the USV-to-USV links in both the 14 m and 24 m EVDs. Assuming a threshold receiver sensitivity in terms of the maximum propagation loss allowable by APM as $L_{APM_{max}} = 135$ dB, the probability of communications was calculated from 49. Shown

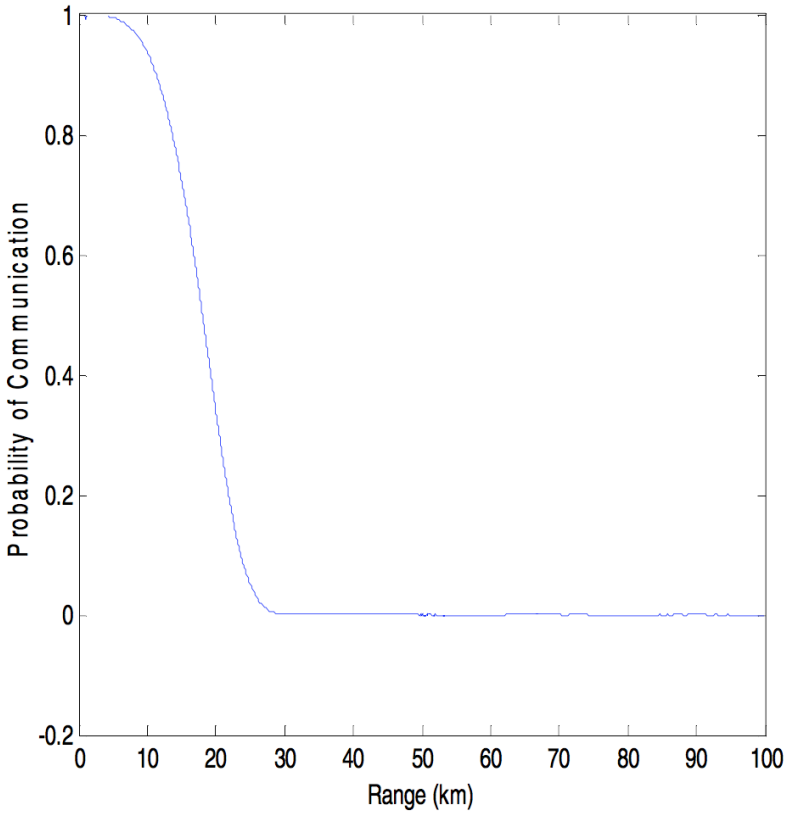


**Figure 60:** Probability of communications for Ship-to-USV link in a 14 m EVD.

in Figs. 60 and 61 are the resulting probability of communications for the Ship-to-USV link under the 14 m and 24 m EVDs, respectively. From these plots, the benefits of the probabilistic approach can be appreciated. The quality of the communication for each link can be quantified by this probability at any given range between a given transmitter or receiver. In the *Communications Awareness Approach*, for the Ship-to-USV link with an Rx Threshold set at 135 dB, it was a sharp cut decision on whether you are in good or bad communications. Now with these probability of communication plots we can measure by means of prediction the quality of the link at any range and give an answer of whether communications are good or bad based on an accepted probability. From Fig. 61, one can still see the skip-zones, indicated by areas of lower probability of communications between 25 and 32 km, and between 55 and 70 km.

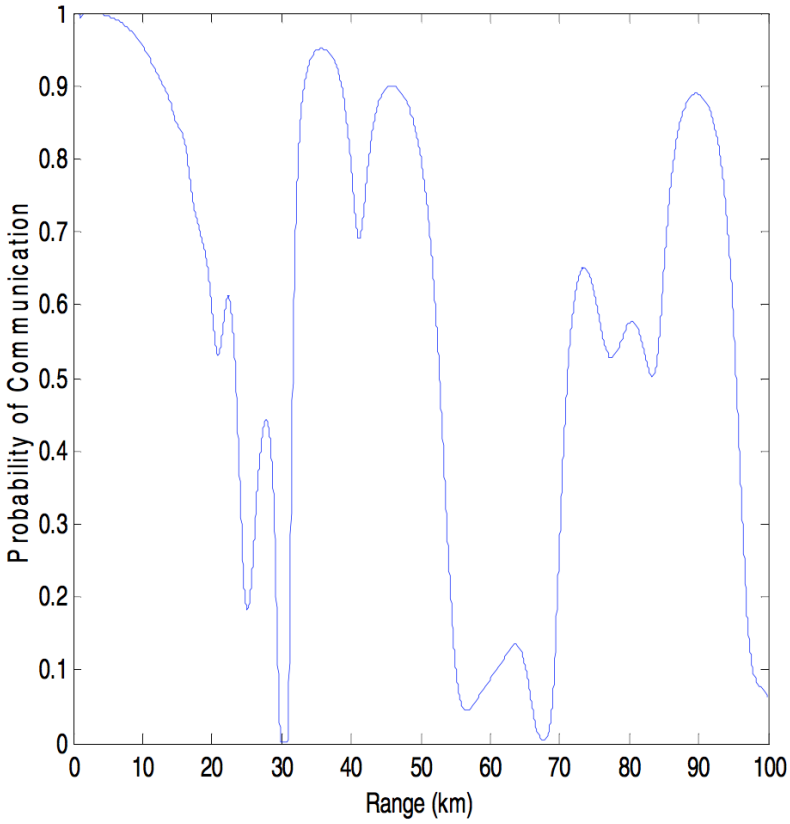


**Figure 61:** Probability of communications for Ship-to-USV link in a 24 m EVD.

Similarly, the probability of communications for the USV-to-USV link was calculated assuming the same maximum propagation loss allowable by APM as $L_{APM_{max}} =$ 135 dB. The plots of the probabilities are shown in Figs. 62 and 63 for the 14 m and 24 m evaporation ducts, respectively. As can be seen in Fig. 62 for the 14 m EVD, if one accepts a probability of communication of 60%, the USV can still communicate with another USV if the range between them is less than 7 km, whereas in the communications awareness approach, by just looking at the APM deterministic large scale fading, USVs can only communicate if the distance between them was less than 5 km. Also shown in Fig. 63 for the 24 m EVD are the probability skip-zones, which can be used to asses ranges of good or bad communications between assets based on an accepted probability of communications.

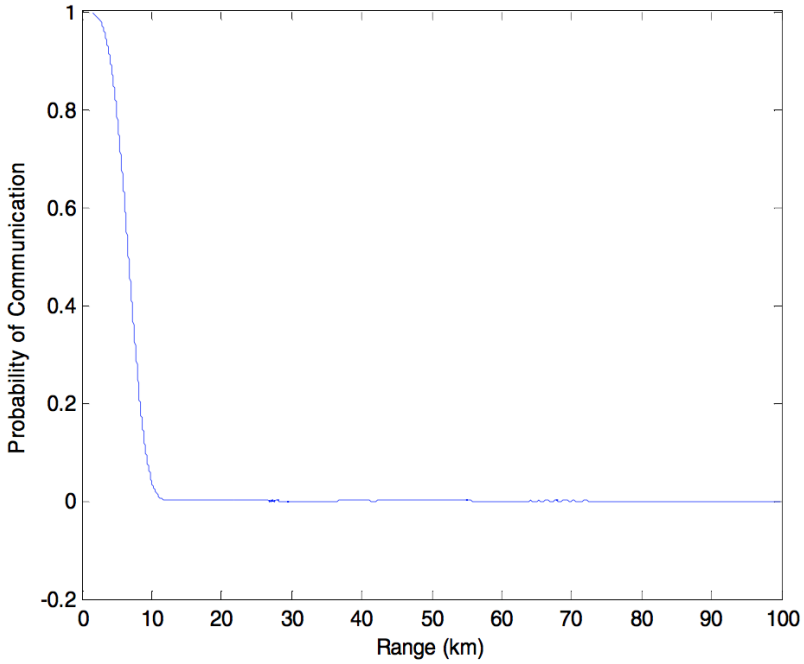


**Figure 62:** Probability of communications for USV-to-USV link in a 14 m EVD.

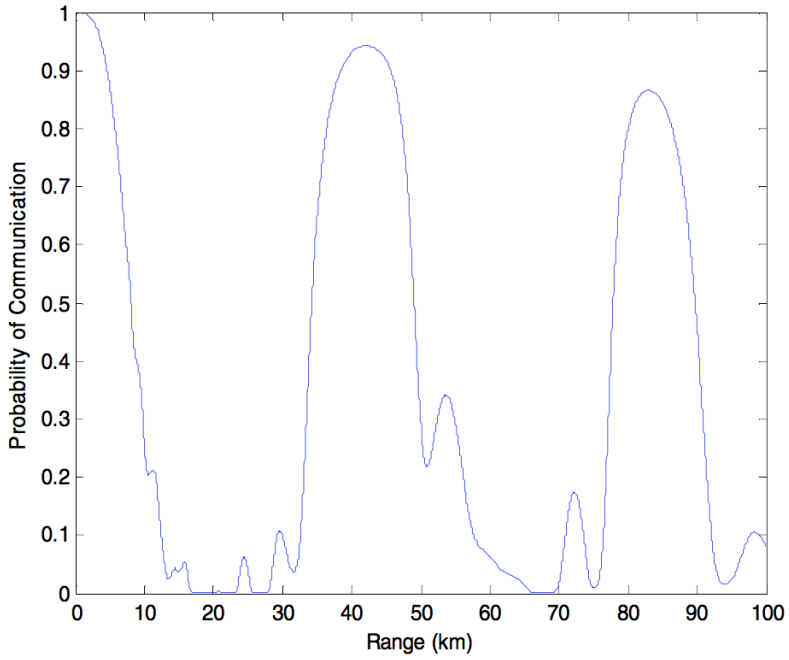


**Figure 63:** Probability of communications for USV-to-USV link in a 24 m EVD.

#### *3.1.7.3 Probabilistic Modeling Guidelines*

The result of Exp1 Part B is a study of the Nakagami-m statistics on the modeling of fading intensities corresponding to different atmospheric conditions found uniquely

in maritime environments. Such atmospheric conditions include evaporation ducts, surface-based ducts, elevated ducts, and other special refractivity conditions.

As shown in our results, the impact of the Nakagami parameter $m$ on the intensity of the fading has been demonstrated in [39] for two fast Nakagami-m fading channel and one slow Gamma fading channel. Their results show that, in general, as the parameter $m$ increases, the smaller the variance and the larger the skewness of the Nakagami distribution. Also, the outage probability, prescribed from the threshold of communications limited by hardware constraints, show that better system performance can be reached in areas of higher $m$ values, namely when desired signal propagates through less severe fading environment. This can be used as general trends when choosing communications hardware and when performing asset allocation during COA development.

When empirical data is available for a given environmental condition, the m-parameter estimation can be made via two major statistical methods used in the literature: (1) method of moments (MoM), and (2) maximum likelihood (ML). In [14], three MoM-based methods were used to find the $m$ parameter that fit a given empirical data. Their results showed that the inverse normalized variance estimator resulted in a better fit, while the Tolparev-Polyakov estimator [209] showed larger sample confidence regions, and the Lorenz estimator [136] showed a positive increasing bias as $m$ was increased. On the other hand, in [56] two ML estimators are compared to the normalized variance MoM estimator from [14] and are shown to have smaller variance. These methods can be used to estimate parameter $m$ and their goodness of fit to the APM deterministic calculation can be compared. Other more general methods may be applied as well, such as the Generalized Moment Estimators, as was used in [57], where real (integer and non-integer) sample moments were used for the derivation of the parameter $m$. These moment calculations are generally more complicated to compute, but may be a possible solution to the parameter $m$

estimation.

### 3.1.8 Ranges of Good Communications

With the capability of modeling the quality of the transmission channel probabilistically with the aid of the APM deterministic approach and the Nakagami-m probability methods, we can now define ranges of acceptable quality of transmission channel links. These ranges of good communications are based on a secondary threshold called the *Probability of good communications threshold* and will be denoted by $Pr_{th}$ from now on. For a given $Pr_{th}$, the probability of communications for each link between a given transmitter and receiver will be compared to this threshold and ranges where the probability of communications is greater than this thresholds will be considered ranges of good communications. In other words:

$$Ranges of communications = \begin{cases} good, & \text{if } Pr(comms, r) \geq Pr_{th} \\ bad, & \text{otherwise} \end{cases}$$

The plots of ranges of good communications will be plots showing distances where vehicles have good communications based on this threshold condition for all azimuths. A depicted plot of ranges of good communications was is shown in Fig. 64 for the main ship emitted signal and trying to communicate with an asset within a target area.

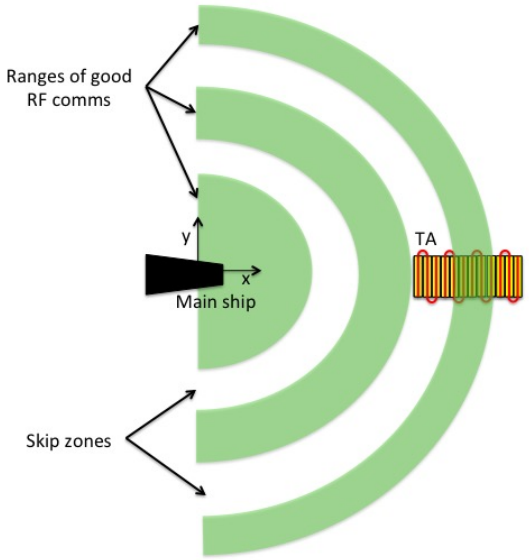


**Figure 64:** Depiction of ranges of good communications and skip zones between main ship and an asset.

These plots will be use throughout this demonstration study to visualize the operational environment and to perform asset allocation.

### 3.1.9 Finite State Markov Channel (FSMC)

In order to take into account the time-variation mechanisms of the channel due to relative UxV motion, which leads to doppler effects, a Finite State Markov Channel (FSMC) model can be used. Based on the Gilbert-Elliot channel model [97] [85], and demonstrated to be effective in the modeling of fading channels [219], FSMC is a probabilistic state transition model implemented in ACF-UV by partitioning the range of the fading amplitude into a finite number of intervals, for which each state is represented as an application-defined communications channel quality [219]. In the FSMC each state represents a defined channel quality. The Gilbert-Elliot channel model represents the special case in which there are two states. Each of these states is represented by a crossover probability which identifies the stability of each channel.

As was stated in the *Fading Channel Modeling* section, we assume a slow time-varying fading channel with flat fading. For these flat-fading channels, there are two important aspects that are studied in the wireless communications community. First, is the channel observation equation, which relates the channel input to the channel output, and is focused on being able to interpret the transmitted signal at the receiver. The second aspect, and key to the FSMC model, is the time-varying nature of the fading channel. A schematic of the discrete-time communications system under consideration is shown in Fig. 65. In a flat-fading channel, all frequency components of the transmitted signal will experience a similar fading fain attenuation. The received signal is sampled at the receiver side at times $t_l = lT_s$ with symbol time $T_s$. Lets denote the channel input as $x_l$, the channel output as $y_l$, and the fading channel gain by $h_l$. Also, lets assume a an AWGN complex valued signal, denoted by $z_l$, with variance $N_0/2$, as was described in the *Fading Channel Modeling* section. The observed signal at the receiver is composed of

$$y_l = h_l x_l + z_l \tag{50}$$

The fading channel gain $h_l$ is a complex-valued random variable with in phase (real) and quadrature (imaginary) components: $h_l = h_{i,l} + jh_{q,l}$, as denoted in [219]. In polar form, the magnitude and phase of the fading channel gain are denoted by $a_l$ and $\theta_l$, respectively: $h_l = a_l e^{j\theta_l}$. We refer to $a_l$ as the fading channel amplitude, and $\theta_l$ as the fading channel phase. If the mean of the fading channel gain, denoted $h_m$, is zero, the fading process is called *Rayleigh* fading, as was described in *Fading Channel Modeling* section. Otherwise, if it is non-zero, that is, if there is a line-of-sight fading amplitude, then it is called *Rician* fading. As was described in *Fading Channel Modeling* section, the Nakagami-m distribution provides a more robust statistical representation of the fading channel that can model different environmental conditions.

The communications channel is a dynamic system where the fading channel gain $h_l$ is a random process that changes over time in a correlated manner. Therefore,

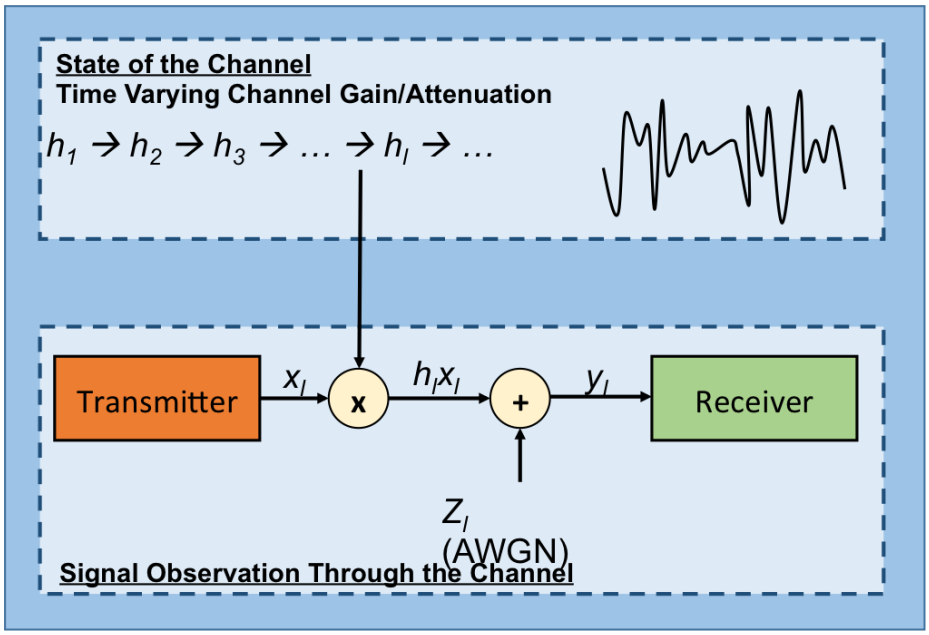


**Figure 65:** Communications system diagram for flat-fading channel under consideration

tractable mathematical models are required to accurately describe time variations of the fading channel gain and its dynamics. One such model is the Clarke's model [60], which is one of the most widely used statistical model for describing the fading random process. In this model, the in-phase and imaginary components of the fading channel gain are intra-correlated and the autocorrelation function is given as [60]

$$\rho = J_0^2(2\pi f_d T_s) \tag{51}$$

where $f_d$ is the maximum *Doppler* frequency, $T_s$ is the symbol time, and $J_0(\cdot)$ is the zero-order *Bessel* function of the first kind. For the observation equation in (50) to be valid, we assumed that the channel gain $h_l$ stays more or less constant during each symbol transmission, which excludes fast time-varying flat-fading channels where the channel coherence time $T_0 \approx \frac{1}{f_d}$ is less than the symbol time $T_s$. Fast fading channels, however, are not common in the majority of practical RF communication systems, where the channel coherence time is at least a few times larger than the symbol period.

A diagram of the FSMC model is shown in Fig. 66 for some discrete time index $l$. The stochastic component of the FSMC model is the state $s_l$. The number of FSMC states is assumed to be finite and equal to $K$. In Fig. 66, at some time index $l$, the state of the channel is equal to an arbitrary state $s_l = m \in \{0, ..., K-1\}$. The channel state is the output of a Markovian chain, where the state transition probability is the probability of moving from state $k$ to state $m$ and is denoted by

$$P_{k \to m} = Pr(S_l = m | S_{l-1} = k) \tag{52}$$

The channel state transition probability matrix is a $K \times K$ matrix given by

$$\mathbf{P} = \begin{bmatrix} P_{0\to 0} & \cdots & P_{0\to(K-1)} \\ \vdots & \ddots & \vdots \\ P_{(K-1)\to 0} & \cdots & P_{(K-1)\to(K-1)} \end{bmatrix} \tag{53}$$

For this study, we will assume that the Markov state process is stationary and, therefore, that the state transition probability is independent of time index $l$. This is a reasonable assumption in many practical communication channels, where the channel statistics do not change rapidly over time. Denoting the stationary probability of being in state $k$ by $\pi_k = Pr(s = k)$, then an important property of the state transition probability matrix is that the stationary state probability vector $\pi = [\pi_0, ..., \pi_{K-1}]^T$ is the solution to the eigenvalue equation given by

$$\mathbf{P}^T \pi = \pi \tag{54}$$

The other stochastic process in the FSMC model is the one that probabilistically maps the channel input $x_l$ to the channel output $y_l$ at each channel state $s_l$, shown in the middle section of the FSMC diagram shown in Fig. 66. For each FSMC state, there corresponds a memoryless channel which determines the channel's input-output relationship. This probabilistic relationship is known as the channel observation law, and is denoted by $Pr(y_l | x_l, s_l)$. Note that the channel observation law is independent of time index $l$ because of the assumption of stationary fading channel states.

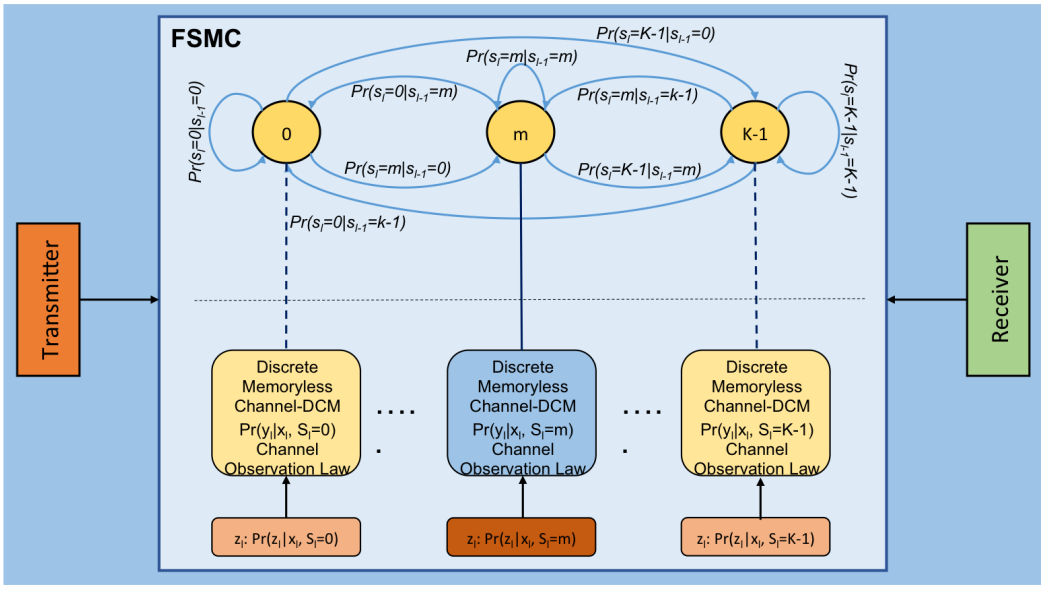


**Figure 66:** FSMC diagram for some discrete time index $l$

It is often useful to introduce the FSMC error or noise $z_l$, which is a function of the current channel input and output, $z_l = f(x_l, y_l)$. The corresponding error probability is given by $Pr(z_l|x_l, s_l)$, which is shown in the lower part of the FSMC diagram in Fig. 66.This FSMC error probability often depends on the type of modulation used by the transmitter, the physical law that governs the he channel input-output relationship, and the type of detection at the receiver.

### 3.1.10 Experiment 2, Part C: Finite State Markov Channel (FCMC) Modeling and Simulation of Network Stability

The FSMC model provides the methods for quantifying and assessing the stability of the communications channel from time-variations in the signal intensity due to asset motion. For this experiment, we again state the assumption that we only consider slow time-varying flat-fading channels (frequency non-selective), which simplifies the FSMC modeling by ignoring complex state transitions that can happen when the coherence bandwidth is less than the signal bandwidth.

For this study, we will define the states of the flat-fading transmission channels as non-overlapping ranges of the signal fading amplitude, as is done by Guan and Turner

[100], and we will ignore the channel phase states which is mainly used in applications where the channel phase can be estimated and compensated prior to decoding [132] [124] [169].

The key benefit of the FSMC for this demonstration study lies in the computation of the state transition probabilities. With the states defined as ranges of the fading signal amplitude, the state transition probabilities provide a way to quantify how stable is each transmission channel in terms of staying within good states that meet our acceptable threshold requirements. The state transition probabilities are computed from the probability model we use to represent the small-scale fading mechanisms. In the next discussion, we will define the state transition probabilities in terms of the general Nakagami-m probability model to keep our modeling open to different signal fluctuation cases.

#### *3.1.10.1 Modeling the Fading Signal Amplitude States*

The transition probability of the Nakagami-m fading channel can be computed using the conditional probability $Pr(x|y)$ that the fading channel is in state $x$ at time $t+1$ given that it was in state $y$ at time $t$:

$$Pr_{x,y}(x|y) = \frac{Pr(x,y)}{Pr_y(y)} \tag{55}$$

Consider two samples of the Nakagami-m fading envelope given by $x = X(t_1)$ and $y = Y(t_2)$. The corresponding instantaneous power levels for the fading envelope are $W_x = X^2$ and $W_y = Y^2$. The joint probability density function of the non-negative random variables $x$ and $y$ can be computed using the derivation provided in [100] as

$$Pr(x,y) = \frac{4(xy)^m exp[-\frac{m}{\Omega}\frac{x^2+y^2}{1-\rho}]}{\Gamma(m)(1-\rho)(\sqrt{\rho})^{m-1}}(\frac{m}{\Omega})^{m+1} I_{m-1}[\frac{2mxy\sqrt{\rho}}{\Omega(1-\rho)}], x, y \geq 0 \tag{56}$$

where $I_m\{\cdot\}$ is the m-th order modified *Bessel* function of the first kind, and where $\rho$ is the correlation coefficient given by

$$\rho = \frac{Cov(x^2, y^2)}{\sqrt{Var(x^2)Var(y^2)}} \tag{57}$$

When samples $X$ and $Y$ are taken $T_s$ seconds apart due to the movements of the UxVs, as was given in Eq. (51) based on Clarke's method [60], the correlation coefficient is given by

$$\rho = J_0^2(2\pi f_d T_s) \tag{58}$$

where $J_0$ is the Bessel function of the first kind of zero order, and $f_d$ is the maximum Doppler frequency. Substituting the joint pdf $Pr(x, y)$ into Eq. (55), an expression for the conditional probability can be generated as

$$Pr_{x|y}(x|y) = \frac{2\Omega^{m-1}x^m exp(\frac{\rho x^2+\rho y^2}{(1-\rho)\Omega})}{y^{m-1}\Omega(1-\rho)(\Omega^2\rho)^{\frac{m-1}{2}})} I_{m-1}\{\frac{2xy\sqrt{\rho}}{\Omega(1-\rho)}\} \tag{59}$$

where $I_m\{\cdot\}$ is the m-th order modified *Bessel* function of the first kind.

We now define the states. Lets define states $k$ and $j$ for which the conditional probability of Eq. 59 is the probability that the fading signal amplitude power level $x_k$ is in state $k$ at time $t_k$ having just being in state $j$, denoted $y_j$, at time $t_j$. We are now able to compute both adjacent and non-adjacent state transition probabilities by integrating the conditional probability density function given by

$$Pr(k|j) = \frac{\int_{\sqrt{S_j}}^{\sqrt{S_{j+1}}} \int_{\sqrt{S_k}}^{\sqrt{S_{k+1}}} Pr(x, y)dxdy}{\int_{S_j}^{S_{j+1}} Pr(y)dy} \tag{60}$$

Where $S_j = (V_j, V_{j+1}]$, and $V_j$ and $V_{j+1}$ represent the boundaries of the state $S_j$. Finally, the probability $Pr(y)$ is the Nakagami-m probability function given by Eq. (30), and repeated here with $Y$ as the random variable for quick reference:

$$P_{Nak}(y, m) = (\frac{2m^m y^{2m-1}}{\Gamma(m)\Omega^m}) \exp(-\frac{my^2}{\Omega}), y \geq 0 \tag{61}$$

With this state representation, we can now compute the probability that the fading signal amplitude $\chi$ is in state $k$ given that it was previously in state $j$.

#### *3.1.10.2 FSMC Simulation and Validation*

In [219], Wang et. al. used the Rayleigh fading channel to model small-scale fading and calculated the SNR of the received signal to discretize the states into ranges

of SNR values. They calculated the state-transition probabilities assuming a steady state probability of cross-over for each neighbor state. They did not consider the state transitions to non-neighboring states.

On the other hand, in [100], Guan and Turner did consider the state transition probabilities of neighboring and non-neighboring states. They used the general Nakagami-m fading model, and defined the states as the fading amplitudes of the signal.

In this small case study we simulate the FSMC under the conditions described by Wang et. al. [219], and by Guan and Turner [100] by modeling the FSMC under a Rayleigh fading channel. The conditions simulated in both papers are the following:

- $m = 1$ (Rayleigh fading probability model).
- $T_s = 10^{-5}$ sec (channel symbol duration)
- $f_d = 10$ (Maximum Doppler frequency)

In each study, eight equi-probable channel states were defined, with lower and upper boundaries $(V_j, V_{j+1}]$ defined in terms of either SNR values or fading amplitude of the signal. The actual values of the boundaries for each state do not matter for this validation study, as long as each state is equally probable, since we are only concerned about the state transition probabilities. Therefore, without loss of generality, we set each state to be $Pr(S_j = k) = 1/8$, that is equally probable. The initial boundary was set to 0, and the final boundary is set to $\infty$. Shown in Fig. 67 are the state transition probabilities approximated by Wang. Note that the sum of the rows is equal to 1, as it is required. Guan and Turner state transition probabilities are shon in Fig. 68. And our simulation calculations of the state transition probabilities are shown in Fig. 69. Note that our state transition probabilities match exactly with Guan and Turner, since we used the same methods. The differences between our

| States j -> k | j = 0 | j = 1 | j = 2 | j = 3 | j = 4 | j = 5 | j = 6 | j = 7 |
|---|---|---|---|---|---|---|---|---|
| k = 0 | 0.993588 | 0.006412 | 0 | 0 | 0 | 0 | 0 | 0 |
| k = 1 | 0.006412 | 0.985521 | 0.008067 | 0 | 0 | 0 | 0 | 0 |
| k = 2 | 0 | 0.008067 | 0.983341 | 0.008592 | 0 | 0 | 0 | 0 |
| k = 3 | 0 | 0 | 0.008592 | 0.983060 | 0.008348 | 0 | 0 | 0 |
| k = 4 | 0 | 0 | 0 | 0.008348 | 0.984205 | 0.007447 | 0 | 0 |
| k = 5 | 0 | 0 | 0 | 0 | 0.007447 | 0.986650 | 0.005903 | 0 |
| k = 6 | 0 | 0 | 0 | 0 | 0 | 0.005903 | 0.990483 | 0.003615 |
| k = 7 | 0 | 0 | 0 | 0 | 0 | 0 | 0.003615 | 0.996385 |

**Figure 67:** State-transition probabilities calculated by Wang et. al. [219].

| States j -> k | j = 0 | j = 1 | j = 2 | j = 3 | j = 4 | j = 5 | j = 6 | j = 7 |
|---|---|---|---|---|---|---|---|---|
| k = 0 | 0.993546 | 0.006454 | 0 | 0 | 0 | 0 | 0 | 0 |
| k = 1 | 0.006454 | 0.985426 | 0.008120 | 0 | 0 | 0 | 0 | 0 |
| k = 2 | 0 | 0.008120 | 0.983231 | 0.008649 | 0 | 0 | 0 | 0 |
| k = 3 | 0 | 0 | 0.008649 | 0.982948 | 0.008403 | 0 | 0 | 0 |
| k = 4 | 0 | 0 | 0 | 0.008403 | 0.984101 | 0.007497 | 0 | 0 |
| k = 5 | 0 | 0 | 0 | 0 | 0.007497 | 0.986562 | 0.005942 | 0 |
| k = 6 | 0 | 0 | 0 | 0 | 0 | 0.005942 | 0.990420 | 0.003638 |
| k = 7 | 0 | 0 | 0 | 0 | 0 | 0 | 0.003638 | 0.996362 |

**Figure 68:** State-transition probabilities calculated by Guan and Turner et. al. [100].

| States j -> k | j = 0 | j = 1 | j = 2 | j = 3 | j = 4 | j = 5 | j = 6 | j = 7 |
|---|---|---|---|---|---|---|---|---|
| k = 0 | 0.993546 | 0.006454 | 0 | 0 | 0 | 0 | 0 | 0 |
| k = 1 | 0.006454 | 0.985426 | 0.008120 | 0 | 0 | 0 | 0 | 0 |
| k = 2 | 0 | 0.008120 | 0.983231 | 0.008649 | 0 | 0 | 0 | 0 |
| k = 3 | 0 | 0 | 0.008649 | 0.982948 | 0.008403 | 0 | 0 | 0 |
| k = 4 | 0 | 0 | 0 | 0.008403 | 0.984101 | 0.007497 | 0 | 0 |
| k = 5 | 0 | 0 | 0 | 0 | 0.007497 | 0.986562 | 0.005942 | 0 |
| k = 6 | 0 | 0 | 0 | 0 | 0 | 0.005942 | 0.990420 | 0.003638 |
| k = 7 | 0 | 0 | 0 | 0 | 0 | 0 | 0.003638 | 0.996362 |

**Figure 69:** State-transition probabilities calculated with our simulations.

simulations and the approximations by Wang can be due to the fact that our model is more general and predicts non-neighboring state transitions.

Next we simulate the Nakagami-m fading channel model with our FSMC framework. The parameters used are as follows:

- $m = 1$ and $m = 2$
- $\Omega = -129dB$ Expected (mean) fading amplitude of signal
- $f_d T_s = 0.05$ (product of Max Doppler frequency and sampling time)

Five states were assumed, partitioned as follows: $S_0 = (-\infty dB, -133dB]$, $S_1 = (-133dB, -131dB]$, $S_2 = (-129dB, -127dB]$, $S_3 = (-127dB, -125dB]$, and $S_4 = (-125dB, 0dB]$. As the UxVs traverse their paths they go through a series of good and bad communication zones. At each distance on their motion, the APM model calculates the large scale fading propagation losses, and the small scale fading of the signal of the transmitted signal. Using the threshold of communications, set by both the minimum received power of the MPU5 radio, and the threshold of probability of communications, the FSMC model is used to predict the probability of the data packets contained within the signal envelope$x$, that have a reception power less than the computed threshold propagation loss value. The results of the simulation are presented in Figs. 70 and 71. From the two figures, it can be seen that the state transition probabilities for the Nakagami-m probability model with $m = 1$ are more spread out than the state transition probabilities with $m = 2$, which is expected since the higher the $m$ value, the less the signal fluctuations we should expect. Note also that now we have state transitions to non-neighboring state occurring for each case. Since the maximum doppler frequency was increased, the effect was greater signal attenuation due to the time-variation of the signal. Note also that, overall, state transition probabilities to neighboring states are higher than non-neighboring states,

| States j→k | J = 0 | J = 1 | J= 2 | J = 3 | J = 4 |
|---|---|---|---|---|---|
| K = 0 | 0.8393 | 0.3052 | 0.0596 | 0.0024 | 0 |
| K = 1 | 0.1297 | 0.3898 | 0.2280 | 0.0311 | 0.0002 |
| K = 2 | 0.0298 | 0.2683 | 0.4663 | 0.2360 | 0.0095 |
| K = 3 | 0.0012 | 0.0363 | 0.2342 | 0.5453 | 0.1472 |
| K = 4 | 0 | 0.0003 | 0.0119 | 0.1852 | 0.8431 |

**Figure 70:** State-transition probabilities with $\Omega = -129dB$ and m = 1.

| States j→k | J = 0 | J = 1 | J= 2 | J = 3 | J = 4 |
|---|---|---|---|---|---|
| K = 0 | 0.7909 | 0.2133 | 0.0148 | 0 | 0 |
| K = 1 | 0.1908 | 0.5128 | 0.1919 | 0.0066 | 0 |
| K = 2 | 0.0183 | 0.2649 | 0.5961 | 0.1988 | 0.0018 |
| K = 3 | 0 | 0.009 | 0.1958 | 0.6680 | 0.1667 |
| K = 4 | 0 | 0 | 0.0014 | 0.1265 | 0.8315 |

**Figure 71:** State-transition probabilities with $\Omega = -129dB$ and m = 2.

which is over all expected given that the signal fluctuation will vary about the mean propagation loss value.

#### *3.1.10.3 FSMC Implementation to Quantify Channel Stability*

Now that we have validated our FSMC model, and provided some test cases for the applicability of the state transition probabilities, we can apply it to our methodology to help us quantify the stability of the transmission channel, and later used to quantify the stability of the communications network.

To make the description of the implementation easier to follow, a simple example will be used throughout this discussion. Consider a UUV trying to communicate back to the main ship (MS). Assume it has the antenna height at 0.5 m from the sea surface, and the MS has a receiver antenna at 21 m, as described in Table 22. Assuming a 24 m EVD, and the radio specifications for the MPU5 COTS radio, given in Table 11. The first step is to use APM to calculate the large-scale fading propagation losses due to the environmental conditions. The propagation loss profile as a function of range and height, and the propagation loss experience at the MS receiver height as a function of range were shown in Fig. 126, and are repeated here for reference 72. The next step was to predict the small scale-fading using our Nakagami-m probability

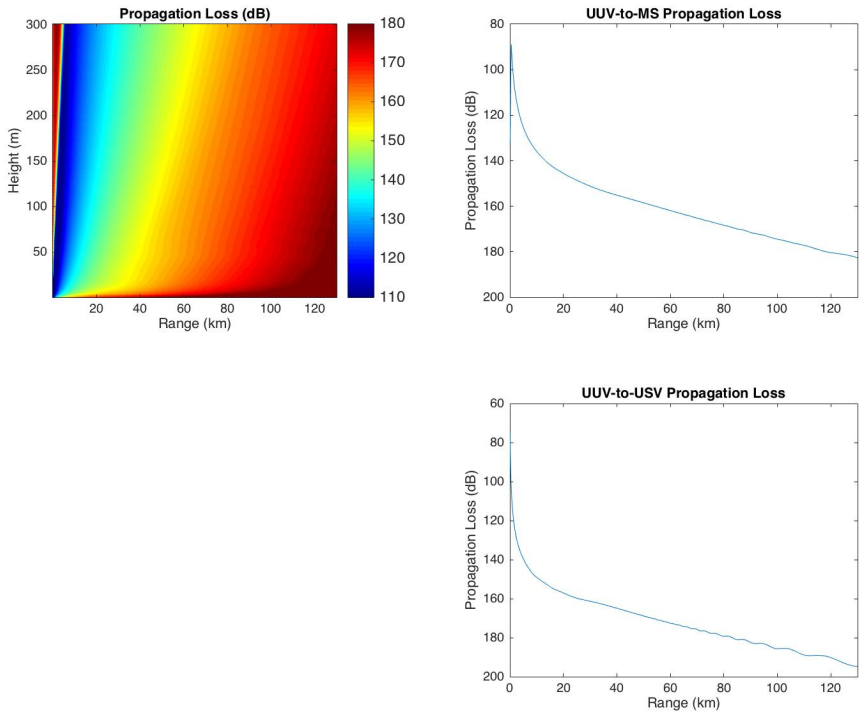


**Figure 72:** Propagation loss profile and corresponding propagation losses for UUV-to-MS and UUV-to-USV links under a 24 m EVD.

model for the fading signal intensity fluctuation. In order to do this, we first used the link-budget equation as a function of distance between transmitter and receiver,

given by

$$P_R(r) = P_T + G_T + G_R - L_{APM}(r) - L_{sys} - L_{cp} \tag{62}$$

Given that the threshold of communications is represented by the minimum receiver power sensitivity threshold of the MPU5, we formulate this condition as the received power being greater than this minimum threshold value:

$$P_{rec_{min}} \leq P_R(r) = P_T + G_T + G_R - L_{APM}(r) - L_{sys} - L_{cp} \tag{63}$$

Solving for $L_{APM}(r)$ gives us an equation based on the condition for the large scale fading propagation loss calculated by APM as

$$L_{APM}(r) \leq P_T + G_T + G_R - L_{sys} - L_{cp} - P_{rec_{min}} = L_{APM_{max}} \tag{64}$$

We then use this maximum propagation loss threshold given by $L_{APM_{max}}$ to calculate the outage probability, that we called the probability of communications, as

$$Pr(comms, r) = 1 - \int_0^{L_{APM_{max}}} (\frac{2m^m \chi^{2m-1}}{\Gamma(m)\Omega^m}) \exp(-\frac{m\chi^2}{\Omega}) d\chi \tag{65}$$

Using the Rayleigh probability model, given by setting $m = 1$, and the average signal fading intensity, given by the APM value $\Omega = L_{APM}(r)$, we integrate and calculate the probability of communications as a function of distance r. We can also track the received power level from the link budget Eq. 62. The results are shown in Fig. 73 This plot is used to determine link quality in terms of the probability of communications at any given range, and determine ranges of good communications given by ranges where the probability of communication is above the threshold probability of communications. But we have no way of determining how stable this link is to the motion of the vehicles as they perform their tasks in the operational environment. That is, the UUV can be at a good communications range, and yet the signal can be unstable enough due to relative motions that the signal can fall below the minimum receiver sensitivity threshold.

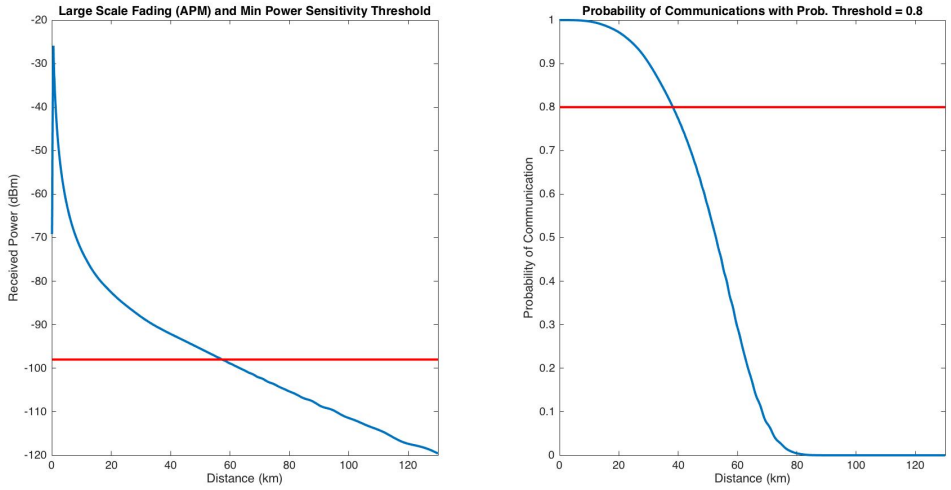


**Figure 73:** UUV-to-MS received power and minimum threshold received power (left), probability of communications and threshold probability of communications (right) in a 24 m EVD.

Therefore, our approach to measure link stability using the FSMC framework is as follows. Using the link budget equation for the threshold maximum propagation loss $L_{APMmax}$ and the values assumed here for hte MPU5 and our assumed gains and losses, we have

$$L_{APM_{max}} = P_T + G_T + G_R - L_{sys} - L_{cp} - P_{rec_{min}} \tag{66}$$

$$= 33.01dBm + 25dBm + 3dBm - 3dBm - 3dBm - (-98dBm) = 153dBm \tag{67}$$

Then we define the states as ranges of fading signal amplitudes nearby this $L_{APM_{max}}$ value. We will discretize the fading signal amplitude around this value into 6 states in such a way that stability can be defined as being 2 dBm away from this threshold value. Therefore we define the states as: $S_0 = (-\infty, -153]$, $S_1 = (-153, -151]$, $S_2 = (-151, -149]$, $S_3 = (-149, -147]$, $S_4 = (-147, -145]$, $S_5 = (-145, 0]$ dBm. Any signal amplitude that lies within the first state $S_0$ is considered unstable, since it violates the threshold propagation loss signal amplitude. Therefore this state will be defined as the unstable state. A signal amplitude that lies in the second state $S_1$ will be considered marginally stable, since it meets the threshold propagation loss signal

amplitude condition, but given that state transition probabilities to neighboring states are overall higher, it has a high probability of transitioning to the neighbor state $S_0$ which is unstable. Any signal amplitude that lies in states $S_2$, $S_3$, $S_4$, or $S_5$ will be considered stable. These stability conditions are shown in Fig. 74.

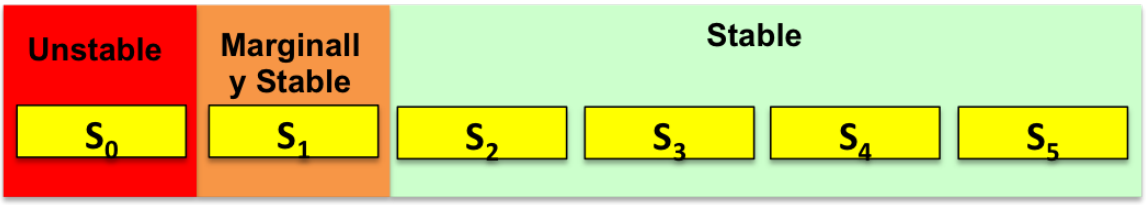


**Figure 74:** FSMC stability conditions.

Given that the average fading signal amplitude calculated by APM $\Omega = L_{APM}$ is a function of the distance between transmitter and receiver, the state transition probabilities are calculated for each distance to determine if communications link is stable. For the UUV-to-MS link, under the 24 m EVD, we calculate the state transition probabilities with the 6 states that were defined. We use the Rayleigh fading probability model, and the same value for the maximum Doppler frequency and sampling time given by $f_d T_s = 0.05$. The results shown in Fig. 75 provide the state of the transmission channel for the UUV-to-MS link as a function of distance between these two vehicles. Assuming the marginally stable state is also considered a bad state, also shown in Fig. 75 is whether the link is in a stable (1) or unstable (and marginally stable) (0) state. We also show in the same figure the sum of the columns of the state transition probability matrix, which helps quantify how stable the link is at each range. As can be seen in the plot of Stability vs. Distance, the link becomes unstable at about 30 km, and stays unstable at any higher distance, since from looking at the State vs. Distance plot, the state of the transmission channel jumps to the marginally stable state at that distance. Comparing this plot to the probability of communications vs. range, if we solely rely on the quality of the link based on the probability of communications, we would say that we can communicate

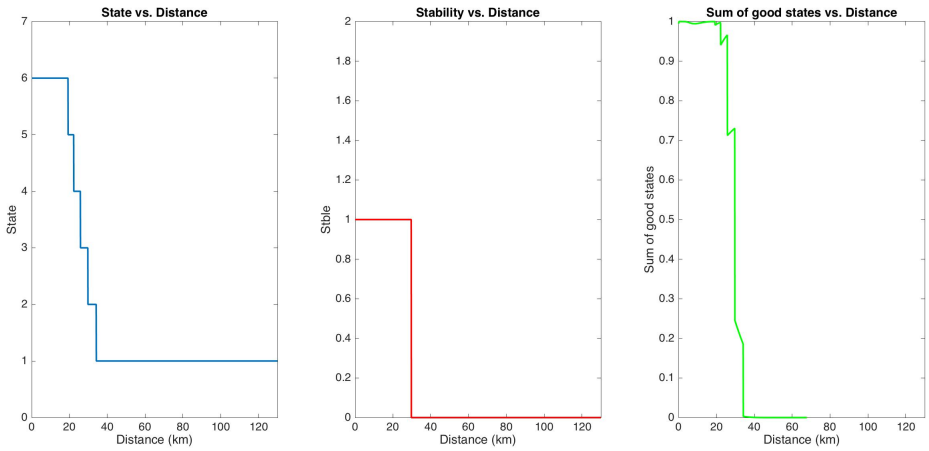


**Figure 75:** FSMC stability test for UUV-to-MS link under a 24 m EVD.

at any distance below 45 km since the $Pr_{th} = 0.8$ threshold was met. However, when looking at the stability of the channel, we deduce that we can only communicate at distances less than 30 km.

The sum of the good states, shown in the 3rd plot in Fig. Fig. 75 can be used to quantify how stable the link is under the given environmental conditions. We will use this information in the communications network analyses to find network topologies that are more stable than others.

## *3.2 Experimental Results and Hypothesis Validation*

From our proposed methodology, our second research question and corresponding hypothesis were the following:

**Research Question 2 (RQ2)**: *How can the fading channel be modeled such that it captures multipath effects and time-variant mechanisms due to relative vehicle motion that is robust to environmental conditions uncertainty and fading fluctuations?*

**Hypothesis 2 (HP2)**: *Given communication constraints that reflect communications hardware limitations, a probability model will provide a robust fading channel*

*model that takes into account multi-path and Doppler effects.*

We showed during the Transmission Channel Modeling that APM can be used to model the large-scale fading mechanims due to the free-space propagation and the multipath created by the refractivity structure of the environment. We used the Rayleigh fading probability model due to the lack of empirical data to fit a more general Nakagami-m probability model, but we left the rest of the statistical modeling and analysis based on this general Nakagami model for future expansion. The time variations of the signal were simulated and validated through a modeled Rayleigh channel and assuming flat-fading non-frequency selective fading. FSMC provided the probability methods to measure stability of the signal due to time-variations of the signal fading amplitude, and the model was validated and simulated through the general Nakagami-m probability model under different signal fluctuation intensities conditions. The links were deemed as robust to environmental conditions in the sense that we set a high threshold of probability of communications to take into account environmental refractivity time variations and modeling errors. Links that met this probability threshold, were more robust to fading signal intensities that could violate a threshold based solely on the receiver specifications, such as the minimum receiver power assumed for our COTS radio. We could not validate Hypothesis HP2 entirely since we could not model a wide range of fluctuation intensities through the m-parameter of the Nakagami probability distribution, mainly due to the lack of empirical data. But we were able to concentrate on a special case of the Nakagami-m probability model, with $m = 1$ and regarded as one of the worse wireless communications conditions, to demonstrate the benefits of small-scale fading channel predictions.

# CHAPTER IV

# COMMUNICATIONS NETWORK

In this chapter, literature background, methods, and models are presented for representing communication networks and analyzing them. This is an important step in the COA Analysis process, shown in Fig. 76, where the composition of links between unmanned vehicles is analyzed to make sure communication is established. Methods are presented to describe the communications network in terms of connectivity, stability, robustness, and reliability.

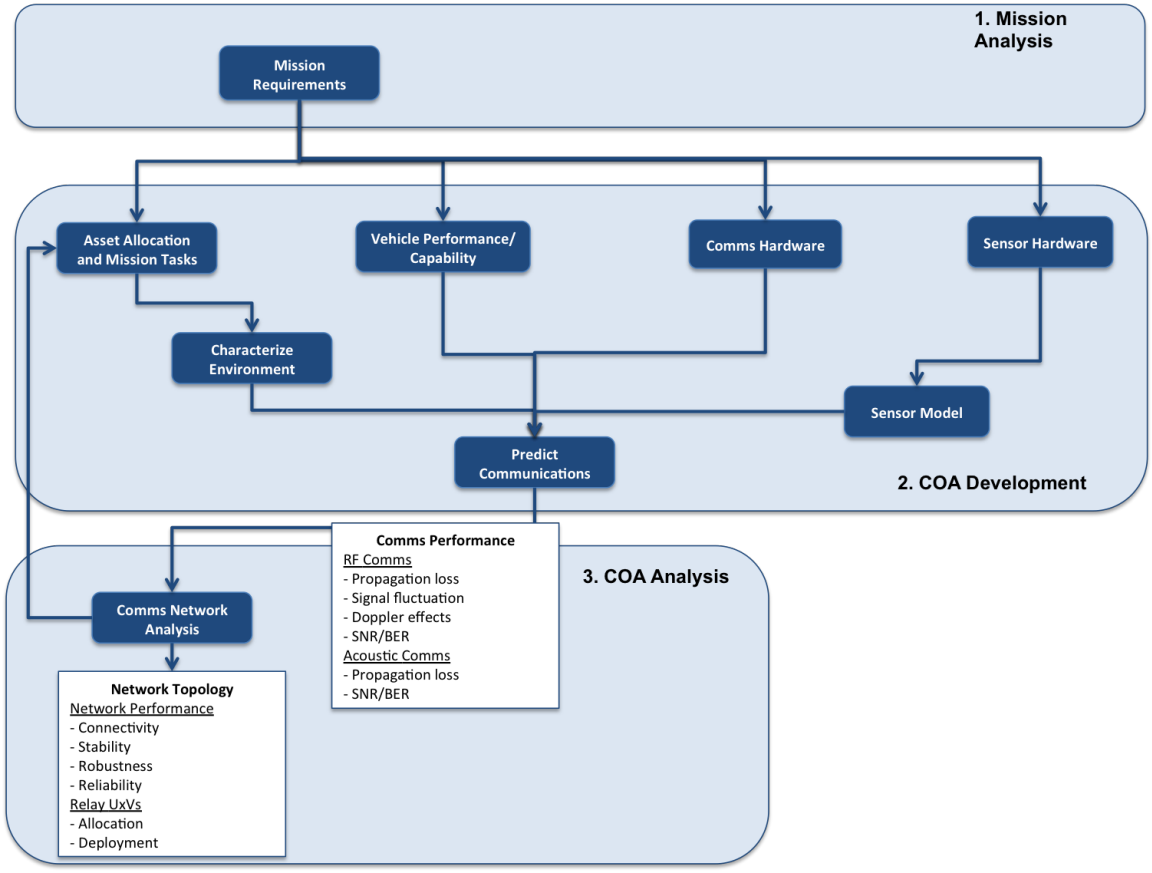


**Figure 76:** Communications network analysis step of the COA Analysis process

## *4.1 Graph Theory for Representing Communication Networks*

Graph theory has been used extensively to model communication networks, where nodes represent vehicles or agents (e.g., UxVs, sensors) and the edges represent the interactions between them (e.g., communication link). These networks can be centralized or descentralized, global or local information.

Communication networks play an important role in achieving various multiagent coordination tasks (e.g., [114], [225], [226]). The performance of sensor networks is highly dependent on the connectivity requirements of the networks [121]. Network connectivity is also critical for surveillance missions, where agents operate away from base and need to stream the surveillance data back to the base through multi-hop communications (e.g., [52] [163]). When a communication link between the nodes fails, there is no guaranteed that the network will remain connected. Therefore, there has been a growing interest for developing strategies that help maintain connectivity in networked systems.

Literature has many examples of the use of graph theory for connectivity control of mobile systems in cases of edge failure including optimization based connectivity control [225], continuous feedback connectivity control [174], and control based on the estimation of the algebraic connectivity [175]. The number of nodes in each of these studies was considered constant, which is not always the case (e.g., when a node is removed), and the uncertainty of the edges was also considered. There has also been a significant interest in addressing agent loss problem in networked systems. In [148], [197] and [31], the focus is on the design of robust network topologies that can tolerate a finite number of agent removals, and propose self-repair strategies that create new connections among the neighbors of the failing agents.

Other studies consider agent motion for connectivity restoration. Some relevant work has been done on distributed connectivity recovery of wireless sensor networks

in agent failure situations. In [16], [12], and [81] the authors propose a set of cascaded replacements for the recovery of network connectivity. Alternatively, the authors of [13] propose block movement of agents instead of cascaded replacements, and their algorithm not only restores connectivity but also does not extend the shortest paths among agents after a failure. In other words, a disconnection due to an agent failure may not be prevented by the remaining agents having too little information.

Also important is how critical is each node in the communication network. That is, if a node or link is removed from the network, how much does it affect the network? Agent criticality is a global type of information that may not be available to all nodes all the time. In [12] for example, it is assumed that each agent has knowledge of its criticality, whereas in [16] nodes do not contain that criticality information, and instead an algorithm given in [68] is used to compute the criticality of a node based on the connected dominating set (CDS) of the whole network. However the methods considered in [16] require large amounts of computation, specially when a topology change has to be made due to agent removal or addition, and refreshing CDS are also time expensive.

Node failure in sensor networks is also studied based on the assumption that agents send periodic heart beat messages (e.g. [13], [16], and [146]). If a heart beat message is not received by the neighbors of node $i$ for some period of time, then node $i$ is assumed dead by the neighbors. Whether these node removals are voluntary (node removal) or not (node failure), this leads to a new network that can be either connected, partially connected, or not connected.

In a networked system, a disconnection can be either avoided or fixed by proactive or reactive approaches, respectively. In proactive approaches, a robust network topology is designed a priori such that the network can tolerate a finite number of agent or link losses (e.g. [148] [83] and [197]). In reactive approaches on the other hand, a control strategy is developed to make sure the network self-repairs itself in

the face of node or edge removal (e.g. [13], and [16]).

Since the methodology involves finding COAs that are reliable to network failures, a network that maintains UxV communications connection in case of link failure(s) is desired. Therefore some of the methods described in the literature can be used to model communication loss as graph edge removal between the vehicles, and determining robust network configurations to ensure that the communication network is still connected to every UxV. The focus of this study is not on agent behavior in case of network failure, but rather to anticipate and assume such possible failures in advance during the mission planning phases and configure a network topology that ensures a reliable network. Therefore, proactive approaches are more suitable in this study. One approach will be to determine possible network topologies, based on asset availability, allocation, mission tasks, and communications predictions, that are reliable to communication link removals.

## *4.2 Communications Network Connectivity*

Whether the communication networks are centralized or not, communicate global or local information, communication networks are critical for teams of heterogeneous unmanned and autonomous vehicles coordination tasks and for providing sensory information to other vehicles or manned assets. Therefore, it is critical to determine whether vehicles are connected or not in a given network, and quantify the connectivity of the network.

First, some assumptions will be made about the graphs that will be considered in this study for modeling communication networks. We will assume that the graphs representing communication networks are composed of undirected links, meaning that direction does not matter: a transmitter can act as a receiver, and vice-versa. In reality, both the forward-link and backwards-links will be different because they will experience different attenuations from atmospheric refractivity variation in space and

time, but we make the assumption that the atmospheric refractivity structure is the same in each direction of azimuth from a transmitter or receiver, and that the refractivity structure stays constant over the time periods we are concerned. The second assumption is that the graphs representing communication networks are simple in the sense that no transmitters communicate with itself, it only communicates with other vehicles, and that no multiple links are used to connect two nodes.

A communications network can be modeled as an undirected graph $G(V, E)$, where $V = v_1, v_2, ..., v_n$ is the set of all nodes (vehicles) and $E = link_1, link_2, ..., link_m$ is the set of all edges (links). In this study, we use a similar approach used in [113] for determining if a communication link exists between nodes. In [113], a disk model is used, in which two nodes are connected if the distance between them is less than the transmission range. They assume all sensors have fixed transmission power and therefore fixed transmission radius. In our study however, the transmission channel is modeled in more detail and probabilistically using the Nakagami-m model. Either through specification of minimum receiver power from communications hardware, or a specified minimum SNR value or BER, a threshold of communications can be set [103]. Therefore, for this study we set a threshold probability of communications $\psi$ from the cumulative distribution function of the Nakagami-m model to determine ranges of good communications, taking into consideration that there might be multiple skip zones, and use this to determine if there is a link between two nodes. Hence, two nodes $v_i$ and $v_j$ are connected if the distance between them is within the ranges of good communications.

For an edge $l$, $1 \geq l \leq m$, connecting nodes $v_i$ and $v_j$, $\{v_i, v_j\} \in V$, define the vector $a_l \in \mathbf{R}^n$, where $a_{l,i} = 1$, $a_{l,j} = -1$, and the rest is zero. The *incidence matrix* $A \in \mathbf{R}^{n \times m}$ of the graph $G$ is the matrix composed by the $l^{th}$ columns given by $a_l$.

The $n \times n$ *Laplacian* matrix $L$ is defined as

$$L = AA^T = \sum_{l=1}^{m} a_l a_l^T \tag{68}$$

The diagonal entry of $L$ , $L_{i,i}$, is the degree of node $i$, and $L_{i,j} = -1$ if $(v_i, v_j) \in E$, otherwise $L_{i,j} = 0$. It should be noted that the summation of the elements in each row (column) of $L$ equals zero. In addition, the Laplacian matrix is positive semi-definite, $L \geq 0$, and its smallest eigenvalue is zero, $\lambda_1(L) = 0$. Even of greater importance with respect to the algebraic connectivity of graph $G$ is the second smallest eigenvalue of $L$, $\lambda_2(L)$, called the *Fiedler value*, which measures how connected the graph is [96] [158]. The Fiedler value is greater than zero, $\lambda_2(L) > 0$ if and only if $G$ is connected and the multiplicity of the zero eigenvalue is equal to the number of connected sub-graphs. The Fiedler value is also monotone increasing in the edge set. That is, if there is a graph $G_1 = (V, E_1)$, and another graph $G_2 = (V, E_2)$ such that $E_1 \subseteq E_2$, then $\lambda_2(L_1) \leq \lambda_2(L_2)$, where $L_1$ and $L_2$ are the laplacian matrices of graphs $G_1$ and $G_2$, respectively [113]. This means that as the number of nodes connected in a graph increases, the Fiedler value also increases, and can be used to quantify the connectivity of a communications network.

Maximum Fiedler value is obtained when all nodes are connected in the graph. In some instances however, complete connectivity is not desired. In some instances, connectivity can be scoped down to being able to reach certain nodes in the graph. For example. we might only care about getting sensory information from a group of UUVs to other nodes, and we don't really care whether those UUVs can connect with each other. In this situation, where the complete connectivity can be relaxed, the Fiedler value can still provide a quantitative measure of the connectivity of the network.

## 4.3 Quality of Communications Network

Although the Fiedler value provides a quantitative measure of the connectivity of the network, it does not provide a measure of the quality of the network in terms of the quality of the communication links representing the edges in the graph. To quantify each link's transmission channel, the graph is weighted with the probability of communications between the nodes. For example, if node $i$ connects with node $j$ because they are within ranges of good communications, then the quality of the link connecting the two nodes is given by the cumulative distribution function of the Nakagami-m distribution function at that range, given by the probability of communications between nodes $i$ and $j$, denoted $P^{i,j}$, which represents the probability that it is above a threshold receiver sensitivity value or SNR value, whichever is used to specify receiver hardware limitations. In this way, each link connecting two nodes $i$ and $j$ in a graph representing a communications network can be weighted as

$$W_{i,j} = P^{i,j} \tag{69}$$

Suppose a node $i$ communicates with node $j$ via a relay node $k$. Then the weight of the path connecting node $i$ to node $j$ is given by

$$W_{i,j} = P^{i,k}P^{k,j} \tag{70}$$

During the COA analysis phase, the planning staff might be interested in different asset allocation configurations based on asset availability and capability of each asset. While the Fiedler value can provide network configurations that guaranteed connectivity, there might be multiple network configurations with the same maximum Fiedler value since they connect the same number of nodes. The quality of the communications network can be used to rank between these different network configurations by weighting each graph according to the quality (probability of communications) of each link. Graphs with greater weights will provide communications

networks that are more robust to time-spreading in the signal intensity due to small scale fading.

## *4.4 Stability of the Communications Network*

The stability of the communications network from time variations in the signal intensity due to vehicle motion can be measured using the Finite State Markov Channel (FSMC) approach. This can be done by discretizing the fading amplitude about the expected fading amplitude into number of fading channel states, and computing the state transition probabilities.

The main question is how can the fading channel be modeled using the FSMC such that the stability of the network can be captured? In order to answer this questions, we need to understand the relationship between the states in the FSMC and the time-variance mechanism of the flat-fading channel. One of the most used practices has been to divide or partition the magnitude of the time-variant flat-fading gain amplitude $a_l$ into a number of non-overlapping states [219], as depicted in Fig. 77. The non-overlapping fading amplitude regions are $[0, V_1), [V_1, V_2), ..., [V_4, \infty)$, where the $V_k$ values denote region thresholds. The FSMC is said to be in state $s = k$ if the time-varying flat-fadding channel amplitude $a$ falls in the region $r_k = [V_k, V_{k+1})$. Referring to Fig. 77, the state transition probability $P_{k\to m} = Pr(s_l = m|s_{l-1} = k)$ is the probability that the fading amplitude $a$ moves from region $r_k$ at time index $l-1$to region $r_m$ at time index $l$. In the example shown in Fig. 77, the state transition probability is given by

$$P_{k\to m} = Pr(a_l \in [V_m, V_{m+1})|a_{l-1} \in [V_k, V_{k+1})) \tag{71}$$

FSMC modeling of the time-varying flat-fading channel amplitude $a$ or the received SNR in this way has been predominantly studied in the literature [218] [201] [27] [26] [59]. In amplitude-only FSMC modeling, the effects of unknown channel phase on the received signal are not considered. This modeling is more suitable for applications,

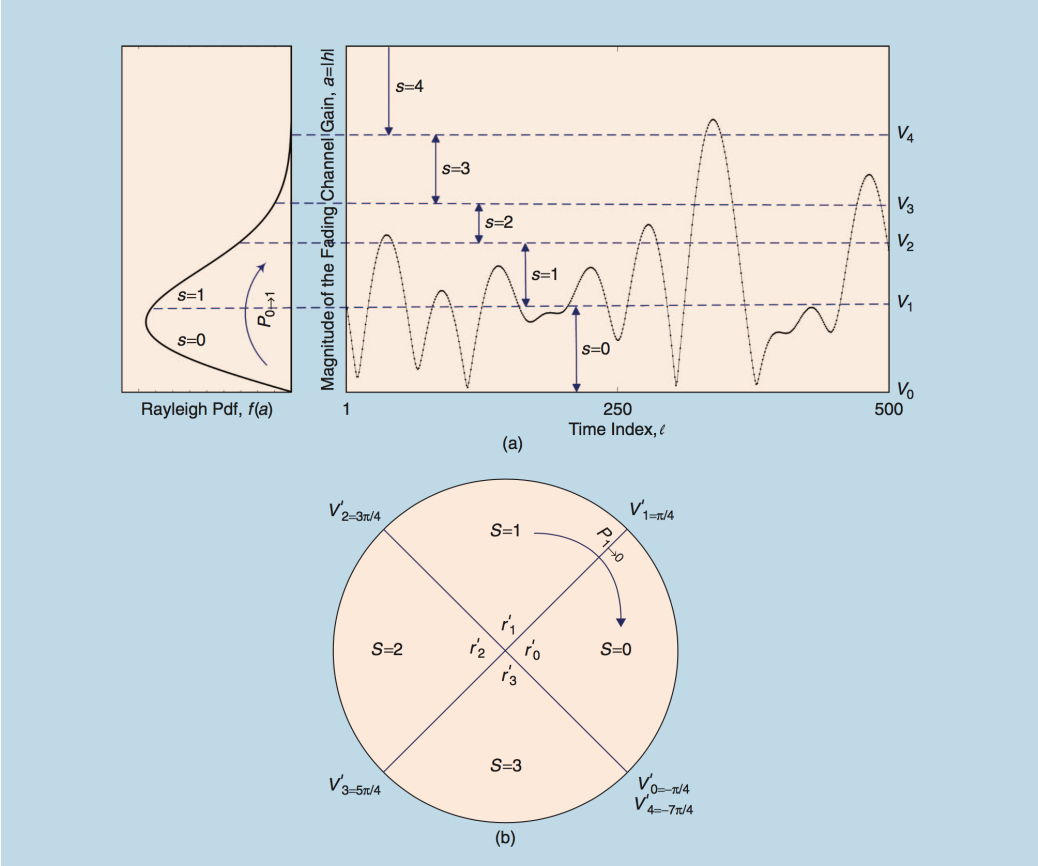


**Figure 77:** An example of the relationship between fading amplitude partitions and FSMC states [176].

where the channel phase can be estimated and compensated prior to decoding or where differential or noncoherent detection is used. Only recently has the FSMC of the time-varying flat-fading channel be modeled using the phase angle $theta_l$ [132] [124] [169].

For our purposes, and as first-order FSMC modeling of the time-varying flat-fading channel, we will consider only fading amplitude states. It should be noted that since the instantaneous received SNR $\chi$ is proportional to the square of the time-varying amplitude $a^2$ ($\chi = a^2 E_s/N_0$), partitioning of the fading amplitude into $[0, V_1), [V_1, V_2), ..., [V_{K-1}, \infty)$ is equivalent to partitioning the received SNR $\chi$ into $[0, E_s V_1^2/N_0), [E_s V_1^2/N_0, E_s V_2^2/N_0), ..., [E_s V_{K-1}^2/N_0, \infty)$. Therefore, it is sufficient to consider FSMC modeling of the time-varying flat-fading amplitude $a$.

## 4.5 Communications-based COAs and Reliability

As UxVs operate in a given UV Sentry mission, they can communicate with other UxVs or manned vehicles. Whom to communicate with, what to communicate, how to communicate, and when to communicate given the environmental conditions are questions that a mission planner is concerned with. UxV capability and task requirements also limit the strategic options for a given mission scenario. Communications scheduling during mission planning can provide communication networks that are reliable and robust to enemy threats and sources of uncertainty. Figure 78 shows communications-based COAs for UxVs in general, as well as specific COAs corresponding to specific vehicles based on their capability.

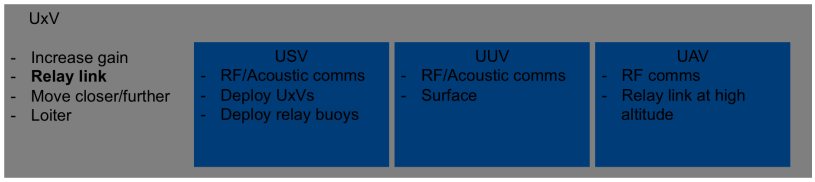


**Figure 78:** Communications-based COAs.

These communications-based COAs and their schedule will be considered as design variables in the optimization methods that will be described in a later section. The space of alternative communication strategies, and how they provide link or node failure tolerance in the communication network, needs to be explored further and analyzed carefully to determine most feasible and reliable solutions.

The feasibility of re-establishing communications is a function of a number of factors, including: speed of the vehicle, vehicle capability (e.g., UUVs that can surface, and UAVs that can loiter) and whether it can deploy other UxVs to relay communications (payload capacity). Reliability depends on whether communications can be actively maintained in the network due to a link or node failure. An important assumption for simplification is that node or link fault detection is done almost

immediately, which allows to concentrate on the temporal and spatial aspects of re-establishing communications using communications-based COAs. Another important assumption is that link or node failures happen one at a time, which is not realistically the case in many interesting and complex scenarios, but it allows us to concentrate on specific scenarios of interest.

One way to provide reliability to a network is by redundancy. There are two forms of redundancy: spatial and temporal [145]. Spatial redundancy replicates the components or data in a system. Transmission over multiple paths through a network and the use of error-correction codes are examples of spatial redundancy, and they try to overcome permanent failures in physical components or individual links. Temporal redundancy deals more with transient errors, and usually done through data re-transmission. Internet's Transmission Control Protocol (TCP), for example, uses automatic repeat requests (ARQ) algorithms to support transmission redundancy. A reliable network usually provides both spatial and temporal redundancy to tolerate faults.

For the scope of this thesis, the faults considered will be limited to link failures (edge failure). Network reliability will be provided by spatial redundancy only, and temporal redundancy will be left to future detail studies on encoding/decoding and communication protocols. Simple communication networks are considered, with multiple heterogeneous UxVs, at varying locations. UxV capability to provide spatial redundancy for node or link failures are considered for communications-based COA, and their effectiveness to re-establish communications are used as a measure of network reliability. Some of these UxV capabilities were shown in Fig. 78. A USV for example, could deploy UAVs to relay communications, and a UUV could surface to communicate sensor information via RF communications instead of acoustic, low-bandwidth, communications.

In this part of the study, for a given mission scenario and assets available, UxV capability and performance are used for comparison between the different re-establishing communication-based COAs possible. Their effectiveness on re-establishing communications are measure as the number of link redundancies it provides to the network, the stability of the links, and the probability of communications it provides for each link. Prior experimental studies on UxV capability are also used for reference and recommendations on how best to use them for communications-based COA.

Literature review on UxVs provide preliminary insights on how can these vehicles be used for communications-based COAs, as compared to manned systems. According to [178], compared to other UxVs, USVs have greater payload capacity, greater endurance, and can use higher-density energy sources (hydrocarbons instead of batteries). USVs also have the capability to operate sensors and communicate both above and below the waterline. In Fig. 79, [178] shows USV capabilities as compared to other similarly-sized UAVs and UUVs. In the same study, the authors performed a suitability analysis for USV on different missions and required functions based on their capability and level of technological maturity (Technology Readiness Levels, or TRL). Their results showed that USVs are expected to be highly suitable for $C^4$ISR, mine warfare, surface warfare, and anti-submarine warfare (ASW) missions in the near future [178].

Clear advantages of UUVs over other unmanned vehicles are that they can operate underwater in denied areas to provide sensor information, and be stealthy. Manned systems, such as the Sea-Air-Land (SEAL) Delivery Vehicle (SDV) or the Advanced Sea Delivery System (ASDS), depend on nuclear submarines for transportation into theater, which limits mission responsiveness, rate at which missions can be performed, and entails human risk for sensitive missions [48]. According to [48], UUVs provide unique capabilities to Navy missions such as ISR, Mine Countermeasures (MCM),

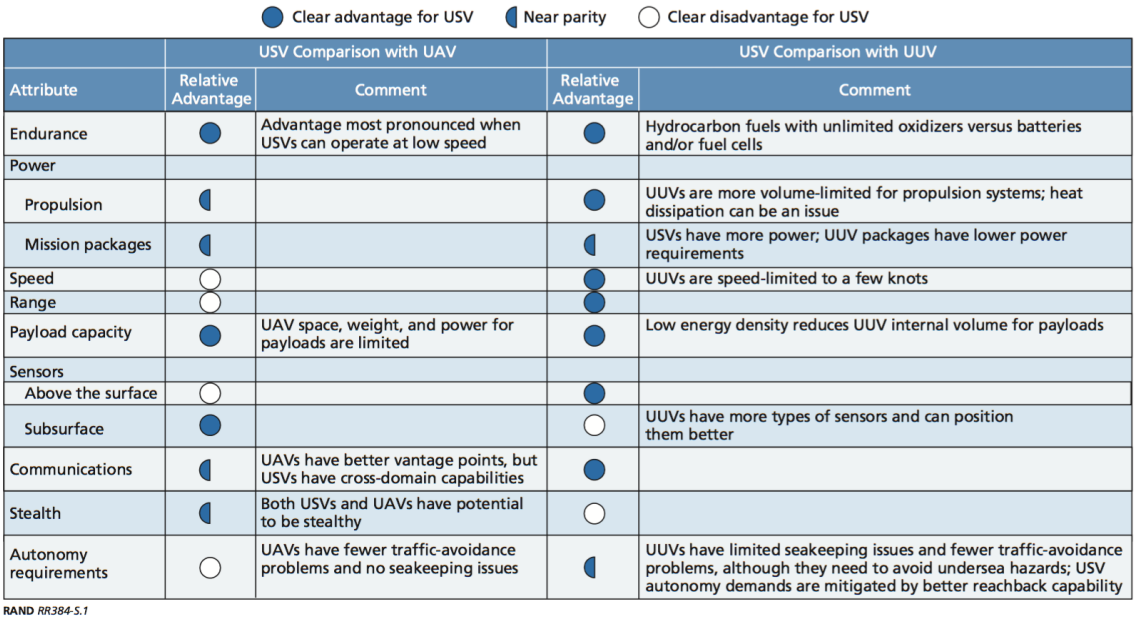


**Figure 79:** USV capabilities as compared to similarly-sized UAVs and UUVs [178].

ASW, inspection and identification missions, and communications/navigation network nodes ($CN^3$). They include mine detection, classification, and neutralization, deploy leave-behind sensor arrays, near-land and harbor monitoring, and detect and track threat submarines. Underwater acoustic communications for UUVs are low bandwidth and slow, and suffer from high levels of noise. However, approaches exist to overcome this limitation, which include surfacing to communicate by RF (at the expense lower stealth), communicating low-resolution data, and relaying acoustic communications.

UAVs have found applications in multiple military domains. From large, long endurance Unmanned Aircraft Systems (UAS) to small-sized, long and short endurance multi-rotor and fixed-wing vehicles, UAVs have shown critical advantages in different missions. In [19], large, long endurance, high altitude UAS are suggested for communication relays to mitigate kinetic and noise jamming threats to satellite communication uplinks by providing alternative links either directly to surface-based terminals or satellites beyond the range of threats. Vertical-takeoff (VT) UAS such

as the Northrop Grumman MQ-8 "Fire Scout", with a fraction of operational footprints from Lockheed Marin's MH-60 Sea Hawk helicopter (used currently for MCM and ASW missions), can provide a wide spectrum of surface vessels with an over-the-horizon maritime surveillance capability [19]. Smaller UAS, such as the ScanEagle, Integrator, Raven, and Puma provide long endurance and varying payload capacity. They can provide communication links in the orders of hours to communication networks. Multi-rotor small UAVs, usually with lower endurance in the order of minutes, can provide additional quick and more stable communication nodes/relays by being able to hover at a specific location, without much deviation.

With these preliminary general guidelines, it can bee seen that different types of UxVs will provide unique communications-based COA to help maintain a reliable communications network. Given the available assets and mission scenario, unique UxV capabilities can be used to provide communications-based COA solutions to re-establishing communications in a network where certain link/node failures are not accounted for during the COA Development process. If no communications-based COAs are possible to re-establish communications in certain scenarios, with the available assets, then network topology may be reconsidered during the COA development process, by moving nodes closer, adding more assets to the fleet, or adding redundant communication paths. To deal with this problem, possible proactive network topologies are investigated, based on asset availability, allocation, mission tasks, and communications predictions, that are reliable to communication link removals and that lead to stable configurations.

Communications networks can be assessed in terms of their connectivity, quality of the links, and their stability due to expected node relative motions, as has been discussed in previous sections. Therefore, the graph corresponding to the communications network can be weighted in terms of connectivity, link quality, and stability in order to determine network topologies that lead to robust and reliable networks.

Reliability can be achieved by link paths redundancy, which can be measured by the degree of each node in the network.

To answer RQ1 and test HP1, the Mine Survey Mission will be used as a demonstration case study, and a limited number of assets and their assigned tasks will be defined. Based on the communication channel prediction for a given environmental condition, the allowable ranges between the vehicles (skip zones) will be determined, and the vehicles motion and schedule will be constrained such that they are always connected with another asset in the network, not necessarily with the main ship.

The expected results of Exp1 will be a set of allowable ranges between vehicles and a minimum required *degree* for each asset such that the communication network is reliable to communication link failures. These ranges will then be considered as constraints during COA optimization of each vehicle during the mission while performing their corresponding tasks.

## *4.6 Reliability Check*

In computer science, formal methods are a collection of notations and techniques for describing and analyzing systems. These methods are *formal* in the sense that they are based on some mathematical theories, such as logic, automata, or graph theory. Formal specification introduce a precise and unambiguous description of the properties of the systems, that can be used to verify that a system satisfies its specification, or to systematically seek for cases where it fails to do so [161]. Automatic verification is the process of automatically inspecting that a given formal specification is met [161]. These methods find applications in software reliability, communication protocols, traffic control, and aerospace systems.

Formal methods and automatic verification can be used in various stages of the software development process, from early design to the acceptance tests of the completed product [161]. In the same way, formal methods and automatic verification can

be used in various stages of the NPP mission planning process, and across all models used to create and evaluate COAs. Optimally, the use of such methods is integrated into the early stages of the NPP through a methodology. A major benefit of early use of formal methods is that errors and communication network failures that are found in early stages of the mission planning process have less chance of compromising the mission.

Once a network topology that is reliable to communication link failures has been found, checks need to be done to ensure that, after optimal communications-based COAs and schedules are determined during the COA analysis, the network is still reliable. Network reliability in this study will be performed using graph theory methods that ensure network is connected in cases of link failures and vehicle position uncertainty.

# CHAPTER V

# PROBABILISTIC ROBOTICS

In this chapter methods are presented for modeling the uncertainty propagation and model integration as the unmanned vehicles perform their required tasks. This is an important step in the COA Analysis process, shown in Fig. 80 as the Bayesian Filter analysis, that helps model the progression of the quality and quantity of information that is communicated over the network.

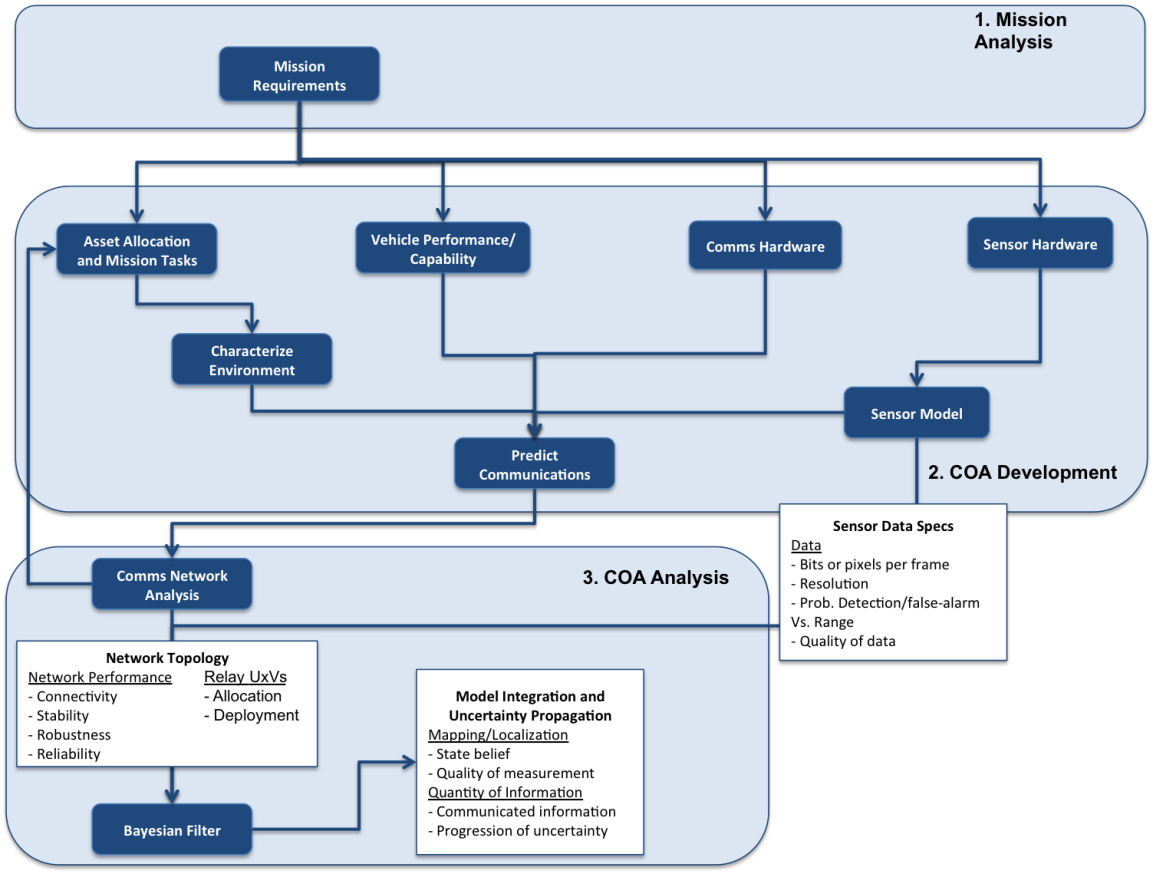


**Figure 80:** Bayesian filter analysis step of COA Analysis process

Experiment 3 is executed in this chapter with the Bayesian filter framework in order to help answer RQ3 and test the validity of hypothesis HP3. A single target

area is considered for the optimization of the quantity of information which is modeled using the Bayesian filter approach.

## *5.1 Model Integration and Uncertainty Propagation*

UxVs are robotic systems to some extent in the sense that they are situated in a physical world, perceive information about their environment through sensors, communicate that information if necessary, and manipulate through physical forces. In the process, the robots need to accommodate for enormous uncertainty that exist. As the UxVs navigate through the operational environment, taking sensor data and performing COAs, different sources of uncertainty affect the state of the vehicles and perception from sensor data. Sources of uncertainty include the environment, sensor models, robot actions (actuation), vehicle internal models, and model approximations.

One way to deal with this uncertainty is to use high-fidelity physics-base models to reduce this uncertainty. One approach is *model-based* motion planning, which assumes that a full and accurate model of the robot and the environment is given, and the robot to be deterministic in nature, as described in [50], and [182]. However most motion planning techniques that have resulted from this *model-based* approach simply produced a single reference trajectory, for example in the control of a manipulator [206]. Applications of these techniques are confined to environments where every little bit of uncertainty could be engineered away or sensed with sufficient accuracy [206].

Another approach is *behavior-based* robotics, which rejects the idea of internal models, and instead focused on the interaction of the robot with the physical environment [115]. Successes that went far beyond the reach of *model-based* motion planning include an hexapod robot which used a relatively simple finite state atutomaton to control the gait of the robot even in rugged terrain [46]. More recently, commercial success through a robotic vacuum cleaner called "Roomba" is another example using *behavior-based* techniques [2]. The success of *behavior-based* robotics

lay in sensing: control is entirely driven by environment interaction as perceived by the robot's sensory information.

The lack of internal models and focus on simple control mechanisms in *behavior-based* robotics led to most robots being confined to relatively simple tasks, where the momentary sensory information was sufficient to determine the right choice of control [206]. Inspired by these limitations, the field of robotics has started to embrace *hybrid control* architectures in which *behavior-based* techniques provide low-level control, and *model-based* planners coordinate the robot's action at a high, abstract level [24]. More recently, *probabilistic robotics* has emerged with the invention of the prolific *Kalman Filter* [116]. In many ways, *probabilistic robotics* is a *hybrid control* method in the sense that models and sensor measurements are used, but they are assumed to be incomplete and insufficient for control [206]. Through the statistical integration of both models and measurements a control action can be devised.

*Probabilistic robotics* provides numerous methods to probabilistically model the temporal integration of models and sensor measurements: *Kalman filter* techniques have been used for high-dimensional perception problems [189], *particle filters* [74] have become more popular with researchers developing new programming methodologies based on Bayesian information processing ([205], [130], and [159]). At the core of *probabilistic robotics* is the idea of estimating the state from sensor data. It estimates quantities from sensor data that are not directly observable, but that can be inferred. Sensors can only provide partial information about the state, and their measurements are also corrupted by noise. Therefore, probabilistic state estimation algorithms compute belief distributions over possible world states [206]. Two main problems of interest in the robotics community are *localization* and *mapping*. The problem of *localization* is to localize the robot within a given map. In this case the state to predict is the location and orientation of the robot within the given map, with the aid of sensory information. The *mapping* problem involves figuring out where

(static or dynamic) objects are. In this case the state to predict is the occupancy of the space around the robot, with the aid of sensory information.

These *probabilistic robotics* techniques can be used in this study to model the *quality* and *quantity* of sensory information communicated during a COA, while taking into account different types of uncertainty using statistics and probability theory. The state can be defined to be threat occupancy within a map (e.g., mines, pirates), and measurements can come from different sensors, such as detection and classification sonars, radars, laser-scanners, lidars, and cameras. As the UxVs navigate through the operational environment, performing their tasks, and executing COAs, they collect measurements from their sensors, which are then used to predict the state, and this is then coded into information that is communicated either to a base ship or to other vehicles, or both. The *quality* of information, for example, can be dictated by the probability of detection, which in turn is a function of the sensor model (e.g, resolution, accuracy, false-alarm rate, etc.). The *quantity* of information can be dictated, for example, by the bits of information that can be send during communications (both RF and acoustic communications). Sensor models also take into account uncertainty in the measurements, and motion models take into account uncertainty in the UxV locations. In this way, probabilistic robotics provides a method to determine the effects of COAs on the ability to predict the state and the amount of information that can be communicated while determining the optimal set of COAs and schedules that optimize a given set of MOPs and MOEs.

## *5.2 Bayesian Filter Framework*

For this thesis proposal, focus is drawn to examining the problem of COA design and scheduling for mobile UxVs carrying sensors while performing required sensing tasks. Active sensing [126] [91] [49] refers to the control of sensor parameters, such as position and orientation, in order to obtain information and reduce uncertainty. Planning for

search and exploration COAs depends on the sensor being used and the quantity of information that is being captured, such as target detection or identification. A method for representing and updating the estimate and associated uncertainty, the belief state, and a way of using the belief state to determine expected information is therefore required.

A general estimation or mapping algorithm can be decomposed into the following steps: 1) update the belief, 2) calculate the expected information, 3) plan the control action, and 4) execute control action and collect measurements. This is an iterative process for a general closed-loop information-based sensing algorithm, as is shown in Fig. 81.

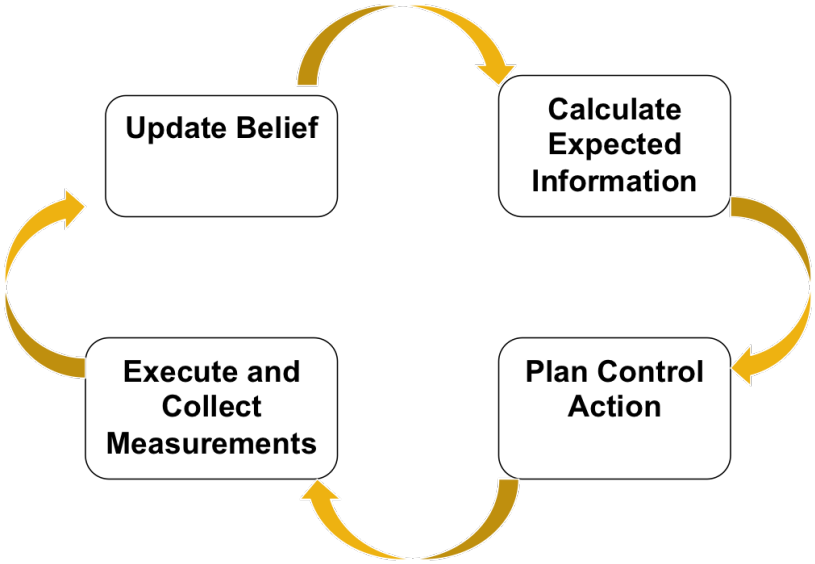


**Figure 81:** General closed-loop information-based sensing algorithm

.

Probabilistic robotics offer techniques to model the relationship between COAs and sensor measurements while taking into account different sources of uncertainty using statistics and probability theory. As the UxVs navigate through the operational environment, performing their tasks defined during the Asset Allocation and Mission Tasks , and executing COAs, they collect measurements from their sensors, which are then used to predict the state, which can be defined to be the occupancy of a

threat in a given target area. This sensory data is then coded into information that is communicated either to a base ship or to other vehicles, or both. The *quality* of information, for example, can be dictated by the probability of detection, which in turn is a function of the sensor model (e.g, resolution, accuracy, false-alarm rate, etc.). The *quantity* of information can be dictated, for example, by the bits of information that can be send during communications (both RF and acoustic communications). Sensor models take into account uncertainty in the measurements, and motion models take into account uncertainty in the UxV locations. In this way, probabilistic robotics provides a method to determine the effects of COAs on the ability to predict the state and the amount of information that can be communicated while determining the optimal set of COAs and schedules that optimize a given set of MOPs and MOEs that were defined in the Mission Analysis step of the NPP process, such as communicating maximum information in the minimum amount of time to provide situational awareness, and doing it in the most efficient way possible.

In order to take into account these uncertainties and making the COAs more robust, the evolution of state and measurements is modeled using the Bayesian Filter [206]. Bayes filter calculates the posterior belief distribution over a state at time $t$ ($x_t$) conditioned on measurement ($z$) and control data ($u$) up to time $t$. It assumes that the state is complete, that is, the world is Markovian, and conditional independence. The dynamic Bayes network that characterizes the evolution of controls, states and measurements is shown in Fig. 82. The general form of the Bayes filter is shown in Eq. 72 for the continuous time case, and in Eq. 73 for the discrete time case.

$$\begin{aligned} \bar{bel}(x_t) &= \int P(x_t|u_t, x_{t-1}) bel(x_{t-1}) dx_{t-1} \\ bel(x_t) &= \eta P(z_t|x_t) \bar{bel}(x_t) \\ \eta &= \frac{1}{\int P(z_t|x_t) \bar{bel}(x_t)} \end{aligned} \tag{72}$$

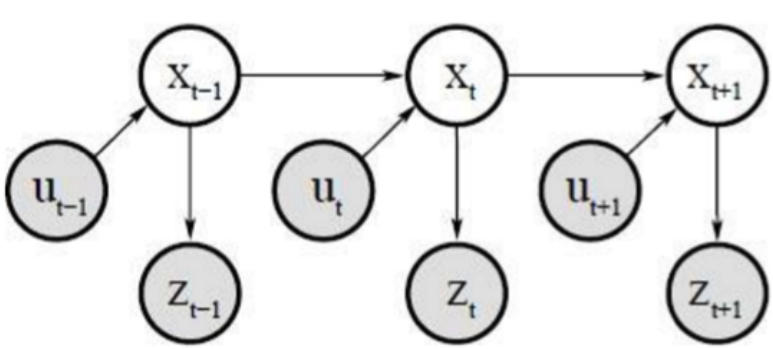


**Figure 82:** Bayesian dynamics using Markovian inference [206].

$$\begin{aligned} \bar{P}_{k,t}(x_j) &= \textstyle\sum_i P(x_{j,t} = x_k | u_t, x_{j,t-1} = x_i) P_{i,t-1}(x_j) \\ P_{k,t}(x_j) &= \eta P(z_t | x_{j,t} = x_k) \bar{P}_{k,t}(x_j) \\ \eta &= \tfrac{1}{\sum_k P(z_t | x_{j,t} = x_k) \bar{P}_{k,t}} \end{aligned} \tag{73}$$

Key elements in the Bayesian filter are the initial belief $P(x_0)$, measurement probability $P(z_t|x_t)$, and state transition probability $P(x_t|u_t, x_{t-1}, z_t)$. Depending on the nature of the problem, there are different types of Bayesian filters that can be used. Figure 83 shows the different types of Bayesian filters available.

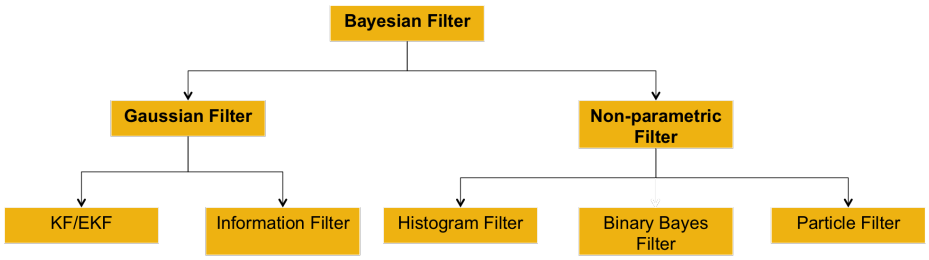


**Figure 83:** Bayesian filters available.

Each Bayesian filter method relies on different assumptions regarding the measurement and state transition probabilities, and the initial belief. These assumptions then lead to different types of posterior distributions, and the algorithms for computing them.

Quantity of information depends on how the state is defined, what types of sensors are used and the quality of information that they provide (sensor models), and how

the motion of the vehicle actions and environment dynamics affect the state. Also important are the assumptions made regarding the measurement and state transition probabilities and the initial beliefs, which lead to different Bayesian filters that can be used, as is shown in Fig. 83. As a general guideline, in applications using active sensing for localization, Gaussian parametric filters may be used, as is done in [131], [90], [215], and [185]. When the posterior is not expected to be approximately Gaussian, non-parametric filters such as Bayesian filters [143] [221], histogram filters [192], or particle filters [127] [172] [139] are often used. For mapping applications, occupancy grids [41] [84], or coverage maps [192] are often used.

Given a belief state and sensing task, either for localization, mapping, or both, not all measurements are equally informative. The quality of the measurement depends on a number of factors, including the sensor resolution and range, which can also be dependent on distance, orientation, and motion. To make sure useful measurements are obtained given realistic restrictions, sensing strategies for mobile sensors should seek to optimize measurement quality [28] [190]. When sensor field-of-view is sufficient to provide useful measurements, they are called *geometric sensing* [139] [70] [227] [102]. On the other hand, other sensors may have sensitivity characteristics within the range threshold that affects sensing capability, such as infrared range sensors, which have a maximum sensitivity region [33], and cameras, which have an optimal orientation and focal length [76].

Different entropy-based measures from information theory and optimal experiment design can be used to predict expected information quantity gain. Shannon entropy has been used for measuring uncertainty in estimation problems [91] [23] [217] [200], also entropy-related metrics including Renyi divergence [126] [131], mutual information [208] [75] [172] [186] [227] [207] [99] [138], entropy reduction or information gain maximization [108] [228], and the Fisher information approach [87] [134] [211] [212] [94] are all possible ways to quantify the information. The choice depends on the

nature of the problem and the application.

Planning the control action that optimizes the quantity and quality of information is a problem of searching for an informative solution over the sensor state space and the belief state, and can be computationally expensive. To actively optimize the control action, it is necessary to calculate an expectation over both the belief and the set of candidate control actions [131] [186] [207] [25]. Some methods rely on decomposing or discretizing the the search space, the action space, or both, and locally selecting the optimal sensing action myopically (selection of only the optimal next configuration or control input) [126] [90]. The expected information gain can be locally optimized, for example, by selecting a control action based on the gradient of the expected information [127] [139] [41] [99]. On the other hand, instead of local information maximization, a sensor can be controlled to move to that state which maximizes the expected information globally over a bounded space [217] [215] [221] [134] [133]. However, while myopic information maximization methods have the advantage in computational traceability, they are usually applied to situations where sensor dynamics are not considered. Even the global myopic methods are likely to suffer when uncertainty is high and information diffuse [192] [137] [166].

Nonmyopic methods, which calculate planning control actions over longer time periods, are also often used. Research on search strategies point out that the most general method for solving nonmyopic control signals involve solving a dynamic programming problem [51] [186] [137], but can be computational intensive. Some heuristic methods have been used to approximate this dynamic programming problem [192] [51] [107] [137]. Common methods involving sampling-based motion planners for maximizing the expected information over a path for a mobile sensor have also been applied to sensor path planning [49] [185] [131] [228] [109] [173].

For this thesis, the path planning will be constrained by UxV required tasks. The control action will be represented as the COA used to communicate information

through the communication network, and mission level objectives such as information gain, situational awareness, and required effort, will be optimized. The bayesian filter is used as a means to capture the time progression of measurements and the change in belief of the state as the UxV perform deterministic control actions involving communicating either via RF or acoustic. The search space is discretized into bits of information that can be communicated, and different measurement and search schedule are used as variables to optimize the objective functions. Although this is a simplified approach, it still provides a benchmark to capture the most important relationships between measurements and the belief of the state, as it is communicated though the network as useful information. It also leaves room for future improvement to include myopic or nonmyopic methods to study the effects of more complex and realistic control actions that UxVs can perform in order to maximize the objective functions.

With these suggestions and simplifications, RQ3 and corresponding HP3 can be tested by an experiment that is mission specific. For example, the state can be defined as the occupancy of a given target area by an object (e.g a mine), the sensors involve sonar measurements of the area, and the motion model is assumed to be deterministic in the sense that the UxV always know its position and velocity with certainty. The quality of information is modeled as the probability of detection, which increases by the vehicle sweeping through the area, and the quantity of information is modeled as the information bits that are communicated to the main ship from the sensor data. Therefore, even though it is mission specific, the next experiment will be used to answer RQ3 and test HP3.

## *5.3 Experiment 3: Using Bayesian Framework to Model Uncertainty Propagation and Information Quantity*

For this experiment, we define the state of a target area as the occupancy of a map and determine how the probability of the state changes due to sensor measurements

and vehicle motion using a histogram and binary Bayesian filter, and determine how the probability of the state affects the quality and quantity of information given a data rate and sensor model. The results of this experiment will be a time evolution of beliefs on the state based on sensor measurements and vehicle motion which may or may not appropriately model the quality and quantity of information.

In this study we consider the scheduling of a UUV performing search and survey of a target area (TA) based on the prediction of communications in maritime environmental conditions. While the UUV sweeps the TA, it gathers sonar data which is communicated back to the main ship via acoustic communications, and via radio frequency (RF) communications by surfacing at the end of a sweep when good communications are predicted. In this study we shown that by placing the most sweeps within the predicted good communication ranges, the information gain rate ($IGR$) can be maximized, therefore demonstrating the benefits of RF communications prediction capability while performing the survey mission.

A general estimation or mapping algorithm can be decomposed into the following steps: 1) update the belief, 2) calculate the expected information, 3) plan the control action, and 4) execute control action and collect measurements. This is an iterative process for a general closed-loop information-based sensing algorithm. Next we will describe the Bayesian framework in detail and provide particular examples to demonstrate our modeling and simulation, and show the benefits of this method with some results.

### 5.3.1 Problem Scope and Definition

Search and survey missions for UUVs include underwater surveillance, search and rescue operations, and seismic monitoring. While performing these tasks, the UUV needs to collect data from different sensors such as sonar data, images, and laser/ladar data. This data, along with general position and vehicle health data, is communicated

to an operator on a main ship and to other vehicles. This information can be dense critical data that needs to be communicated fast enough for the operator to make further decisions. The quality of the information is also affected by the path the vehicle takes and how the information is communicated. UUVs are usually equipped with acoustic modems for communication, but the communication underwater is very low bandwidth and is greatly affected by noise [195]. Some of these UUVs are also equipped with RF communications package, which when on the surface, allows them to communicate much faster. RF communications however is also affected by noise, atmospheric conditions, and distance.

Extensive work has been done for online path planning and navigation of UUVs and autonomous underwater vehicles (AUV) while performing object detection and classification. In [177] Sariel et al. investigates an online dynamic task allocation (and reallocation) system that aims to achieve a team goal while using resources effectively between AUVs. During the detection phases, searching paths have been proposed for efficient and complete coverage of an area. For example, in [15] a comparison is made between random and complete lawn-mower pattern search, and the benefits of a complete search is discussed as being more efficient and more useful for the classification stages. In [95] search strategies are presented based on a-priori spatio temporal distributions of targets. Also, line-sweep directions which minimizes time for area coverage have been proposed in [110]. But neither of these studies consider the ability to communicate the information both by acoustic and RF communications. Therefore, the scope of our work is to incorporate the capability to predict communications in the path planning and scheduling of UUV operation, especially for cases where quality and quantity of information communicated to a main ship is crucial as the detection of objects is taking place. Specifically, we focus in the mission planning phases, before the UUV is deployed, and account for the effects of maritime environmental conditions on the state of the transmission channel.

#### 5.3.1.1 *Problem Statement*

Consider an example survey mission scenario in which only one TA is searched for objects of interest. Assume the tactical situation is such that there exists a deep water maneuver box that provides the necessary geometry in which UUVs can operate to conduct area search and survey. We assume the UUV sweeps in a lawn-mower pattern at some depth. As it sweeps through the area, the side-scan sonar collects a number of discretized cells based on its resolution. These cells can be translated into bits of information that are communicated via acoustic, or via RF communications by surfacing at the end of each sweep, as we depict in Fig. 84. If an object is located

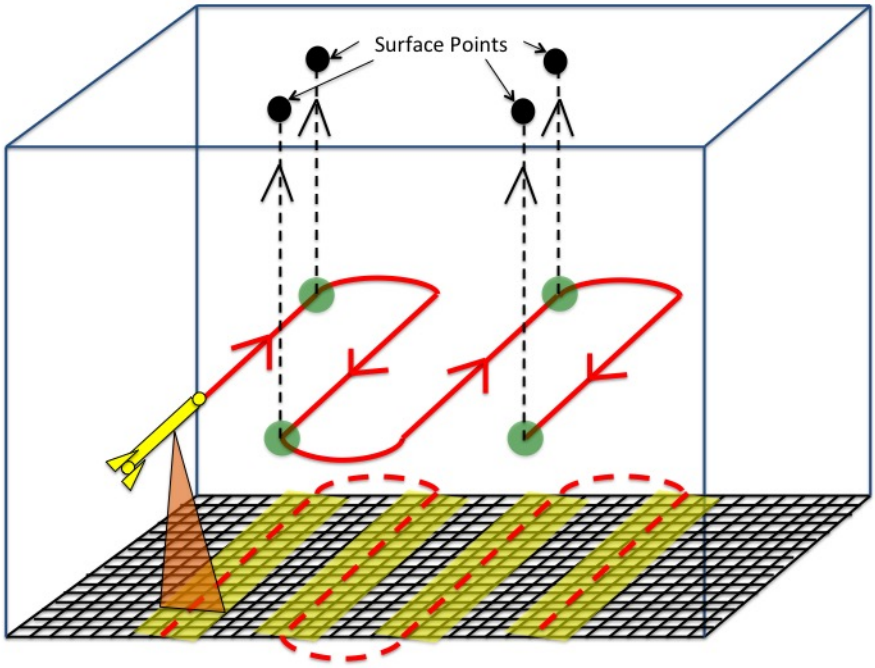


**Figure 84:** TA discretization based on sonar resolution and UUV path.

within the TA, it will occupy a number of cells that can be detected by the sonar.

We use an optimization routine to find optimal course of actions (COAs) in the form of communication scheduling during a given mission. For this study, the function to optimize is the information gain rate ($IGR$), which will be defined in a later section, subject to mission-level, vehicle, and communication constraints. The design variables

consists of scheduling the communications between the UUV and main ship, as the mission takes place, in the form of separation distance between each sweep and the availability prediction of RF communications based on the environmental conditions.

Let $\mathbf{X}$ be the vector of sweep distances from one edge of the TA, $\mathbf{X} = [x_1, x_2, ..., x_i, ..., x_n]$, as is shown in Fig. 85. At the end of each sweep, if the surface point, denoted *Sp*, is within good communication ranges, the UUV surfaces and communicates sonar sensor data via RF communications, else, if the *Sp* lies within skip zones, it does not surface and continues with the next sweep while it communicates sensor information via acoustic communications. Communication constraints come in the form

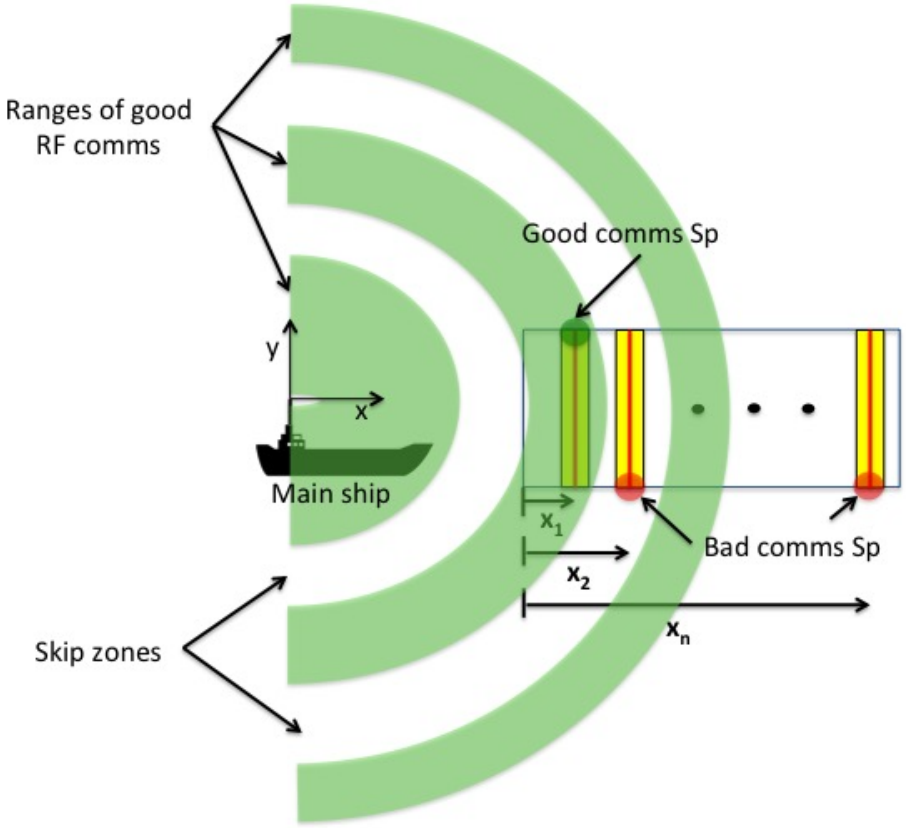


**Figure 85:** Mission scenario with target area and distance between sweeps design variables.

of ranges of good RF communications, depicted in Fig. 85, and mission level constraints come in the form of required percentage area coverage. Percentage area

coverage constraint can be posed as a given number of required sweeps that do not overlap. Therefore, once the number of $n$ required sweeps is determined, given that the sensor range is $R$, the constraint can be formulated in terms of the $Sp$ locations $Sp_1(x_1), Sp_2(x_2), ..., Sp_i(x_i), ..., Sp_n(x_n)$ as

$$g_1(x_i) = 2R - |Sp_i(x_i) - Sp_j(x_j)| \leq 0 \tag{74}$$

for $i, j = 1, 2, ..., n$ and $i \neq j$. The constraint in (74) enforces that the separation distance between each sweep is at least two times the range of the side-scan sonar range, therefore not allowing sonar scans to overlap. The other two constraints involve the lower and upper bound requirements for the sweep locations based on where the TA is located. Denoting the lower and upper bounds as $LB$ and $UB$, respectively, these two constraints are defined as

$$g_2(x_i) = LB + 2R - Sp_i(x_i) \leq 0 \tag{75}$$

$$g_3(x_i) = Sp_i(x_i) - UB - 2R \leq 0 \tag{76}$$

for $i = 1, 2, ..., n$. We use constraints in (75) and (76) to ensure the surface points lie within the length of the TA. The requirement for each of these three constraints is that $g_k(\mathbf{X}) \leq 0$, for $k = 1, 2, 3$.

The goal is to maximize $IGR$ while trying to meet the constraints the best possible. This can be posed as the following constrained minimization problem:

$$\begin{aligned} \min_{\mathbf{X}} \quad & -\sum_{i=1}^{n} IGR(x_i) \\ \text{subject to} \quad & g_k(\mathbf{X}) \leq 0,\ k = 1, 2, 3 \end{aligned} \tag{77}$$

To formulate the optimization problem as an unconstrained minimization problem, we used an external penalty function, where the objective function includes the degree to which the constraints are met [216]. The goal is to maximize $IGR$ while trying to meet the constraints the best possible. This can be posed as the following

unconstrained minimization problem, where we take the objective function in 77 and add the constraints to it in the following form

$$F(\mathbf{X}) = -\sum_{i=1}^{n} IGR(x_i) + r_p \sum_{k=1}^{3} max[0, g_k(\mathbf{X})]^2 \tag{78}$$

where $r_p$ is the weight on the constraint, and can be modified in each iteration.

Since most of the variables have non-linear impact on the constraints and objective functions, we selected genetic algorithm (GA) as an evolutionary optimization method. The GA routine starts with an initial random population of $N$ designs with varying sweep distances, $[\boldsymbol{X_1}, \boldsymbol{X_2}, ..., \boldsymbol{X_N}]$, each design with $n$ number of required sweeps to meet percentage area coverage. A roulette wheel is built from the fitness level from each design point $\mathbf{X}$, and used to determine which design points cross-over. Cross-over is performed by swapping sweeps from each design point that meet a biased coin toss condition. Mutation is performed by adding or subtracting a random value to the sweep locations from design points that meet certain biased coin toss condition. The new generation is fed back to the GA iteration until a certain running time is achieved [58]. In the next section we present a way to model the amount of cells data from the sonar sensor that is available to be communicated based on the UUV path.

### 5.3.2 Binary Bayes Filter

We use Binary Bayes filter (BBF) Markov process in this study for modeling the probabilistic nature of the temporal integration of sensor data during survey missions. For a given target area (TA) $A$, the finite state random variable $Y$, a static state, consists of the occupancy of each cell $j$, denoted by $y_j$. Each cell is in either an occupied state $y_j = 1$, or not occupied state $y_j = 0$. The probability that cell $j$ is in an occupied state is denoted by $P_O(y_j)$. Key assumptions made using the BBF are: (1) occupancy of individual cells are independent, (2) UUV motion is deterministic, and (3) occupancy of the TA is static [206] (does not change with time, only the

probability of it being occupied changes as new measurements are made). The lack of a time index on the state $y$ reflects the assumption that the state does not change.

Initially, all cells are unknown to be occupied, with probability $P_{O_0}(y_j) = 0.5$. Using conditional independence, and the assumption that the state is static, we assume the belief that cell $j$ is occupied at time $t$ given measurements $z_{1:t}$ and control actions $u_{1:t}$, is approximated as a Markov process. Thus, we have the following approximation

$$\begin{aligned} bel_t(y_j|z_{1:t}, u_{1:t}) &\approx bel_t(y_j|z_t, u_t) \\ &\approx P_O(y_j|z_t, u_t) \end{aligned} \tag{79}$$

Cells that lie within the side-scan sonar range are detected by the sonar and their occupancy probability either decreases or increases from the initial unknown probability, as is depicted in Fig. 86.

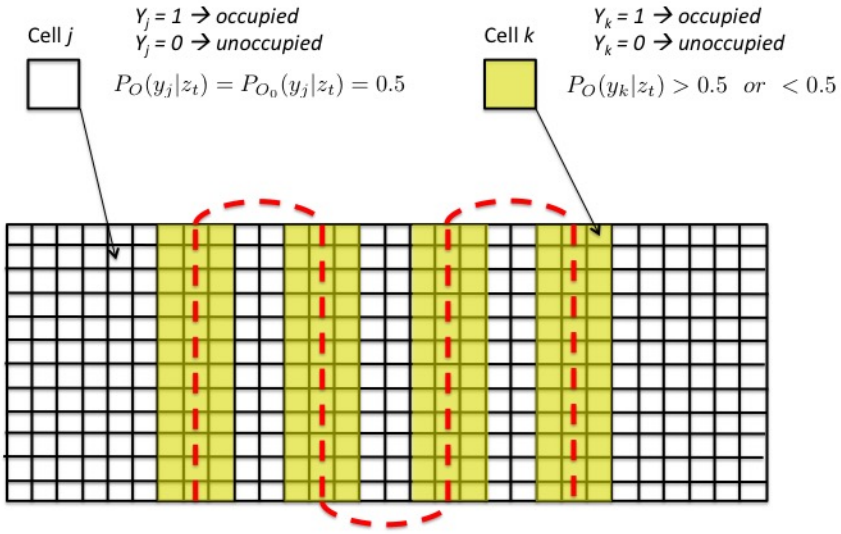


**Figure 86:** TA discretization into occupancy cell map.

For BBF, the belief is commonly implemented as a *log odds* ratio. The *odds* of a state $y_j$ is defined as the ratio of probability of an event and the probability of its

negative, given by

$$odds(y_j) = \frac{P_O(y_j)}{1 - P_O(y_j)} \tag{80}$$

The *log odds* at some time $t$, denoted $l_t$, is then the logarithm of this expression, given by

$$l_t(y_j) = \log_e \frac{P_O(y_j)}{1 - P_O(y_j)} \tag{81}$$

The BBF update formula using the *log odds* representation [206] is given as

$$\begin{aligned} l_{t+1}(y_j|z_{t+1}, u_{t+1}) = &\log_e \frac{P_O(y_j|z_{t+1}, u_{t+1})}{1 - P_O(y_j|z_t), u_t} \\ &- \log_e \frac{P_{O_0}(y_j)}{1 - P_{O_0}(y_j)} \\ &+ l_t(y_j|z_t, u_t) \end{aligned} \tag{82}$$

The first term in the right-hand-side of (82) is the *log odds* of the *inverse* sensor model, the second the initial *log odds* belief, and the third the previous time step *log odds* belief. The *inverse* sensor model specifies a distribution over the binary state variable as a function of the measurement $z_t$. The initial *log odds* belief can also be written as

$$\begin{aligned} l_0(y_j) &= \log_e \frac{P_{O_0}(y_j)}{1 - P_{O_0}(y_j)} \\ &= \log_e \frac{0.5}{0.5} \end{aligned} \tag{83}$$

Once the *log odds* for each time step is calculated, the corresponding posterior occupancy belief for that time-step can be retrieved using

$$bel_t(y_j|z_t, u_t) = 1 - \frac{1}{1 + exp(l_t(y_j)|z_t, u_t)} \tag{84}$$

This belief for each cell is updated as new sonar measurements are made, using the Markov process provided by the BBF to capture the effect of vehicle path and sensor measurements on the information to be communicated. Figure 87 shows the Bayesian dynamics using the BBF Markov process used for this study. The more measurements are made of any cell $j$, the higher or lower is its belief of being occupied based

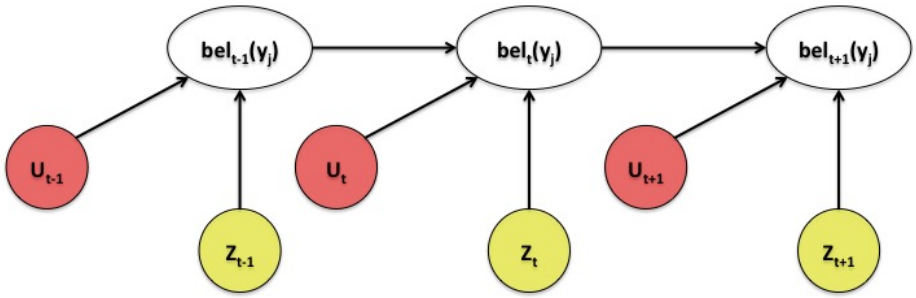


**Figure 87:** Bayesian dynamics for BBF Markov process.

on the detection capability of the sonar. Cells that have more certainty about its occupancy probability provide less information than those for which it is unknown. Next we present how we model area coverage as the amount of information entropy communicated using information gain and rate.

### 5.3.3 Information Gain

Information can be represented by the amount of cells transmitted to the main ship. If a given TA $A$ contains $N_p$ number of cells, then the survey objective can be translated to minimizing the information entropy parameter $H$ of the TA $A$, denoted $H(A)$, of the probability distribution equation defined over all cells $y_j \in A$ [49]

$$H(A) = -\sum_{y_j \in A} P_O(y_j) \log(P_O(y_j)) \tag{85}$$

Using our Markovian approximation through the BBF, we can rewrite (85) as the entropy at a given time $t$

$$H_t(A) = -\sum_{y_j \in A} bel_t(y_j|z_t, u_t) \log(bel_t(y_j|z_t, u_t)) \tag{86}$$

Initially each cell has unknown occupancy, $P_{O_0}(y_j) = 0.5$ for all $y_j \in A$, and the initial entropy of the TA $H_0(A)$ is at its maximum. For survey missions, the value of $H_t(A)$ is of little importance, what is relevant is the information gain ($IG$) , denoted $\triangle I_t(u_t)$, which is given by the absolute value of the difference in entropy before $H_t(A)$

and after a particular control action $u_t$, denoted $H_{t-1}(A)$, given by [172]

$$\triangle I(u_t) = |H_t(A) - H_{t-1}(A)| \tag{87}$$

The particular action $u_t$ could be a complex maneuver, consisting of a number of control actions and observations $z_t$ that spans multiple time steps. For our demonstration study, the only control actions considered are: 1) transmit bites of cells by acoustic communications, and 2) surface at available surface points to transmit bites of cells by RF communications. Both control actions will provide information gain, but at different quantities and rates. During surveys, the rate at which information is gained is critical (i.e. the faster the information is available, the better). Therefore, it is useful to denote information gain rate $IGR$ as

$$IGR = \frac{\triangle I(u_t)}{t} \tag{88}$$

While the UUV is underwater sweeping through the TA, bites of cell information are transmitted to the main ship every $t_a$ time steps using acoustic communications. At the end of each sweep, if RF communication is possible at that surface point, the UUV surfaces and transmits the rest of cell information to the main ship via RF communications at a given time $t_{rf}$, and submerge back down to continue the rest of the sweeps. In the next section we present the model used to predict whether surface points lie within good RF communications based on environmental conditions.

### 5.3.4 Communications Modeling for Surface Point Thresholds

For this study, lets assume the TA to be 10 km from the main ship, with a length of $L = 7\ km$, width of $W = 3\ km$, and at a depth of $D = 0.2\ km$, representative of deep-water regime [150]. Under the maritime conditions considered here, low altitude propagation on over-water paths between the main ship and a UUV at the water surface can be characterized by a "standard atmosphere" with some degree of evaporation ducts. A 24 m evaporation duct height was considered, which has been shown

to result in lower signal attenuation and larger number of skip zones compared to the worldwide mean 14 m evaporation duct height during RF communications between a ship and unmanned surface vehicles (USVs) [62]. The modified refractivity profile corresponding to the 24 m evaporation duct is the input to the APM propagation model, along with the radio transmitter and receiver characteristics from Table III. The output of APM is a propagation loss profile with range and height, and the same profile is assumed for all azimuths about the UUV transmitter, as is shown in Fig. 88. Threshold signal-to-noise ratio ($SNR$), denoted by $\omega_T$, is also computed by APM,

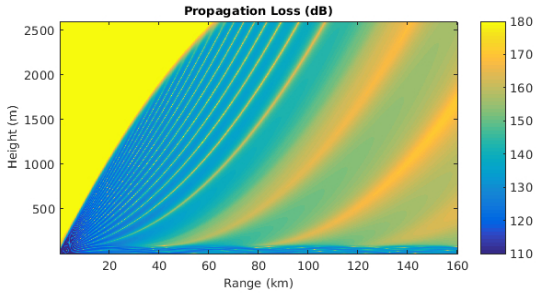


**Figure 88:** Propagation loss profile computed by APM.

and is given by

$$\omega_T = P_T + G_T + G_R + L_{rs} - L_{sys} - L_{cp} \tag{89}$$

where $P_T$ is the transmitter power, $G_T$ the transmitter antenna gain, $G_R$ the receiver antenna gain, $L_{rs}$ the receiver sensitivity, $L_{sys}$ are assumed system losses, and $L_{cp}$ is cross polarization loss. The received power $P_R$ can be decomposed into gains and losses in the following link budget given by

$$P_R = P_T + G_T + G_R - L_{APM} - L_{sys} - L_{cp} \tag{90}$$

where $L_{APM}$ is the propagation loss calculated by APM corresponding to the given antenna heights for the transmitter and receiver from the propagation loss profile.

The instantaneous $SNR$ parameter is computed as

$$SNR = P_R - P_N \tag{91}$$

where $P_N$ is the additive white gaussian noise (AWGN) power. Shown in Fig. 89 is the resulting received power as a function of range and the threshold power received corresponding to the given receiver sensitivity as the threshold value from APM.

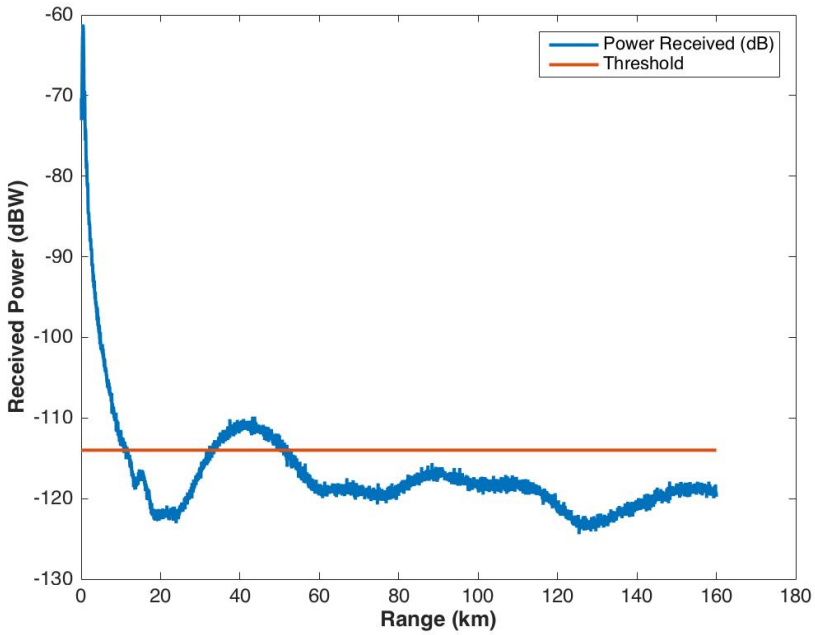


**Figure 89:** Received power $P_R$ profile and threshold of communications $\omega_T$.

The instantaneous $SNR$ is compared to the threshold of communications as follows to determine ranges of good communications and skip zones. Ranges with received power above the threshold values are regarded as ranges with good communications, and those below as ranges of bad communications, given by

$$SNR - \omega_T \begin{cases} > 0, \textit{good communications range} \\ \leq 0, \textit{skip zone} \end{cases} \tag{92}$$

Sweeps with surface points within good RF communication ranges allow UUVs to transmit data at a faster rate than those within bad RF communications. Next we give specifications of the UUV, the acoustic and RF communications, and define the sonar notional capability that we consider for this study.

**Table 3:** EdgeTech Side-Scan Sonar Assumed Operating Conditions and Specifications [82]

| | |
|---|---|
| Water temperature (°C) | 6-10 |
| Water salinity (ppt) | 32-34 |
| Height above sea floor (m) | 10 |
| Frequency (kHz) | 540 |
| Maximum range, R (m) | 100 |

### 5.3.5 Vehicle Sonar Sensor and Communications

The UUV is modeled after the Remus-600, powered by two rechargeable lithium-ion batteries, equipped with a side-scan and a gap-filling sonar, and acoustic and RF communications packages. Based on the Remus-600 vehicle specifications [125], the UUV is assumed to have a max forward speed of 4 knots, a nominal sweeping speed of 2 knots, and 24 hr endurance.

The side-scan sonar sensor on board the UUV is assumed to be comparable to the AN/AQS-20A system, currently used as a tow body that provides detection and classification capabilities [86]. Together with the gap filling sonar, the sonar system is assumed to cover a given range right underneath the UUV for the detection of objects on the sea floor. Figure 110 shows a depiction of the side-scan sonar and gap-filling sonar as it scans the sea floor, with the overall sonar range $R$ defined. The range of the side-scan sonar is itself a function of a number of factors, which include ambient noise, water temperature and salinity, water depth, and height above the sea bottom [38]. Table 12 shows specifications for the EdgeTech side-scan sonar under general and typical conditions used for this study [82].

The UUV is assumed to be equipped with the Woods Hole Oceanographic Institution (WHOI) Micro-Modem for the acoustic communications package. The WHOI Micro-Modem is a compact, low power, underwater acoustic communications and navigation subsystem that is used in multiple platforms as a baseline [93]. The modem specifications are given in Table 10.

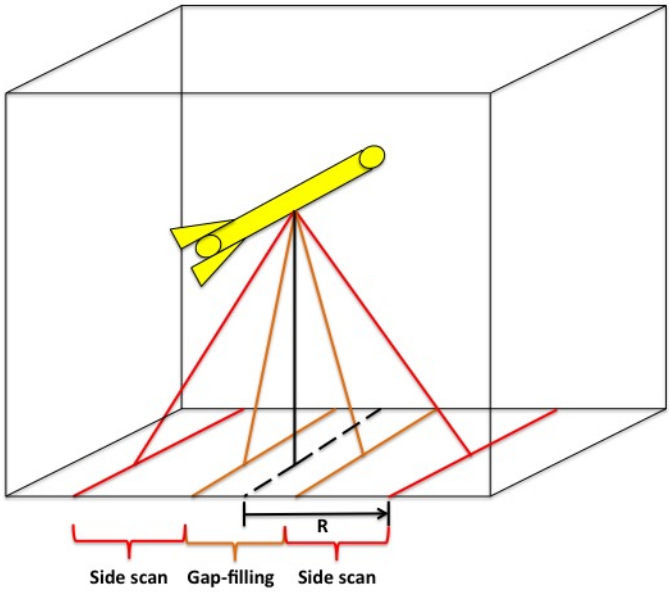


**Figure 90:** Side-scan and gap-filling sonar range.

**Table 4:** WHOI Acoustic Micro-Modem Specifications [93]

| | |
|---|---|
| Frequency (kHz) | 25 |
| Bandwidth (kHz) | 4 |
| Modulation scheme | PSK |
| Data rate (bytes/sec) | 10 |
| Time between updates, $t_a$ (sec) | 4 |

A FreeWave 900 MHz industrial radio was chosen as the RF communications package for its long range and representative data rate [92]. Radio specifications and power requirements are given in Table 5. An omnidirectional antenna was chosen, with given specifications and propagation angle also given in Table 5.

As the UUV sweeps through the TA, collecting cells of data from its sonar sensor, it communicates that data to the main ship via acoustic communications, and via RF communications at the end of each sweep if is possible.

**Table 5:** FreeWave Radio Specifications [92]

| | |
|---|---|
| Frequency (MHz) | 900 |
| Bandwidth (kHz) | 230 |
| Modulation scheme | 2-level GFSK |
| Data rate (kbps) | 154 |
| Propagation angle (deg) | 3 |
| Transmitter antenna height (m) | 0.5 |
| Receiver antenna height (m) | 25 |
| Receiver propagation loss sensitivity (dB) | -135 |
| Time spent communicating, $t_{rf}$ (sec) | 10 |

### 5.3.6 Results

For a required 60% TA percentage coverage, corresponding to $n = 90$ required sweeps, representative of a mission-level Measure of Performance (MOP) metric, the sweeps were distributed across the TA, and a comparison was made between the COA to surface within good RF communications ranges, or not. The three cases considered are summarized as follows:

- Case 1: Sweeps are evenly distributed along length of the TA, and communication is restricted to only acoustic communications.
- Case 2: Sweeps are evenly distributed along length of the TA, and both acoustic and RF communications are allowed. RF communications happen at end of each sweep if it is within good communication range.
- Case 3: Optimal sweep distances are found that maximize *IGR* using both acoustic and RF communications.

For Case 3, the GA optimization method was set up with an initial population of 100 randomly chosen design points. The weight on the constraint in the penalty function $r_p$ was increased by one unit each iteration to consider a broader design space initially and to make sure that constraints are met as the GA converged to a solution.

The TA location for the search and survey mission under the environmental conditions we considered is shown in Fig. 91.

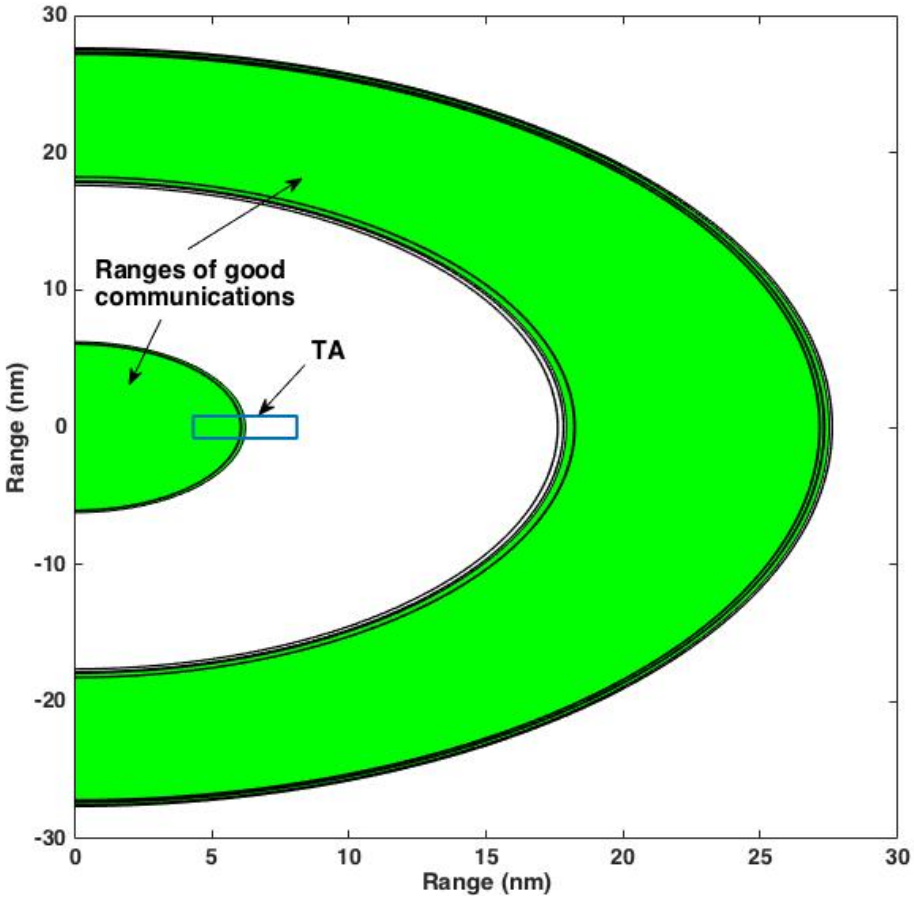


**Figure 91:** Search and survey mission scenario with TA and ranges of good communications.

The resulting sweep locations for cases 1, 2, and 3 are shown in Figures 92, 93, and 94, respectively, with green points denoting surface points within good communication ranges, and red points denoting surface points within skip zones.

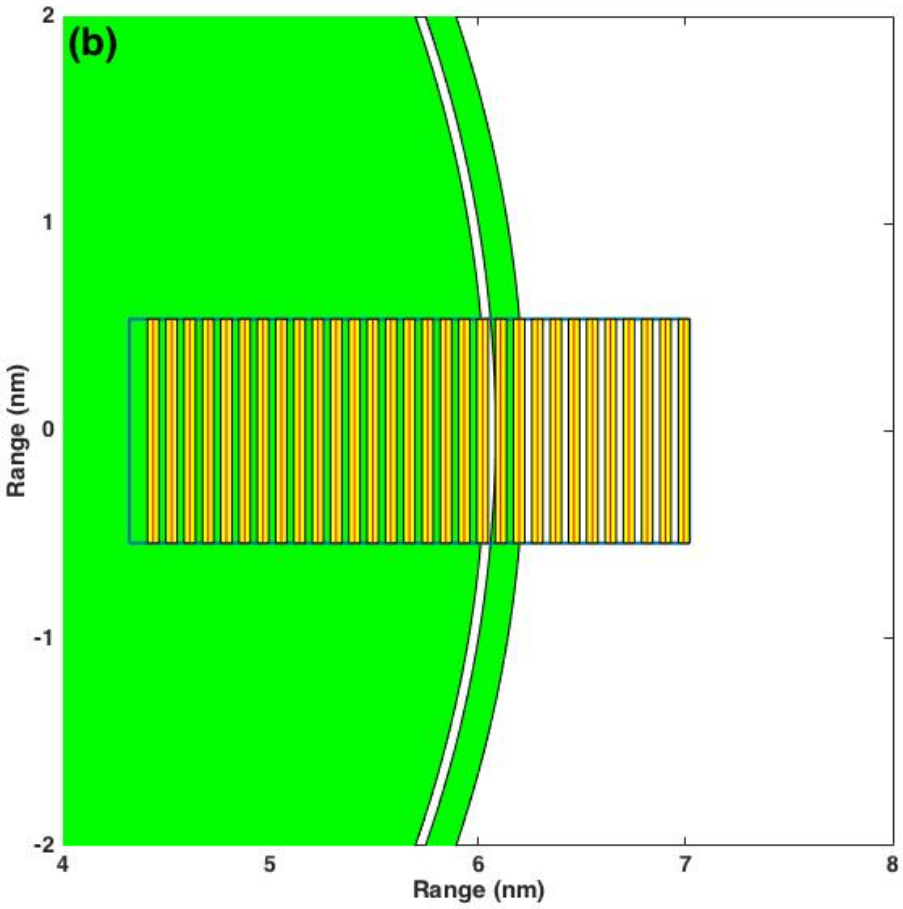


**Figure 92:** Case 1 sweep locations.

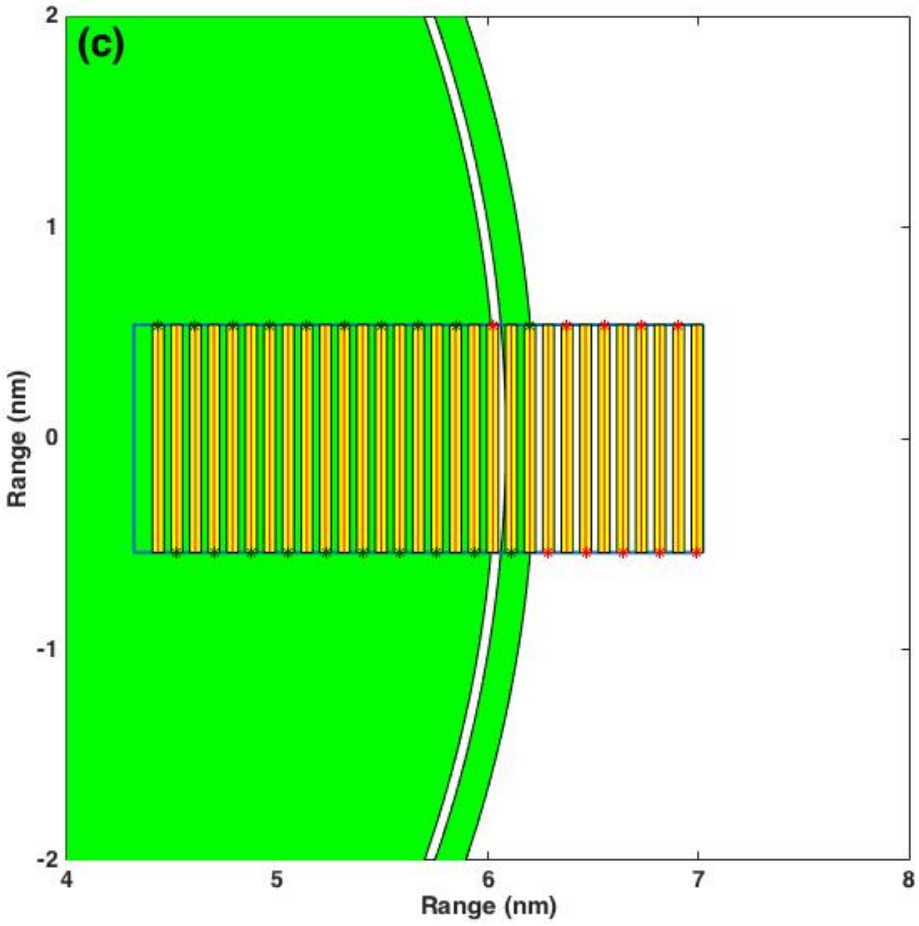


**Figure 93:** Case 2 sweep locations.

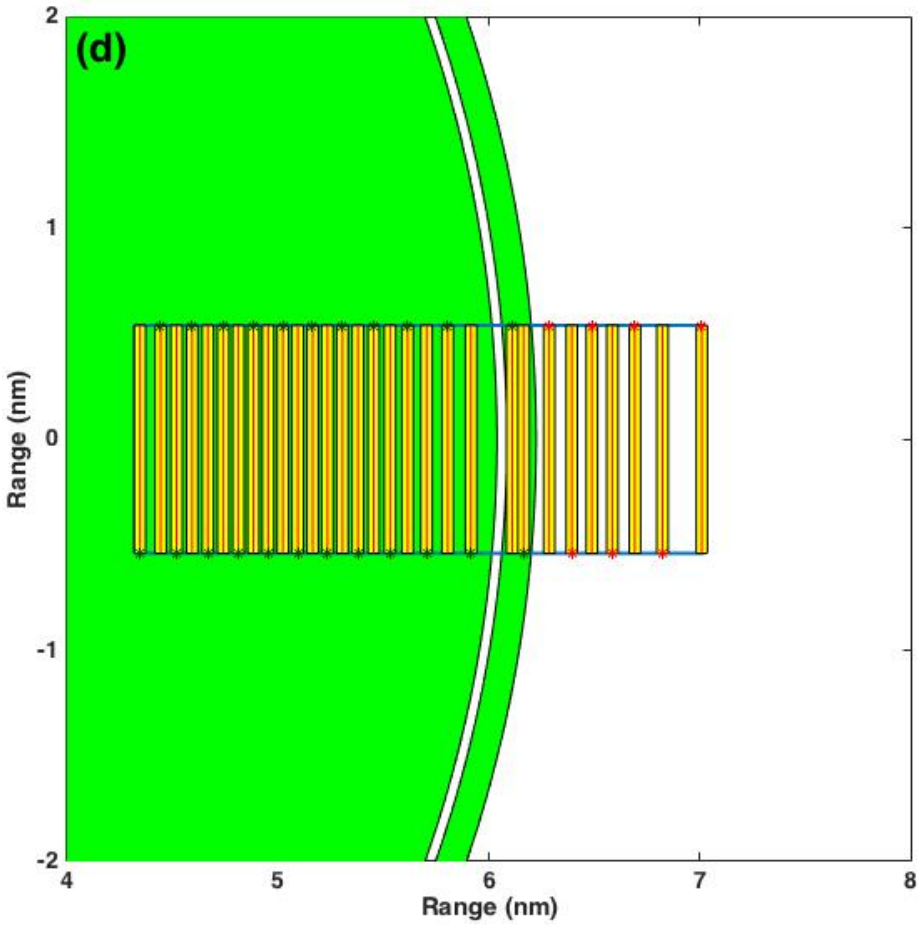


**Figure 94:** Case 3 sweep locations.

In each case, the information entropy and corresponding *IGR* is measured from the amount of sonar sensor data communicated to the main ship. The entropy for case 1 stays almost constant with time, with very small slope, as compared to cases where RF communications are allowed, as shown in Fig. 95. Entropy is reduced significantly more in case 3 when the sweeps distances are separated enough from each other that more can fit within good communication ranges (23 good surface points, as compared to 20 in case 2).

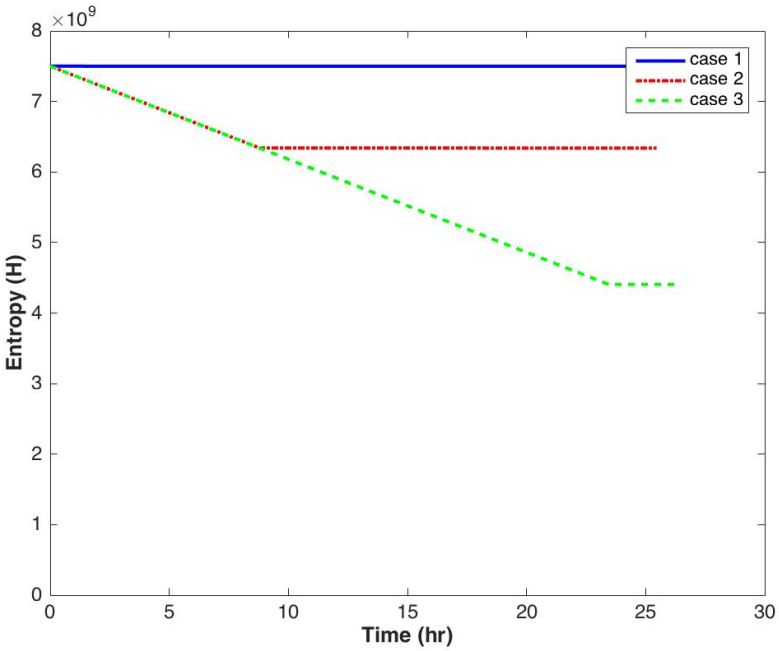


**Figure 95:** Entropy vs. time for each case.

In Fig. 96 the *IGR* is plotted as a function of time for each case. It can be seen in this plot that the rate of *IG* is greater when RF communications are used. Case 3 provides greater *IGR* for longer duration of time than case 2.

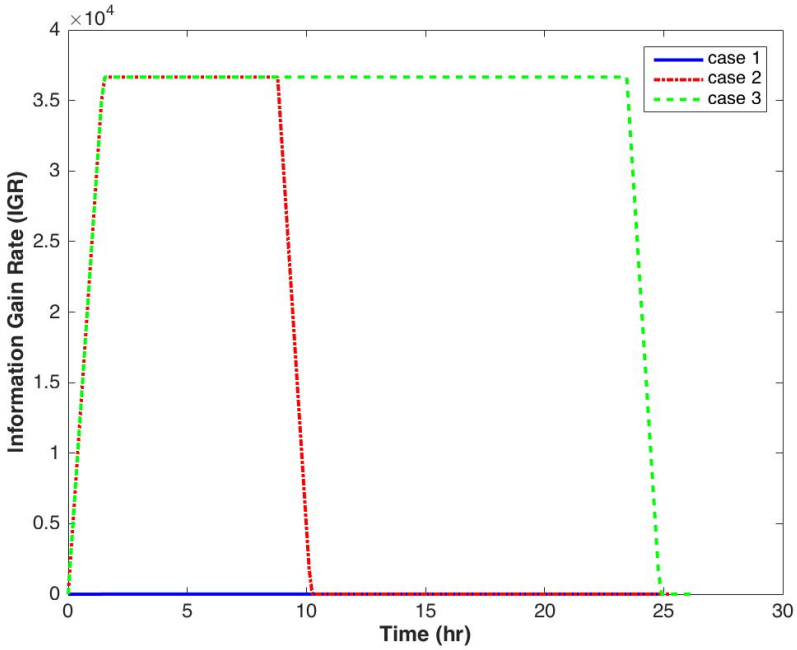


**Figure 96:** IGR vs. time for each case.

Time to complete 60 % area coverage was 25 hr, 25.5 hr, and 26.2 hr for cases 1, 2, and 3, respectively. While communicating via RF takes more time due to surfacing and coming back to cover the rest of the TA, its not much different from having the UUV communicating only via acoustic communications the whole time. Since cases 2 and 3 use RF communications to complete the mission, and provide more *IG* within almost the same amount of time, it can be concluded that allowing UUVs to surface and communicate by RF within predicted good communications areas can be more strategically beneficial in terms of situational awareness during search and survey missions.

## *5.4 Experiment 3 Results and Hypothesis Validation*

The third research question and corresponding hypothesis posed in the Proposed Methodology are repeated here for quick reference:

**Research Question 3 (RQ3)**: *How to model the effect of COAs on the quality and quantity of information communicated through the communications network?*

**Hypothesis 3 (HP3)**: *A sensor model can model Quality of information, and quantity of information can be modeled as the amount of state uncertainty that is communicated through the network.*

In Experiment 3 we presented scheduling solutions for a search and survey scenario where a UUV is allowed to communicate sonar data through acoustic and RF communications. The prediction of RF communications in maritime environmental conditions was useful in determining ranges of good communications and surface points that the UUV can use to communicate sensor data at a faster rate. The results showed that optimal *IGR* can be achieved if the distance between sweeps are varied in such a way that they lay within ranges of good communications, while still separated good enough so that they meet the percentage area coverage requirement. While this is a simple notional example, it captures the advantage of communications predictions due to environmental conditions.

We discretized the target area into a number of small cells of information that is picked up by the side-scan sonar sensor, and used our sensor model to capture the quality of information in terms of the probability of detection. The progression of sensor measurements and belief of the state of the occupancy of the cells in the target area was modeled and quantified by the Bayesian filter. The amount of information, in terms of the information entropy of each measurement, can be quantified by the information gain. Since we are concerned about getting valuable information as quick as possible during the mine-survey mission, we concentrated on the rate of the gain of information, or Information Gain Rate (IGR). We demonstrated through an example

how we can find optimal sweeping distances which maximize the IGR. Our analysis was based on our modeling of the transmission channel between the UUV and the main ship at each possible surface point location. Our results showed the benefit of using the Bayesian filter to help us define the quality and quantity of information we can transmit through our RF channel, while sweeping through a given target area. Therefore, we have validated Hypothesis 3.

In future work, we would like to investigate scenarios with more target areas, and under different environmental conditions. Temporal variation of the communications channel is another aspect we would like to account for and model, especially for long duration missions. Sweep overlaps will be allowed in the future to model the effects of detection probability on the amount of information being communicated. Other communication metrics we want to consider are signal bandwidth, the state of the transmission channel, modeled as a Markov fading channel, due to variations in the environmental conditions, and model how it affects other mission level metrics such as sensor area coverage, time to complete mission, and quality of information.

# CHAPTER VI

# COMMUNICATIONS-BASED OPTIMIZATION

Optimization of communications-based mission objectives and meeting mission level requirements are considered in this chapter. An important step in the COA Analysis process of the methodology is to perform optimization that meet constraints imposed on the COAs developed, as is shown in Fig. 97. The wargame is to find the optimal COA that meets all these requirements and maximize/minimize MOPs and MOEs. General guidelines and optimization methods are described and recommendations are made based on particular problems.

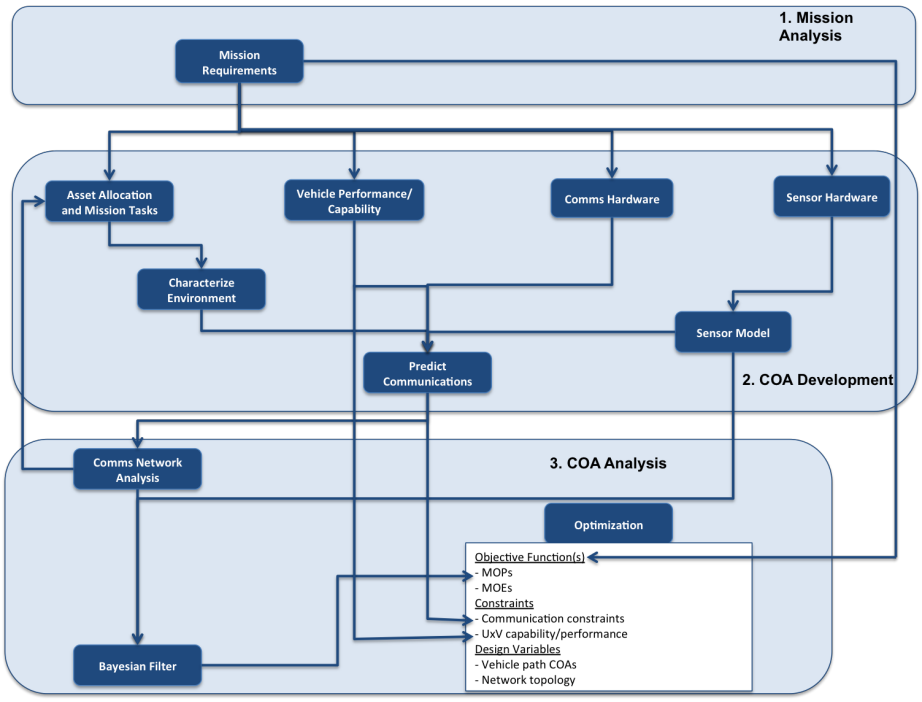


**Figure 97:** Optimization step of COA Analysis process

## *6.1 Optimization for Mission Planning*

The tools and optimization methods used in mission planning are established methods that are continuing to be explored and improved. Boukhtouta et. al. [40] provides several general categories of mission planners. According to Boukhtouta, good mission planning is generally characterized by quick response, decisive action and flexibility to adapt to the exogenous events and changing situations. A COA developed for a mission must consider an employment plan for dealing with one or more enemy COAs and should identify a deployment plan for moving forces and their equipment. By performing mission planning, plans are developed to bring the appropriate combat and supporting forces including their equipment and supplies to the operational field in time for the successful completion of their mission planning hierarchy [40].

Route planners are well established categories of mission planning that use optimization methods. These planners often developed to run onboard autonomous vehicles to response to dynamic environments and vehicle actions, and determine routes which are optimal relative to some metric (e.g., minimum power consumption and minimum risk). Genetic algorithms are used frequently to solve these route planning optimization problems to reduce runtime while maintaining high-fidelity models [204] [20].

Administrative support tools help the mission planner by automating large amount of details of mission planning found primarily in step 5 of the NPP. APGEN for example, is a planning tool developed by the Jet Propulsion Laboratory which allows a planner to work at a higher level while the tool automates allocation of the subtasks associated with high-level tasks [142]. Another example is agent support for policy-driven collaborative mission planning, which aids the planner working as part of a coalition by automatically detecting and preventing policy violations [199]. While these tools do not help to generate COAs, they still inform expected functionalities of mission planning tools.

Logistics and transport optimizers, such as the Combat Logistic Force Planner [47], focus on supply chain optimization. These tools benefit from predictable actions and the ability to use average trends rather than high-fidelity simulation. Run-time is not a concern in these tools since supply missions can take days to months. While predictability and long-time scales are not characteristics of Navy battle missions, logistic optimization tools show potential for tools that cover multiple steps of the NPP since they generate, analyze, and recommend COAs.

Battle planners belongs to a category of tools which assist planning operations for combat forces. The Naval Postgraduate School's Autonomous Unmanned Vehicle Workbench (AUVW) for example is a high-fidelity simulator which enables accurate and rapid wargaming within the current planning process, but does not perform any optimization of plan recommendations [72]. High-fidelity simulators do provide planners with accurate results and near-real-life wargaming scenarios to make better COA decisions during COA analysis, but do not aid planning in any other way other than merely visualization. FOX-GA, an academic tool which simulates infantry maneuvers and uses genetic algorithms to generate, evaluate, and recommend a set of plans to a commander [180], is an exception however. FOX-GA demonstrates the potential of optimization in battlefield planners by producing good, if not optimal, plans in less time than typical human planners and the ability to develop and evaluate many diverse COAs.

Therefore, while optimization-based tools are present in logistics and path planning, there is a demonstrated need for maritime battlefield planners which perform optimization routines. The current state of the art are mission simulation and visualization tools which only facilitate step 3 of the NPP, but do not really aid interpreting the overall vision of the mission and developing COAs. This leads to the following identified gap:

**Gap**: *Mission planning tools are needed that incorporate optimization routines and help mission planners during the NPP steps of mission analysis and COA development.*

## *6.2 Optimization Methods*

In light of the need for optimization during the NPP steps of mission planning, this section provides brief literature review on tools and methods that can be used for different optimization problem formulations. The general constrained optimization problem can be formulated as follows:

$$\begin{aligned} \min_{\mathbf{X}} \quad & F(\mathbf{X}) \\ \text{subject to} \quad & g_j(\mathbf{X}) \leq 0 \quad j = 1, ..., \ell \\ & h_k(\mathbf{X}) = 0 \quad k = 1, ..., b \\ & X_i^l \leq X_i \leq X_i^u \quad i = 1, ..., n \end{aligned} \tag{93}$$

where $\mathbf{X}$ is the vector of design variables, $F(\mathbf{X})$ represents the objective functions, $g_j(\mathbf{X})$ represents inequality constraints, $h_k(\mathbf{X})$ represents the equality constraints, and each design variable may have lower $X_i^l$ and upper $X_i^u$ limits, also known as side constraints. The objective function, inequality and equality constraints may be linear or non-linear, and explicitly or implicitly a function of the design variable $\mathbf{X}$.

Depending on the nature of the problem, different optimization method alternatives can be used. The problem may be unimodal, with only one optimal solution, or multi-modal with multiple possible optimal solutions, or may not have any optimal solution [216].

If the optimization problem can be formulated with the objective function and constraints as linear functions of the design variable $\mathbf{X}$, then Linear Programming (LP) optimization methods can be used [216]. If the objective and constraints are

not linear, often is possible to linearize them about a point and solve using LP techniques, such as the simplex method [69]. For linearization, a first-order Taylor series expansion is made of the objective and constraint functions, and the resulting linear problem is solved using LP routines. The result is again linearized and the process repeated until some convergence criteria is achieved [216]. The benefits of such techniques are that computer codes based on this method are widely available, have been extensively tested and are highly reliable [216]. As a relevant study, an Integer Linear Programming (ILP), which is a LP with the variables being strictly *integers*, is used in Erkan et. al. to determine energy-optimal UUV surfacing and slave/master configurations in a 3-dimensional communications network [88]. Another relevant study used Mixed Integer Linear Programming (MILP), which is a LP with *some* variables being integers and others real, to find the optimal communication point of communication that minimizes energy consumption while operating in a realistic communication environment, and under a given time budget after visiting a number of points of interest [222].

If the optimization problem can be formulated as unconstrained, then special methods and techniques can be used to find the optimal. The different methods available to solve unconstrained optimization problems rely on different type of information that needs to be provided in searching for the minimum of the function [216]. Zero-order methods require only function evaluations, first-order methods require also function evaluations and the gradient of the objective function information, and second-order methods rely on function evaluations, gradient information, and the Hessian matrix [216]. In general, the more information is available and used in the process of finding the optimal solution, the faster the optimization procedure and the more accurate the solution. The only drawback is that getting this information may not be trivial or available, and may require additional effort. If the optimization problem contains constraints, sequential unconstrained minimization techniques can

be used by setting up the problem as an unconstrained problem by adding penalty functions to the objective function [216].

On the other hand, if the optimization problem involves discrete variables, the function evaluations are cheap to compute, and the objective function is multi-modal (it contains a global minimum and many relative minima), then Genetic Algorithms (GAs), a type of evlolutionary algorithm [71], are the attractive optimization methods to use [216]. Key features of GAs are that: (1) it uses function values only, (2) it naturally handles discrete variables, (3) it is easy to program, and (4) it requires large number of function evaluations, but if approximation techniques are used, they can be made fast [216] [73].

Another optimization method used if the optimization problem involves discrete variables and the objective function is cheap to compute is Simulated Annealing. Annealing is a process in metallurgy where metals are slowly cooled to make them reach a state of low energy where they are very strong. Simulated annealing is an analogous method for optimization. It is typically described in terms of thermodynamics. The random movement corresponds to high temperature; at low temperature, there is little randomness. Simulated annealing is a process where the temperature is reduced slowly, starting from a random search at high temperature eventually becoming pure descent as it approaches zero temperature [11]. The randomness should tend to jump out of local minima and find regions that have a low heuristic value; greedy descent will lead to local minima. At high temperatures, worsening steps are more likely than at lower temperatures. This process is done until some convergence criteria is met.

In the case where the optimization problem is unconstrained and involves continuous variables, then Particle Swarm can be an attractive optimization method. This method is based on the idea of a population with each member of the population being a particle that has a position in space defined by its vector of design variables $X^i$, and also will have a velocity vector $v^i$ [216]. The method can be thought of as

modeling a swarm of bees seeking food, and making decisions based on neighbor's location and speeds. [118].

Novel optimization techniques based on biologic systems and social interactions have been developed over the years which provide global distributed optimization and control. One of these is the Bacterial Foraging Optimization Algorithm (BFOA) proposed recently in [160], which mimics how bacteria optimizes the time spent in searching for food given different available paths and corresponding rewards and risks [37]. These methods can be used in cases where time, reward, and risks play an important role in selecting among different options.

### 6.2.1 Mission Objectives and Constraints

The formulation of the multi-objective optimization problem can be posed as given in Eq. 93. The objective function $F(\mathbf{X})$ is based on quantifiable mission-level objectives: MOPs and MOEs. These MOPs and MOEs are high-level measures of both mission-level and communication network performances. Depending on the mission, mission-level effectiveness can be measured by quantifying how good tasks are being performed by UxVs. Representative mission-level MOP and MOE for UV Sentry missions are shown in Fig. 98.


**Figure 98:** Representative MOPs and MOEs for UV Sentry missions.

Quality of communications network can be quantified in terms of the states of individual transmission channels, and in terms of situational awareness provided by the communications network (information quality). State of transmission channels can be measured by the SNR/BER provided by the communications models. Situational awareness provided by the communication network can be measured as the quality and quantity of information provided by the communications network to the

main ship and between UxVs. Quantity of information can be mapped to decrease of entropy in the mission by communicating UxV states and sensor data during the mission for example, as is modeled in the Bayesian filter. And this measure of quantity and quality of information will be different for RF and acoustic communications (see right side of Fig. 98).

Inequality and equality constraints represent the vehicle capabilities, environmental constraints, mission requirements, sensor capability, and communications constraints, which were mostly defined during the COA development step of the NPP mission planning process. An additional constraint will be added in a later section to impose reliability in the communications network due to communications failures.

Design variable vector $\mathbf{X}$ consists of communication-based COAs and schedules used to optimize the objective function.

### 6.2.2 Network Reliability Constraints

When communication failures occur, either due to environmental conditions, hardware failure, or vehicle failure, the communication network may be compromised. When failures occur, potential methods for re-establishing the communication network are: continue trying to communicate, increase the communications power gain, move to another location and re-try, etc. Usually these methods are inefficient and do not always guarantee that communications network will be re-established.

As stated in the RO, one of the proposed goals is to find optimal communication-based COAs that are reliable to network failures. One method for modeling the communication network is as an undirected graph, with nodes representing the vehicles, and edges representing the communication channels between the vehicles , as was demonstrated in [18] and [17]. The quality of the resulting communication network from link failures (edge removals) can be used to constraint the vehicle locations, COAs, and schedule during the mission as part of the mission analysis.

### 6.2.3 COA Design Variables

The optimization method for finding optimal communications-based COAs and schedules is highly dependent on the nature of the problem, the constraints, and the design variables in the formulation of the multi-objective optimization problem given by Eq. 93. Since most of the variables used are of discrete nature and have non-linear impact on the constraints and objective functions, selecting an evolutionary optimization method seems to be a viable option. Genetic algorithm is an evolutionary optimization method that is simple to use and is well documented. The major drawbacks of such evolutionary optimization methods is its complexity and its non-deterministic nature (e.g., is hard to track the solution from its inputs). However, a major advantage is that they are suitable for multi-objective non-linear, discrete problems. Converting all MOPs and MOEs to costs removes sensitivity to weights of aggregate objective function. Each solution from the population, corresponding to a set of COAs and schedules, can be tested for network reliability constraints as described in the previous sections.

Once optimal communications-based COAs and schedules are found and selected as feasible and viable solutions for the mission at hand, a separate optimization routine is performed to find optimal re-establishing communication COAs in cases when link and nodes fail unexpectedly. The goal is to anticipate some level of UxV autonomy for choosing how to re-establish a lost communication link. One way to do this is by using Foraging techniques which has been used to find residence time looking for food in microbial bacteria. The method involves looking for food using different search patterns and rank them in terms of the amount of reward that they provide. These Foraging techniques can be used to rank different re-establishing communication COAs by time spent, processing time, and the potential risk. Prey and patch methods are then used to determine which COAs to use and for how long. The selection of the method will be based on the mission at hand and the importance

of the message to be sent. Some of these re-establishing COAs include relaying communications through another close-by UxV, return to last successful transmission location, loiter for some time and retry, adjust heading towards higher probability of communications, or return to base.

# CHAPTER VII

# METHODOLOGY DEMONSTRATION: MINE SURVEY MISSION SCENARIO

To demonstrate the proposed methodology for meeting the RO, a Mine Survey mission scenario will be considered. Mine survey mission vision for the future involves using UUVs to detect mine-like objects (MLO) at specific target areas from the sea-base. The UUVs carry sonar sensors for the detection and classification of mines, and are equipped with both RF and acoustic communications hardware for both types of communications. They are assumed to be deployed from a main ship, and must perform lawn-mower pattern sweeps surveys during the detection task.

In the following sections, the proposed methodology will be followed step by step. Since the methodology will be demonstrated using this particular case study, certain mission requirements and environmental constraints will be assumed. However, the benefits and effectiveness of the methodology during the mission planning phases will be pointed out in the process for use in other similar unmanned vehicle mission scenarios.

## *7.1 Step 1: Mission Analysis*

This is the first step of the methodology, shown in Fig. 99, where mission requirements are explicitly specified in the mission statement. In this step we specify the TAs locations, their dimensions, and percentage area coverage requirements around the sea base. We also specify the communication network requirements.

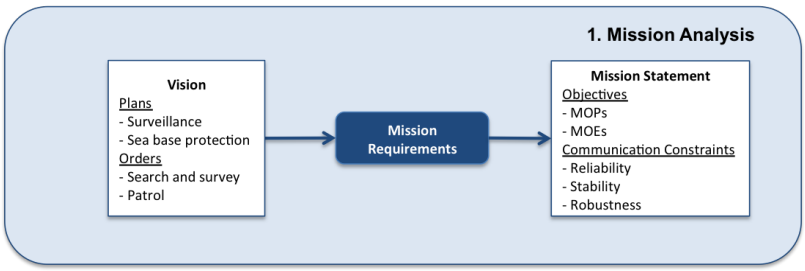


**Figure 99:** Step 1: Mission Analysis.

### 7.1.1 Sea Base and Target Areas Specifications

To demonstrate our methodology using the UV-Sentry vision, the search and survey mission is modeled after the mine-counter-measures (MCM) mission, which needs to be performed around a given sea-base. We only model the search and survey of target areas, where detection of objects of interest needs to be performed. We do not concentrate in later phases of the MCM mission such as identification, classification, and neutralization.

The sea-base is stationed in a littoral combat environment, where there might be different types of threats, such as piracy attacks, mines, underwater vehicle attacks, etc. For this demonstration study, we only concentrate on the mine threat. In littoral environments, mines can be of different types, shapes, and be triggered in different ways [150]. In general, depending on the depth, certain types of mines can be expected, as is shown in Fig. 100.

For the mine search and survey mission, suppose the main ship, from which the commander and mission planning staff use the propose methodology, is located at the center of the ship zone radius inside the sea base. The sea base is supplied through a corridor at the lower-left side of the sea base, with ships going in and out of the sea base at some frequency. The search and survey needs to be performed from the ship zone radius to some radius, called the mine detection radius, as is shown in Fig. 101. TAs are distributed within this mine detection radius. For this study, assume 4 TAs are distributed around the main ship, at locations shown in Fig. 101. Assume there

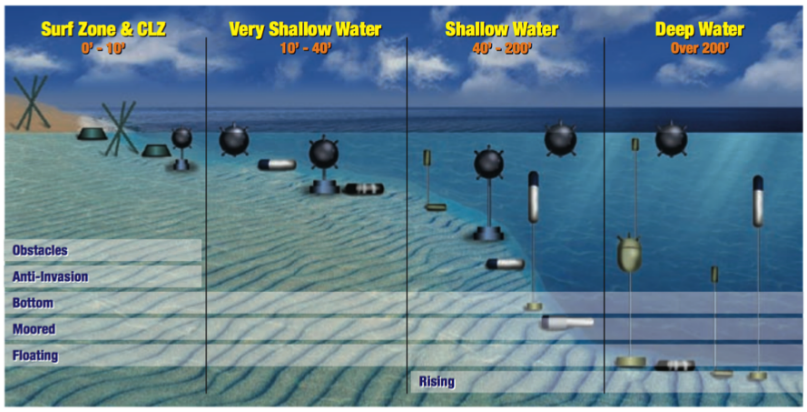


**Figure 100:** Expected mine depths for littoral environments [150]

are also 3 TAs along the supply lane, as shown in Fig. 101. All TAs are of the same dimensions and at the same depth, representative of deep water regime, as is shown in Fig. 100. The dimensions and locations of each TA are shown in Table 6.

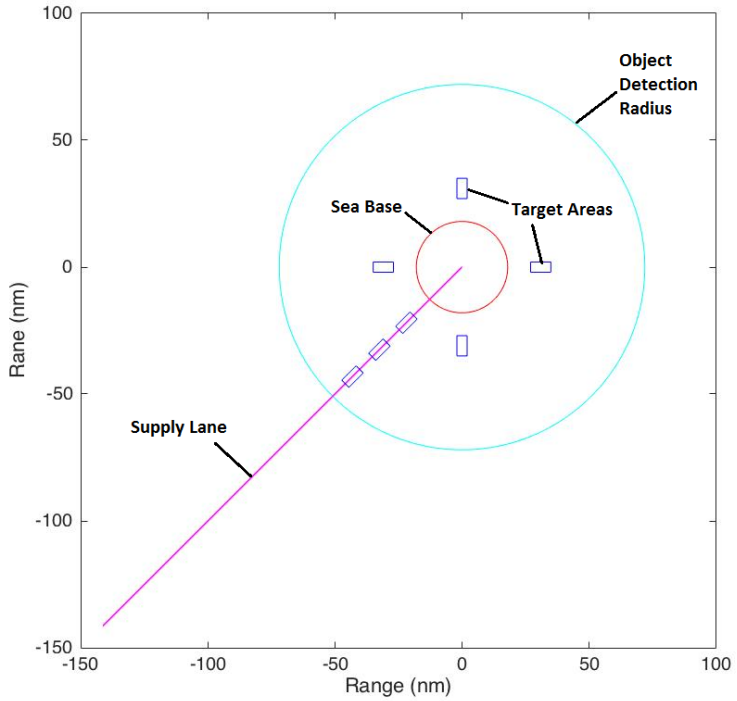


**Figure 101:** Sea base environment for search and survey mission.

The selected TA locations and dimensions are such that they provide some area

**Table 6:** TA Locations and Dimensions

| TA | Distance (nm) | Azimuth $\theta$ (deg) | Length (nm) | Width (nm) | Depth (m) |
|---|---|---|---|---|---|
| 1 | 31 | 0 | 8 | 4 | 200 |
| 2 | 31 | 90 | 8 | 4 | 200 |
| 3 | 31 | 180 | 8 | 4 | 200 |
| 4 | 31 | 270 | 8 | 4 | 200 |
| 5 | 31 | 225 | 8 | 4 | 200 |
| 6 | 46 | 225 | 8 | 4 | 200 |
| 7 | 61 | 225 | 8 | 4 | 200 |

coverage around the sea base and the supply lane. The choice of locations and dimensions are chosen for simplicity and to keep track of TAs.

We assume further that only 60% of the area of all TAs need to be covered during the detection phases, representative of an initial detection phase that needs to be done as quick as possible and provide as much information as possible about potential threats.

We also assume that the specified communication requirements derived from the Commander's vision are the following:

- Each UUV must be able to communicate at a given location in the operational environment back to the main ship.
- Consider using available UxV assets to help relay communications.
- Provide communications that have good quality, that are robust to environmental conditions, stable to vehicle motions and signal fluctuations, and reliable to link failures.
- Provide path navigation that maximize the amount of information sent back to the MS through the use of both acoustic and RF communications.

## *7.2 Step 2: COA Development*

The next step in the methodology is the COA Development, where based on mission requirements from the mission statement, the planning staff identifies available

unmanned vehicle assets and their capability and performance in terms of motion, communications, and sensors. From these generated COAs, the user also characterizes the environment based on the domains and ranges that these vehicles are expected to operate at. Finally, the user predicts communications between vehicles and from vehicles to main ship to determine if the COAs are feasible. If they are not feasible, an iteration is done to allocate assets or select other suite of unmanned vehicles that lead to a better communications network.

The first step of the COA Development process is to identify COAs that meet the mission requirements, as is shown in Fig. 102. These COAs involve identifying what available unmanned vehicle assets can be used to meet the mission requirements, what their capability are, what communications hardware do they carry, what sensor information can they provide to meet the mission requirements, and how to distribute the tasks among these assets. In the following subsections, we will walk through each phase of the COA development in detail using our case study as an example.

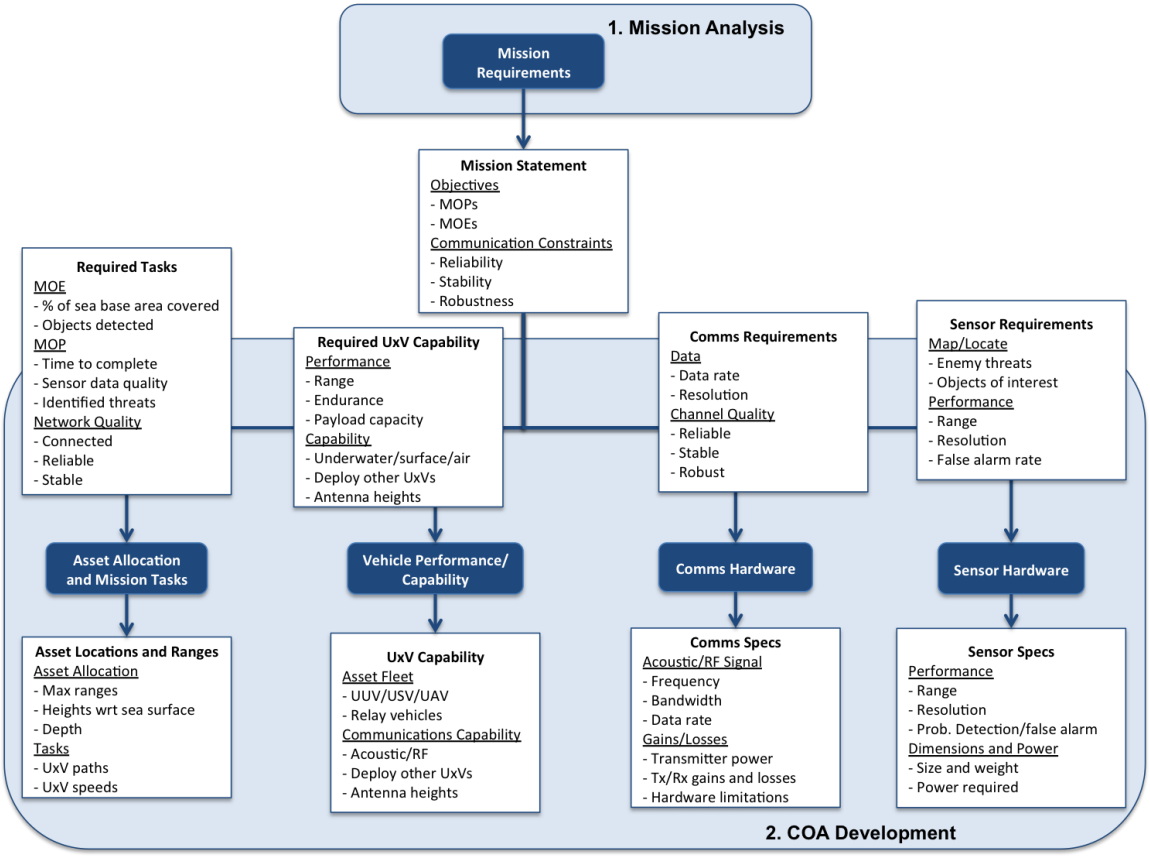


**Figure 102:** Step 2: COA Development phase 1.

### 7.2.1 Vehicle Performance and Capability

Vehicle performance and capability is based on existing state of the art unmanned vehicles from which data is available or from which our laboratory has experience with. Three main types of UxVs are considered in this study: UUVs, USVs, UAVs, and Cormorant, a hybrid aerial and underwater vehicle. Next, the performance and capability of a main ship, from which all UxVs are deployed, and each UxV, are specified with corresponding references, and assumptions made are explicitly stated.

#### *7.2.1.1 Main Ship Performance and Capability*

For this case study, the main ship stationed inside the sea base within the ship zone, from which all unmanned vehicles are deployed, is assumed to be comparable

**Table 7:** LCS-2 Independence Specifications [3]

| | |
|---|---|
| Max speed (knots) | 40 |
| Height (m) | 31.6 |

to the Littoral Combat Ship (LCS) by General Dynamics. Specifically, the LCS-2 Independence Class, shown in Fig. 103, is assumed for this study, for its high speed, agility, and shallow draft [3]. LCS specifications on relevant performance and dimensions are shown in Table 7.

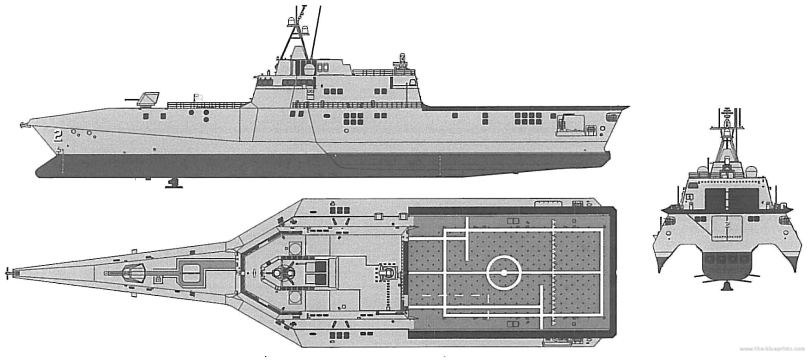

**Figure 103:** LCS-2 Independence by General Dynamics [3].

#### *7.2.1.2 UUV Performance and Capability*

The UUV performance and capability is based on the Remus 600 by Kongsberg Maritime [125]. The Remus 600, shown in Fig. 104, is an autonomous underwater vehicle designed to support Navy's growing need for operations requiring extended endurance, increased payload capacity, and greater operating depth (up to 600 m). Specifications of the Remus 600 used for this demonstration study are shown in Table 8.


**Figure 104:** Remus 600 by Kongsberg Maritime [125].

**Table 8:** Remus 600 Specifications [125]

| | |
|---|---|
| Max forward speed (knots) | 4 |
| Nominal sweep speed (knots) | 2 |
| Vertical surfacing speed (knots) | 1.5 |
| Max endurance (hr) | 24 |

**Table 9:** WAM-V Specifications [6]

| | |
|---|---|
| Max speed (knots) | 11 |
| Nominal speed (knots) | 3 |
| Max Range (nm) | 100 (at 3 knots) |

#### *7.2.1.3 USV Performance and Capability*

The USV performance and capability is based on the 16 ft Wave Adaptive Modular Vessel (WAM-V) from Marine Advanced Research Inc. [6]. The WAM-V, shown in Fig. 105, is suited for unmanned operation during surveillance, sensor and vehicle delivery, and communications node [6]. The same USV is used in our laboratory at ASDL to compete at the bi-annual Maritime Robot-X challenge, hosted by the Association for Unmanned Vehicle Systems International (AUVSI) [9]. Although other USVs are available with better performance, for this study we selected this USV due to our experience with the vehicle, and the possibility to test our results from this demonstration study in the near future. Specifications on the WAM-V used for this demonstration study are shown in Table 9.

**Figure 105:** WAM-V by Marine Advanced Research Inc. [6].

## *7.3 Communications and Sensor Hardware*

In this section, specifications about the communications and sensor hardware are given. We also provide a sensor model for modeling uncertainty in measurements, which will be used in later sections to define sensor data information.

### 7.3.1 Communications Hardware

The communications hardware carried by each unmanned vehicle is based on its payload capability and operation domain. For this demonstration study, it will be assumed that all vehicles carry the same RF communications packages, but with different antenna heights. UAVs and Cormorant will be capable of changing the antenna heights, but the main ship, USVs, and UUVs RF antenna heights will be assumed constant. UUVs and Cormorant will be assumed to be capable of both acoustic and RF communications, by UUVs capability to surface and Cormorant's capability to surface and fly at some altitude and hover. The communications hardware packages used for this study were selected on the state-of-the-art in acoustic and RF communications for small vehicles and based on available hardware that can be tested in the future.

#### *7.3.1.1 Acoustic Communications Package*

A Woods Hole Oceanographic Institution (WHOI) Micro-Modem, shown in Fig. 106 is selected for the acoustic communications package. The WHOI Micro-Modem is a compact, low power, underwater acoustic communications and navigation subsystem that is used in multiple unmanned vehicle platforms as a baseline [93]. The modem specifications are given in Table 10.

**Table 10:** WHOI Acoustic Micro-Modem Specifications [93]

| | |
|---|---|
| Frequency (kHz) | 25 |
| Bandwidth (kHz) | 4 |
| Modulation scheme | PSK |
| Data rate (kbps) | 0.08 |
| Time between updates, $t_a$ (sec) | 4 |

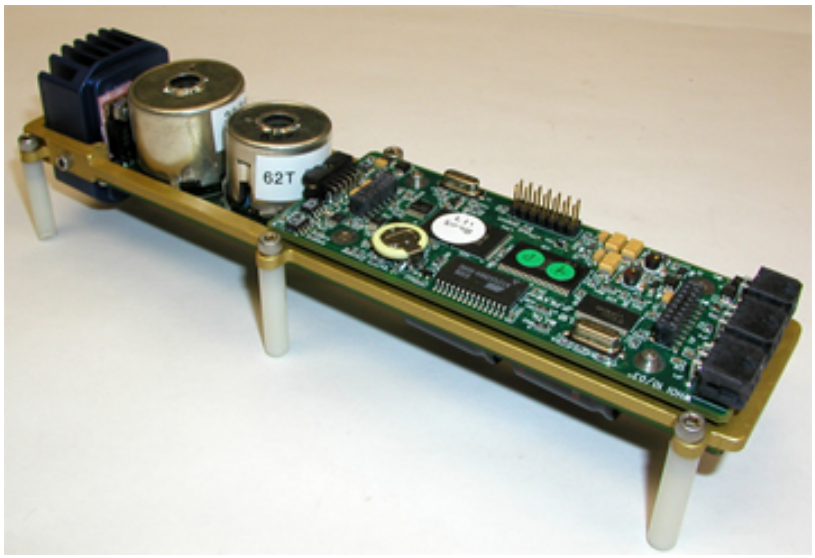

**Figure 106:** WHOI Acoustic Micro-Modem [93].

#### *7.3.1.2 RF Communications Package*

An MPU5 Wave Relay smart radio from Persistent Systems, shown in Fig. 107, was selected as the RF communications package for its long range, military rated performance, reliability, durability casing design, 3x3 multiple-input-multiple-output (MIMO) configurable network, and high data rates [7]. MPU5 radio specifications and receiver sensitivity are given in Table 11. An omni-directional antenna was chosen for each radio. Our laboratory also acquired 3 MPU5 radios for transmitting sensor data of our unmanned vehicle during competitions and for research purposes. These can be used to test our predicted performance and models in the near future.

**Table 11:** MPU5 Persistent Systems Radio Specifications [7]

| | |
|---|---|
| Frequency (MHz) | 2400 |
| Bandwidth (MHz) | 20 |
| Modulation scheme | OFDM (BPSK, QPSK, 16QAM, 64QAM) |
| Data rate (Mbps) | 150 |
| Minimum Receiver Sensitivity (dBm) | -98 (BPSK) |


**Figure 107:** MPU5 smart radio from Persistent Systems Wave Relay [7].

The MPU5 radio can operate in two different bands, the S-band (2200-2507 MHz) and the L-band (1350-1390 MHz), however, the L-band is restricted to military operation only. Within the S-band frequency spectrum, the frequency allocations in the United States, enforced by the National Telecommunications and Information Administration (NTIA) [5], limits the frequency of operation to within 2400 MHz, where amateur frequencies are open for operation without the need of a license, as is shown in Fig. 108.

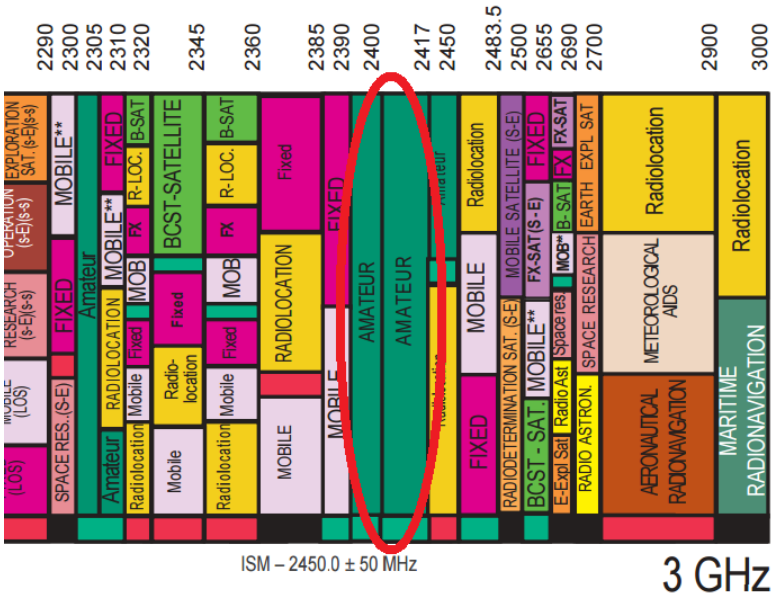


**Figure 108:** Unites States frequency allocation and selected frequency of operation [5].

### 7.3.2 Sensor Hardware

For this mine search and survey mission case study, objects of interest need to be detected within the percentage area coverage of underwater TAs. Typically a sonar sensor is used to provide underwater detection of objects. Sonar sensor is based on active acoustic sound waves emitted from a source and determining the object shape baed on the reflected echoes of the signal [198]. For this study, UUVs will be assumed to be equipped with sonar sensors to provide the object detection task within the TAs. A side-scan sonar and a gap filling sonar will be used for their applicability at deep water regimes assumed for this study.

The side-scan sonar sensor on the UUVs is assumed to be comparable to the EdgeTech side looking sonar on the AN/AQS-20A Mine Reconnaissance Sonar System (RMSS), shown in Fig. 109, currently used as a tow body that provides mine detection and classification capabilities through its Volume Search Sonar (VSS), Forward Looking Sonar (FLS), Gap Filler Sonar (GFS), and Side Looking Sonar (SLS) [86].

**Table 12:** EdgeTech Side-Scan Sonar Assumed Operating Conditions and Specifications [82]

| | |
|---|---|
| Water Temperature (°C) | 6-10 |
| Water Salinity (ppt) | 32-34 |
| Frequency (kHz) | 540 |
| Depression Angle $\Phi$ (deg) | 50 |
| Pixel Resolution $(x_p, y_p)$ (m/pixel) | (0.1, 0.1) |
| Bytes per pixel (Bpp) | 10 |

Together with the gap filling sonar, the sonar system is assumed to cover a given range right underneath the UUV for the detection of objects on the sea floor. Figure 110 shows a depiction of the side-scan sonar and gap-filling sonar as it scans the sea floor, with the overall sonar range $R$ defined. The range of the side-scan sonar is itself a function of a number of factors, which include ambient noise, water temperature and salinity, water depth, and height above the sea bottom [38]. Table 12 shows specifications for the EdgeTech side-scan sonar under general and typical conditions used for this study [82].

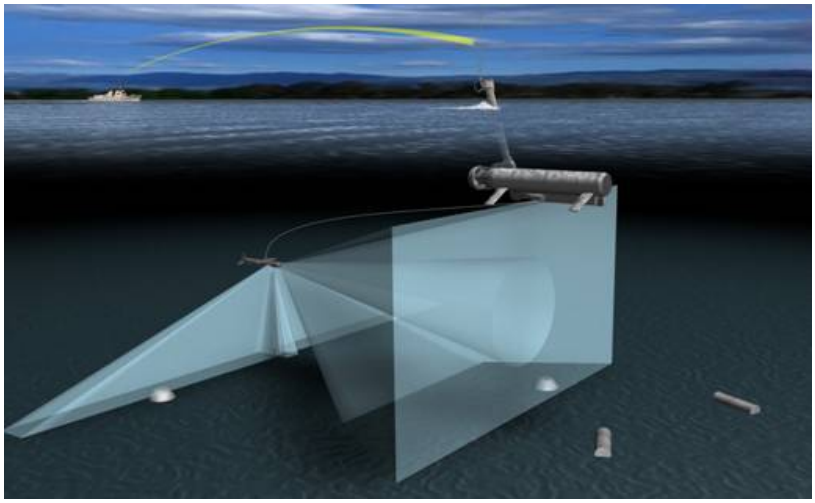

**Figure 109:** Mine Reconnaissance Sonar System (RMSS) by Raytheon [86].

Assuming the UUV sweeps at a height above the TA of $h_{uuv}$ m, with a depression angle of $\Phi$, as is shown in Fig. 111, then the range $R$ of the side-scan sonar is given

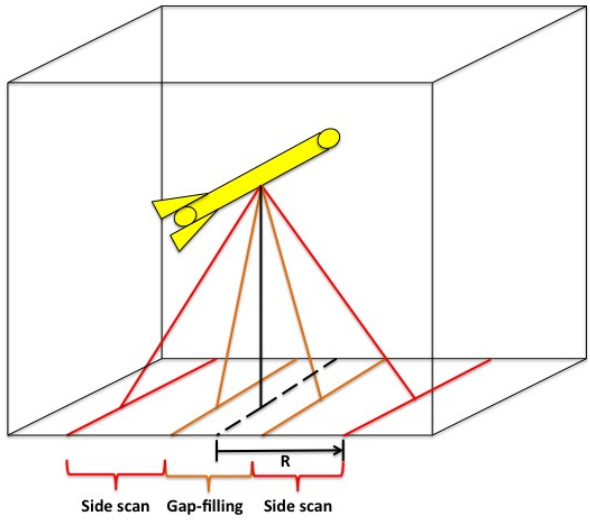


**Figure 110:** Side-scan and gap-filling sonar range.

by

$$R = h_{uuv} \tan(\Phi) \tag{94}$$

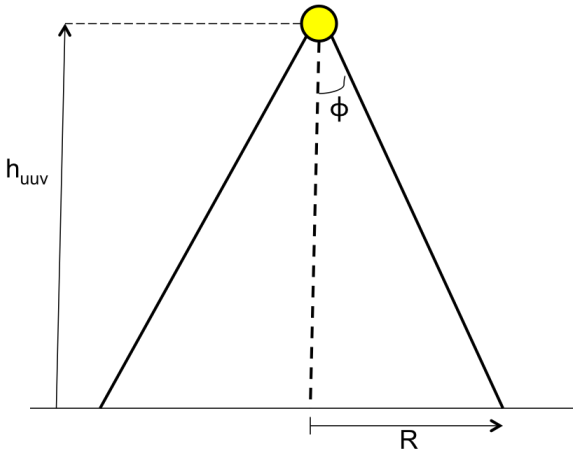


**Figure 111:** Side-scan sonar geometry.

Using EdgeTech side-scan sonar specs in Table 12 for the depression angle $\Phi = 50$ deg, and assuming the UUV sweeps over the TA at a height of $h_{uuv} = 84$ m, then the side-scan sonar range is $R = 100$ m.

Each TA is discretized in such a way that the length and width distances are

divided by the pixel resolution $(x_p, y_p)$ of the side-scan sonar, and rounded to the closest integer value. This leads to a total number of pixels $N_p$ for each TA, each of which can contain multiple bits of data, depending on the bits per pixel $b_p$. This can be translated to a total number of bits of information for a given TA (Fig. 112), given by $N_b$.

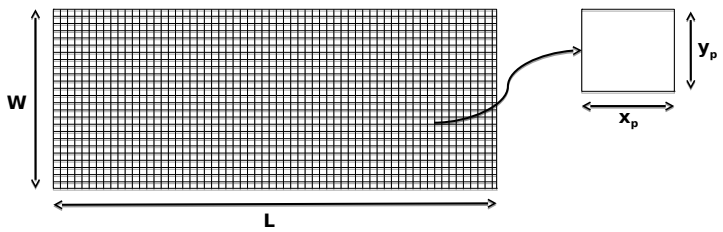


**Figure 112:** Discretization of target areas and pixel resolution.

As the UUV surveys the TA, the side-scan sonar images laterally with objects on the ocean floor giving strong returns. A series of acoustic pings are transmitted and the amplitude and timing of the returns combined with the speed of sound are used to detect mine-like objects (MLO) located perpendicular to the direction of motion. While surveying, it is assumed that the UUV sweeps at a constant translational speed $v_t$. For a given amount of time $t$, the UUV sweeps thorough a distance $d_t = (v_t)t$. This sweeping distance and lateral distance covered by the side-scan sonar can be divided by the pixel resolution, and rounded to the nearest integer value, to get the total number of pixels measured at a given time $N_{pc} = (R/x_p)(d_t/y_p)$. These measured pixels can be converted to number of bites covered $N_{bc} = (N_{pc})(b_p)$.

### 7.3.3 Sensor Model

The next step in the COA Development process is to model the sensor performance, as is shown in Fig. 113. For this study, it is assumed that all objects are discrete and protrude above the seabed, but are still connected to it. Another assumption is that the side-scan sonar sound pulses move without refraction, and can therefore be modeled as straight tracing rays. The denser the object and the more reflective compared to the background, the stronger the return from the object. This model is accurate for short ranges and non-floating objects, such as mines in shallow and deep waters shown in Fig. 100.

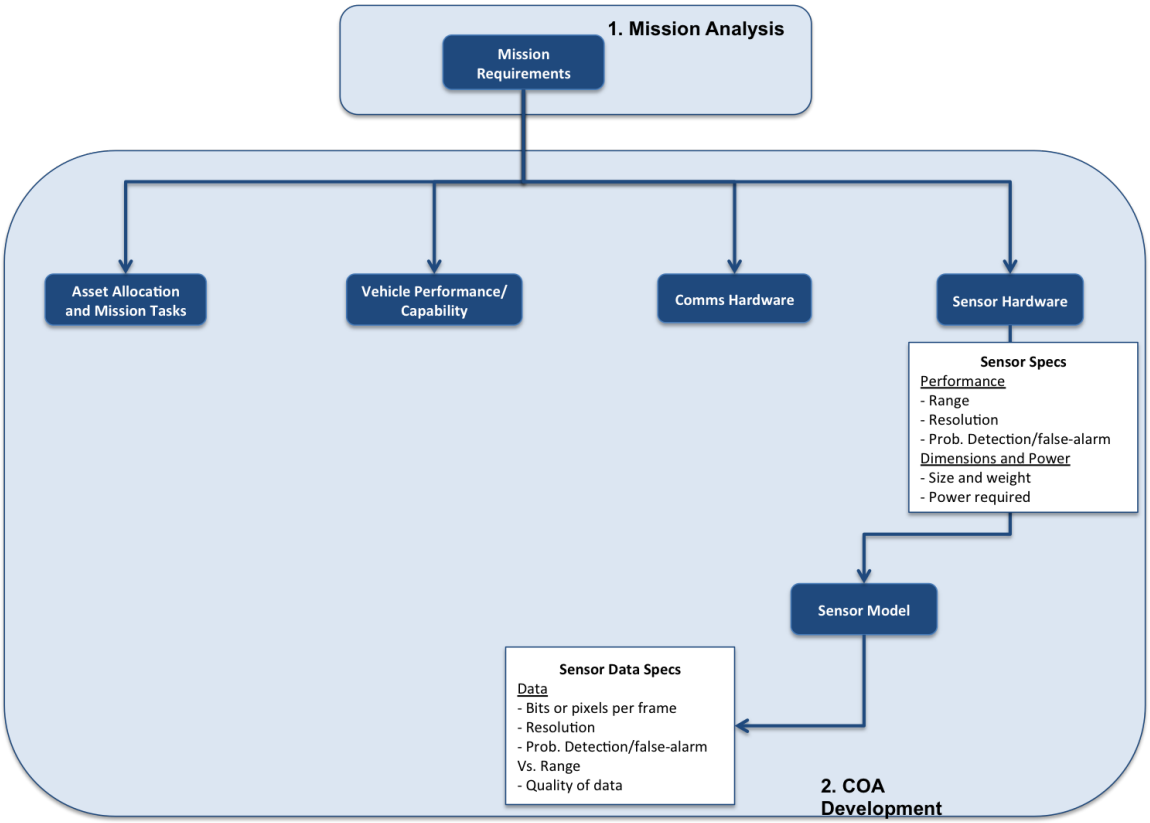


**Figure 113:** Sensor modeling step of the COA Development process.

The sonar model follows a process of using the propagation loss model to determine how signals propagate through water, a scattering model to determine how

signals disperse and attenuate as s function of range, and signal loss and noise model to determine how the signals are attenuated due to other losses and noise. Once this is calculated in the form of link budget equation, a SNR of the signal can be determined. From this SNR value, a corresponding Receiver Operating Characteristic (ROC) curve can be used to determine the probability of signal detection, given a required probability of false alarm rate required [112]. This process is shown in Fig. 114.

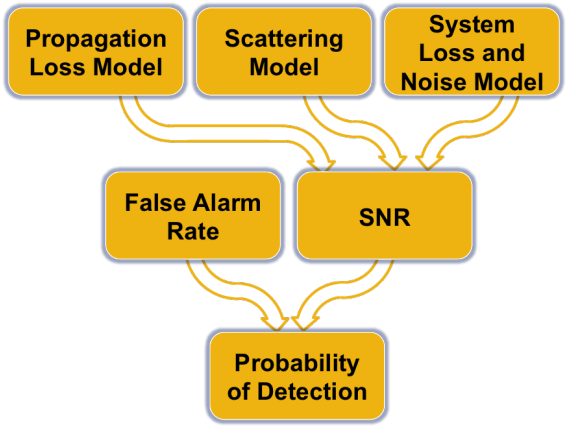


**Figure 114:** Stochastic sensor model process [112].

The sonar equation, a link budget equation, is used to estimate the expected SNR of sonar acoustic waves. Similar to the process of establishing link budgets for reliable communications, a link budget is used for acoustic sonar model. The SNR determines whether or not a sonar will be able to detect a signal in the presence of background noise in the ocean. It takes into account the source level, sound spreading, sound absorption, reflection losses, ambient noise, and receiver characteristics [213].

The side-scan and gap filling sonars are active sonars which transmit a pulse of sound and listen for echoes. In this way, the source also acts as the receiver. The sonar equation must account for how loud the sound source is (source level), sound spreading and attenuation as the sound pulse travels from the sonar to the target (transmission loss), the amount of sound reflected back toward the sonar by the target

(target strength), sound spreading and attenuation as the reflected pulse travels back to the receiver (transmission loss), the background noise at the receiver (noise level), and the receiver characteristics (array gain).

As the sonar transmits a signal with source level $SL$ (in dB), the sound propagates through water and becomes weaker as it travels due to spreading and absorption. The reduction in signal intensity is called the transmission loss $TL$ (in dB). The signal intensity of the transmitted signal is then $(SL - TL)$ dB. Only part of the signal that hits the target is reflected back towards the sonar. The intensity of the echo relative to the intensity of the sound hitting the target is called the target strength $TS$ (in dB). The intensity of the returned signal or echo $SI$ (in dB) at the receiver is given by

$$SI = SL - 2TL + TS \tag{95}$$

If the noise level at the receiver is $NL$ dB, then the ratio of the signal level to the noise level at the receiver, called signal-to-noise ratio (SNR), is

$$SNR = SL - 2TL + TS - NL \tag{96}$$

#### *7.3.3.1 Transmission Loss*

The transmission loss $TL$ can be determined from calculation of propagation loss as a function of distance from side-scan sonar to target. Such calculations are very dependent on the signal specifications and water properties, such as sound velocity profile, salinity, temperature, etc. If such data is made available for certain operating conditions and signal characteristics, then it can be used to extract the propagation loss. EdgeTech provides such propagation loss data for their side-scan sonar hardware for specific application scenarios. For example, 2-way transmission loss for a 410 KHz signal is shown in Fig. 115 for both fresh and salt water [82].

For littoral sea environments, we can assume salt water, and the calculated range of $R = 100$ m can be used to extract the expected transmission loss from red curve

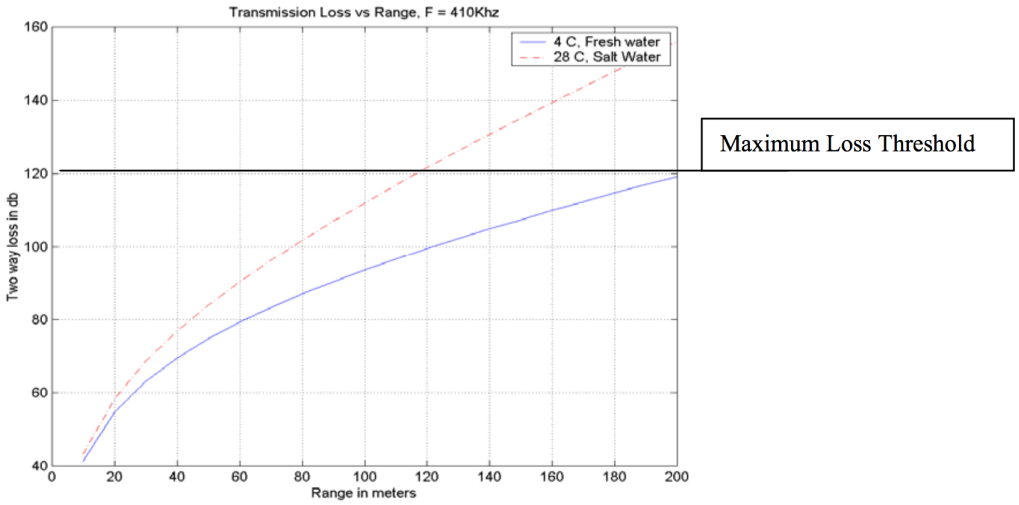


**Figure 115:** Transmission loss (TL) vs. Range for fresh and salt water [82].

in Fig. 115, which is about $TL = 110$ dB.

#### *7.3.3.2 Target Strength*

The target strength $TS$ is the ratio of the intensity of the reflected wave at a distance of 1 meter to the incident sound wave in dB, and is given by

$$TS = 10Log(\frac{I_r}{I_i}) = 10Log(\frac{\gamma}{4\pi}) \tag{97}$$

where $I_r$ is the intensity reflected from target, $I_i$ the intensity incident on target, and $\gamma$ the backscattering cross-section. $I_r$ depends on the physical characteristics of the target and the characteristics of the signal (angle and frequency). The backscatter cross section is a number that represents the degree to which sound is scattered off a target. It is related to the size, shape and reflectivity of a target. The $TS$ can be calculated analytically for simple geometric shaped objects, such as convex, sphere, and cylindrical objects [213].

For this study, it will be assumed that objects of interest, or targets, are simple rigid spheres laid on the bottom of the sea. For rigid spheres, the reflected back scattering is dependent on the size of the sphere, or radius of the sphere $a$, compared to the wavelength of the side-scan sonar wave, denoted by $k = c_{sound}/f_{sonar}$, where $c_{sound}$

is the speed of sound. The following two subsections provide analytical calculation of $TS$ for a rigid sphere for cases when $ka >> 1$, or specifically $ka > 10$, and $ka < 1$.

*7.3.3.3 Rigid Sphere Target Strength, Case 1: $ka >> 1$*

When the rigid sphere target is large compared to the wavelength of the incident sound wave and the sphere is assumed to be an isotropic reflector (reflects sound equally in all directions), we have the case shown in Fig. 116.

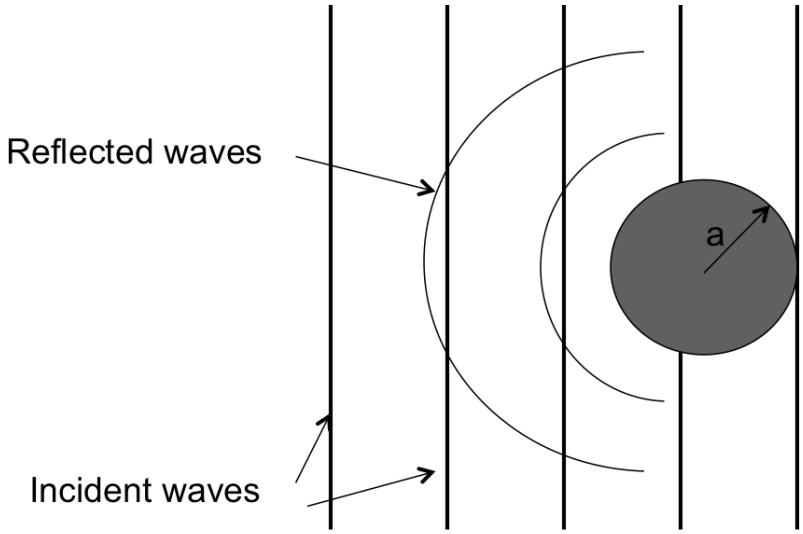


**Figure 116:** Rigid sphere target incident and reflected waves.

The power of the incident wave that will be reflected is that power of wave incident on a cross-section of the sphere where

$$P_i = I_i \pi a^2 \tag{98}$$

Since the power of the incident wave is all reflected back, we find that the reflected power is equal to the incident power, $P_r = P_i$, and therefore

$$I_r 4\pi r^2 = I_i \pi a^2 \tag{99}$$

or

$$\frac{I_r}{I_i} = \frac{a^2}{4r^2} \tag{100}$$

Using the definition of target strength, we get

$$TS = 10Log\frac{I_r}{I_i} = 10Log\frac{a^2}{4r^2}|_{r=1m} = 10Log\frac{a^2}{4} \tag{101}$$

Note that for this case, the target strength is independent of the frequency, as long as the $ka > 10$. This simple approximation is only meaningful for high frequencies where the wave effects can be average out. For lower frequencies (longer wavelengths), the wave effects must be taken into account, as shown in the next case.

#### *7.3.3.4 Rigid Sphere Target Strength, Case 2: $ka < 1$*

When the wavelength of the incident wave is larger than the size of the sphere, some of the wave will appear to continue past the sphere as if it did not exist. There will be very little scattering. For this case, Lord Rayleigh showed that

$$\frac{I_r}{I_i} = \frac{\pi^2 V^2 k^4}{r^2}[\frac{3}{2}cos(\theta) - 1]^2 \tag{102}$$

where $V$ is the volume of the sphere and the angle theta is the incident angle, shown in Fig. 117.

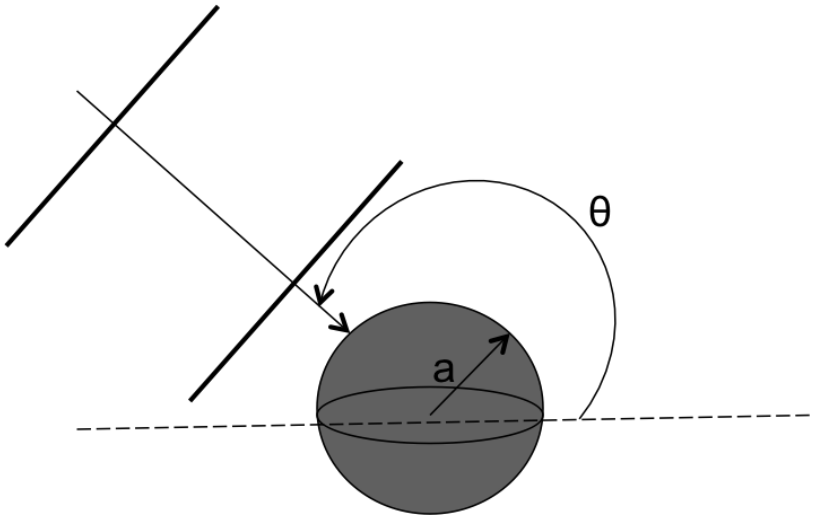


**Figure 117:** Rigid sphere target incident waves and incident angle $\theta$.

Assuming straight back scatter, with $\theta = 180\,\text{deg}$ and $r = 1m$, the target strength is given by

$$TS = 10Log[(ka)^4\frac{25}{36}a^2] \tag{103}$$

For this case the ratio of the effective backscattering cross section to the geometric cross section would be

$$\frac{4\pi\frac{25}{36}k^4a^6}{\pi a^2} = 2.8(ka)^4 \tag{104}$$

Notice that this ratio increases very rapidly with frequency ($\propto f_{sonar}^4$), therefore the target is barely detectable hen the size is much smaller than the wavelength.

For this study, we will assume the targets to be of much greater size than the wavelength of the incident sonar waves, and therefore use *case 1* for the analytical calculation of the target strength. From the sonar specifications given in Table 12, we have $f_{sonar} = 540$ kHz, corresponding to a wavelength of $k = 0.0028$ m. Rigid spherical targets of with radius $a = 1$ m will be assumed, which is much greater than the sonar wavelength. Using the analytical derivation above, the target strength is given by

$$TS = 10Log\frac{a^2}{4} = 10Log[\frac{(1)^2}{4}] = -13.9dB \tag{105}$$

*7.3.3.5 Noise Level*

A typical sonar receives signals over frequency bands greater than 1 Hz wide. The frequency band over which the receiver operates is called the bandwidth, denoted $BW_{sonar}$ in Hz. Given the bandwidth, the noise level $NL$ can be computed as follows

$$NL = 10LogBW \tag{106}$$

Shorter sonar pulses provide broader bandwidths, and means the receiver bandwidth must be greater. The receiver bandwidth can be roughly estimated as

$$BW = \frac{1}{T} \tag{107}$$

where $T$ is the sonar pulse length in seconds. For this case study, we assume the sonar transmits a 0.1 second long pulse, corresponding to a bandwidth of $BW = 10$ Hz. The receiver noise level is then given by

$$NL = 10Log(10) = 23.0dB \tag{108}$$

#### *7.3.3.6 Total SNR Calculation*

Assuming a source level for the sonar of $SL = 238$ dB, and using the calculated transmission loss, target strength, and noise level, the resulting $SNR$ can be computed from 96 as

$$SNR = SL - 2TL + TS - NL = 238dB - 2(110dB) + 13.9dB - 23dB = 9dB \quad (109)$$

From Fig. 114, a false alarm rate can be used together with the calculated $SNR$ to determine the probability of detection. Receiver Operating Characteristic (ROC) curves can be used to determine such probability of detection, described in the next section.

#### *7.3.3.7 Receiver Operating Characteristic (ROC)*

ROC curves are used to assess the performance of radar and sonar detectors. ROC curves are plots of the probability of detection $P_d$ vs. the probability of false alarm $P_{fa}$ for a given $SNR$. The probability of detection $P_d$ is the probability of saying that "1" is true given that event "1" occurred. The probability of false alarm $P_{fa}$ is the probability of saying that "1" is true given that the "0" event occurred. In applications such as sonar and radar, the "1" event indicates that a target is present, and the "0" event indicates that a target is not present. A detector's performance is measured by its ability to achieve a certain probability of detection and probability of false alarm for a given SNR. Examining a detector's ROC curves provides insight into its performance [4]. For example, in Fig. 118 the ROC curves are plotted for various SNR values.

Given an SNR value, we can calculate the $P_d$ and $P_{fa}$ values that a linear or square-law detector can achieve using a single pulse. Using our calculated $SNR$ value of 9 dB for our side-scan sonar, and certain requirements that dictate a $P_{fa}$, what value of $P_d$ can the detector achieve? We can start with a plot of the ROC curve corresponding to our side-scan sonar, given in Fig. 119.

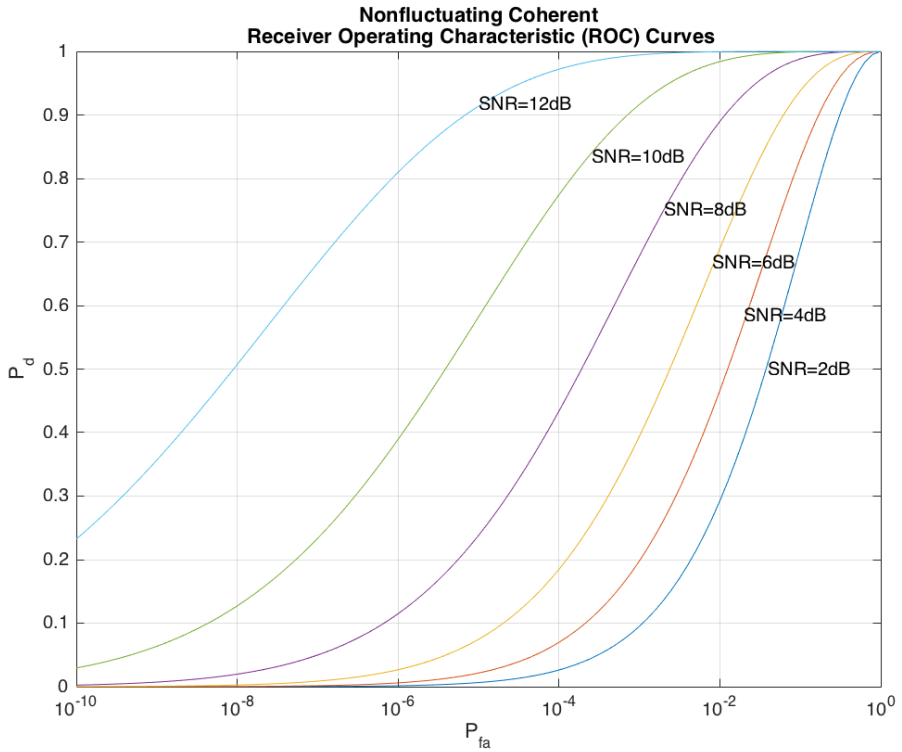


**Figure 118:** ROC curves for different SNR values.

The false alarm rate $P_{fa}$ can be dictated by sensor performance data or by requirement. For example, if data is available for the sensor, and the target locations are known, a calibration method can be used to determine the $P_{fa}$. Shown in Fig. 120 is a notional side-scan sonar data that can be used to extract the false alarm rate.

The $P_{fa}$ can also be dictated by requirement, therefore making sure the sensor is accurate enough. For this case study, we will assume a given false alarm rate of $P_{fa} = 0.001$, which corresponds to a probability of detection of about $P_d = 0.8$ according to the ROC curve in Fig. 119.

The probability of detection and classification is also a function of the image itself (i.e., size, shape, shadow), number of pixels corresponding to a given target (resolution and size of target), and the receiver voltage sensitivity. For simplicity, this study only considers individual pixels for mine occupancy, instead of dealing with multiple pixels and try to classify MLO from a training set of data, as is done in

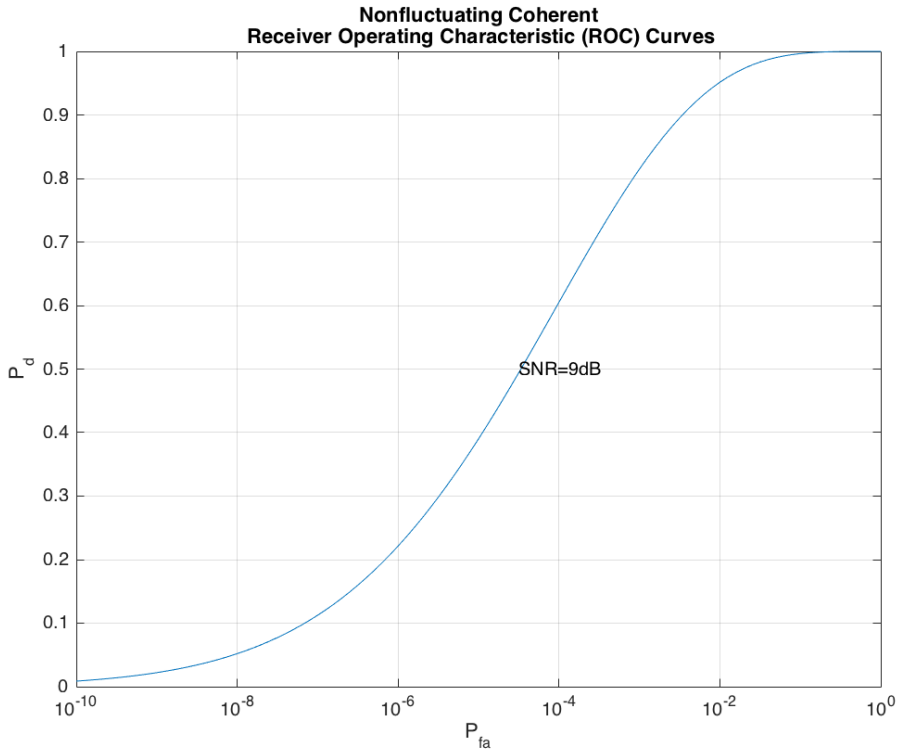


**Figure 119:** ROC curve for calculated side-scan sonar $SNR = 9$ dB.

[54], and [168]. This model however allows for the specification of the receiver voltage sensitivity in terms of false alarm rate and probability of detection. As is shown in Fig. 120, depending on the sonar sensor receiver sensitivity (voltage threshold), certain signals will result in target detection or false alarms. Lowering the receiver voltage sensitivity leads to higher probability of detection, but also increases the probability of false alarms. Increasing it leads to the opposite effect of lower probability of detection but lower probability of false alarms. The selection of receiver sensitivity is therefore a compromise between detection capability and effort needed to classify between actual and false targets.

#### *7.3.3.8 Probability of Detection Sweep*

The probability of object detection as a function of lateral distance for the side-scan and gap filling sonars can be modeled as a step function $P_d = [0, P_{ag}]$, with

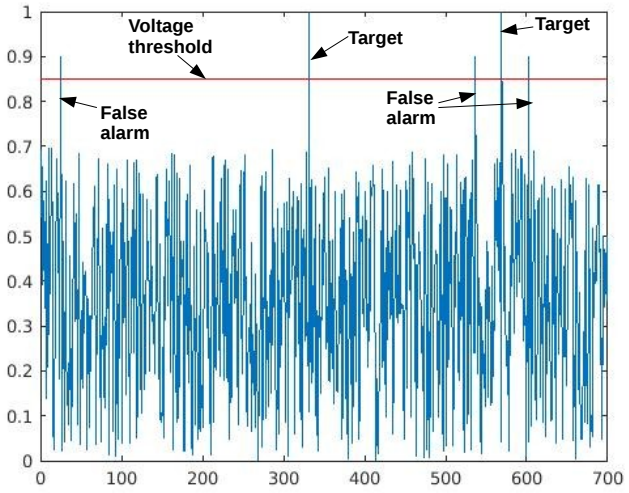


**Figure 120:** Notional side-scan sonar target detection and false alarms.

the aggregate sweep detection probability $P_{ag}$ being the product of the characteristic search width $d_A$ and the average probability of successful detection $B$, where $P_d(R)$ is the probability that the vehicle correctly detects an object at a location within range $R$, as shown in Fig. 121. This allows for the profile to model the zero probability of detection within the dead zone distance $d_{dz}$ right below the vehicle and at far lateral distances. For sake of simplicity, we will assume the probability of detection is swept over the whole horizontal range of the side-scan sonar, and assume there are not gaps in the sensor, or that there is a gap filling sonar that takes into account the area right below the UUV at the same detection probability.

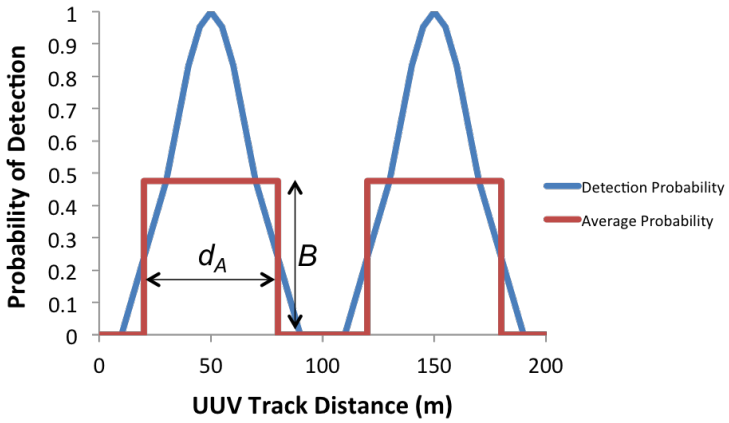


**Figure 121:** Target area surface points and side-scan sonar ranges.

### 7.3.4 Characterize the Environment

Once the available assets and their domain of operation, communications, and sensor information have been chosen from available options, then next step within the COA Development is to characterize the environment, as is shown in Fig. 122.

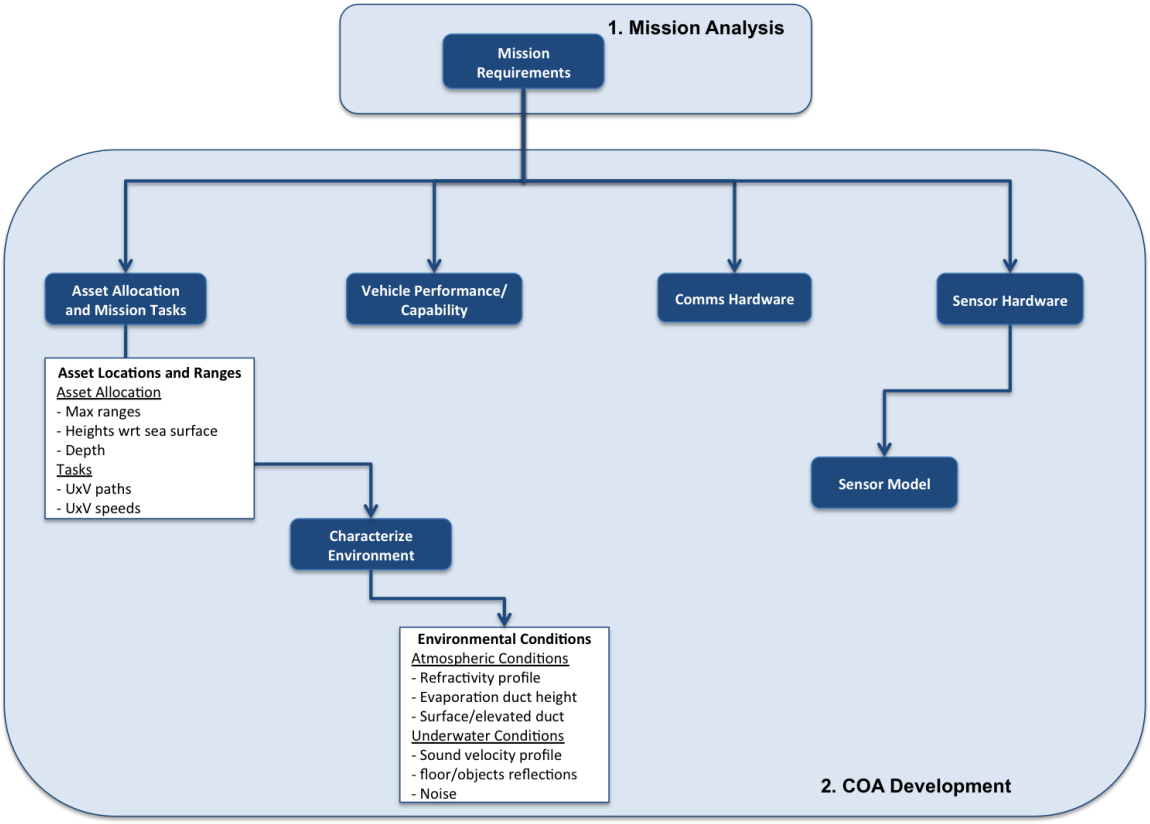


**Figure 122:** Characterize the environment step of COA Development process.

#### *7.3.4.1 Atmospheric Environment and Propagation Loss*

Changes in EM wave speed leading to changes in the propagation direction or bending are caused by changes in temperature, moisture, and pressure in the atmosphere. These changes in speed can be captured by the *modified refractivity* $M$ as given by Eq. (4). Different $M$ profiles as a function of altitude lead to different refraction conditions, such as evaporation ducts and trapping layers. The modified refractivity gradient as a function of altitude is used in Ocean and Atmospheric Sciences to easily identify the different refractivity conditions. Table 13 identify the different refractivity conditions based on the modified refractivity gradients.

A tool was developed to create modified refractivity profiles and gradients that correspond to the different atmospheric conditions. The tool is shown in Fig. 123. The tool allows the user to specify the $M$ profile by manually specifying the trapping

**Table 13:** Modified Refractivity Gradient Conditions

| Condition | M-Gradient (M/km) |
|---|---|
| Trapping | $\frac{dM}{dh} \leq 0$ |
| Superrefractive | $0 < \frac{dM}{dh} \leq 78$ |
| Standard | $78 < \frac{dM}{dh} \leq 157$ |
| Subrefractive | $\frac{dM}{dh} > 157$ |

layer altitude and duct heights, and corresponding $M$ gradients. It then performs a smooth curve fitting with desired degree of polynomial fit that can be used as input to the APM model.

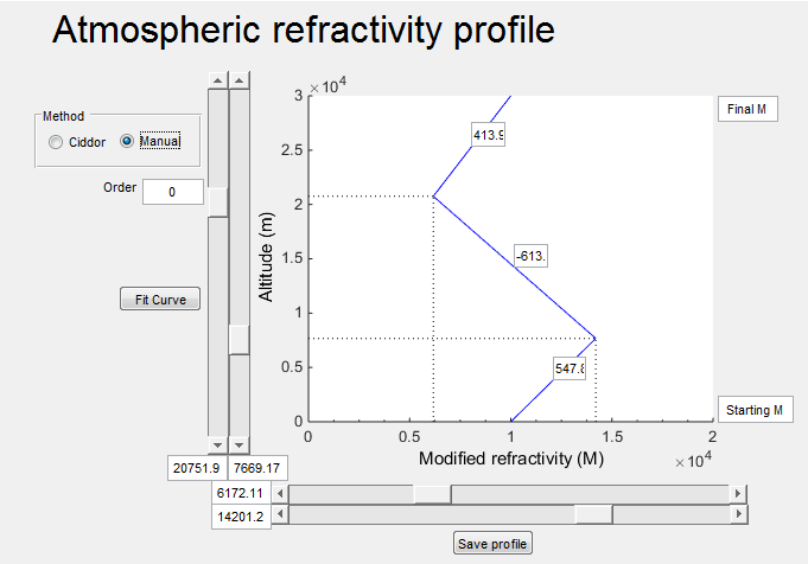


**Figure 123:** Manual refractivity profile generator.

Under the maritime conditions considered here, low altitude propagation on over-water paths for these vehicles at the water surface can be characterized by a "standard atmosphere" with some degree of evaporation duct and surface-based ducts. Three atmospheric conditions were chosen to study their effects on the amount of attenuation from multi-path fading due to the reflections and refractions of the radio waves. The first condition is a 24 m height evaporation duct, which has been shown to result in lower signal attenuation and larger number of skip zones compared to the worldwide mean 14 m evaporation duct height during RF communications between main ship

and USV [62]. Evaporation ducts are created by a rapid decrease of relative humidity immediately adjacent to the air-sea interface. The second condition is a 90 m surface-based duct (SBD), caused when the air aloft is exceptionally warm and dry compared with the air at the water surface, which creates a trapping layer for the radio waves, and can be used for beyond line-of-sight communications. The third condition is a combination of the 24 m evaporation duct and the 90 m SBD, to study the effects of more complex and realistic environments. The M-profiles generated with our tool for each atmospheric condition are shown in Fig. 124.

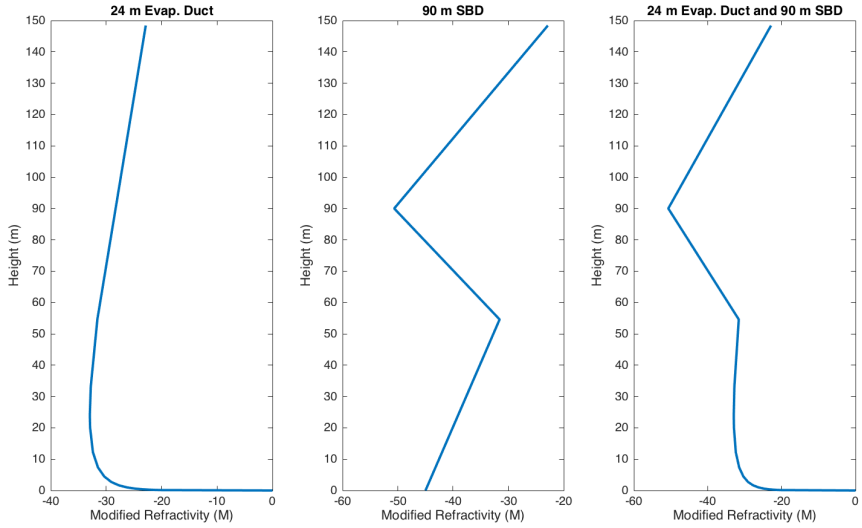


**Figure 124:** M-Profiles for 1) 24 m evap. duct, 2) 90 m SBD, and 3) combination of both.

### 7.3.5 Asset Allocation Based on Communication Predictions

Next we perform communications predictions to make better decisions on asset allocation, which is the next step of the COA Development process shown in Fig. 125.

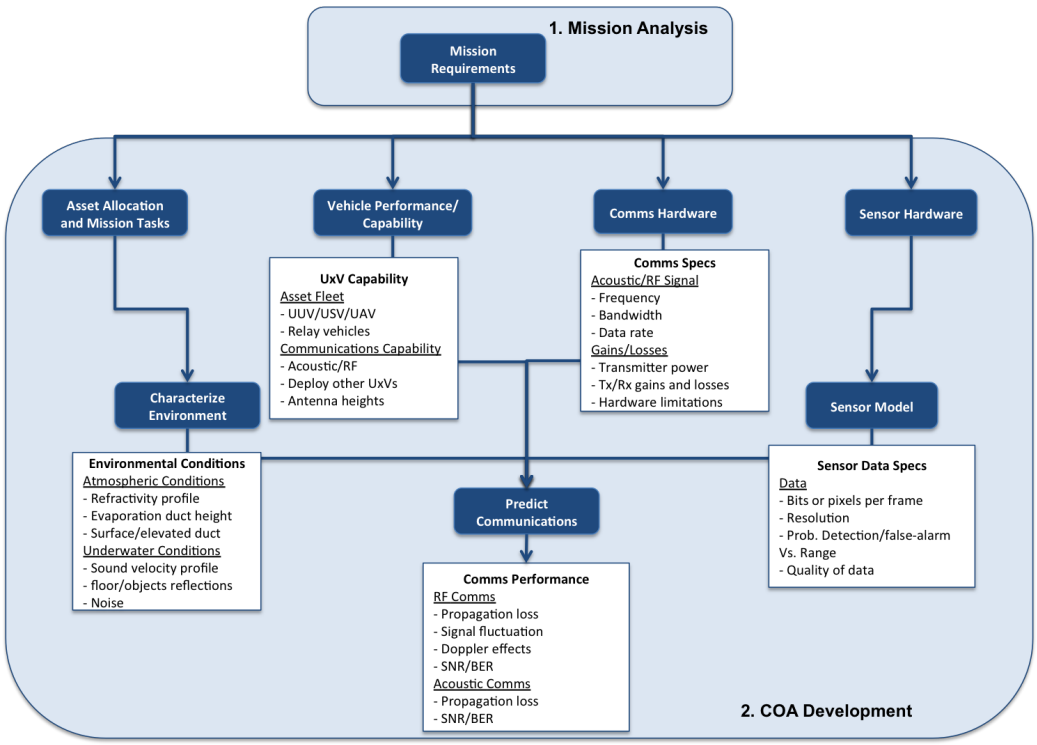


**Figure 125:** Predict communications for asset allocation step in COA Development proces.

If ranges of good communications leads to vehicles not being able to communicate at any point back to the main ship or with other unmanned vehicles, then the user has the option of performing asset allocation once more to make sure vehicles are assigned to tasks that lead to a connected communication network.

#### *7.3.5.1 Initial Asset Allocation*

From the Mission Analysis step of the NPP applied to our demonstration study, we can perform an initial asset allocation and predict the quality of the transmission channels between our assets and the main ship. We will consider the 3 atmospheric conditions described during the *Characterize the Environment* step given by (1) 24 m EVD, (2) 90 m SBD, and (3) 24 m EVD plus 90 m SBD.

The antenna heights, based on vehicle capability, for the UUV, the USV and

**Table 14:** Main Ship, UUV, and USV Antenna Heights

| | |
|---|---|
| UUV (m) | 0.5 |
| USV (m) | 3.5 |
| Main Ship (m) | 25 |

the main ship (MS) are shown in Table 14. Note that these antenna heights are constrained at that altitude due to the vehicle capabilities of the UUV, USV and MS.

Next, the propagation loss from APM was calculated for each of the 3 weather conditions and extracted the propagation loss at the given receiver heights. Shown in Figs. 126, and 127 are the propagation loss (PL) profiles for the UUV-to-MS, the UUV-to-USV, and the USV-to-MS links under the 24 m EVD. Similar plots can be

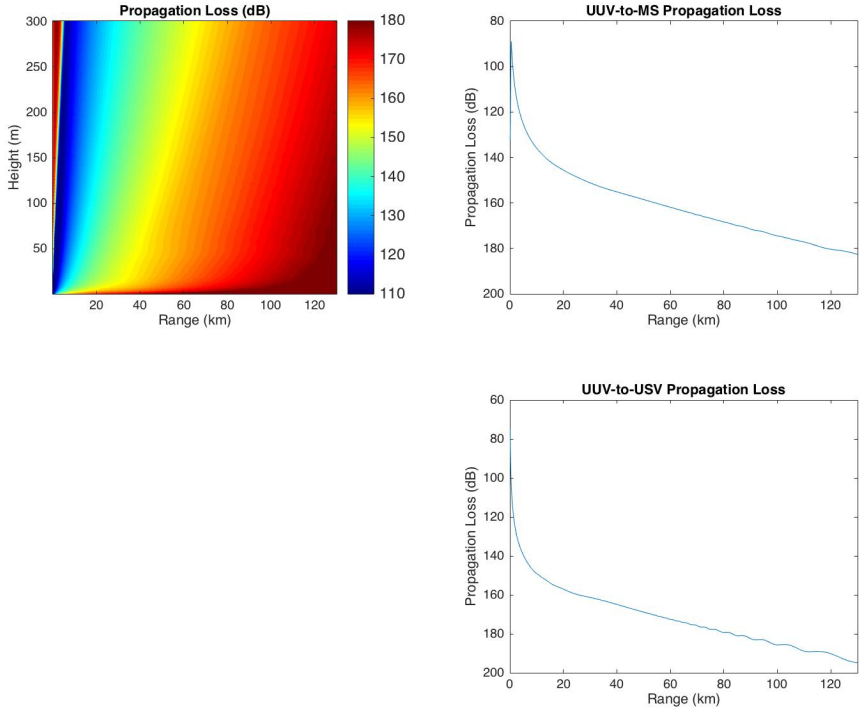


**Figure 126:** Propagation loss profile and corresponding propagation losses for UUV-to-MS and UUV-to-USV links under a 24 m EVD.

made for the other two environmental conditions considered. From the plots, it can

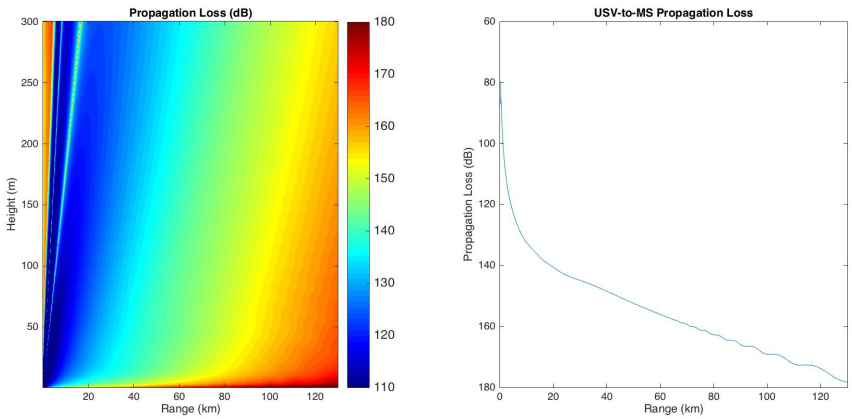


**Figure 127:** Propagation loss profile and propagation losses for USV-to-MS link under a 24 m EVD.

be seen that the propagation loss increases significantly over the considered range.

Next we add the small scale fading signal intensity attenuation to the signal by using our probabilistic modeling of the transmission channel. Given that the minimum received power threshold specified by the MPU5 radio is set to $P_{rec_{min}} = -98dBm$, the probability of communications $Pr(comms, r)$ as a function of range can be calculated.

In order to make our modeling and calculations robust to uncertainties in weather conditions and modeling errors, we conservatively assume a probability of good communications threshold high enough to $Pr_{th} = 0.8$. This means that the probability of communications needs to be higher or equal to 0.8 in order for the link to be considered in good communications range. Assuming the same link budget with all gains and losses given in Table 2, the probability of communications are calculated and shown in Figs. 128, 129, and 130 for the UUV-to-MS, UUV-to-USV, and USV-to-MS links, respectively, for the 24 m EVD weather condition. As can be seen in these plots, the USV-to-MS link offers greater ranges of communications, up to about 95 km, when compared to the UUV-to-MS link, which can only offer good communications up to about 40 km, less than half of what the USV can provide. However, the UUV-to-USV link offers smaller range of communications, up to about 22 km, when compared to the UUV-to-MS link, which is due to the greater antenna height of the

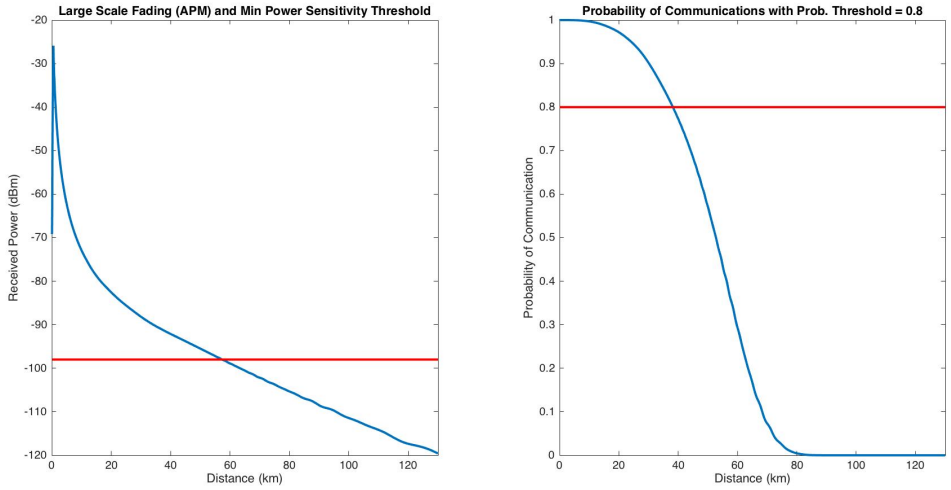


**Figure 128:** UUV-to-MS received power and minimum threshold received power (left), probability of communications and threshold probability of communications (right) in a 24 m EVD.

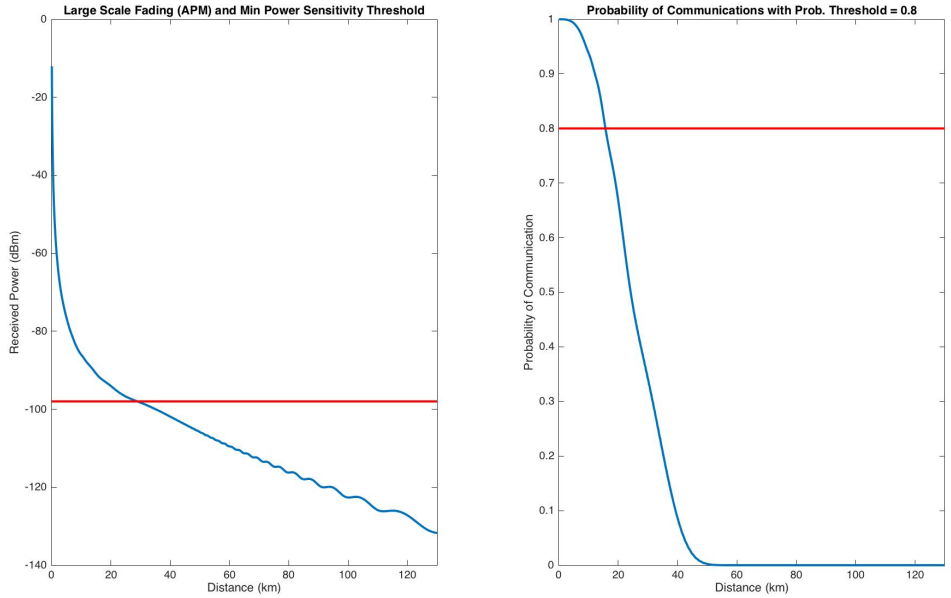


**Figure 129:** UUV-to-USV received power and minimum threshold received power (left), probability of communications and threshold probability of communications (right) in a 24 m EVD.

MS receiver. This can also be explained by the fact that the closer the transmitter is from the sea surface, the more attenuation it will experience from the reflected paths

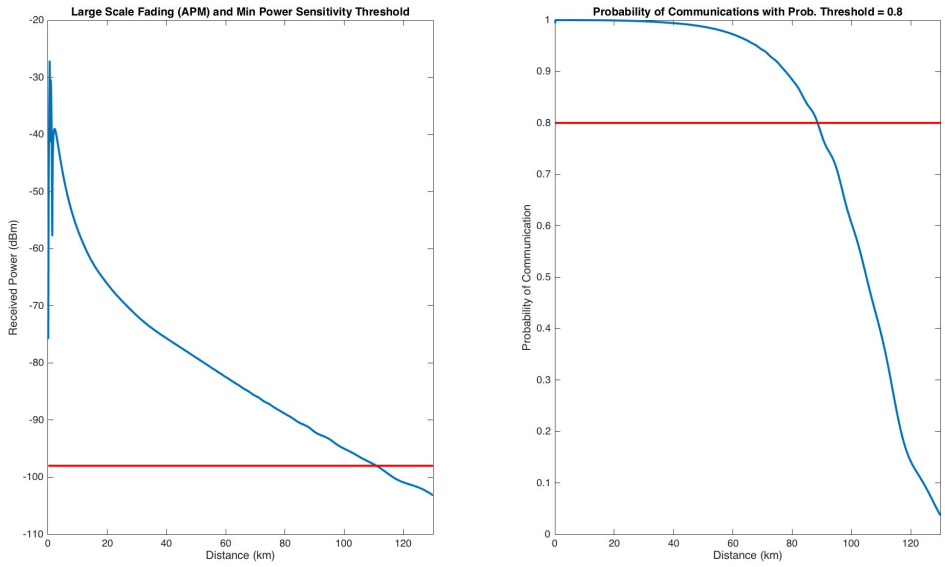


**Figure 130:** USV-to-MS received power and minimum threshold received power (left), probability of communications and threshold probability of communications (right) in a 24 m EVD.

that bounce off the sea surface since the angle of reflection is greater. It can be deduced from this experiment that link transmissions from the UUV to any other asset will experience greater attenuation due the transmitter antenna being closer to the sea surface. Therefore, when considering relaying communications between assets, it would be ideal to have the capability to change the height of the antenna relative to the water surface and the duct height.

With these results in mind, and the need to account for these environmental propagation conditions, a study was done to come up with a UAV design and capability that can be deployed from the MS and the USV which can provide the antenna height needed to relay communications between our assets. In the next section, we provide design considerations based on desired capability, show some preliminary results on prototype design, and size the UAV to meet our communications-based COAs.

## *7.4 UAV Design Considerations for Enhanced Communications Capability*

For this demonstration study, we considered novel UAV technology and capability that is relative maturing in recent years to provide enhanced communications in the maritime environment. Due to the complex atmospheric environment in maritime environments, with evaporation ducts and elevated ducts refractivity profiles that bend and refract RF signals leading to multipath fading, a UAV capable of operating at different heights relative to the ducts is desired. As heterogeneous groups of UxVs operate in the maritime environment, they may change their positions and paths, and also change their operational domain from water surface, to high above in the atmosphere, or go underwater. Therefore, it is desired to have a vehicle that is capable of operating in all these three domains. In many maritime applications, it is also desired to be able to hold position and orientation in all these three domains. For example, when communicating with other assets, it may be desired to stay at a given height relative to a surface duct, and hold position to avoid entering a shadowing or skip zone. In the realm of maritime, open sea environments, current remote underwater object detection and classification is typically performed by UUVs which either need to communicate the sensor data via acoustic or radio frequency (RF) systems. However, acoustic communications underwater affords relatively low bandwidth and is greatly affected by noise [195], and therefore cannot send as much information underwater as when they surface to communicate via RF. However, surfacing and communicating via RF may be expensive in terms of power if they are operating at significant depths, and the time between each surface may be long if they are performing object detection or classification over large areas. A vehicle capable of submerging to a given depth and communicate using acoustics with the UUV or groups of UUVs to collect sensor data or get UUV states and coordinate positions would be benecifial. Therefore it would also be desired for the proposed design to have the capability of

submerging underwater and hop back up relay information from underwater vehicles to surface platforms.

In the literature, there has been certain proposed UAV designs that provide unique capability in maritime environments. To sample water along a river, certain methods are currently used as noted in Ore et al.[153], grab sampling (technician grabbing sample), statically deployed systems, autonomous surface vehicles (ASVs), and autonomous underwater vehicles (AUVs). These methods are not ideal for many scenarios due to additional manpower required, slow speeds, and/or spatial restrictions. For instance, using an AUV along a river might be restricted if changes in depth restrict its motion or if obstructions block the waterway. It would be very beneficial to be able to accommodate these instances but this is not readily possible with current technology. Using aerial vehicle technology could help improve riverine and other water sampling methods and is a current research topic for others as well. Ore et al.[153] used a UAV to sample water at high spatial frequency in rivers and lakes by tethering a small pump about a meter long to collect water. Ore et al. were mainly interested in sampling water at different points in a river and or lake(s). The tethered method restricts sampling water to relatively shallow depths. If one is interested in collecting sensor data from UUVs, then greater diving depth may be required and it would require another system.

Young[224] and Yang et al.[223] present different options that could offer the benefits of aerial coverage and underwater sensor data collection. Young presents an air launched vehicle that can impact the water and then submerge as a typical AUV. This system was meant to be launched from a larger aircraft and was not meant to takeoff out of the water. Yang et al. studied a system very similar to how a Gannet bird plunges into the water. The system studied flies as a typical aircraft does but to transition into the water, much like the bird, it dynamically changes shape which allows it to plunge deeper into water. Their system was meant to be able to take-off

out of the water and repeat transitions. This system has the benefits of the speed and range of an aircraft with more aerodynamic shape underwater. However the system needs to change configuration drastically which could be difficult to robustly design, resulting in a relatively complicated system.

Drews-Jr et al.[80] came up with a different hybrid water-air system which combined the propulsion systems of both UAV and AUV systems. They conducted trade studies on the efficiencies of different vehicle types in both air and water. Their conclusions pointed to a system that consisted of both drive train systems of UAVs and AUVs. When in the air, the UAV propulsion system is used. Once on the water the AUV thrusters allow downward forces to pull the vehicle under and also allow underwater navigation. From a complexity point of view this system is very good as both UAV and AUV systems are not overly complex and are rather robust. The main issue with including both is the weight penalties in the air. Carrying around additional payloads can drastically affect flight time.

With these desired capabilities and literature review in mind, we examined UAV design considerations for two vehicles:

- (1) a submergible unmanned flying vehicle (SUFV) capable of collecting underwater sensor data and providing unique operational communications both underwater and above water, and

- (2) a long endurance UAV that can hover to high altitudes to relay communications

We limited our UAV design considerations to multi-rotor UAVs due to their capability to maneuver in any direction and be able to hold position for a given amount of time. They also provide the capability for vertical take-off and landing, and hovering, however at the cost of lower endurance than fixed-wing UAVs. In this study, we consider pushing the envelope of multi-rotor technology to provide the communications

re-establishing COAs that are needed to complete the mission.

The first vehicle, named Cormorant, is a multi-rotor vehicle that provides the capability of underwater and air mobility to communicate with other assets in both domains. The second vehicle, named Eagle, is a multi-rotor UAV that is deployed from USVs to help relay communications during the periods of time that are needed at heights above and below an evaporation duct encountered in maritime environments. For this proposed work, the main considerations were being able to quickly and effectively collect data along a given path at a given depth, and being able to fly up in the open ocean and hover to relay RF communications from a UUV to a main ship in an evaporation duct maritime atmospheric environment. It was also desired for the vehicle to be able to cover ranges on the order of 10 to 20 nautical miles from a deployable and rechargeable station or platform.

For this effort, we focus on two application case studies for the proposed SUFV design and Eagle. The first case study involves a scenario where the vehicle needs to collect subsequent underwater sensor data within a given range. The second case study involves using the proposed vehicle to hep relay communications in a multi-vehice operational environment, where UUVs relay communications via the Cormorant vehicle back to the main ship. In each case, the benefits of the proposed Cormorant SUFV design in terms of its capability to operate underwater, on the surface, and fly and hover above the surface will be demonstrated and compared to current approaches.

### 7.4.1 Motivational Case 1: Underwater Sensor Data Sampling

For the first case study, assume the requirements are to collect underwater sensor data for a given range $R$ at some depth $D$. In order to collect the data, the vehicle needs to submerge every $S$ distance, collect the sensor data, and submerge back up to the surface to communicate the sensor information. The mission profile for a typical UUV will involve submerging, collecting sensor data at different depths, moving forward

to a distance $S$, surfacing to communicate the data, submerge back down to collect more data, and so on until the range $R$ is covered, as it is depicted in Fig. 131 (a). For our proposed SUFV vehicle, the mission profile involves submerging, collecting data at different depths, surfacing and flying to next measurement location a distance $S$ away and so on until the range $R$ is covered, as is depicted in Fig. 131 (b).

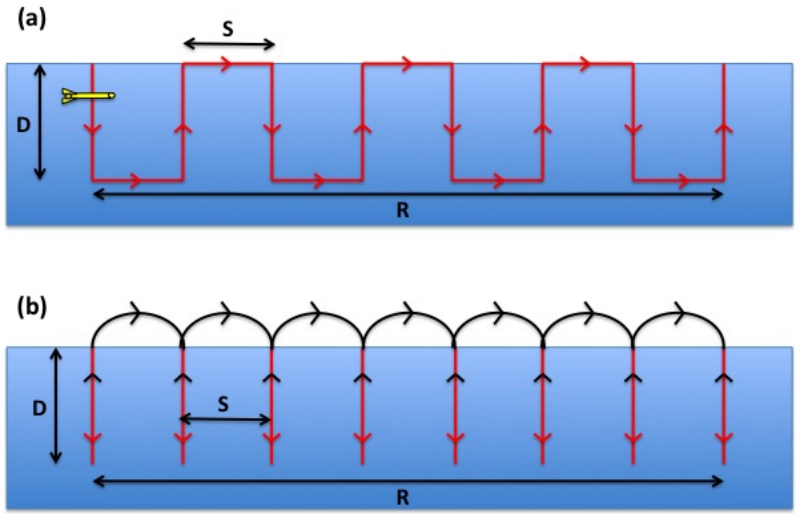


**Figure 131:** Motivational case 1 scenario for (a) a typical UUV, and (b) for the proposed SUFV Cormorant design.

### 7.4.2 Motivational Case 2: Underwater Object Detection

For the second case study, the requirements are to provide underwater detection and classification of objects of interest at depths of 60 ft, representative of shallow-water regime [150]. A target area (TA) is assigned to a UUV for conducting detection and classification of objects using sonar. While sweeping through the TA, the vehicle needs to communicate the sonar data back to the main ship via RF communications. However, due to an evaporation duct, there are skip zones where the UUV cannot communicate. We consider a scenario where the proposed SUFV helps relay communications between UUV and main ship, as is depicted in Fig. 132. We compare the ability to communicate sonar data back to the main ship by a direct link from the UUV and using our proposed Cormorant vehicle design as a communications relay.

After we define the sensor and communications hardware, and characterize the en-

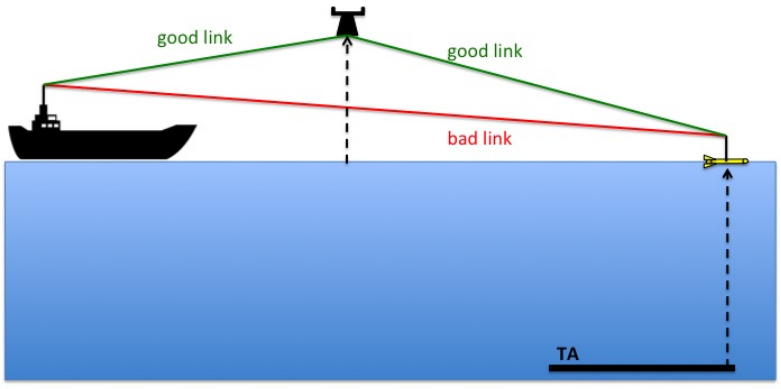


**Figure 132:** Side view of case 2 scenario with main link between UUV and main ship and relay link using proposed SUFV.

vironment, we determine design considerations for building a prototype and testing the design, which can be sized for the mine survey mission demonstration study.

### 7.4.3 Overall Cormorant and Eagle UAV Design Considerations

#### *7.4.3.1 Vehicle*

Next, we performed a trade study for the selection of the overall UAV vehicle design. Among those studied were multi-rotors, single main rotor (SMR) and coaxial helicopters, and free-wing vehicles [105]. The quadrotor configuration was chosen as it has the major advantage of propulsive system simplicity as compared to the other concepts. For example, the generally smaller blade diameter as compared to that of the SMR and coaxial helicopter design has operator-safety advantages. In addition, these smaller rotors may be turned underwater if needed to apply forces and moments to the vehicle in a way that would not be possible with a traditional helicopter. Also, the obvious complexity advantages in the linkage between the power plant and the

propeller make the multirotor a reasonable choice. The use of a multirotor with homogenous rotors for aerial and underwater propulsion comes with several complications, including increase in power required to turn a propeller under water, which has three orders of magnitude higher density than air. Another albeit more complicated possibility is to use variable pitch propellers to lower the load when operating underwater. This of course adds the mechanical complications of such a system.

#### *7.4.3.2 Sensor placement*

While it is possible to do underwater sensor sampling with a detachable and/or slung-loaded sensor suite as referenced , the complexities associated with such a system are not attractive. The subsystem also then needs to have a navigation solution and potentially control (if imaging sonar is required, for example), adding another level of complexity. A slung-loaded sensor has additional requirements, such as a winch mechanism if depth control is desired. These may be heavy (mechanism plus tether), may jam, and may also become tangled on underwater obstructions. Slung load dynamics also may need to be considered if the load is not rigidly attached to the vehicle during use, adding further complications to such a system.

Operationally, submerging the entire vehicle has several advantages. For example, a vehicle squatting several inches below the surface may be more immune to wave action and/or environmental effects (wind, sun) than one on the surface. This may be of value for stabilizing a vehicle with a sonar imager sensitive to platform movement, or cooling motors on a hot day. Another advantage is the ability to negotiate obstacles should a complicated mission be required, such as inspecting an underwater structure where maneuvering might be required to reach areas of interest. Submerging may also allow the vehicle to operate in areas with heavy surface traffic, submerging to a safe depth while scanning or loitering to avoid collisions.

#### *7.4.3.3 Depth Control*

For depth control, several strategies were considered including positive buoyancy with propulsion, dive planes, compressed gas and bladder, as well as different types of pumps (peristaltic, diaphragm, stepper/piston) moving air, water, or oil. Using a positively buoyant vehicle with propulsive control for diving [140] is ruled out due to its inefficiency in required power. Making multiple measurements down to tens of feet (up to 60 ft as required for some missions to acquire sensor data) require a more efficient depth control system. This decision also rules out the use of dive planes, as these rely on relative water velocity to function. Compressed gas and bladder (with the bladder on the external part of the vehicle) is useful in case of emergency ascent but having to replace gas canisters is undesirable for normal operation. The main disadvantage of this system is it may become the limiting factor for mission endurance. That is, it may limit the number of dives possible with the vehicle should a dense desired dive grid be required and/or an efficient propulsion system be used [36]. Different pumps moving different media are also considered. Other systems, including oil pumps may be considered in the future as well due to the relatively better incompressibility of oil, which is useful at greater depths. A stepper with a piston is also good for heavy vehicles, but has disadvantages for a SUFV. First, it tends to be heavy, requiring a rigid container and a stepper motor with associated electronics. This is not beneficial for flight endurance. Second, a stepper motor continuously draws power even if not in use, further reducing flight endurance.

#### *7.4.3.4 Waterproofing*

The Brushless DC motors selected are waterproof but not corrosion resistant. If they are to be used in a salty environment, they should be cleaned with fresh water and sprayed with an anti-corrosion lubricant after each use. Motor damage may result from debris sticking between these two during operation. Salt water also presents

electrical complications for exposed electronics. Silicon is used to seal through-holes and exposed terminals and electronics.

#### *7.4.3.5 Submersible Prototype*

For the Cormorant, the primary goal of the prototype was to test the depth control system, so the flight time was limited to only 10 minutes of hover endurance. The propulsion system was optimized using the methods described in [36]. The optimizer outputs are shown in Table 15. We chose the 17 inch diameter 5.5 inch pitch propellers for additional payload capacity in case predictions were incorrect. Carbon fiber is chosen for the blade material so that, in case it is desired to turn them as underwater screws, they will not deform along or around their radial axis. In Fig. 133, the Cormorant SUFV vehicle design is shown operating underwater. Inside

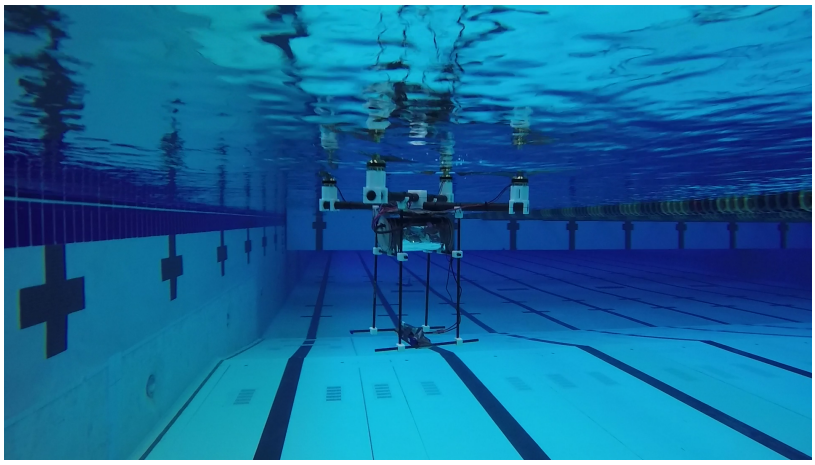

**Figure 133:** Cormorant proof of concept SUFV design operating underwater. (Video: https://www.youtube.com/watch?v=U7vl7uqwN4I)

the water tight compartment (WTC), the avionics (box A in Fig. 134) control the vehicle's electronics. It interfaces with a receiver for manual mode, and is capable of autonomous operation. A hobby-grade 72 MHz receiver is used to allow operation in several feet of water. A more recent hobby-grade 2.4 GHz receiver may also be used but due to the attenuation in water, its efficacy is limited to about one foot underwater. The prototype Cormorant employs an Ardupilot (APM) with custom

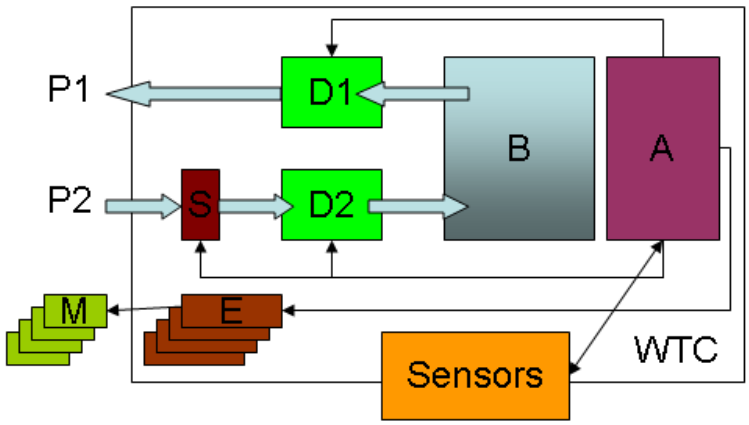


**Figure 134:** Schematic of Cormorant. D1, D2 are pumps, B is a bladder, A is the avionics suite, S is a solenoid, E are ESCs, M are rotors. P1 is the ascent pathway and P2 is descent. Most electronics and communications package are contained inside the water tight compartment WTC.

code. To fly, the APM commands the motors (M) via electronic speed controllers (E) in the standard multirotor configuration. As the vehicle lands on the water, the APM spools down the rotors. To descend, the APM commands the solenoid (S) and the diaphragm pump D2 to activate, pulling water into the bladder (B). This increases the weight of the vehicle, causing it to sink. As the vehicle descends, the APM interacts with a barometer which is modified to measure water depth. When it detects a pre-set depth, the APM closes S and D2 and waits for the next pre-set depth to enable D1 to begin ascending. If the descent rate exceeds a particular value, the rotors may be used to arrest it. As D1 empties the bladder, buoyancy overwhelms weight, and the vehicle begins to ascend.

The first system for depth control tested uses air to inflate/deflate a bag attached outside the WTC. To surface, the air is compressed from inside the WTC using an air pump, and forced out into the bag. This increases the buoyancy of the vehicle which causes it to surface. To dive, the opposite happens. In this case, a solenoid is energized, dumping the compressed air in the bag back into the WTC. This system has the drawback that should the pump fail, the vehicle may be lost. Peristaltic

**Table 15:** Optimizer output for rubber propulsion system requirements for Cormorant prototype, 10 minute hover

| Parameter | Value (rubber) | Value (built) |
|---|---|---|
| Battery configuration | 4S | 4S |
| Battery capacity | 4322 mAh | 4000 mAh |
| Propeller diameter | 16” | 17” |
| Propeller pitch | 3.5” | 5.5” |
| $RPM_{hover}$ | 2700 RPM | 2520 RPM |
| $K_v$ | 364 RPM/V | 390 RPM/V |
| $P_{hover}$ | 252 W @ 14.8 V | 263 W @ 14.8 V |

pumps were found to be functional to about 6-7 ft of depth in this design. It is possible to increase the efficiency of the system by allowing the WTC to have more air (less electronics) but this increases the weight of the vehicle in trimming it to be near neutrally buoyant. The second system tested uses a water bladder inside the WTC. To descend, a diaphragm pump pulls water from the environment into the bladder, and the opposite to ascend. A solenoid is required to keep water from leaking backwards through the diaphragm pump into the bladder, slowly sinking the vehicle. If this happens and the vehicle surfaces, the extra pressure inside the WTC will likely cause a blowout or a leak once the vehicle surfaces and experiences lower external pressure. One advantage of this system is that greater depths are attainable, although two diaphragm pumps and at least one solenoid are required to operate it. Another advantage of this system is no extra ballast needs to be carried, and the vehicle can trim itself to be nearly neutrally buoyant using the water surrounding it. The Cormorant prototype was tested successfully down and back up from 21 feet of chlorinated water in this configuration, limited by the depth of the pool that was used to test it. The test was done untethered and a barometer was used to automatically detect depth and reverse the pumps to surface. The static margin, which may change as vehicle submerges due to water filling the bag inside the WTC, depends on the depth control system. The cormorant has a low-mounted battery to keep it statically stable in an upright attitude, although this may be adjusted a priori or propellers

may be used underwater if necessary to change attitude.

#### *7.4.3.6 Eagle Long Endurance prototype*

As described above, the Cormorant prototype was built to refine the depth control system for a flying submersible vehicle. A larger vehicle named Eagle[36] has been built to test the "long" endurance aspect of the final Cormorant configuration; a combination of the Eagle and Cormorant prototype capable of long-endurance and diving. The Eagle is designed to have a hover endurance of over two hours. Table 15 shows optimization output of the two configurations. The difference between the Eagle and the final configuration is the payload/battery tradeoff. The Eagle flies a 40.8 Ah battery, while in the final configuration, half of the battery is removed and replaced by about 1.8 kg of sensors, avionics, and depth control equipment. This drops the calculated hover endurance from about 140 minutes to around 50-60 minutes.

**Table 16:** Optimizer output for rubber propulsion system requirements for Eagle, 140/60 min hover, 0/1.8 kg payload

| Parameter | Value (rubber) | Value (built) |
|---|---|---|
| Battery configuration | 6S | 6S |
| Battery capacity | 44378 mAh | 40800/20400 mAh |
| Propeller diameter | 30" | 30" |
| Propeller pitch | 10.5" | 10.5" |
| $RPM_{hover}$ | 1400 RPM | 1390 RPM |
| $K_v$ | 112 RPM/V | 100 RPM/V |
| $P_{hover}$ | 417 W @ 22.2 V | 409 W @ 22.5 V |

### 7.4.4 Motivational Case Studies Results

For the first motivational case study, consider a specific scenario in which underwater sensor data needs to be collected with the following dimensions and requirements: $R = 7$ nm (half of the maximum range of the Cormorant to allow for a return trip), $D = 15$ ft, and $S = 300$ ft, corresponding to 141 sensor data samples required. Next we make a comparison between time to complete the sensor sampling range using a

*Remus 100* and our Cormorant design. Specifications of the Remus 100 are given in Table 17 [111].

**Table 17:** Remus 100 Specifications [111]

| Parameter | Value |
|---|---|
| Max. depth (m) | 100 |
| Max. endurance (hr) | 8-12 |
| Max. range (nm) | 64.3 |
| Cruise speed (m/s) | 1.5 |
| Sink/ascend rate (m/s) | 1 |

Sizing the Cormorant vehicle for maximum range, replacing 1.8 kg of batteries with avionics and sampling sensors, leads to the performance metrics shown in Table 18. The sink/ascend rate varies between 1-3 ft/sec, therefore a conservative 1 ft/sec rate was chosen for analysis. The power required to dive and surface is very minimal, since it only requires inflating/deflating the ballast system with a small amount of water, and the brushed DC motors in the diaphragm pumps use very little power (on the order of 500 mA at 7 m). This accounts for about 2% of hover power, and a conservative value of 5% is used for analyses. Therefore, the maximum range for the Cormorant was for the most part restricted to power required to fly to subsequent sampling locations, and the power available from the batteries.

**Table 18:** Cormorant Specifications (Calculated unless otherwise specified)

| Parameter | Value |
|---|---|
| Max. depth tested (m) | 7 |
| Dive/surface rate tested (m/s) | 0.3-1 |
| Max. range (nm) | 13 |
| Max. endurance (min) | 56 |
| Cruise speed, max. range (m/s) | 7.6 |
| Cruise speed, max. endurance (m/s) | 3.1 |

Results show that to sample the sensor data at the required range, it would take the Remus 100 a total of 4.9 hr, where as it only takes 2.1 hr with the proposed Cormorant design. The better performance by our Cormorant design is mainly due

to its ability to get to traverse the horizontal distance $S$ faster than a UUV with its ability to fly. Note however that if the mission profile requires horizontal water columns instead of vertical, the UUV clearly has the upper hand.

For the second case study, consider a specific scenario in which a TA needs to be completely covered by a UUV to detect and classify objects of interest using sonar. Assume the TA is at 60 ft deep, and the UUV needs to be able to surface at any point during the detection and classification phases to communicate sensor data to a main ship. The atmospheric conditions are such that a standard 24 m evaporation duct is present at any azimuth within 90 miles from the ship.

Lets also assume the UUV carries the MPU5 RF radio communicating at 2.4 GHz, with antenna height of 0.5 m. Also assume the main ship antenna is located 21 m above the surface of the water, as was shown in Table 14. For our Cormorant vehicle, assume it also communicates at 2.4 GHz using the same MPU5 radio, and can communicate at 20 m height, well above the USV antenna height at 3.5 m which limited our communications relay capability, but below enough from the 24 m evaporation duct that it can be trapped within the inside of the layer where the MS receiver is located.

Using the APM model to calculate the signal propagation loss due to large-scale fading mechanisms, the resulting propagation loss profiles for both UUV-to-Ship and Cormorant-to-Ship links are shown in Figures 135 and 136, respectively. It can be seen that greater propagation loss is experienced when the transmitter and receiver are within the evaporation duct for UUV-to-Ship links, since the duct acts as a waveguide for the links that are trapped within the duct, bouncing between the ocean surface and the upper layer of the duct.

The MPU5 minimum receiver power sensitivity was used $P_{R_{min}} = -98dBm$. Using a Rayleigh distribution for the modeling of the small-scale fading, the propagation

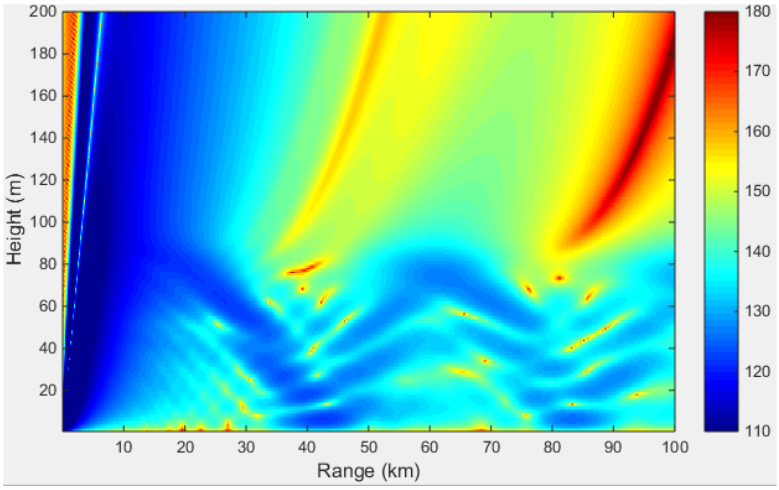


**Figure 135:** Propagation Loss profiles for UUV-to-Ship link in a 24 m evaporation duct.

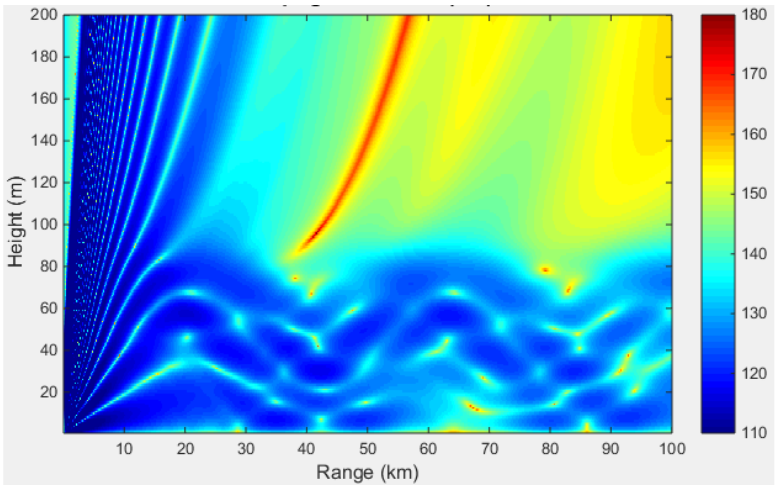


**Figure 136:** Propagation Loss profiles for Cormorant-to-Ship in a 24 m evaporation duct.

loss at the receiver, with corresponding probability of communications for UUV-to-Ship, UUV-to-Cormorant, and Cormorant-to-Ship cases are shown in Figures 137, 138, and 139, respectively.

Assuming a probability of good communications threshold high enough to $Pr_{th} = 0.8$, we can calculate ranges between transmitter and receiver at which good communications ranges and skip-zones are located. Shown in Figures 140, 141, and 142 are the ranges of good communications for UUV-to-Ship, UUV-to-Cormorant, and

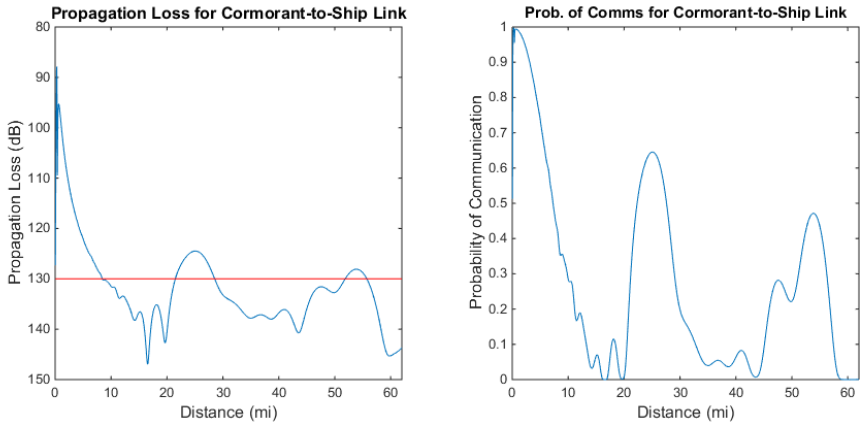


**Figure 137:** Propagation loss at the receiver height and probability of communications for UUV-to-Ship link.

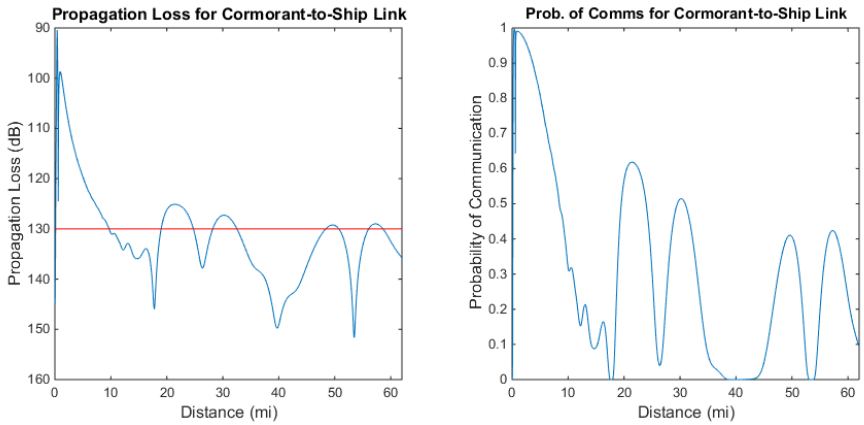


**Figure 138:** Propagation loss at the receiver height and probability of communications for UUV-to-Cormorant link.

Cormorant-to-Ship links, respectively.

As can be seen from Fig. 140 for the UUV-to-Ship good communication ranges, the location of the TA is limited to lie within 8 miles from the main ship, or between 23 and 27 miles from the main ship, which highly restricts the TA ranges and UUV RF communications as it sweeps through the TA. From Figures 141, and 142, it can be seen the benefit of having Cormorant as a communications relay above the 24 m evaporation duct by allowing the TA to be at multiple ranges from the main ship, as long as the TA is within good communications ranges with the Cormorant, and as long as the Cormorant is in good communications ranges from the main ship. As a

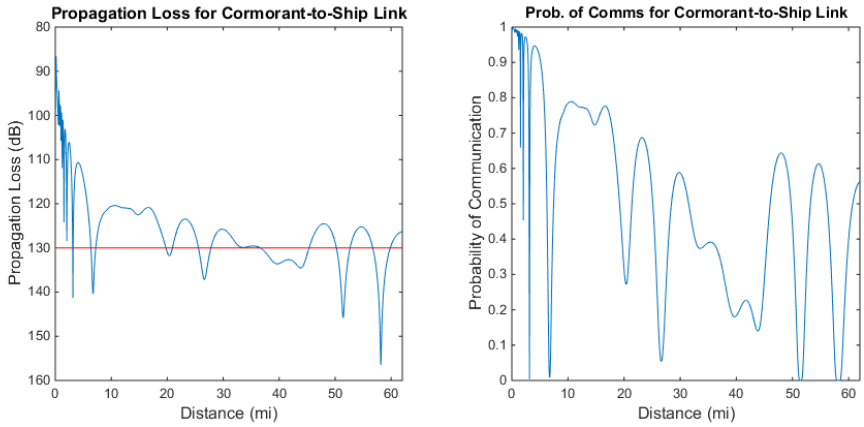


**Figure 139:** Propagation loss at the receiver height and probability of communications for Cormorant-to-Ship link.

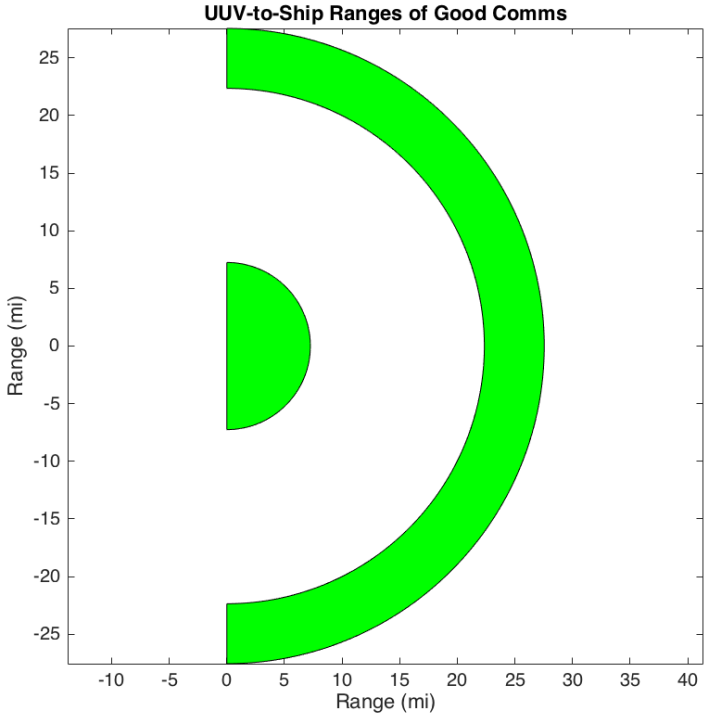


**Figure 140:** Ranges of good communications and skip zones for UUV-to-Ship links.

simple specific example, a TA at 20 miles from the main ship will not allow the UUV to communicate back to the ship while it sweeps through the TA. However, the same TA at 20 miles from the main ship can be located using the following configuration:

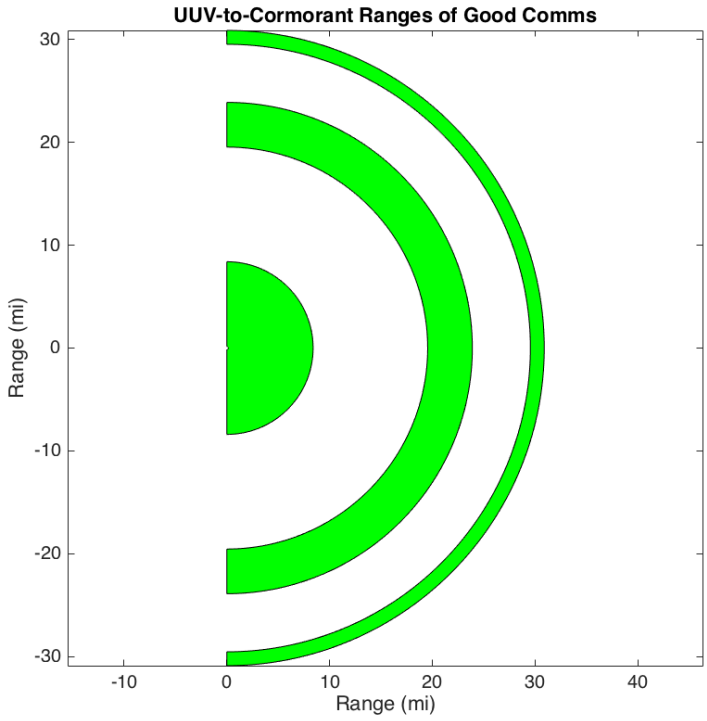


**Figure 141:** Ranges of good communications and skip zones for UUV-to-Cormorant links.

place the TA 8 miles from the Cormorant vehicle, and make sure the Cormorant is 12 miles from the main ship. As the threshold of probability of communications is increased, the ranges of good communications start to shrink, and UUV-Cormorant-Ship placement configuration possibilities start to decrease, but still provide more options than not having the Cormorant as a communications relay. The Cormorant design can also be sized for greater hover endurance for cases where the UUV needs to relay communications during further classification of objects of interest, and for cases with more than one TA.

### 7.4.5 Conclusions of Proposed UAV Vehicle Design Capability

The SUFV enables maritime operations in situations not possible by using solely a UAV, ASV, or UUV by leveraging the benefits of each type of vehicle. For some conditions, the SUFV also outperforms traditional sampling methods. We show how

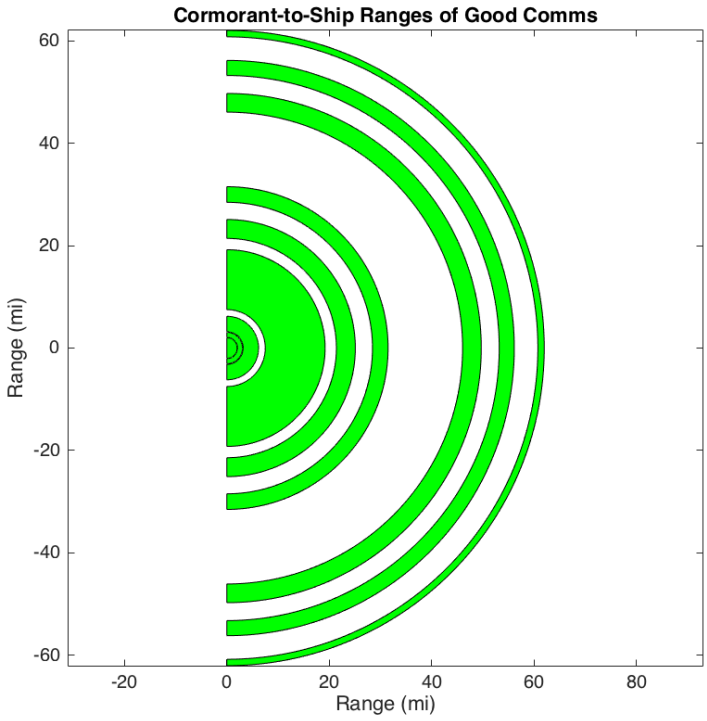


**Figure 142:** Ranges of good communications and skip zones for Cormorant-to-Ship links.

the Cormorant design outperforms a typical UUV while sampling sensor data for a given range, by completing the sampling more than two times faster. We also showed the benefits of the Comorant's long hovering endurance while relaying communications between a UUV and a main ship for a given evaporation duct atmospheric environment.

For the mine survey mission demonstration case study, we will assume that a multi-rotor UAV comparable to Eagle vehicle, shown in Fig. 143, is able to be deployed off from top of a WAM-V USV, hover to relay communications, and come back and land on the WAM-V to recharge for the next flight. Performance specifications for Eagle are shown in Table 19. Since It will be able to be deployed from the WAM-V USV, it will have a the same range as the USV in the operational environment.

A Cormorant SUFV, will be deployed from the main ship only to help relay

**Table 19:** Eagle UAV Specifications

| | |
|---|---|
| Max Endurance (hr) | 2 |
| Vertical Flying Speed (knots) | 3 |
| Max Altitude (m) | 100 |

communications nearby. We will also assume that the Cormorant vehicle can be used within the maximum range of 13 nm, but still providing both underwater and above water capabilities. Cormorant's specifications are shown in Table 20.

**Figure 143:** Eagle multi-rotor UAV bult by Georgia Tech UAV Research Facility [10].

**Table 20:** Cormorant SUFV Specifications

| | |
|---|---|
| Max Endurance (hr) | 1 |
| Max Range (nm) | 13 |
| Max Depth (tested) (m) | 7 |
| Dive/surface rate (tested) (m/s) | 0.6 |
| Vertical Flying Speed (knots) | 2 |
| Cruise speed, max range (m/s) | 7.6 |
| Cruise speed, max endurance (m/s) | 3.1 |
| Max Altitude (m) | 100 |

## *7.5 Step 3: Course of Action Analysis (Wargaming)*

The next step in the NPP mission planning process is to conduct COA Analysis of the communications-based COA develped from the previous step. It involves a detailed assessment of each COA as it pertains to the adversary and the OE [151]. Each friendly COA is war-gamed against selected adversary COAs. This step assists planners in identifying strengths, weaknesses, and associated risks, and in assessing shortfalls for each prospective friendly COA. Wargaming also identifies branches and potential sequels that may require additional planning. COA wargaming provides the most reliable basis for understanding and improving each COA. This step also allows the planning staff to refine its initial estimates based on a more refined understanding of the COA that is gained through the war game.

The wargaming analysis will be done through the use of graph theory to model the communications network made up of our fleet of assets. We will assume we have a limited number of assets, with capability as has been previously defined in the COA Development step. The communications network modeling through graph theory will be used to measure the connectivity of the network, the quality of the transmission channel links, the stability of the network, and the reliability of the network to link

failures. The end goal is to consider different friendly COAs in terms of different proactive network configurations and war-game them against network connectivity that is robust and stable to small scale fading uncertainty, and reliable to possible link failures possibly due to adversary jamming.

Once a network configuration is selected that meets the connectivity, robustness, stability, and reliability constraints, it will be used to find optimal path navigation and schedule for UUVs during the detection of objects in the mine-survey mission. A Bayesian filter is used to model the evolution of state and measurements as the UUVs sweep through a target area. In the process, entropy information gain will be measured to optimize rate at which information is communicated to the main ship.

For our initial iteration, we will assume that our fleet is composed of one UUV for each TA, one main ship, and that we have one of each possible relay vehicle: 1 USV, 1, Eagle, and 1 Cormorant. The result of the COA Analysis is a solution or set of solutions in terms of combinations of these vehicles that meet the mission requirements which can be further compared in the next step during the COA Comparison and Decision.

### 7.5.1 Communications Network Analysis

The first phase in the COA Analysis step is to analyze potential network configurations based on our available fleet of assets and their capability, as shown in Fig. 144. In order to do so, we need to model the communication channels between each asset, and determine ranges of good communications between each combination of assets. Different possible network topologies are analyzed in terms of network connectivity, quality of the communication links, stability, and reliability. Each of these steps are described in detail in the next subsections.

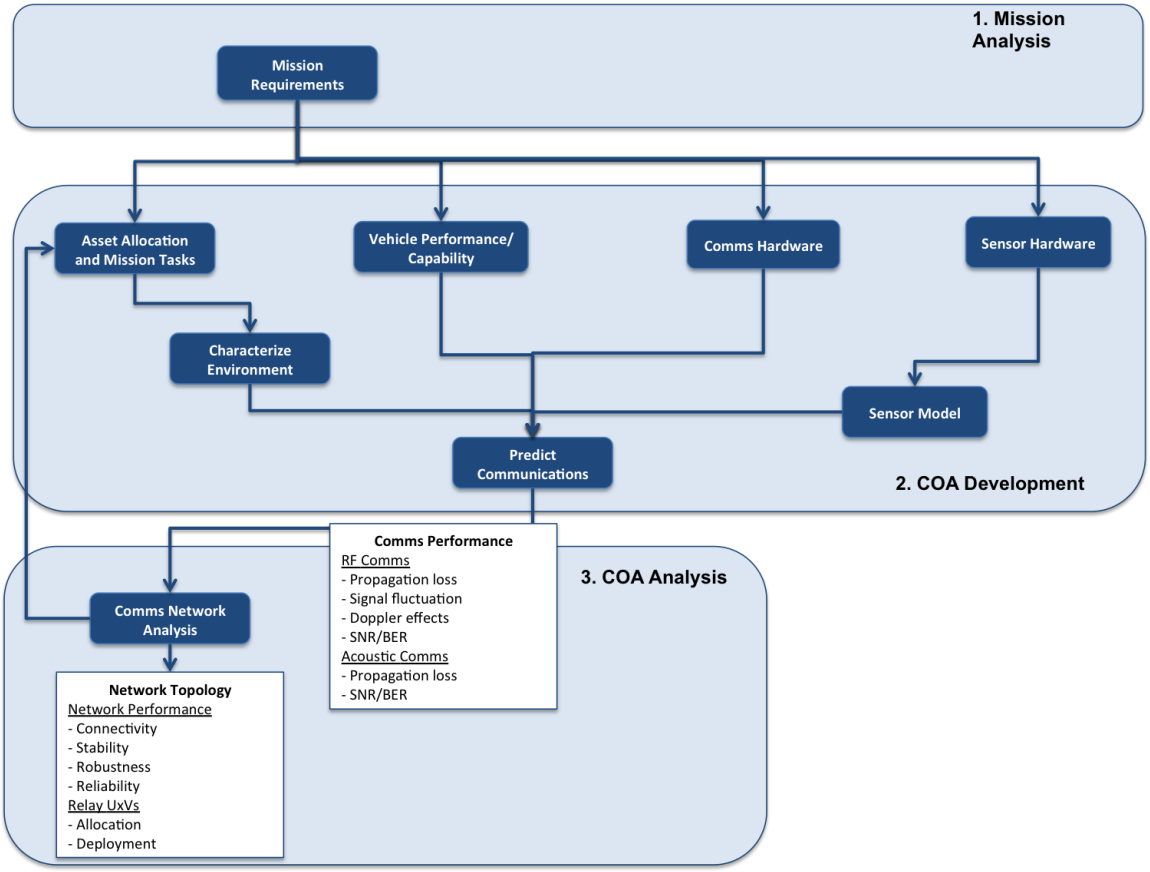


**Figure 144:** Communications network analysis phase of the COA Analysis step.

#### *7.5.1.1 RF Antenna Heights*

Effects of evaporation ducts on signal frequency diversity were analyzed in previous sections for wideband and narrowband communications between a ship and a USV, and between USVs, assuming a Nakagami fading channel model with parameter $m = 1$ (Rayleigh fading). The results showed that the lower the elevation duct, the higher the signal attenuation. In this study it was found that antenna height relative to the duct elevation is critical for transmission performance. Results moreover indicated that better signal transmission occur for USV-to-USV communications, most likely due to the height of their transmitting antenna relative to the evaporation duct elevation. The 14m and 24m duct elevations allow the transmitting signals of the USVs 3m antennas to be better trapped within the confines of the waveguide-like

ducts. Wide frequencies propagation loss differs greatly, even at the same range. However, when looking at a narrowband of 16 MHz, it was observed that the 16 MHz bandwidth will offer a substantial advantage over wideband transmissions.

From the USV and UUV trade studies, we concluded that transmitting communications from UUVs to MS directly has greater ranges of communications than when we use the USV as a relay, which is due to the higher antenna height provided by the MS. We also found that the higher the transmitter antenna is from the sea surface, the more attenuation the signal experiences, and was explained in terms of the higher multipath fading experienced by the reflected paths from the sea surface. These results led to the UAV design considerations and motivational studies to provide unique UAV capability for communications-based COAs help relay communications from a UUV back to MS and that can also submerge underwater and fly to relay either acoustic or radio communications, or collect underwater sensor data. These trade studies led to the design of the Cormorant design for a SUFV that can operate both above and underwater, and Eagle, which has a long hover endurance to relay comms from different assets. Both vehicles were sized and their capability was tested experimentally with prototype designs.

In light of these results, the antenna heights for each UxV and main ship, based on their operational domain, dimensions, and capability, are chosen so that they are within our outside the surface based or evaporation ducts. Flying vehicles contain a range of values based on their service ceiling. Eagle UAV antenna height varies from USV altitude to the service ceiling altitude. Cormorant's antenna height varies from sea surface to its service ceiling. The antenna height of each UxV and main ship are shown in Table 21.

**Table 21:** UxV and Main Ship Antenna Heights

| | |
|---|---|
| UUV (m) | 0.5 |
| USV (m) | 3.5 |
| Eagle UAV (m) | 3 - 100 |
| Cormorant UAV (m) | 0 - 100 |
| Main Ship (m) | 25 |

#### *7.5.1.2 Large-scale Fading of Transmission Channels*

The modified refractivity profile corresponding to the 24 m EVD, 90 m SBD, and 24 m EVD plus90 m SBD are input to the APM propagation model, along with radio transmitter and receiver characteristics for the MPU5 COTS RF radio. The transmitter and receiver heights used for each asset and main ship are extracted from Table 21. For Eagle, two operating transmitter/receiver heights are chosen, at 30 m, just above the evaporation duct height, and at 100 m, well above the evaporation duct and just above the surface-based duct height. This allows for determining the effects of duct heights on the positioning of the transmitter/receiver. Cormorant's transmitter/receiver height was chosen at 0 m, right on the water surface, and at 20 meters, right below the evaporation duct height. UUV transmitter was set at a constant 0.5 m, and the USV also set at a constant 3.5 m. Finally, the main ship receiver height was set at 25 m. These chosen heights for this case study are shown in Table 22.

**Table 22:** Transmitter and Receiver Selected Heights

| | |
|---|---|
| UUV (m) | 0.5 |
| USV (m) | 3.5 |
| Eagle UAV (m) | 30 and 100 |
| Cormorant UAV (m) | 0 and 20 |
| Main Ship (m) | 25 |

For this case study, only one relay at a time is considered for simplicity. There may be multiple relays to chose from given the deployment of available assets, but each relay only communicates sensor data from the UUV to the main ship. An Operational View (OV-2) is provided in Fig. 145 for the operational node connectivity and links between the different assets.

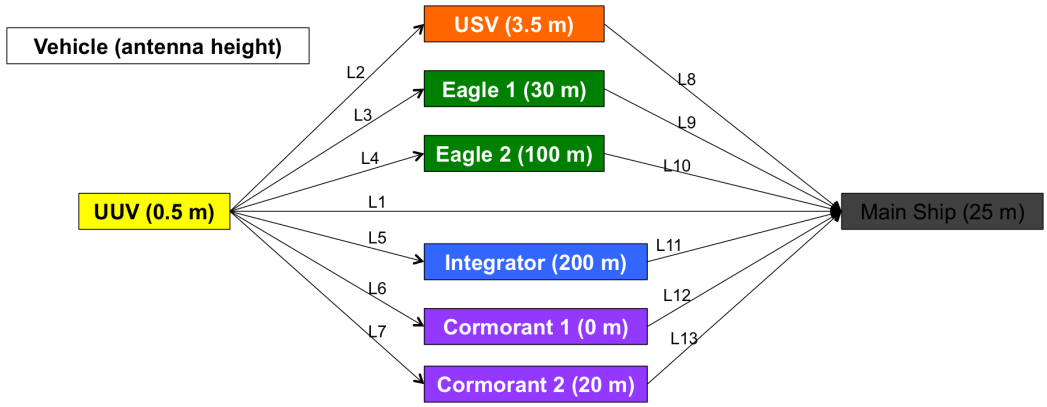


**Figure 145:** OV-2 Operational Node Connectivity and Links.

Propagation loss profiles (PLPs) corresponding to links $L1$ to $L7$ can be studied from a single profile generated for each atmospheric condition, with the UUV transmitting antenna and the receiving antenna set up for each other vehicle. The signal attenuation is propagated over the maximum ranges within the sea-base and at maximum altitudes. The rest of the links will be studied with PLPs corresponding to given transmitter and receiver heights, and all the atmospheric condition. These

propagation loss profiles and corresponding link transmitters and receivers are shown in Table 23.

**Table 23:** Propagation Loss Profiles (PLPs)

| PLP | Atmospheric Condition | Links | Transmitter | Receiver(s) |
|---|---|---|---|---|
| 1 | 24 m evap. duct | 1 - 7 | UUV | MS and UxVs |
| 2 | 90 m SBD | 1 - 7 | UUV | MS and UxVs |
| 3 | 24 m evap. duct plus 90 m SBD | 1 - 7 | UUV | MS and UxVs |
| 4 | 24 m evap. duct | 8 | USV | MS |
| 5 | 90 m SBD | 8 | USV | MS |
| 6 | 24 m evap. duct plus 90 m SBD | 8 | USV | MS |
| 7 | 24 m evap. duct | 9 | Eagle 1 | MS |
| 8 | 90 m SBD | 9 | Eagle 1 | MS |
| 9 | 24 m evap. duct pus 90 m SBD | 9 | Eagle 1 | MS |
| 10 | 24 m evap. duct | 10 | Eagle 2 | MS |
| 11 | 90 m SBD | 10 | Eagle 2 | MS |
| 12 | 24 m evap. duct plus 90 m SBD | 10 | Eagle 2 | MS |
| 16 | 24 m evap. duct | 12 | Cormorant 1 | MS |
| 17 | 90 m SBD | 12 | Cormorant 1 | MS |
| 18 | 24 m evap. duct plus 90 m SBD | 12 | Cormorant 1 | MS |
| 19 | 24 m evap. duct | 13 | Cormorant 2 | MS |
| 20 | 90 m SBD | 13 | Cormorant 2 | MS |
| 21 | 24 m evap. duct plus 90 m SBD | 13 | Cormorant 2 | MS |

The output of APM are propagation loss profiles (PLPs) with range and height. The PLP and corresponding propagation loss to the receiver antenna height for links 1 to 7 for the 24 m evaporation duct, 90 m SBD, and combination of both are shown in Fig. 146, Fig. 147, and Fig. 148, respectively.

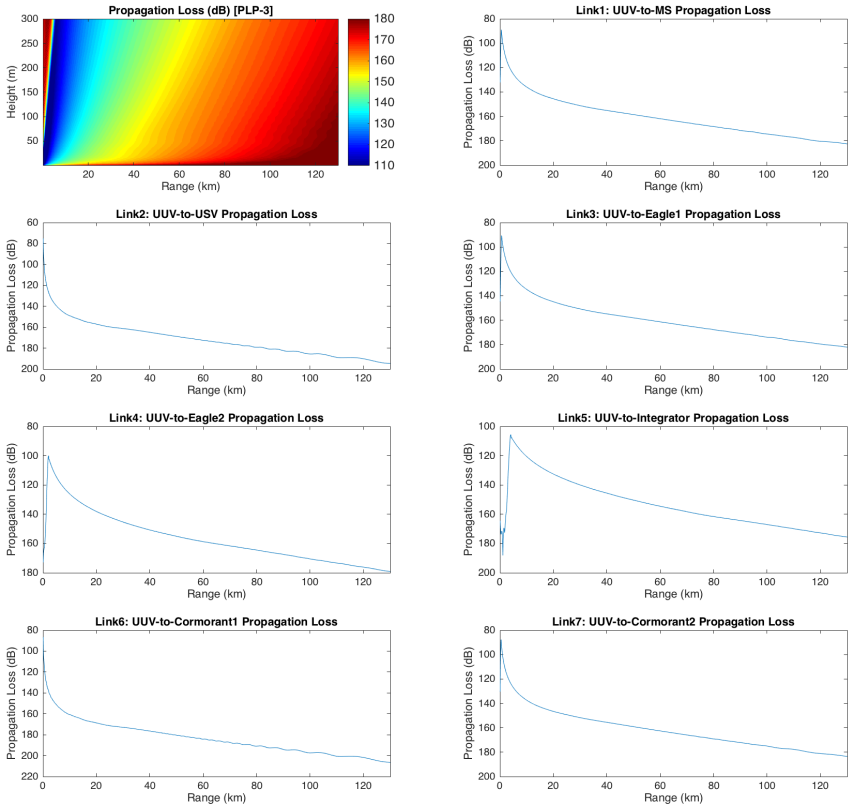


**Figure 146:** PLP-1 for 24 m evaporation duct and receiver propagation losses for links 1 to 7.

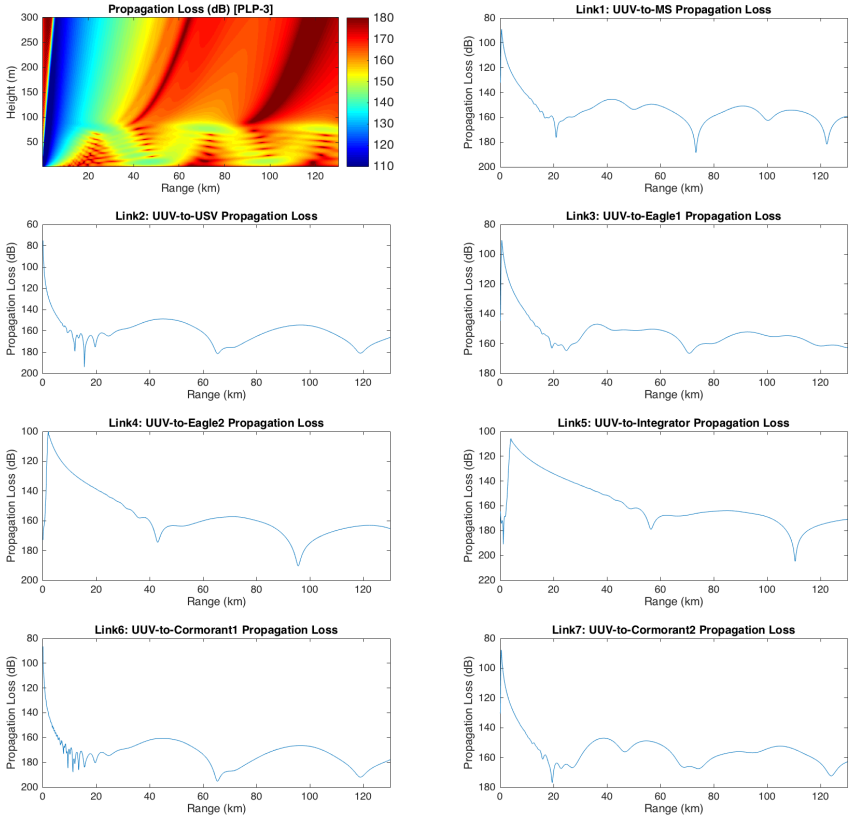


**Figure 147:** PLP-2 for 90 m SBD and receiver propagation losses for links 1 to 7.

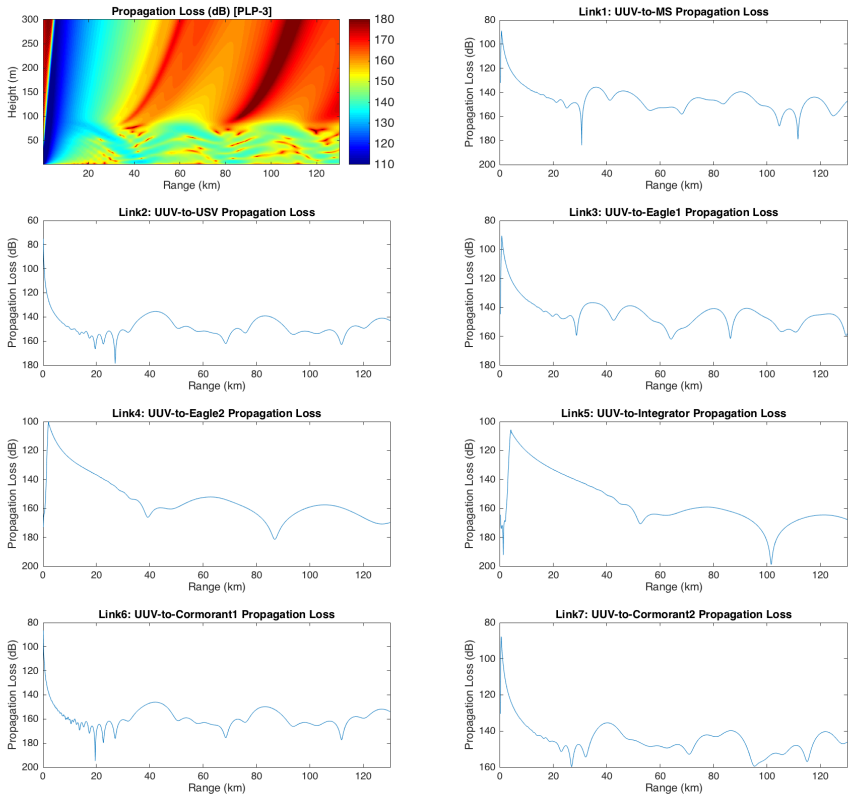


**Figure 148:** PLP-3 for 24-m evaporation duct and 90 m SBD and receiver propagation losses for links 1 to 7.

Propagation loss profiles PLP-4 to PLP-21 were generated also from APM model, for each atmospheric environment, with transmitter and receiver heights corresponding to each vehicle in links 8 to 13, as shown in Table 23. PLPs 4, 5 and 6 corresponding to USV to MS links for each atmospheric condition are shown in Fig. 149.

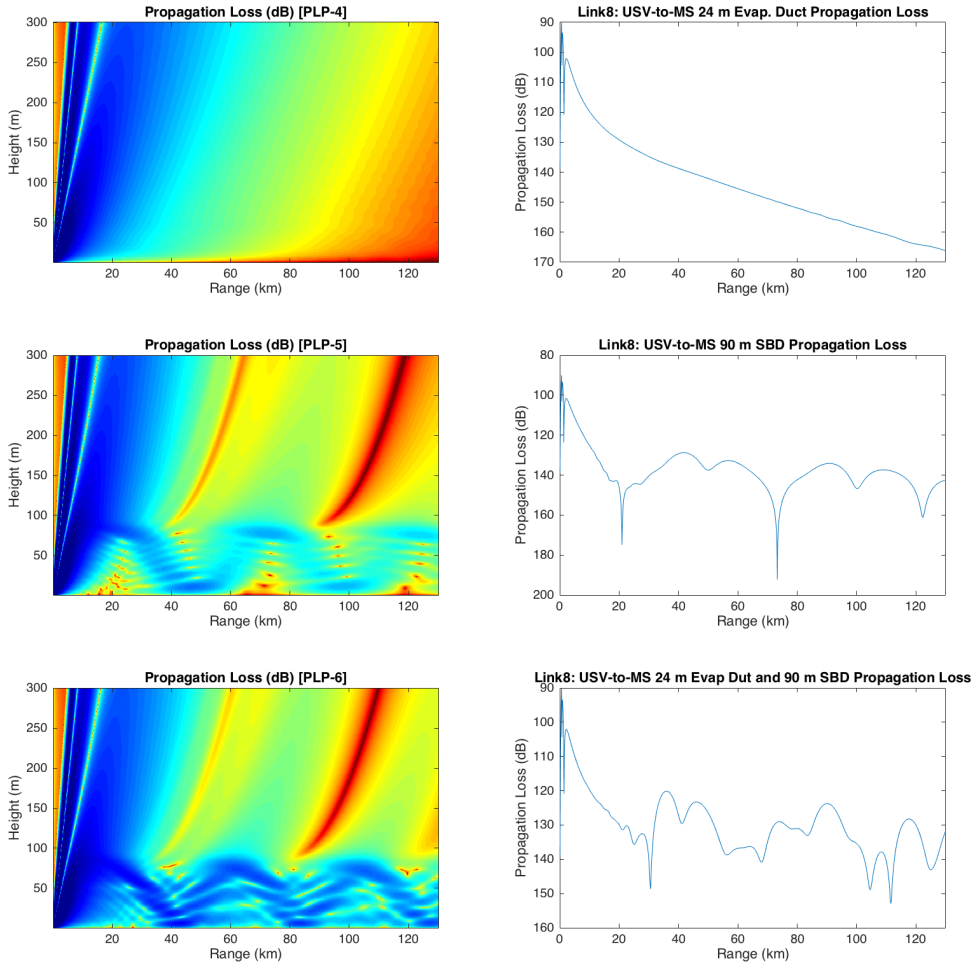


**Figure 149:** PLP-4 to PLP-6 and corresponding receiver propagation losses of link 8 under each atmospheric condition.

PLP 7 to PLP 21 in Table 23 generated by APM for each link under the three atmospheric conditions are given in Appendix A.

#### *7.5.1.3 Propagation Loss over Signal Bandwidth*

The operating frequency of the signal, from MPU5 radio specifications is at 2.4 GHz, with a signal bandwidth of $BW = 20MHz$. The propagation losses calculated so far are only at the center frequency of the radio, at 2.4 GHz and do not take into account

the propagation losses over the whole bandwidth of operation. Therefore, next we use the APM model to calculate the propagation losses over the channel bandwidth, and compare them to the mean large-scale propagation losses calculated previously at the center frequency. Whichever propagation loss is higher, that becomes the propagation loss at that given range and height.

Since the center frequency is at $f = 2400MHz$ and the bandwidth is $20MHz$, the frequency was varied from a low frequency of $f_L = 2390MHz$ to a high frequency of $f_H = 2410$. Using the same MPU5 radio properties, and antenna heights given in Table 22, APM was used to calculate the propagation loss profiles vs. frequency and range for each asset combination under the three atmospheric weather conditions considered in this study. Shown in Figs. 150, 151 and 152 are the resulting frequency-range propagation (FRPs) losses calculated by APM for each configuration in each weather condition.

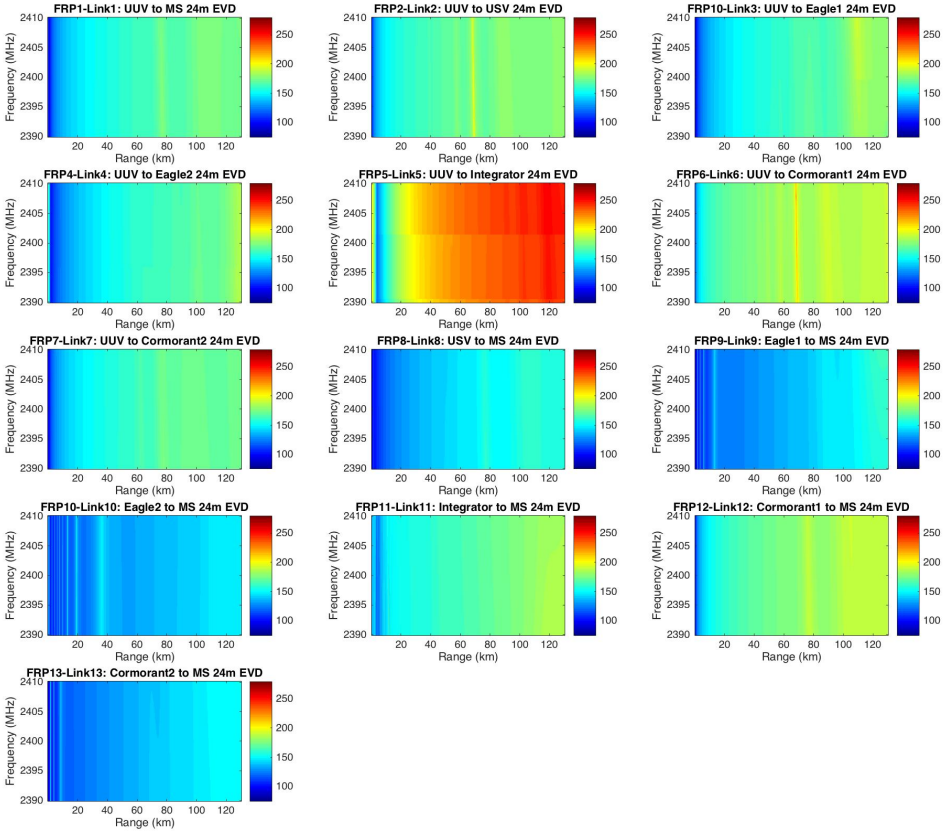


**Figure 150:** FRPs for each link in a 24m EVD.

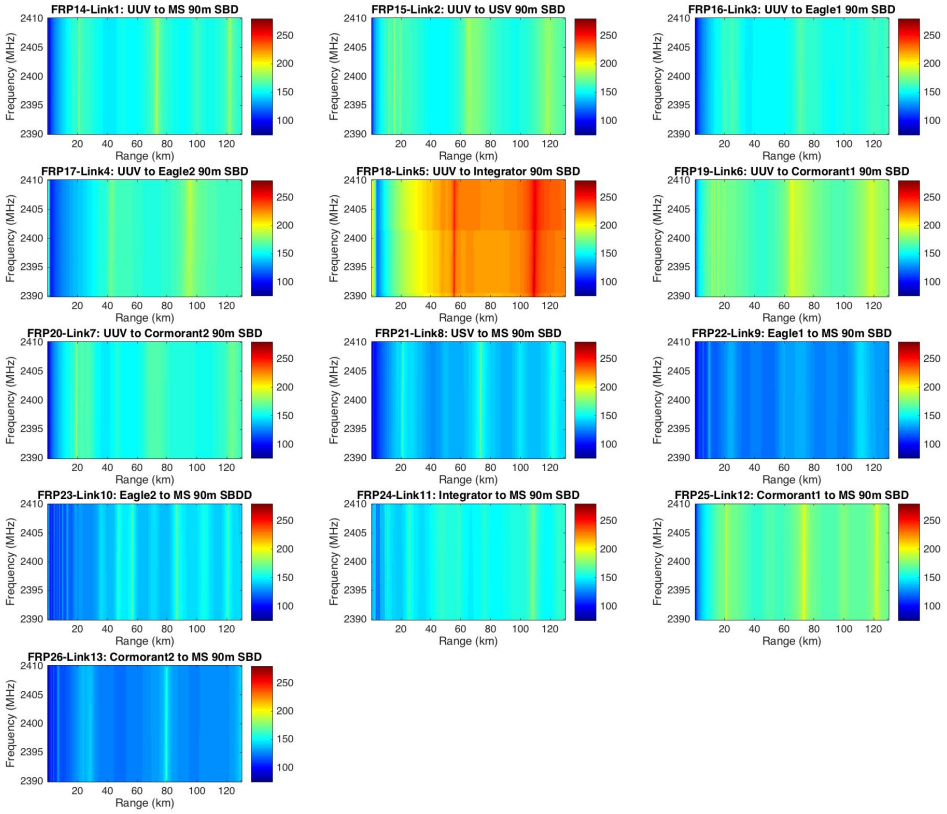


**Figure 151:** FRPs for each link in a 90m SBD.

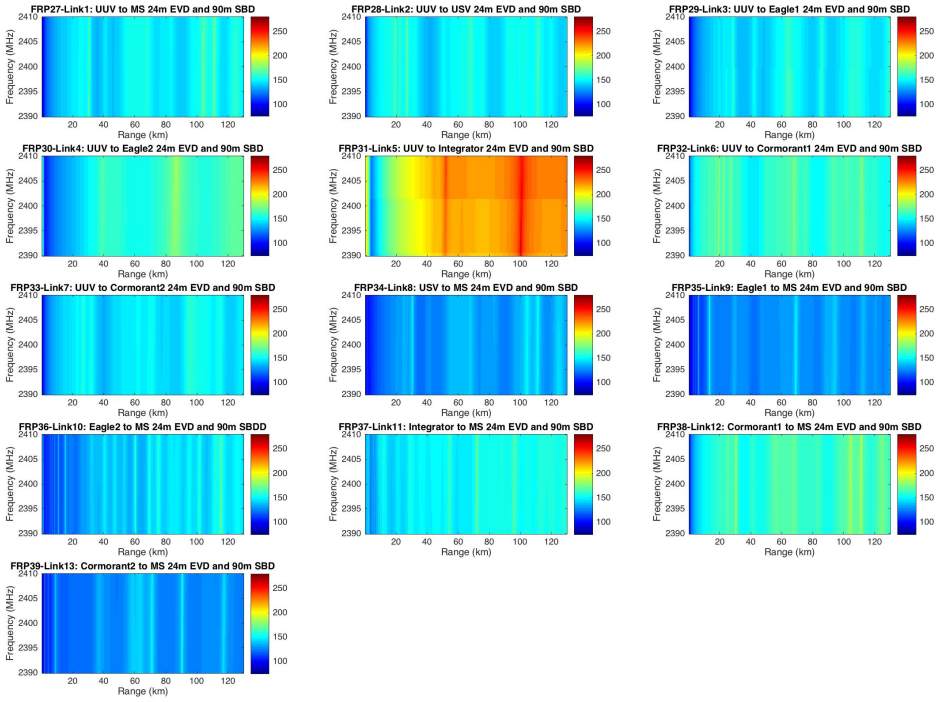


**Figure 152:** FRPs for each link in a 24m EVD plus 90m SBD.

As can be seen in each of these FRPs, the propagation loss stays pretty much constant, but there were instances where the propagation loss was higher at certain frequencies other than the center frequency, which was used instead to resemble the maximum propagation loss experienced over the channel bandwidth at that range and height. Next we add the small scale signal intensity effects of the transmission channel.

#### *7.5.1.4 Small-scale Fading of Transmission Channels*

The small-scale fading of each channel was modeled using the Nakagami-m probability model with parameter $m = 1$, or Rayleigh fading probability model. The link budget was composed of the gains and losses given in Table 2. The same minimum receiver power threshold for the MPU5 at $P_{R_{min}} = -98dBm$ was used to calculate the CDF for

the outage probability of communications. The probability of good communications threshold was again set high enough to $Pr_{th} = 0.8$ to take into account errors in the modeling and uncertainty in environmental conditions. The resulting received power from the link budget equation with the minimum receiver power threshold shown, and the corresponding probability of communications with the threshold of probability of communications shown, for the first links are shown in Fig. 153.

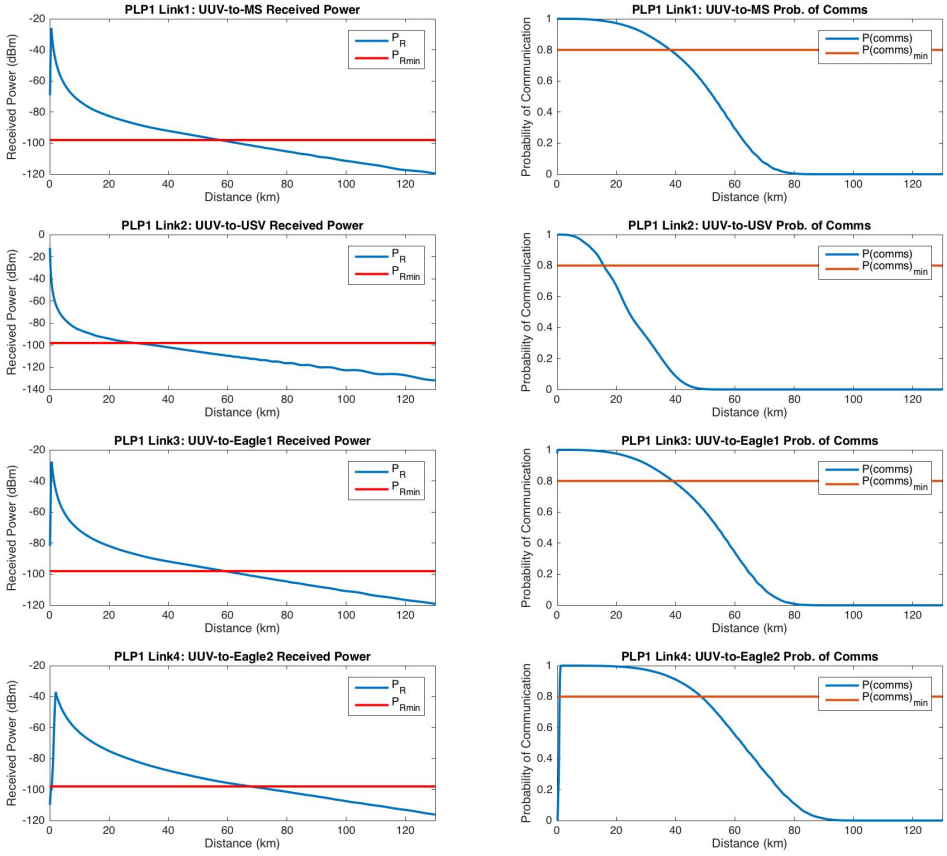


**Figure 153:** Received power and probability of communications for first set of links under the 24 m EVD.

The received power and probability of communication profiles for the rest of the links under the different environment conditions are given in Appendix B.

### 7.5.2 Experiment 1: Network Topology Analysis

Our final experiment deals with our first RQ1 and corresponding hypothesis HP1 posed on finding proactive communications network topologies that are reliable to communication link failures based on asset availability, and which has the best network quality and is stable due to vehicle relative motions. We will use our available assets, relay UxVs, their capability and performance, and their communications and sensor capability to find network topologies that meet the mission level requirements that deal with communications.

We present methods in graph theory to create communication network topologies that meet our mission constraints. In this discussion, vehicles or agents are represented by the set of nodes $V = v_1, v_2, ..., v_n$ where $n$ is the number of vehicles, and the set of links (edges) between the nodes are represented by $E = Link_1, Link_2, ..., Link_M$, where $M$ is the number of links. A given graph topology is represented by $G(V, E)$. The graph theory assumptions regarding the types of communication networks we model for this case study are the following:

- Undirected links: we do not model the direction of the communications transmission, and assume both ways are equally represented.
- Graphs are simple: no transmitters communicate with itself, and no multiple links are used to connect two nodes.

For a link $Link_k$, $1 \geq k \leq M$, connecting nodes $v_i$ and $v_j$, $\{v_i, v_j\} \in V$, we define the vector $a_k \in \mathbf{R}^n$, where $a_{k,i} = 1$, $a_{k,j} = $ -1, and the rest are zero. The *incidence matrix* $A \in \mathbf{R}^{n \times m}$ of the graph $G$ is the matrix composed by the $k^{th}$ columns given by $a_k$. The $n \times n$ *Laplacian* matrix $L$ is defined as

$$L = AA^T = \sum_{k=1}^{M} a_k a_k^T \tag{110}$$

The diagonal entry of $L$ , $L_{i,i}$, is the degree of node $i$, and $L_{i,j} = -1$ if $(v_i, v_j) \in E$, otherwise $L_{i,j} = 0$. As was previously described, It should be noted that the

summation of the elements in each row (column) of $L$ equals zero. In addition, the Laplacian matrix is positive semi-definite, $L \geq 0$, and its smallest eigenvalue is zero, $\lambda_1(L) = 0$.

As was also noted in the literature review, even of greater importance with respect to the algebraic connectivity of graph $G$ is the second smallest eigenvalue of $L$, $\lambda_2(L)$, called the *Fiedler value*, which measures how connected the graph is [96] [158]. The Fiedler value is greater than zero, $\lambda_2(L) > 0$ if and only if $G$ is connected and the multiplicity of the zero eigenvalue is equal to the number of connected sub-graphs. The Fiedler value is also monotone increasing in the edge set. That is, if there is a graph $G_1 = (V, E_1)$, and another graph $G_2 = (V, E_2)$ such that $E_1 \subseteq E_2$, then $\lambda_2(L_1) \leq \lambda_2(L_2)$, where $L_1$ and $L_2$ are the laplacian matrices of graphs $G_1$ and $G_2$, respectively [113]. This means that as the number of nodes connected in a graph increases, the Fiedler value also increases, and can be used to quantify the connectivity of a communications network.

#### *7.5.2.1 Network Topology Assumptions and Constraints*

In this section, we enumerate the assumptions and constraints used to investigate possible communication network topologies among the different assets. These constraints help us scope our problem to one can be analyzed in this study and that provides network solutions that show the benefits of our methodology.

For this case study, the are only concerned about the communication of sensor information from the UUVs back to the main ship (MS). Each UUV is tasked with surveying a given target area during the objet detection phase. As they sweep through their corresponding TA, they will communicate sensory information back to the MS both acoustically and by RF communications. We focus on a specific location of the UUV for re-establishing communications with the MS. This location is chosen to be the lower-left corner of each TA, the starting point of each UUV before they start

sweeping the TA, as are shown in Fig. 154. We concentrate our network analysis to the communication of UUV sensory information back to the MS through direct or relay links at this specific UUV starting point location. The selection of this starting

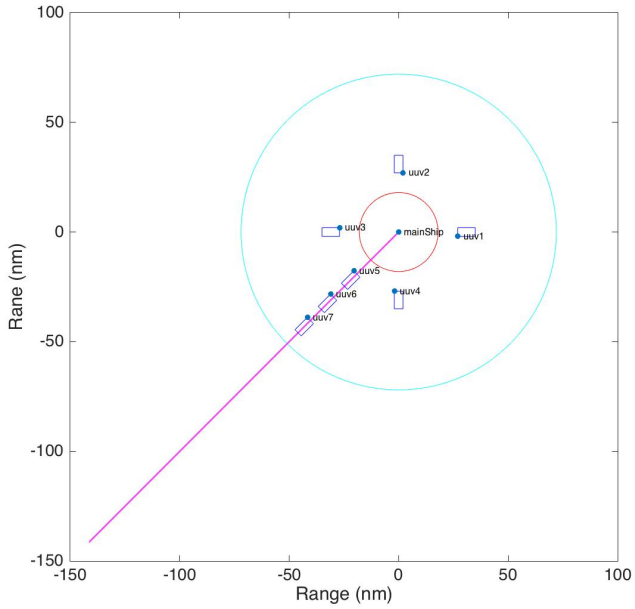


**Figure 154:** Initial UUV and MS configuration at the starting points for each TA.

point may seem arbitrary to some degree, but it provides some valid logistics. If the UUV loses communication at any other point during the object detection phase while surveying the TA, it can come back to this starting point and connect back to the MS. The UUV can also take a shorter path to the starting point through the area that was surveyed up to that point. And if relay vehicles are needed to relay the communications back to the MS, the relay vehicles can be in a safe cleared location between the MS and the starting point.

The next assumption will be that relay vehicles, composed of USV, Cormorant, and Eagle unmanned vehicles, will only relay communications from one or more UUVs back to the MS. That is, we will not consider network topologies where relay vehicles relay the communications through other relay vehicles. This is done to simplify our analysis while scoping the problem to a manageable space of relay alternatives, and

also due to the fact that frequency bandwidth is usually lost as the number of relay nodes are added to the transmitted signal.

Another assumption is that relay vehicles are added to the network topology only if it relays communications from a UUV or group of UUVs back to the MS. If not, it is not considered in the network topology, and the connectivity of the network, as measured by the Fiedler value, is not affected.

The network topologies that result from this study will be assessed in terms of their connectivity, the quality of the communication links, their stability, and in terms of their reliability to link failures. The end goal of this study is to meet our mission requirements on the robustness of the communication network towards environmental conditions, the stability of the network towards signal fluctuations and vehicle motions, and reliability to unexpected link failures.

The first requirement to meet is network connectivity. We make sure that each UUV can communicate back to the main ship at its starting point. The less the number of relays we need to use, the better. And this will be measured by the Fiedler value, since the node set will be kept constant (all relays are considered in any graph, but not necessarily connected) and the edge set will be increasing or decreasing which is a direct measure of the connectivity.

The second requirement to meet is the stability of the communication network. There might be different network topologies that have the same maximum Fiedler value, and which are not stable. The stability of the network is measured by the stability of each link in the network. As explained in the FSMC section, this can be done by summing the state transition probabilities of the good states from the state transition probability matrices. This is done for each path connecting a UUV to the MS, via a relay or not. If any of the links in the path is not stable, then the path is considered unstable. This can be used to rule out network topologies that do not meet our stability requirements.

The third requirement to meet is the quality of the communication network. There might be the case where two or more network topologies have the same connectivity and have the same stability. Therefore, it will be useful to compare the quality of the communications network in terms of the quality of the communication links that compose it. This is done by adding weights to the graph given by the probability of communications of each link. Each path then takes the weight of the product of the probability of communications that compose it. We then add each paths weights to get the network probability of communications weight. This network probability of communications is then used as a measure of the quality of the network, and can be used to compare among candidate network topologies with the same connectivity.

Finally, the fourth requirement to meet is the reliability to link failures. We will assume that link failures happen one at a time. We are going to assess reliability by the degree of each UUV node, which measures how many paths there are to communicate back to the MS. To meet this reliability constraint, we will require that each UUV node has a degree $\geq 2$, such that if a link fails in any of the paths connecting the UUV to the MS, there is at least one more path for the UUV to connect back to the MS at the starting point.

To summarize, network topologies will be assessed in the following order:

- 1) Network connectivity
- 2) Network stability
- 3) Network quality
- 4) Network reliability

#### *7.5.2.2 Space Exploration of Communication Network Topologies*

In this study, the goal is to fully enhance the connectivity of the communications network by using our available set of relay unmanned vehicles to the network. We

use the Fiedler value to quantify the connectivity of the network for each possible network topology. We aim at finding the optimal locations of the relay UxVs in order to maximize the Fiedler value of the resulting graph.

Finding the optimum locations for each relay is a difficult problem due to the continuous nature of the problem, which results in an infinite number of possible topology configurations. To overcome this problem, we propose discretizing the space into $n_c$ possible candidate locations for each node, at each of the RF antenna heights considered for each vehicle. This method is inspired by the work of Ibrahim et. al. [113] which used a network-maintenance algorithm to find the near-optimum locations for a set of available sensor relays. However, we stop at the first level of Ibrahim's method, instead of going to higher levels of more granular discretization of the space.

The connectivity problem is posed as follows. The set of deployed UUVs to each TA, as described in the Mission Analysis step, and the stationary MS at the center of the sea base, together define the initial graph $G_0(V_0, E_0)$. This initial graph will be constant since the MS location at the center of the sea base is fixed, and the starting point for each UUV (the lower left corner of each corresponding TA) is also fixed. The question becomes: given a set of $Q$ available relay UxVs, deployed over a square $[x_c, y_c]$ area with $n_c$ possible candidate locations, resulting in the graph $G_c(V_c, E_c)$, what are the optimum locations for these UxV relays such that the Fiedler value is maximized for the resulting graph? Adding relays (nodes) to the initial graph can result in connecting UUVs to the MS that were not initially connected due to the environmental conditions and the small scale fading signal fluctuations and attenuations. The added relay can be within good communication ranges of the UUV and the MS, and hence it can relay the sensor data from the UUV to the MS, which results in the addition of edges to the initial graph. Letting $E_c(Q)$ denote the set of edges resulting from adding a candidate set of $Q$ relays, the network connectivity

problem can be formulated as

$$\max_{E_c(Q)} \quad \lambda_2(L(E_0 \cup E_c(Q))) \tag{111}$$

We solve this problem by dividing the $[x_c, y_c]$ area into $n_c$ equal small areas, each of width $w$. With $x_c = y_c$, this results in $n_c = (\frac{x_c}{w})^2$ number of possible relay locations. Each relay will be considered placed at the center of that location. We want to choose the optimum $Q$ relay locations among these $n_c$ relays. This optimization problem is formulated as

$$\begin{aligned} &\max && \lambda_2(L(p)) \\ &\text{subject to} && \mathbf{1}^T p = Q, p \in \{0,1\}^{n_c} \end{aligned} \tag{112}$$

where

$$L(p) = L_0 + \sum_{k=1}^{n_c} p_k A_k A_k^T \tag{113}$$

where $\mathbf{1} \in \mathbf{R}^{n_c}$ is the all-ones row vector, $A_k$ is the incidence matrix resulting from the addition of relay $k$ to the original graph $G_0$, and the optimization vector $p \in \mathbf{R}^{n_c}$ where each element is either 1 or 0, denoting whether this relay should be used or not.

The optimization problem in Eq. (112) can be formulated as a standard semi-definite programming (SDP) optimization problem and can be solved using an SDP solver. However, due to the small number of relay assets we consider, we will use an exhaustive search, which is done by computing the Fiedler value for $\binom{n_c}{Q}$ combination of Laplacian matrices.

#### *7.5.2.3 Network Connectivity Analysis*

Here we show the results of our network analysis. We discretized our sea-base area into $n_c = 961$ of grid points within a square area $[-75nm, 75nm]$ of width $w = 5nm$, centered about the MS location at the origin, as is shown in Fig. 155.

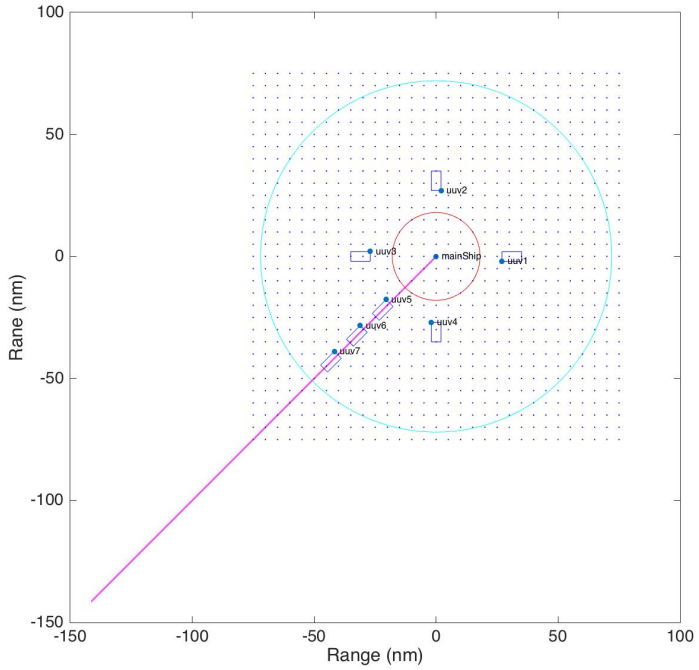


**Figure 155:** Grid points discretization for possible candidate relay locations.

Each relay UxV was placed at each grid location, without overlapping with other UxVs, except for Eagle which is assumed to be able to hover above the USV from which it is deployed. The USV relay was placed at each of these grid locations with an antenna height at 3.5 m (below the 24 m EVD). The Eagle relay, when considered, it was tested at the two considered antenna heights: 30 m and 100 m (below and above the 90 m SBD). The Cormorant vehicle was constrained y its range at 13 nm, which was only deployed from the MS. Its considered heights were 0 m and 20 m (both below the 24 m EVD). These antenna heights were given in Table 22.

Combination of relays are considered as choosing 1 to Q relay UxVs from the $n_c$ possible locations, and at each of the 2 possible heights for the Eagle and Cormorant UAVs. Each possible combination of UxVs is tested at each possible grid point location using an exhaustive search. For a given potential grid point of each relay vehicle, it is compared to the ranges of good communications between each UUV

and that relay vehicle and the ranges of good communications between each relay vehicle and the MS. If both links, the one from the UUV to the relay vehicle and the link from the relay vehicle to the MS are in good communication ranges (they meet the threshold of probability of communications), then the grid point is considered as a potential location for that relay vehicle. This is done for each vehicle in each combination, at each grid point and possible relay height. Next we asses our network connectivity analysis for each environmental condition. Given that the lower the evaporation duct the more the signal attenuation, as was shown from our previous results, we consider the different environmental conditions based on their complexity in the following order: 1) 24 m EVD plus 90 m SBD, 2) 90 m SBD, and 3) 24 m EVD.

#### *7.5.2.4 24 m EVD Plus 90 m SBD Network Analysis*

The initial graph of the network under the 24 m EVD plus 90 m SBD, given by the UUVs and the MS nodes, with the ranges of good communications shown, is given in Fig. 156. The corresponding graph showing the quality of the links, stability, and whether each link is in a stable (1) or unstable (2) state is shown in Fig. 157.

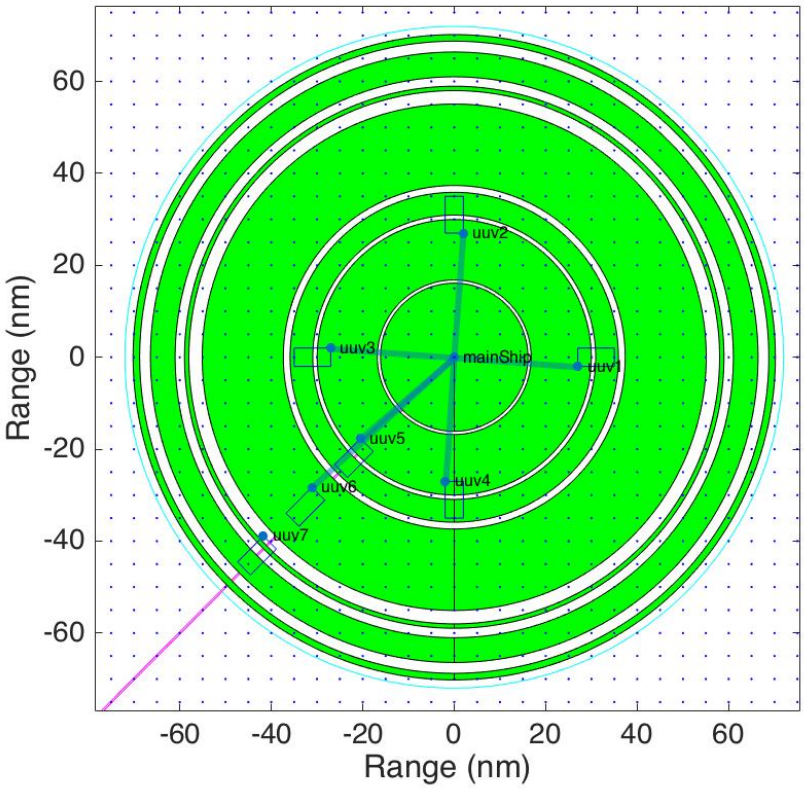


**Figure 156:** Initial graph $G_0$ under 24 m EVD plus 90 m SBD with ranges of good communications between UUVs and MS.

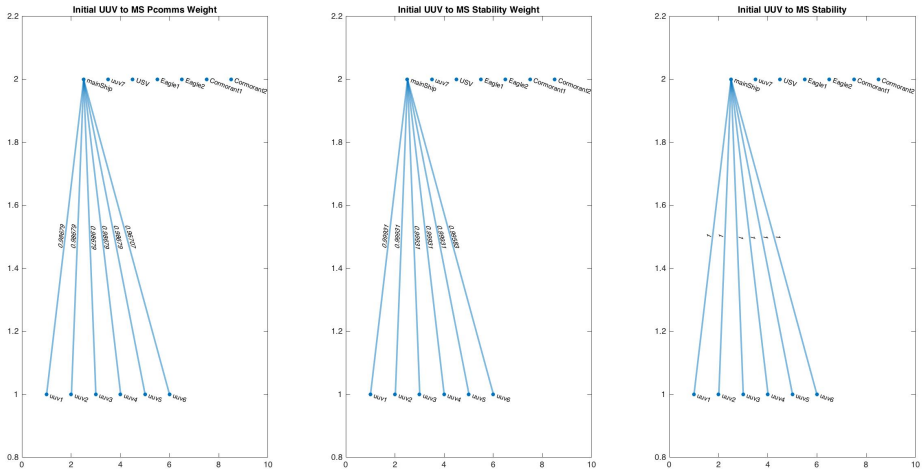


**Figure 157:** Initial graph $G_0$ under 24 m EVD plus 90 m SBD with link quality weights (left), stability weights (middle), and stable states logical values (right).

As can be seen in each plot, the initial set of connected nodes are UUV1 to UUV6. The only UUV not connected to the main ship is UUV7. To meet our first connectivity constraint, we consider adding relays to the network, and look at possible network topologies that help meet our first connectivity criterion.

Next we performed a search for finding network topologies that maximize the Fiedler value according to Eq. 112. Since under this environmental conditions, the RF signals tend to be trapped within the 24 m EVD and the 90 m SBD, there were 150 solutions that yielded the same Fiedler value. The next step was to select the best combination out of these 150 solutions that meet the stability, quality, and reliability criteria.

Out of these 150 solutions, we compared them in terms of their stability. The network topology with the highest number of stable paths was the one that involved using Eagle1 and Cormorant2 as relay UxVs. The graph corresponding to this network topology, with stability, quality of link weights and logical representation of being in stable (1) or unstable (0) state are shown in Figs. 158, 159, 160. Table 24 shows the

reliability of this network topology in terms of the number of link paths available for each UUV to connect with the MS, and the main path that has the most stable paths and highest probability of communications.

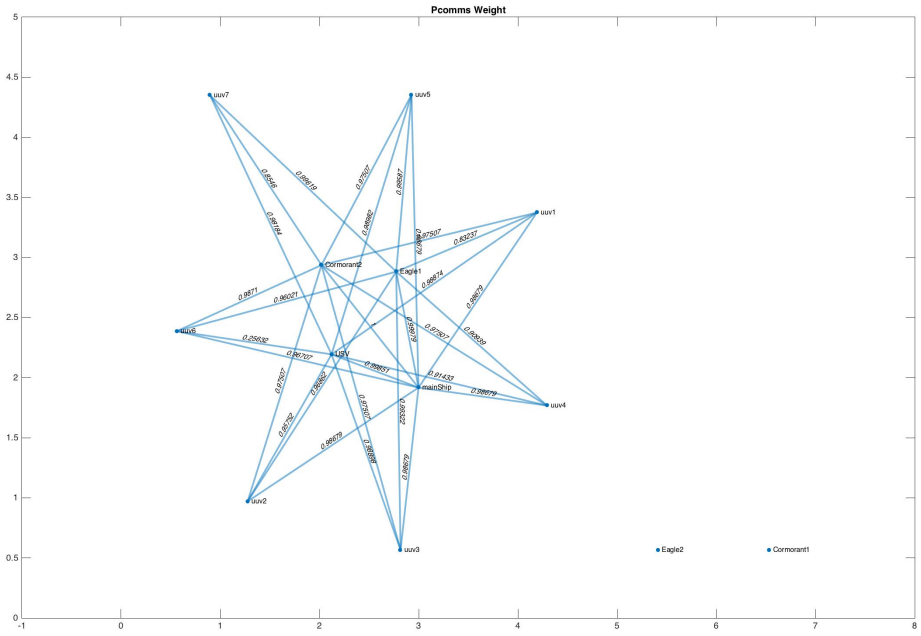


**Figure 158:** 24m EVD plus 90m SBD best network topology with quality weights.

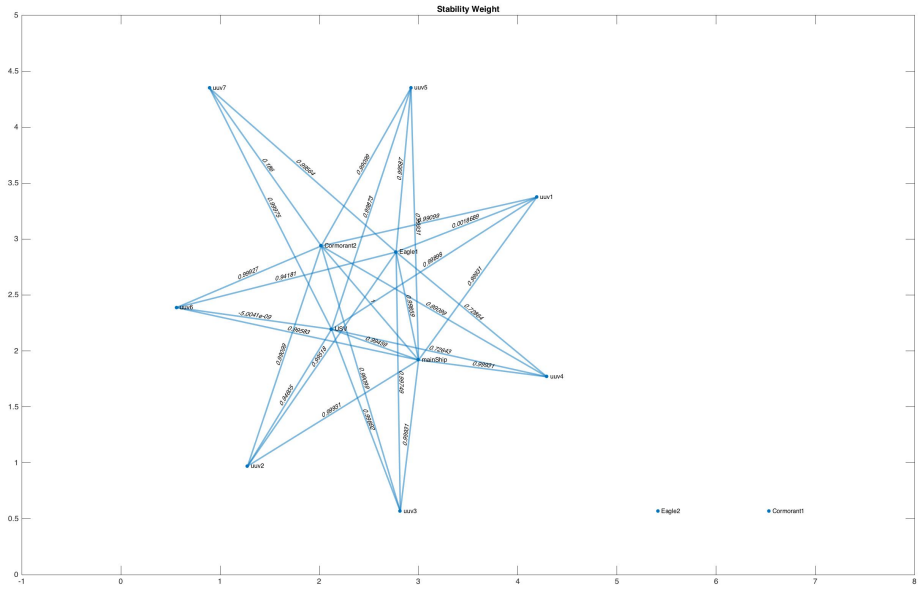


**Figure 159:** 24m EVD plus 90m SBD best network topology with stability weights.

**Table 24:** Network Topology Analysis for 24m EVD plus 90m SBD

| | UUV1 | UUV2 | UUV3 | UUV4 | UUV5 | UUV6 | UUV7 |
|---|---|---|---|---|---|---|---|
| **Degree** | 3 | 4 | 4 | 4 | 4 | 3 | 2 |
| **Main Relay** | MS | MS | Eagle1 | MS | Eagle1 | Cormorant2 | Cormorant2 |

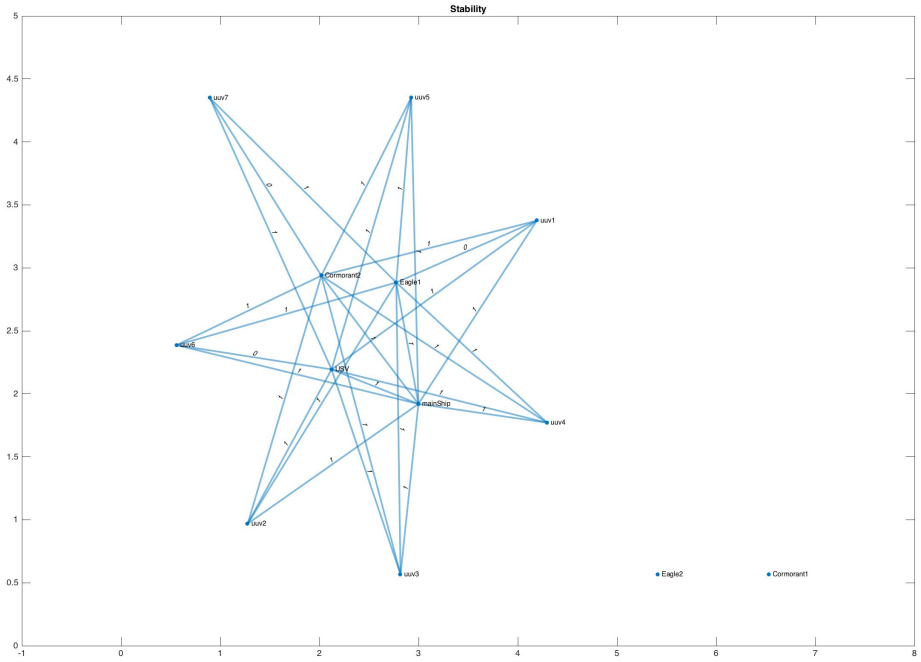


**Figure 160:** 24m EVD plus 90m SBD best network topology with stable state logical values.

The final network topology can be shown in the following plots for the UUVs connected with straight to the MS in Fig. 161, using Eagle1 as a relay in Fig. 162, and using Cormorant2 as the relay in Fig. 163.

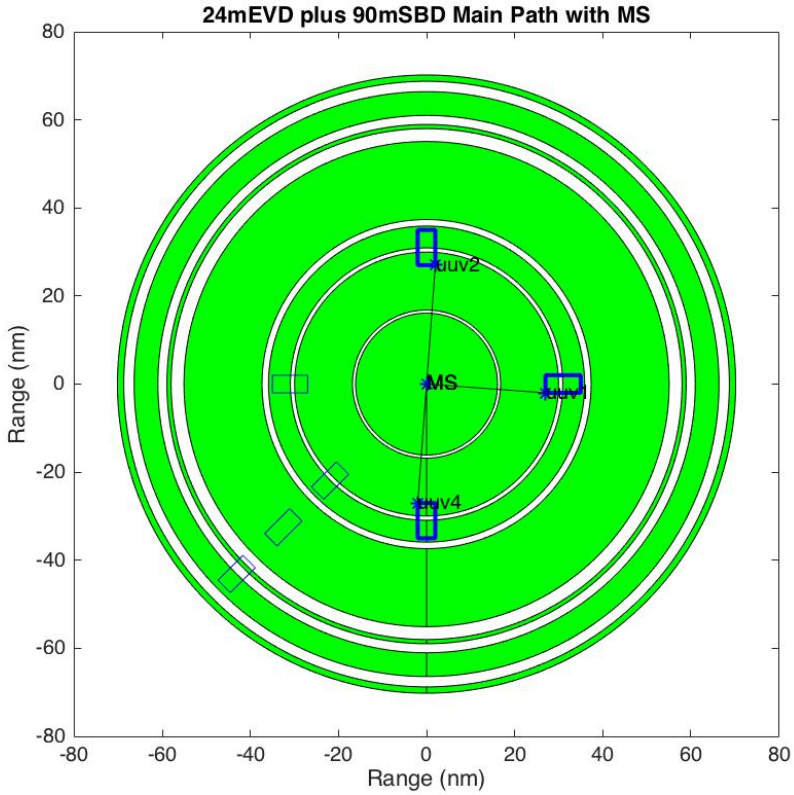


**Figure 161:** Final network topology with ranges of good communications for UUVs connected directly to MS in a 24m EVD plus 90m SBD.

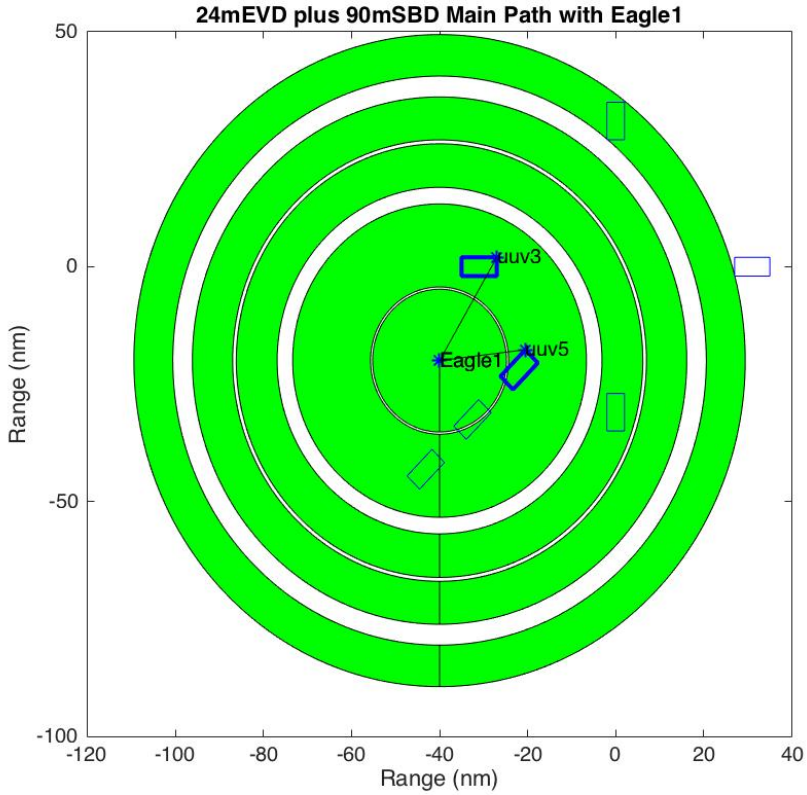


**Figure 162:** Final network topology with ranges of good communications for UUVs connected with relay Eagle1 in a 24m EVD plus 90m SBD.

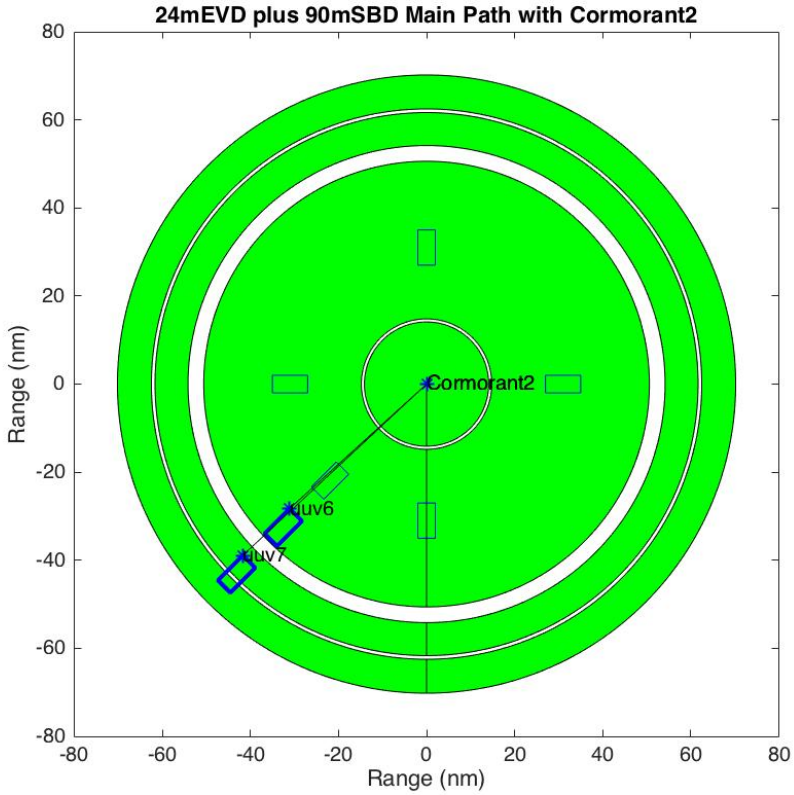


**Figure 163:** Final network topology with ranges of good communications for UUVs connected with relay Cormorant2 in a 24m EVD plus 90m SBD.

#### *7.5.2.5 90 m SBD Network Analysis*

The initial graph of the network under the 90 m SBD, given by the UUVs and the MS nodes, with the ranges of good communications shown, is given in Fig. 164. The corresponding graph showing the quality of the links, stability, and whether each link is in a stable (1) or unstable (2) state is shown in Fig. 165.

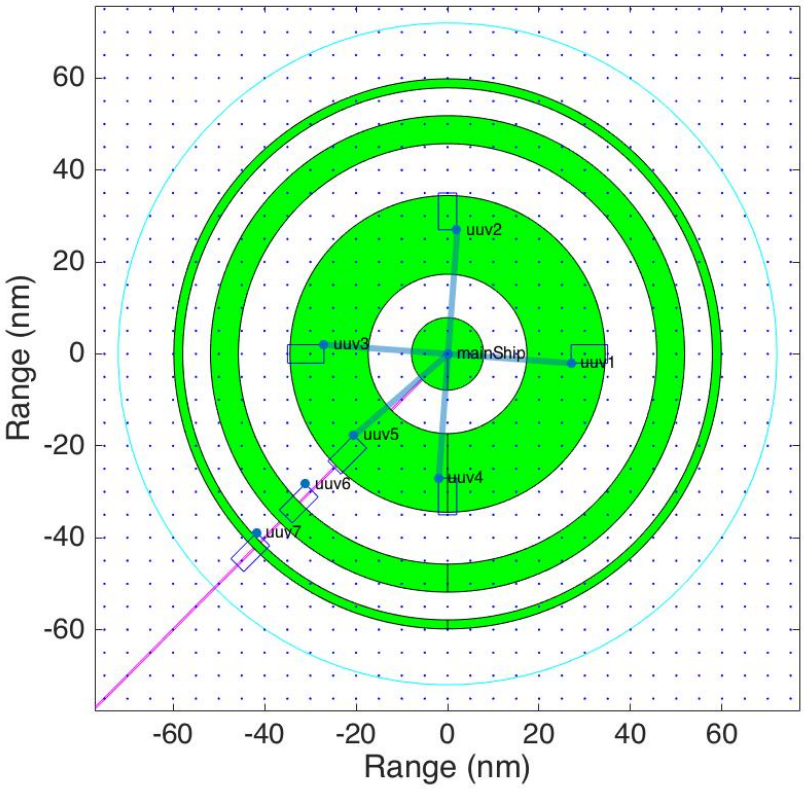


**Figure 164:** Initial graph $G_0$ under 90 m SBD with ranges of good communications between UUVs and MS.

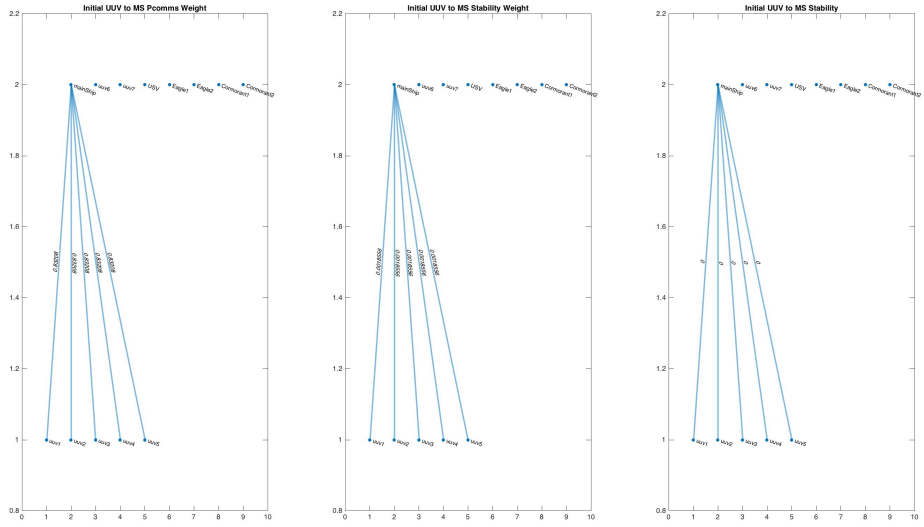


**Figure 165:** Initial graph $G_0$ under 90 m SBD with link quality weights (left), stability weights (middle), and stable states logical values (right).

As can be seen in each plot, only UUVs 1 to 5 are connected to the MS, however neither of the links are stable, as is shown in the stable states logical values of Fig. 165. Therefore, in order to meet our connectivity and stability constraints, we consider adding relays to the network, and look at possible network topologies that help meet our first connectivity criterion.

When we performed our search for the optimum network topologies that maximize the Fiedler value, only 6 solutions yielded the same maximum Fiedler value. Next we selected the best combination out of these 6 solutions that meet the stability, quality, and reliability criteria.

First, we compared the 6 possible solutions in terms of their stability. The network topology with the highest number of stable paths was the one that involved using USV as a relay UxV. The graph corresponding to this network topology, with stability, quality of link weights and logical representation of being in stable (1) or unstable (0) state are shown in Figs. 166, 167, 168. Table 25 shows the reliability of this network

topology and the main path that has the most stable paths and highest probability of communications.

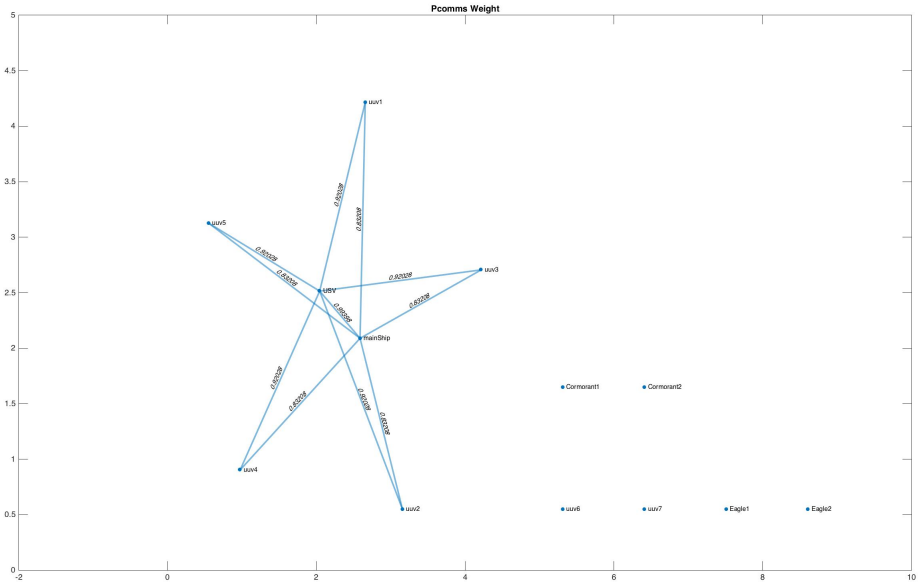


**Figure 166:** 90m SBD best network topology with quality weights.

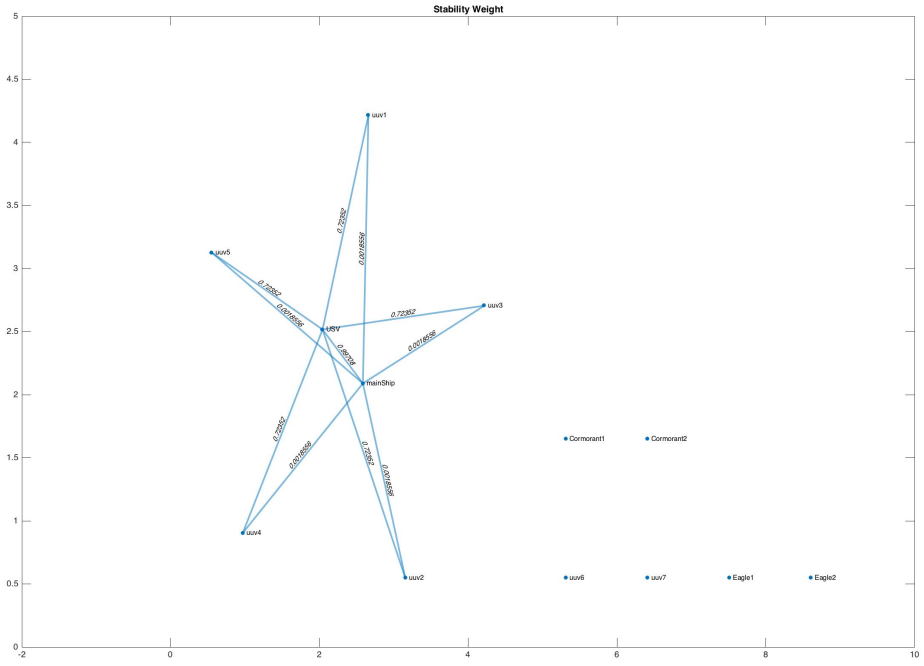


**Figure 167:** 90m SBD best network topology with stability weights.

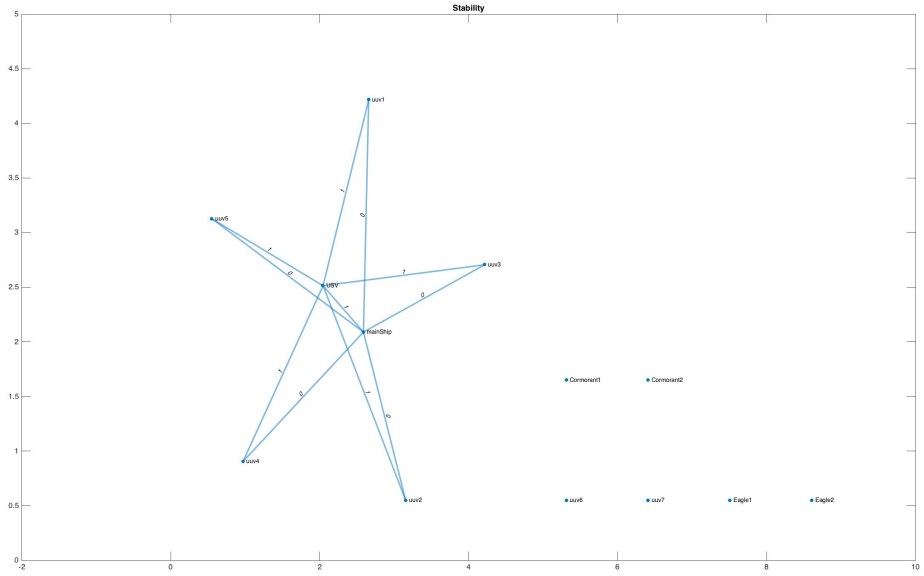


**Figure 168:** 90m SBD best network topology with stable state logical values.

**Table 25:** Network Topology Analysis for 90m SBD

| | **UUV1** | **UUV2** | **UUV3** | **UUV4** | **UUV5** | **UUV6** | **UUV7** |
|---|---|---|---|---|---|---|---|
| **Degree** | 1 | 1 | 1 | 1 | 1 | 0 | 0 |
| **Main Relay** | USV | USV | USV | USV | USV | | |

Only UUVs 1 to 5 are able to be connected to MS, while UUV6 and UUV7 are not connected. Note also that although UUVs 1 to 5 are connected, and stable, they are not reliable, since the path through the USV is the only path available. If the link fails, they have no other path available to communicate with the MS. Therefore, we conclude that for this 90 m SBD environment condition, connectivity and reliability cannot be met with the available set of assets. We will need to consider other options, such as increasing the gain of the transmission, adding more assets to the fleet, decreasing our thresholds of probability of communications such that links with lower probability of communications become acceptable, or allow the states of the transmission channels to be in the marginally stable state with the hope that some communication paths will become available. We can also vary the height of the relaying antennas and try to find a height that provides additional communication paths.

The approach we take here in order to meet the connectivity and reliability conditions is to add more assets to the fleet until we can meet all criteria. We add one UxV relay at a time until we can meet all requirements. When we add an Eagle UAV as a relay, we assume that the USV is within reach to be deployed from and land back on it. For each addd relay, we again look for the network topology that maximizes the Fiedler value. The UUVs that were already connected (UUV1 to UUV5) can only be increasing their reliability by the possible increase of their degree in the new network topologies. When we do this, on the second iteration we find a configuration where by adding an Eagle 2 vehicle deployed from a USV, both Eagle2 and the USV provide relay paths for UUV 6 and UUV7, which helps us meet our first connectivity criteria.

The graphs with link quality weights, stability weights, and stable logical values are shown in Figs. 169, 170, and 171, respectively.

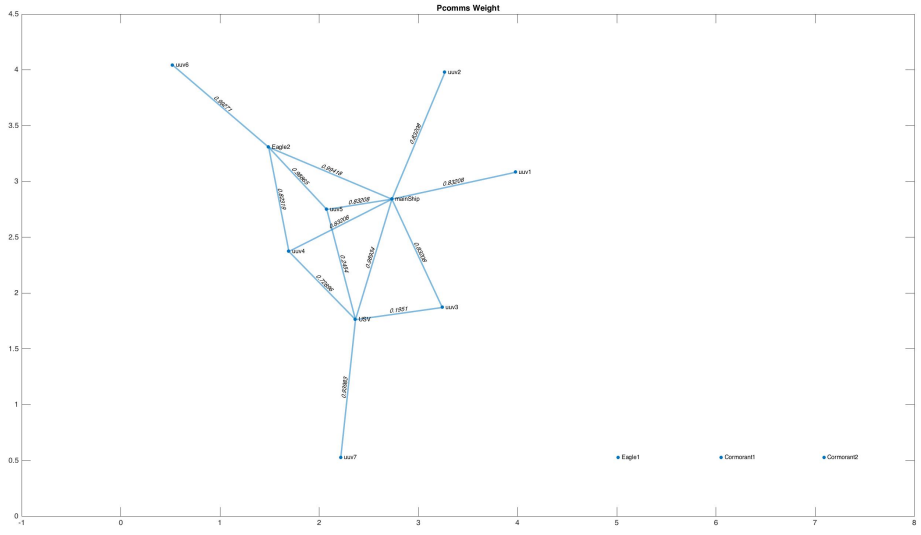


**Figure 169:** 90m SBD best network topology with link quality weights for the added assets.

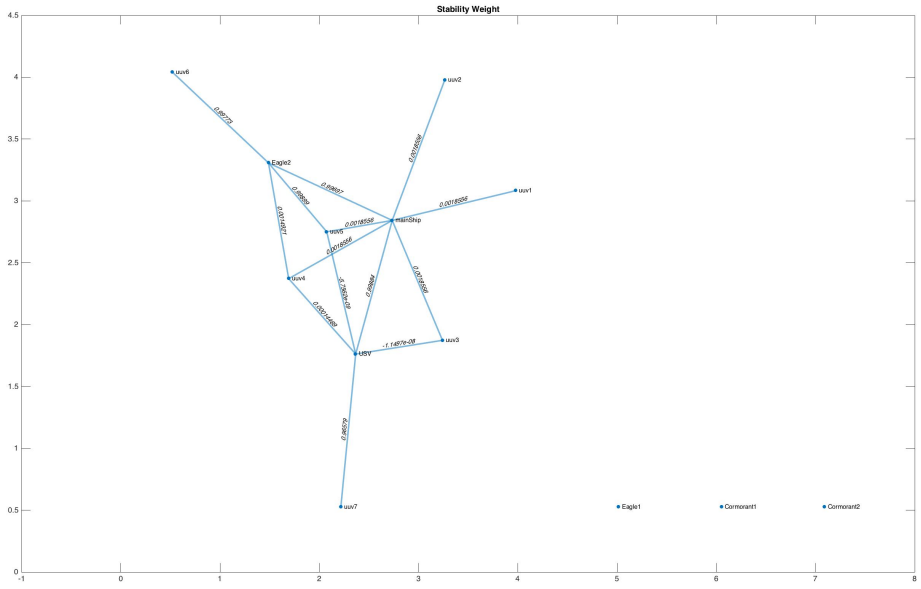


**Figure 170:** 90m SBD best network topology with stability weights for the added assets.

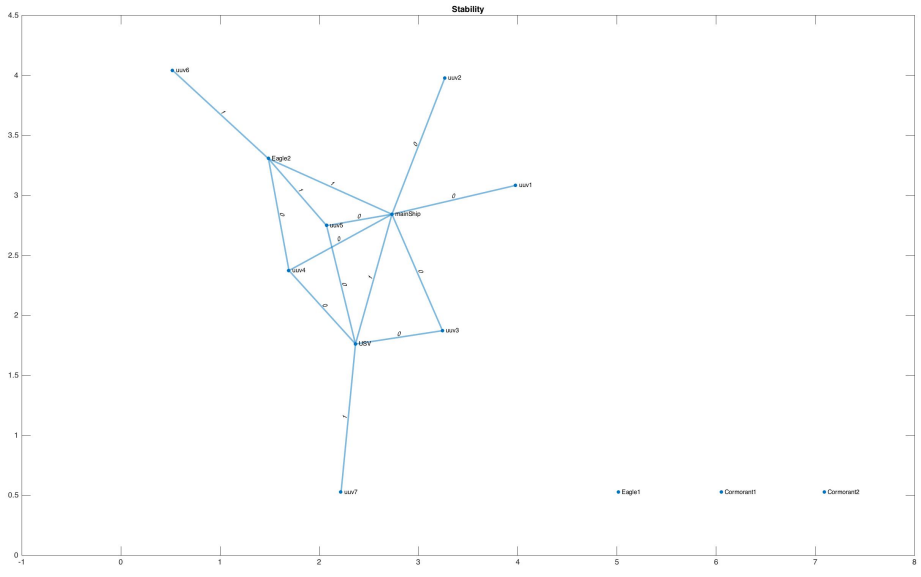


**Figure 171:** 90m SBD best network topology with stability logical values for the added assets.

**Table 26:** Network Topology Analysis for 90m SBD

| | **UUV1** | **UUV2** | **UUV3** | **UUV4** | **UUV5** | **UUV6** | **UUV7** |
|---|---|---|---|---|---|---|---|
| **Degree** | 1 | 1 | 1 | 1 | 2 | 1 | 1 |
| **Main Relay** | USV | USV | USV | USV | USV | Eagle2 | USV |

Note that the combination of graphs from the first iteration from using the USV as a relay and the second iteration from using the USV and Eagle2 as relays, allows us to meet the connectivity and stability conditions. However, we have not yet met our reliability conditions for all UUVs, only for UUV5, as is shown in Table 26. Therefore we will still need to consider other way to meeting this requirement. Further iterations show that reliability criteria can be met when another USV and an Eagle 1 are added to the fleet of assets. The final configuration of the network for this environmental condition using 2 USVs and one Eagle 2 as relays are shown in Figs. 172, 173, and 174, with respective ranges of good communications.

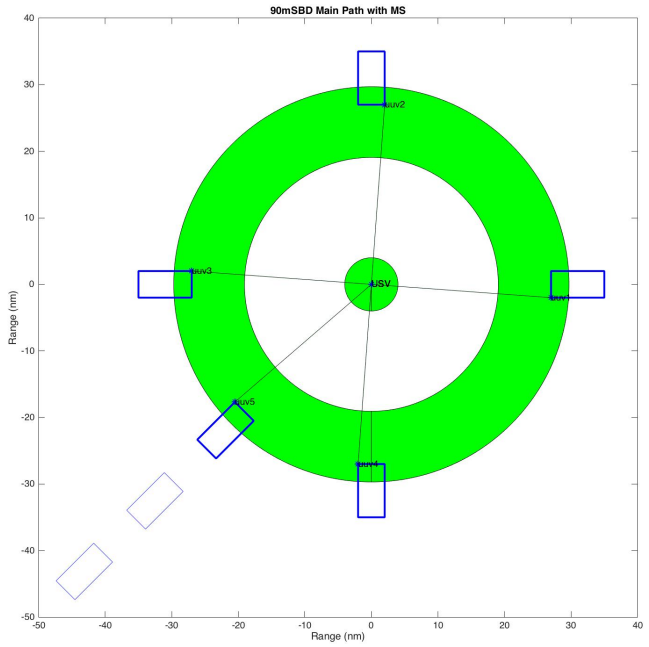


**Figure 172:** Final network topology with first USV used as relay under a 90m SBD.

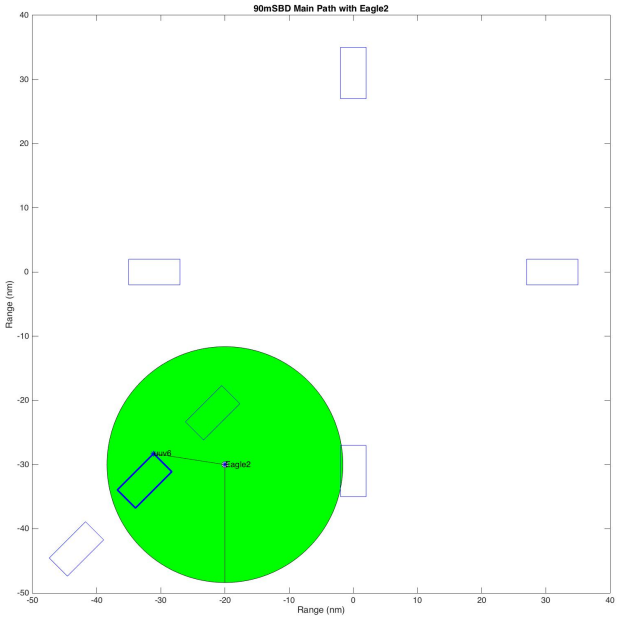


**Figure 173:** Final network topology with Eagle2 used as relay under a 90m SBD.

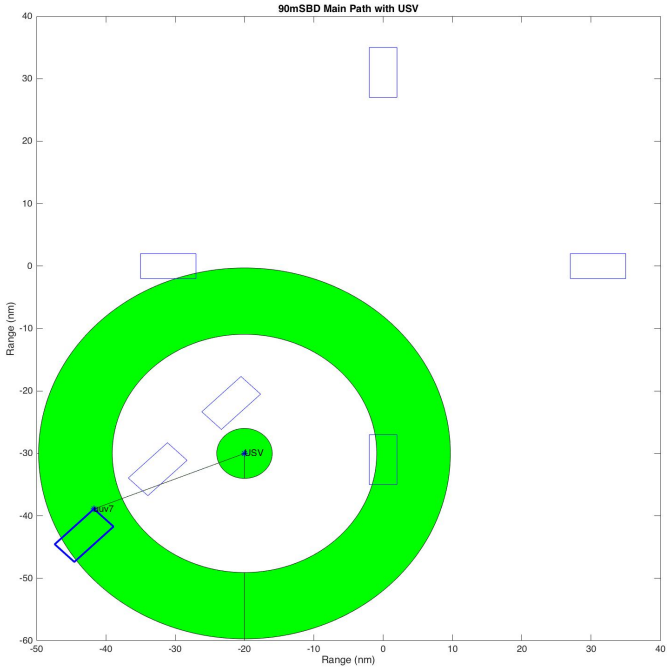


**Figure 174:** Final network topology with second USV used as relay under a 90m SBD.

#### *7.5.2.6 24 m EVD Network Analysis*

Finally, for the 24 m EVD, the initial graph composed of UUVs and the MS is shown in Fig. 175, with ranges of good communications between UUVs and the MS also depicted. It can be seen that the only range of good communication goes up to 20 nm in radius, and does not reach any of the UUVs. Therefore there is no connectivity, and we cannot meet any of our criteria.

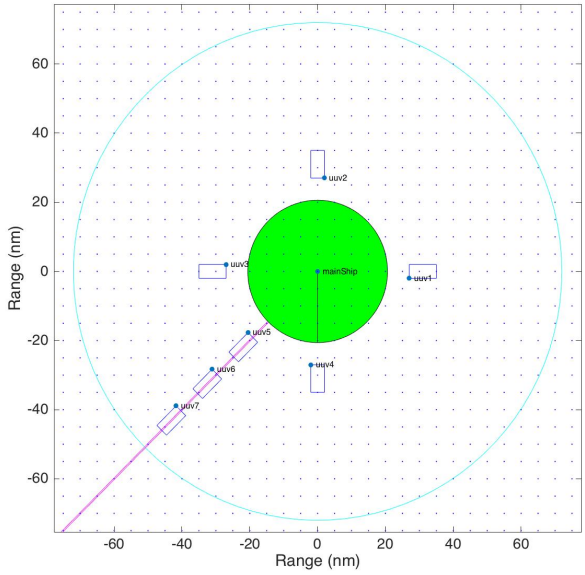


**Figure 175:** Initial graph $G_0$ under 24 m EVD with ranges of good communications between UUVs and MS.

Performed our search for the optimum network topologies that maximize the Fiedler value results in 41 solutions with the same maximum Fiedler value. Next we selected the best combination out of these 41 solutions that meet the stability, quality, and reliability criteria. The network topology that provided the most number of stable paths is shown in Figs. 176, 177, and 178, with channel quality weights, stability weights, and stable state logical values, respectively.

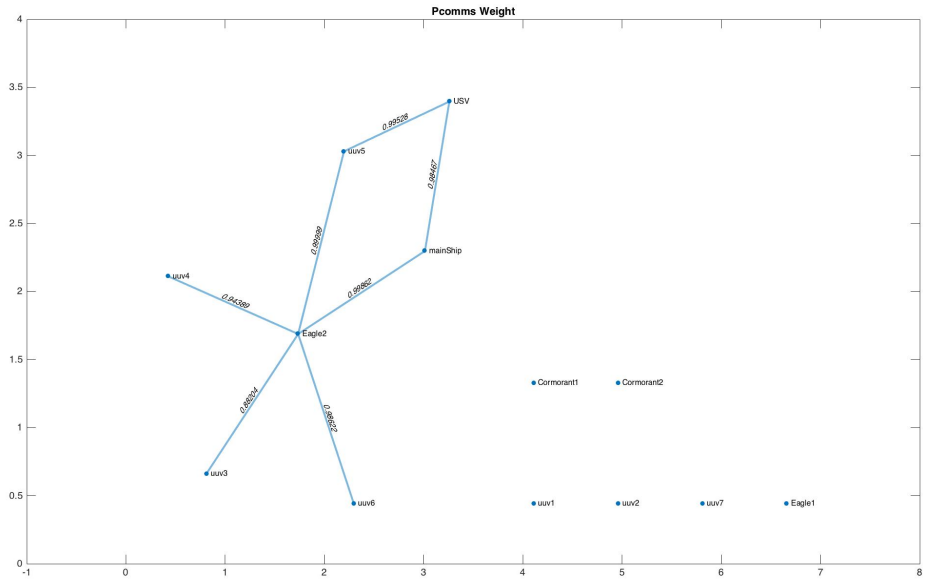


**Figure 176:** 24m EVD best network topology with quality weights.

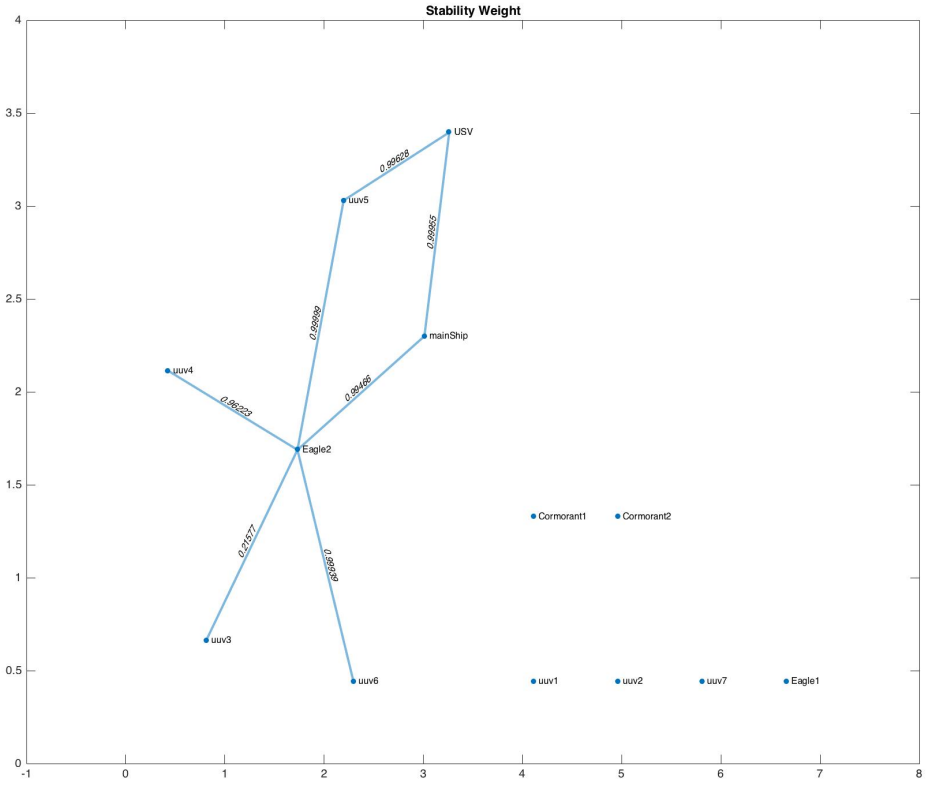


**Figure 177:** 24m EVD best network topology with stability weights.

**Table 27:** Network Topology Analysis for 24m EVD

| | UUV1 | UUV2 | UUV3 | UUV4 | UUV5 | UUV6 | UUV7 |
|---|---|---|---|---|---|---|---|
| **Degree** | 0 | 0 | 0 | 2 | 1 | 1 | 0 |
| **Main Relay** | | | | Eagle2 | Eagle2 | Eagle2 | |

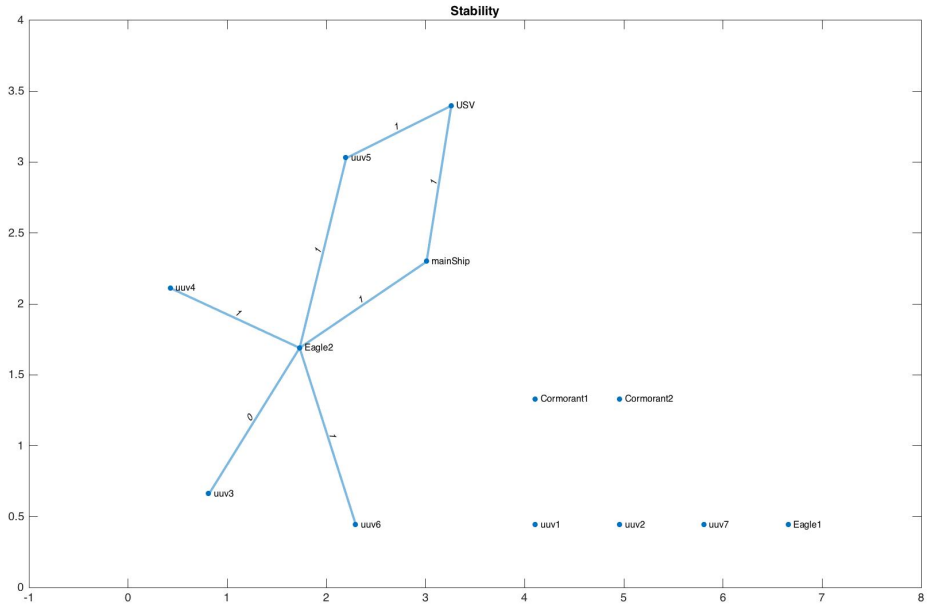


**Figure 178:** 24m EVD best network topology with stable state logical values.

As can be seen from the graphs, only UUV4, UUV5, and UUV6 are connected through the Eagle2 relay, and each path is stable. However, we cannot meet the reliability criteria for any UUV, as is shown in Table 27 for this first iteration.

In order to meet the connectivity and stability requirements, for this environmental condition we needed to run 4 more instances and therefore add 4 more relay to our fleet of assets. The graphs corresponding to each of these 4 instances are not shown here for sake of space, but the relay information of the connected and stable final network is shown in Table 28 and depicted in Figs. 179, 180, 181, 182, 183.

**Table 28:** Network Topology Analysis for 24m EVD

| | UUV1 | UUV2 | UUV3 | UUV4 | UUV5 | UUV6 | UUV7 |
|---|---|---|---|---|---|---|---|
| **Degree** | 1 | 1 | 1 | 1 | 4 | 4 | 1 |
| **Main Relay** | USV | USV | Eagle2 | Eagle2 | Eagle2 | Eagle2 | Eagle1 |

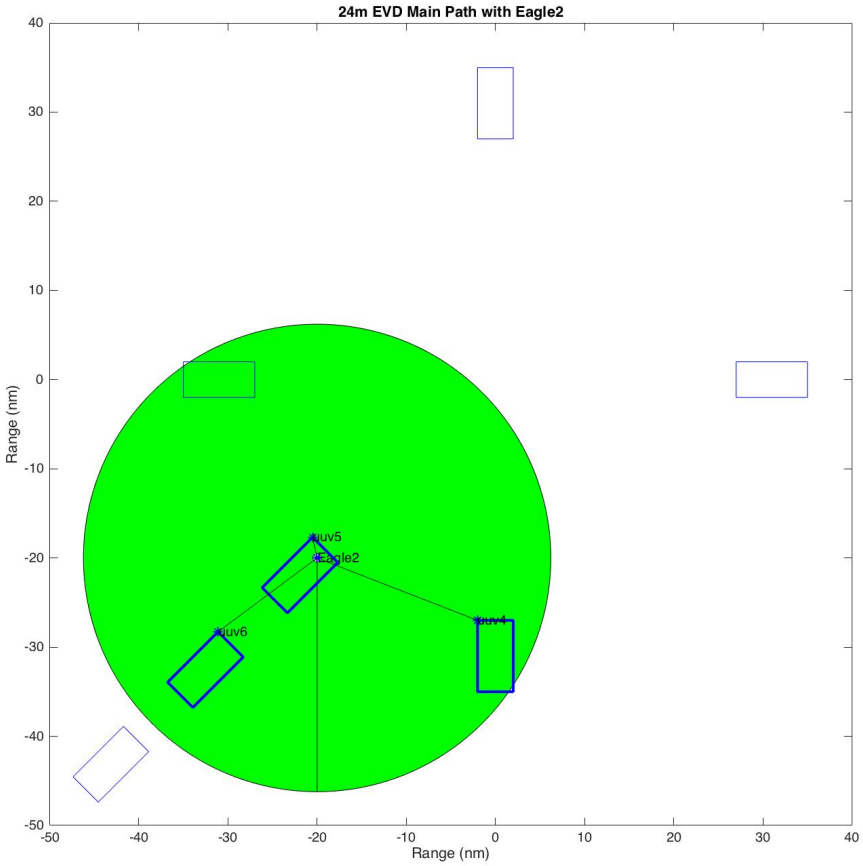


**Figure 179:** Final network topology with Eagle2 used as relay under a 24m EVD.

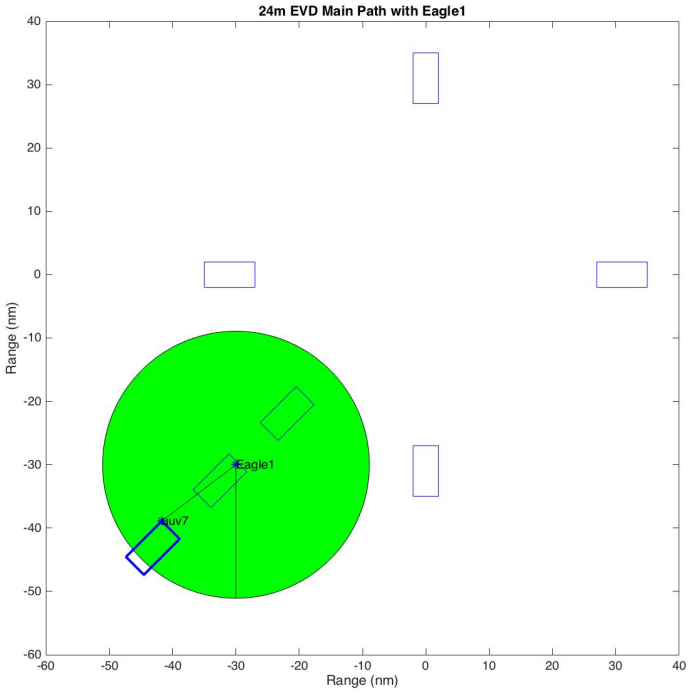


**Figure 180:** Final network topology with Eagle1 used as relay under a 24m EVD.

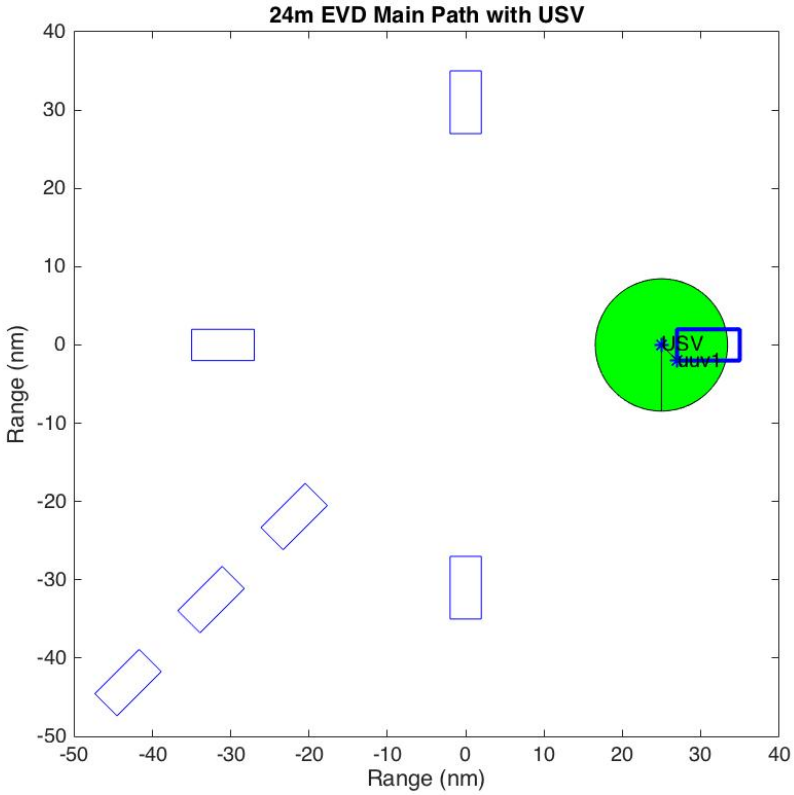


**Figure 181:** Final network topology with a USV used as relay under a 24m EVD.

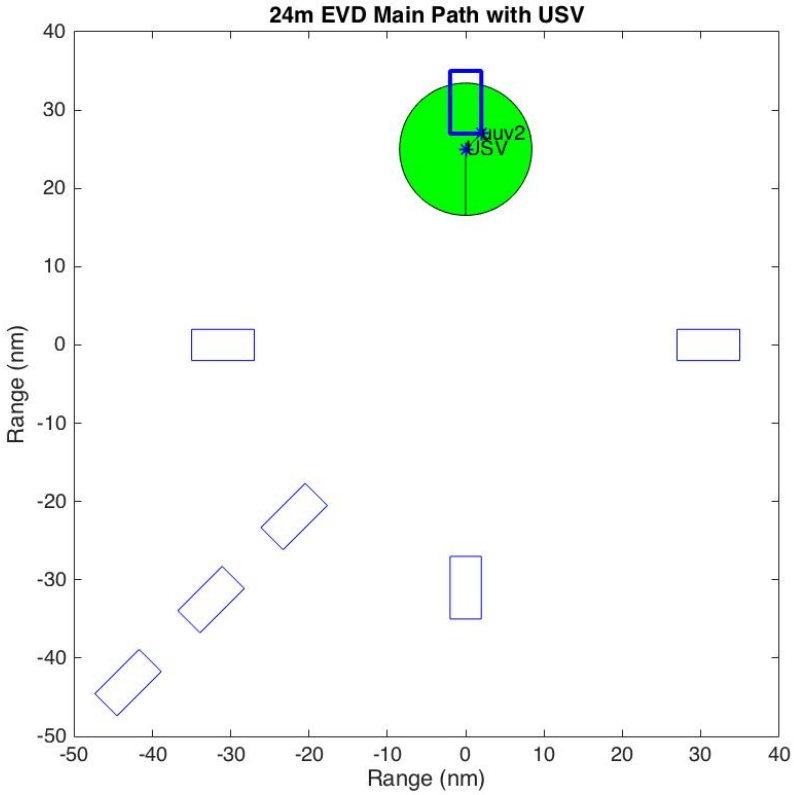


**Figure 182:** Final network topology with a second USV used as relay under a 24m EVD.

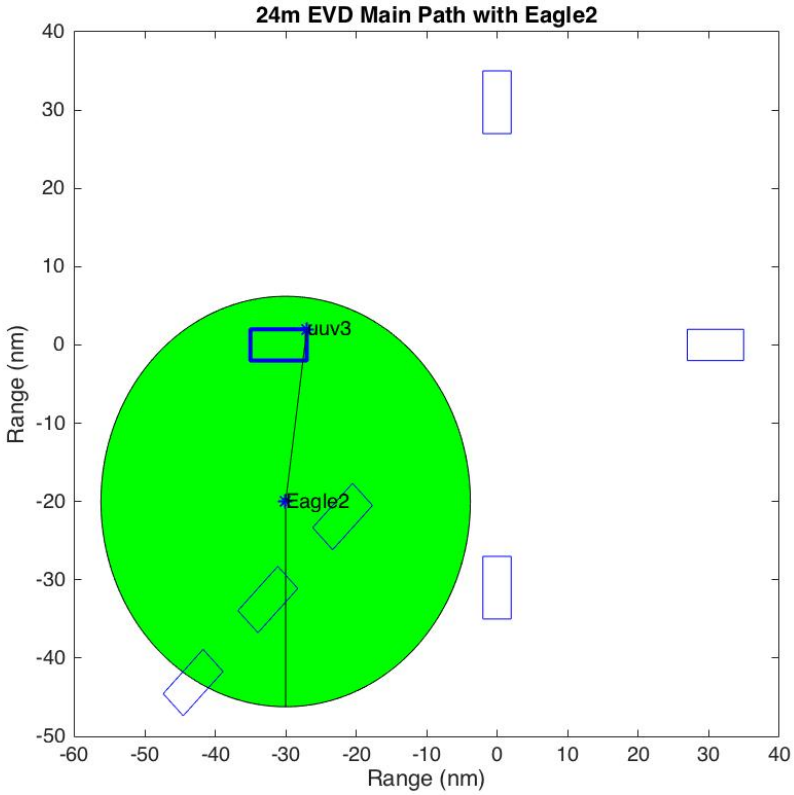


**Figure 183:** Final network topology with a second Eagle2 used as relay under a 24m EVD.

So far we have met the connectivity, the quality of the communications, and the stability requirements. We have yet to make the network topology reliable. In order to do so, 5 more iterations had to be done by adding 3 more USVs, an Eagle 2 and one Eagle1 relay.

## *7.6 Experiment 1 Results and Hypothesis Validation*

Research question RQ1 and corresponding hypothesis HP1 posed in the Proposed Methodology are repeated here for quick reference:

**Research Question 1 (RQ1)**: *What communication network topology is reliable*

*to communication link failures based on asset availability, which has the best network quality and is stable due to vehicle relative motions?*

**Hypothesis 1 (HP1)**: *A network topology that takes into account acceptable probability of communications, require the time-varying fading amplitude of the signal to be within certain thresholds, and which requires each asset to have spatial redundancy, will result in a reliable communications network.*

In the Network Analysis Section of the Mine Survey mission case study, we made assumptions about our graphs, and went further to define connectivity, stability, and reliability of the network. We broke down a set of criterions that were analyzed in order to come up with the best network topology that met all of our requirements. We first checked for connectivity through the use of the Fiedler value, and found that there can be multiple graph topologies that meet this condition. Our next criterion was to make sure the links in the graph were stable. We showed that a signal can be regarded as in good quality in terms of probability of communications, but may be unstable in terms of the relative motions with other vehicles. Stability criterion was based on discretizing the states of the transmission channels into good and bad states, and defining stability in terms of the transitions probability of transitioning from any state to the bad state. Given that neighboring state transition probabilities are higher, we defined the marginally stable state to be a bad state, and we disregarded network topologies which where in unstable or marginally stable states. The states were defined in the FSMC model in terms of the time-varying fading amplitudes of the signal near the APM large scale fading mean value $\Omega$, and we computed this state transition probabilities at each range for each APM propagation loss value. Our final criterion was to make sure the network is reliable to possible link failures. We

showed that this condition is harder to meet with limited number of assets for certain environmental conditions, and therefore we proposed keep adding assets to the fleet until we were able to meet this criterion. With this, we can say that we validated our first hypothesis HP1.

## *7.7 Bayesian Framework*

The next phase in the COA Analysis step is to model the progression of state estimation and sensor measurements to come up with optimal path navigation that maximizes the quality and quantity of information. In this phase of the methodology, shown in Fig. 184, we model the quality and quantity of information using the Bayesian framework. Focus is drawn to examining the problem of COA design and scheduling for mobile UxVs carrying sensors while performing required sensing tasks. Active sensing [126] [91] [49] refers to the control of sensor parameters, such as position and orientation, in order to obtain information and reduce uncertainty. Planning for search and exploration COAs depends on the sensor being used and the quantity of information that is being captured, such as target detection or identification. The methods for representing and updating the estimate and associated uncertainty, the belief state, and a way of using the belief state to determine expected information analyzed in the *Probabilistic Robotics* chapter are used here to find optimal sweep distances for each UUV that maximizes information gain rate.

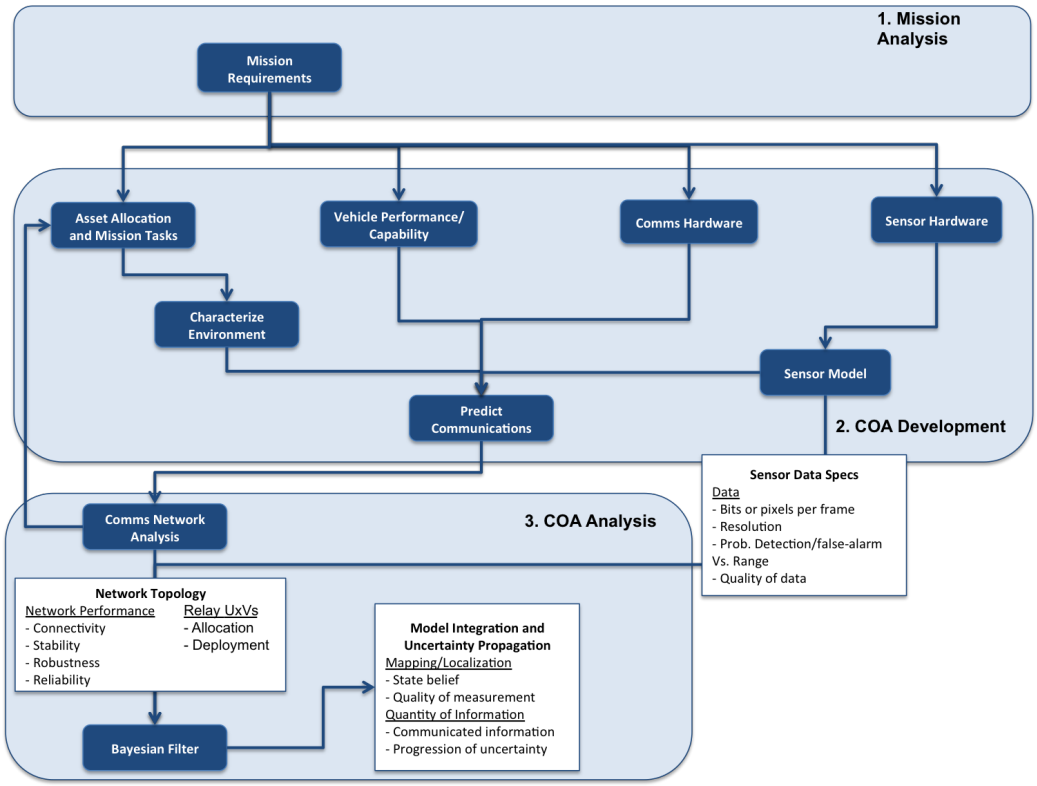


**Figure 184:** Bayes filter modeling of information phase in COA Analysis step.

## *7.8 Information Gain Optimization*

With the Bayesian framework used as a way to quantify quality and quantity of information, we wan to meet the last mission requirement of our demonstration case study. The requirement is to provide path navigation that maximize the amount of information sent back to the MS through the use of both acoustic and RF communications. We have demonstrated in the previous section that $IGR$ can be optimized over the sweep distance between each sweep measurement. We showed that by taking into account ranges of good communications, predicted with the methods described in this thesis, we can maximize the $IGR$ by surfacing at points with good RF communications. As the next phase of the COA Analysis step, shown in Fig. 185, we apply the same optimization procedure to our case study, but with our mission requirements, radio specifications, and environmental conditions.

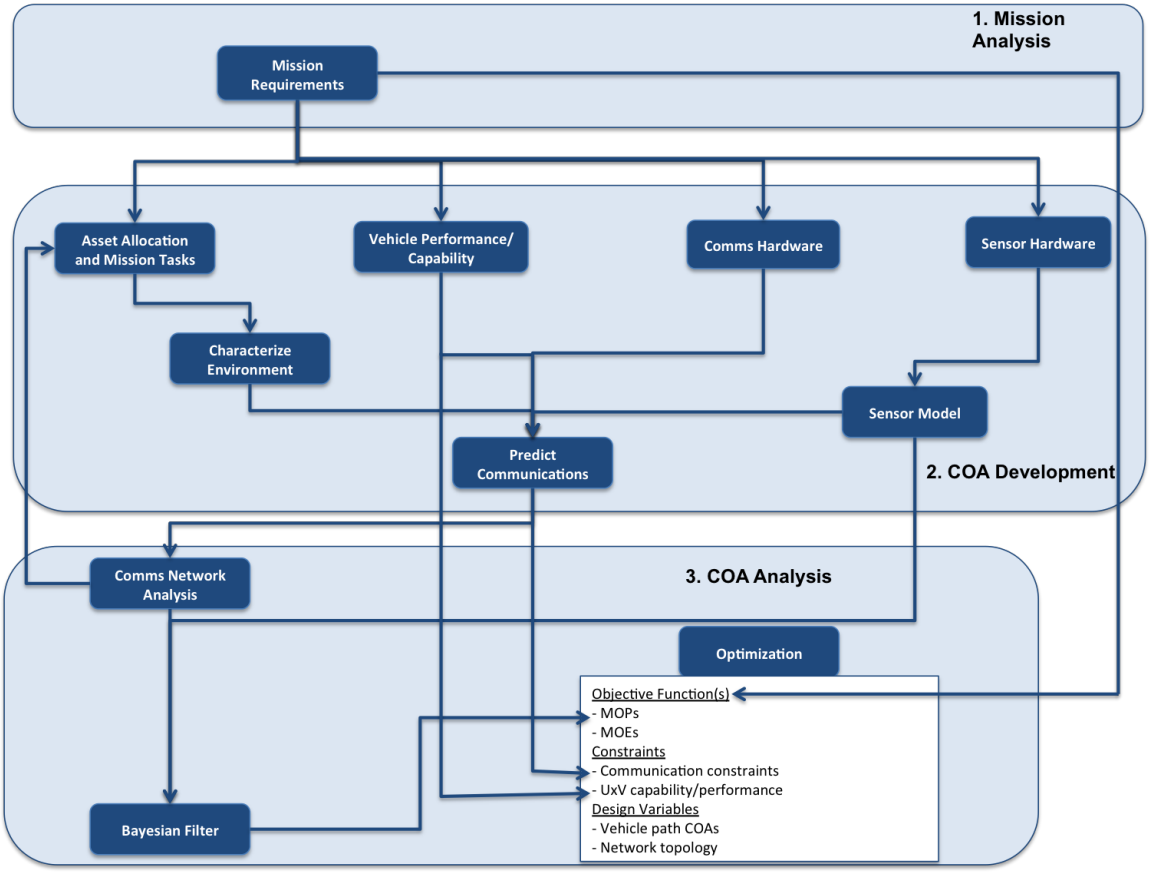


**Figure 185:** Path-planning optimization phase of COA Analysis step.

### 7.8.1 Problem Definition

We again consider the case where 60% of each TA needs to be surveyed by its assigned UUV. Each UUV will perform the same object detection procedure for the TA assigned, as was described in the previous study and depicted in Fig. 84. The UUVs have the option of communicating information back to the MS using acoustic communications, or surface and communicate by RF. Now however, we have defined a communication network during the *Network Topology Analysis* phase, that we showed it connects every UUV to the MS, and which is stable and reliable, for each environmental condition. In these network topologies, UUVs do not necessarily communicate the information to MS by a direct link, but may have to relay communications through another UxV. We use the quality of each link in the network to

find the best communications path between each UUV and the MS. Therefore, this path will be used instead in the search of optimum sweep distances for each UUV that maximize the $IGR$.

### 7.8.2 Optimization Results and Discussion

The results obtained from all the target areas optimization for each of the three environmental conditions are shown next.

#### *7.8.2.1 24 m EVD plus 90m SBD Optimization Results*

For the 24 m EVD plus 90 m SBD environmental condition, we showed that the network topology that provided the most stable, reliable, and robust communications was given in Figs. 161, 162, and 163. Therefore, using the main paths in the optimization method to maximize $IGR$, we get the the following surface points and sweep distance locations for each sweep for each UUV, shown in Figs. 186, 187, and 188.

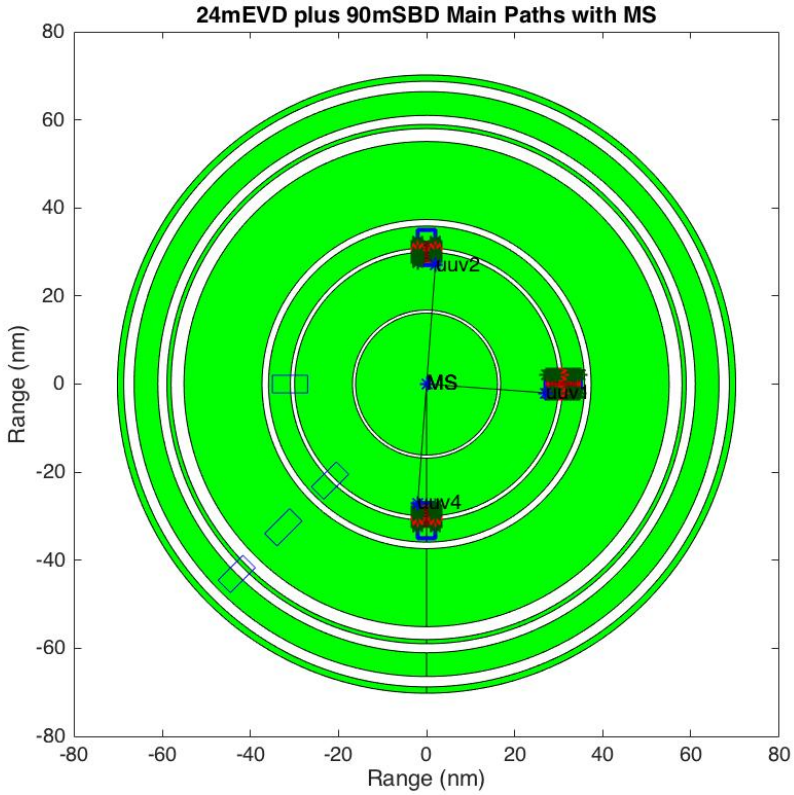


**Figure 186:** Optimal sweep distances and surface points for UUVs 1, 2, and 4 under 24 m EVD plus 90 m SBD.

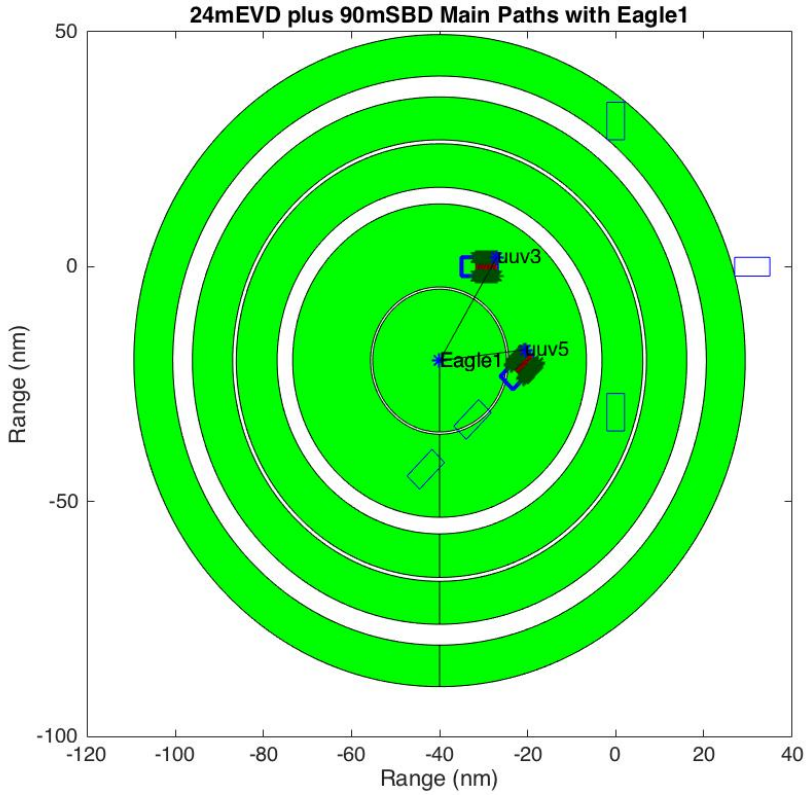


**Figure 187:** Optimal sweep distances and surface points for UUVs 3, and 5 under 24 m EVD plus 90 m SBD.

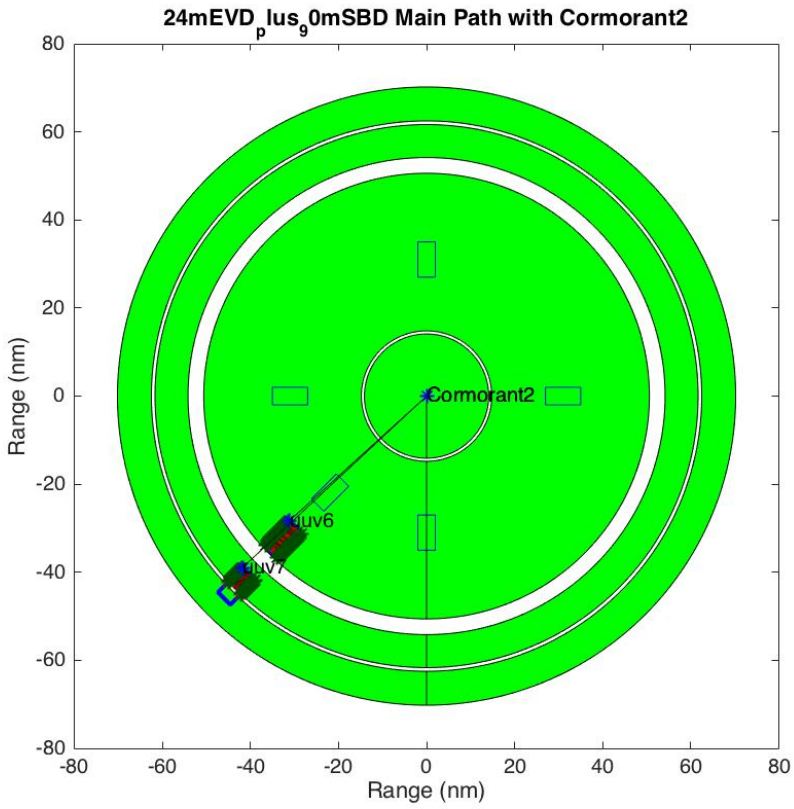


**Figure 188:** Optimal sweep distances and surface points for UUVs 6 and 7 under 24 m EVD plus 90 m SBD.

Note that for each UUV, the optimal surface points are those that lie within good communication ranges that are closer to the MS or relay location, which provide the most $IGR$ by surfacing as soon as it is possible to communicate using RF communications instead of underwater acoustic. Note that although the main paths between UUV3, UUV5, and UUV6 are in good communication ranges with the MS, they are not as stable and as reliable as the suggested paths using relays Eagle 1 and Cormorant 2. This is another benefit of this methodology, that it is able to determine main paths of communication that provide the most stable and reliable, even though other main paths may seem more convenient or trivial.

Next we compare our optimal results with the following cases: 1) evenly-spaced

sweeps with only acoustic communications with MS, 2) evenly-spaced sweeps with both acoustic and RF communications with MS. In case 2, the UUV takes advantage of the prediction of good communication ranges to determine if it can surface to communicate via RF. In each of these two cases, the Link 1 is used, if available, to communicate the sensor data straight to the MS. Shown in Fig. 189 is the plot corresponding to case 2 for this environmental condition.

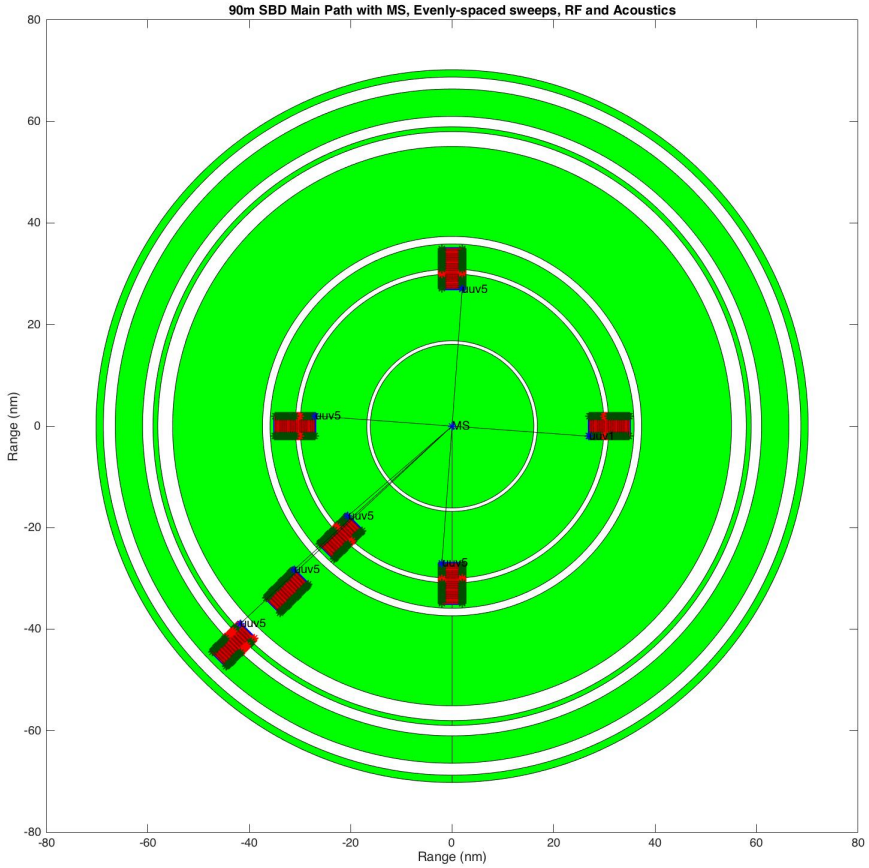


**Figure 189:** Evenly-spaced sweeps case 2 for 24m EVD plus 90m SBD.

The $IGR$ as a function of time was calculated for each of these two cases, and were plotted with our optimal solution for comparison in Fig. 190.

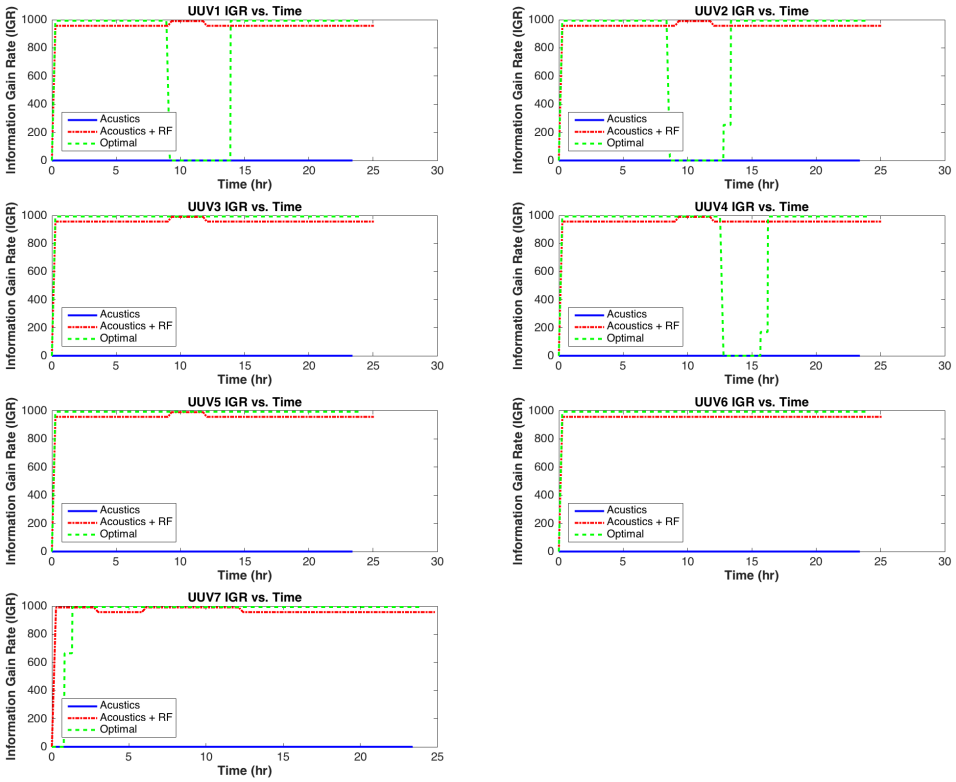


**Figure 190:** IGR vs. time for each case and our optimal solution for 24m EVD plus 90m SBD.

As can bee seen in this plot, the $IGR$ for case 2 tends to be slightly lower than the optimal value when the surface points are used to communicate sensor data. This is due to sweeps being separated over longer distance in the evenly-spaced configuration, which means that the same information gain is communicated over a longer period of time due to moving from one sweep to the next. There are times, specifically for UUVs 1, 2, and 4 which use a relay to communicate with MS, when case 2 has higher $IGR$ than the optimal, and this is due to our optimal solution being based on choosing the relay that provides robustness, stability and reliability. Although the link straight to the MS leads to higher $IGR$, it does not meet the other criteria and constraints we posed for stability and reliability. Case 1 $IGR$ is much lower than

case 2 and the optimal since it communicates sensor information only by acoustic communications. The $IGR$ for case 1 stays constant at a very low value throughout the mission (it is not zero).

#### *7.8.2.2 90m SBD Optimization Results*

For the 90 m SBD environmental condition, we showed that the network topology that provided the most stable, reliable, and robust communication network was given in Figs. 172, 173, and 174. Using these main paths in the optimization method to maximize $IGR$ we get the the following surface points and sweep distance locations for each sweep for each UUV, shown in Figs. 191, 192, and 193.

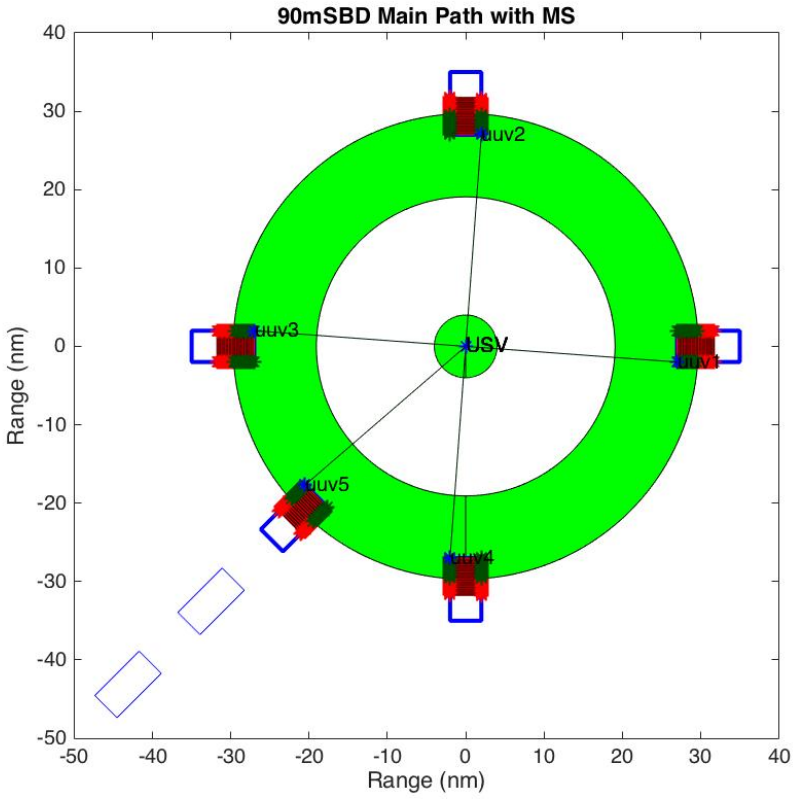


**Figure 191:** Optimal sweep distances and surface points for UUVs 1, 2, 3, 4 and 5 under 90 m SBD.

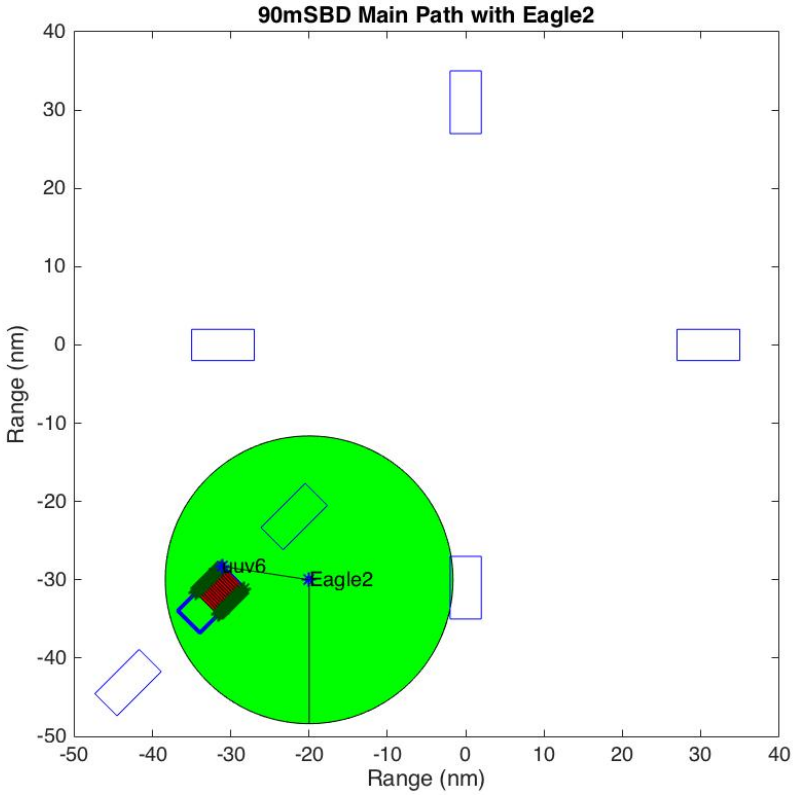


**Figure 192:** Optimal sweep distances and surface points for UUV 6 under 90 m SBD.

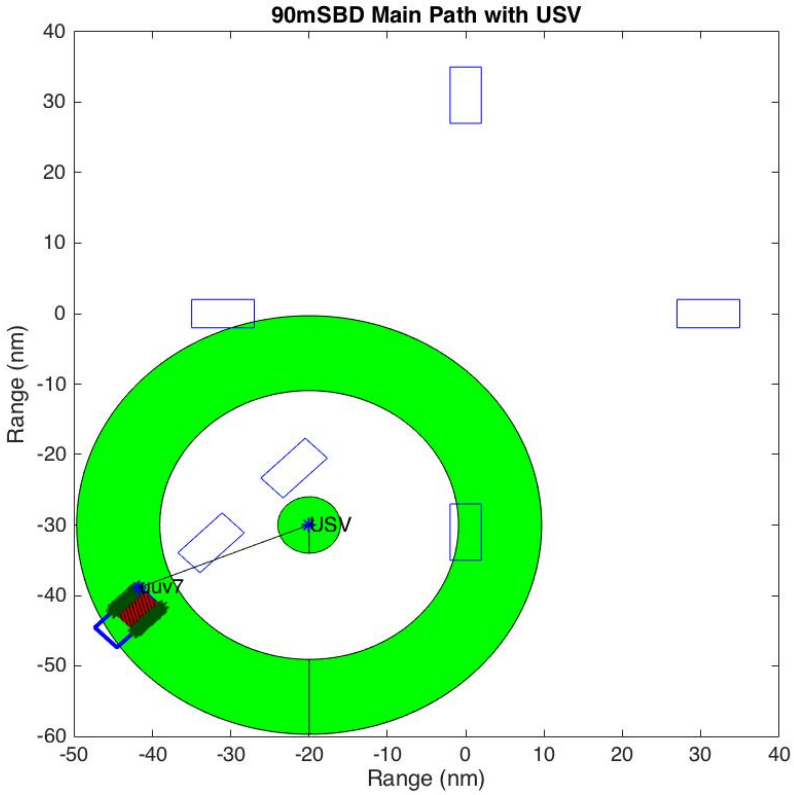


**Figure 193:** Optimal sweep distances and surface points for UUV 7 under 90 m SBD.

Note that for this environmental condition, UUVs 1 to 5 have surface points outside of the ranges of good communications, which is due to the non-overlapping sweep constraint. Since the number of sweeps that can fit within the ranges of good communications was at its maximum, the rest of the sweeps needed to be done by sending the rest of the information by acoustic communications.

Next we compare our optimal solution to the same two cases (evenly-spaced sweeps with acoustics communications only, and with RF communications at ranges of good communications) as in the previous environmental condition. Shown in Fig. 194 is the plot of case 2 for this environmental condition. Again, the UUV takes advantage of the ranges of good communications to surface and communicate via RF to the MS.

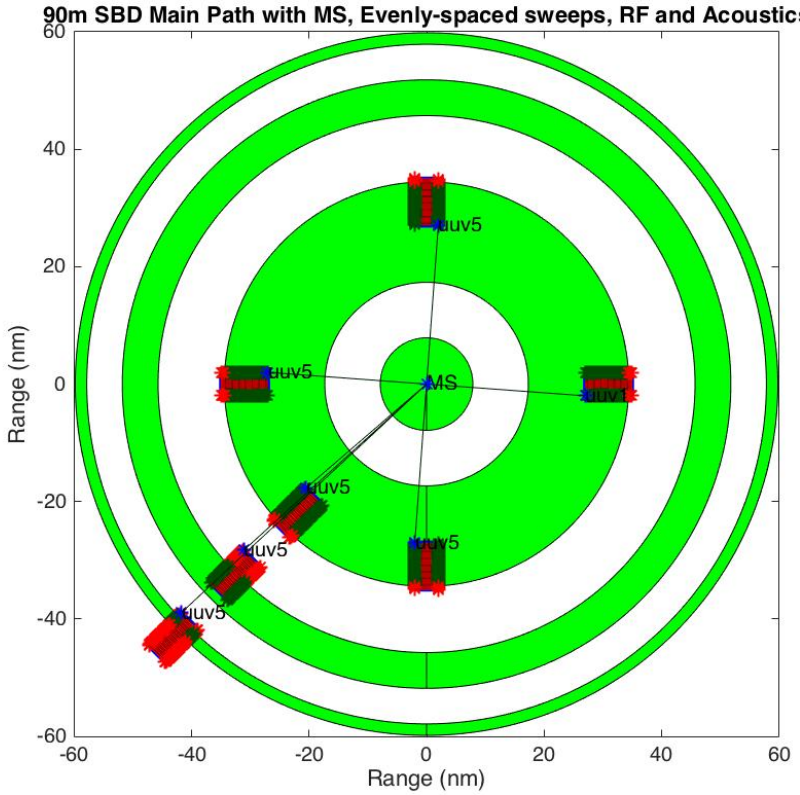


**Figure 194:** Evenly-spaced sweeps case 2 for 90m SBD.

The $IGR$ as a function of time was calculated for each of these two cases, and were plotted with our optimal solution for comparison in Fig. 195.

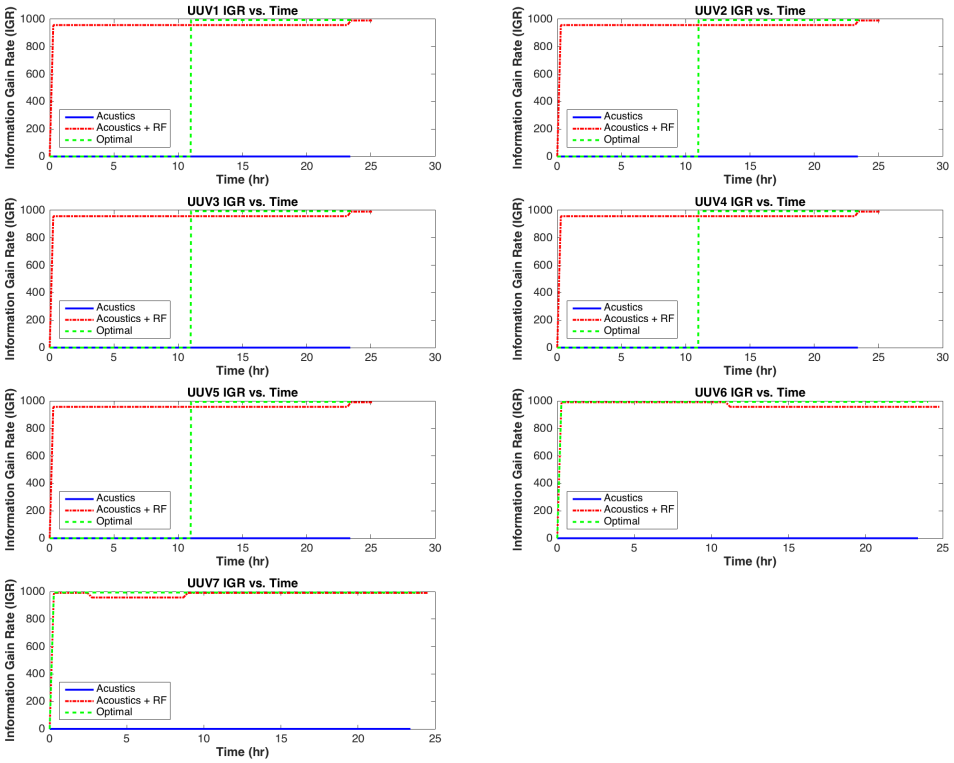


**Figure 195:** IGR vs. time for each case and our optimal solution for 90m SBD.

From these plots, it can be seen that, again, case 2 provides higher $IGR$ than the optimal for some times, but when surface points become available, the optimal solution provides higher $IGR$. As explained earlier, case 2 may provide higher $IGR$, but the link straight to the MS used is not reliable or stable. Therefore, the mission planner has the option of giving up reliability and stability of the network for higher information gain rates provided by case 2. Case 1 again provides the least $IGR$ throughout the whole mission since it only communicates via acoustics communications.

#### *7.8.2.3 24m EVD Optimization Results*

For the 24 m EVD environmental condition, we showed that the network topology that provided the most stable, reliable, and robust communication network was given in Figs. 179, 180, 181, 182, 183. Using these main paths in the optimization method to maximize $IGR$ we get the the following surface points and sweep distance locations for each sweep for each UUV, shown in Figs. 196, 197, 198, 199, 200.

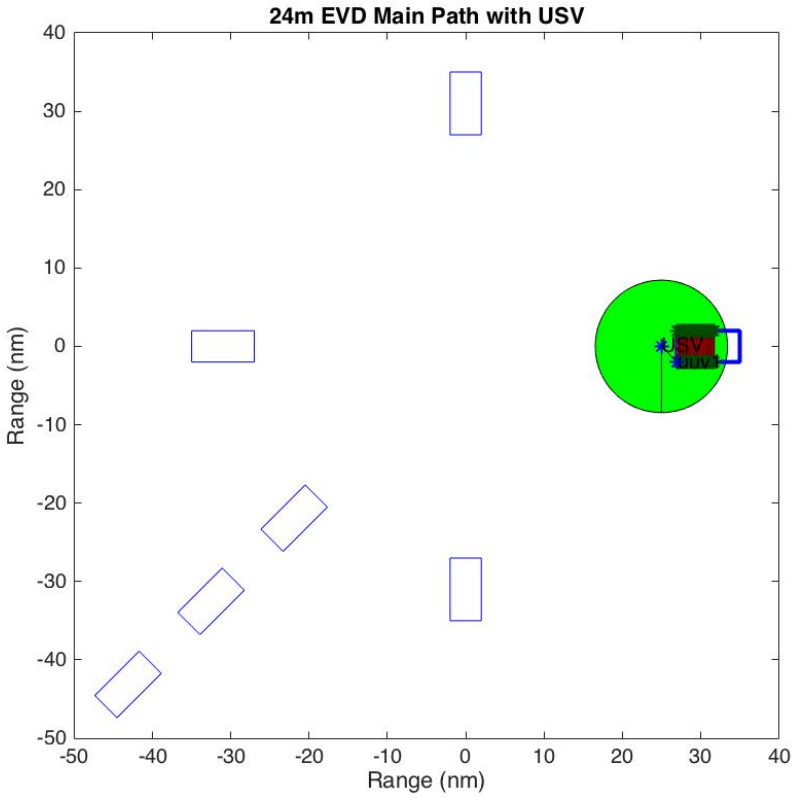


**Figure 196:** Optimal sweep distances and surface points for UUV 1 under 24 m EVD.

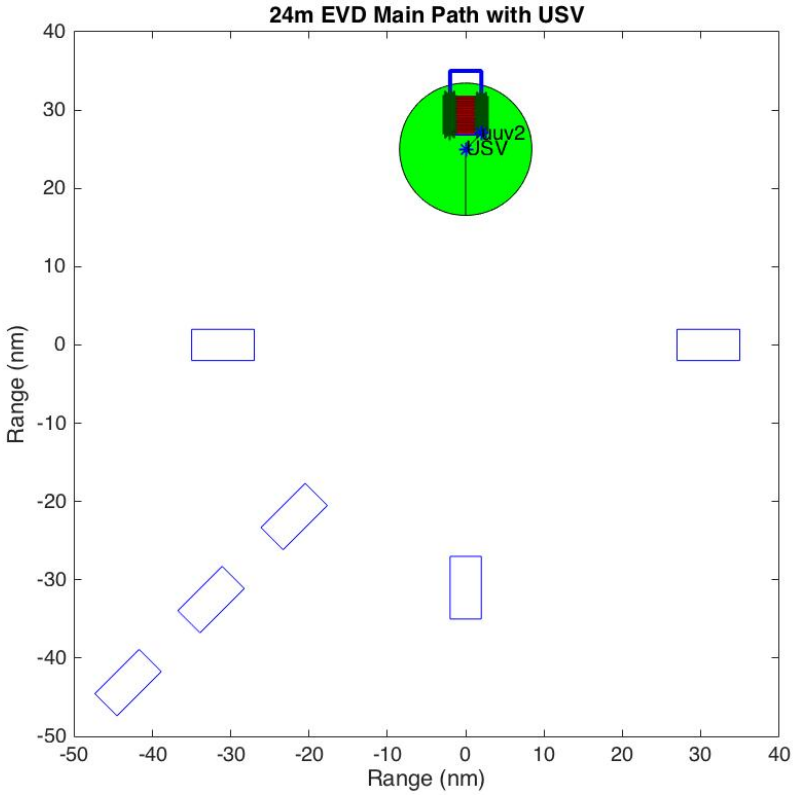


**Figure 197:** Optimal sweep distances and surface points for UUV 2 under 24 m EVD.

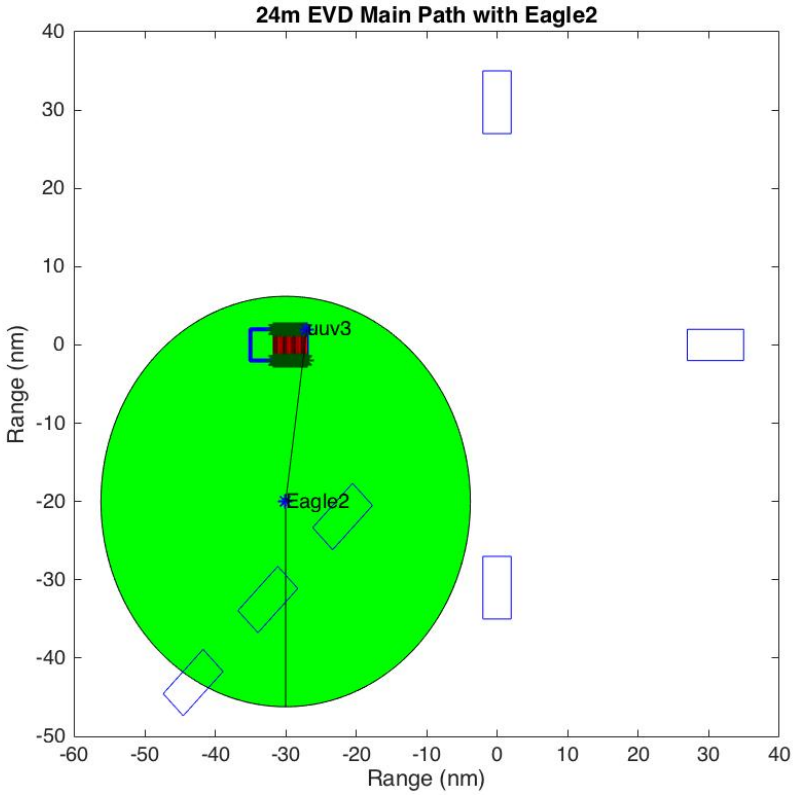


**Figure 198:** Optimal sweep distances and surface points for UUV 3 under 24 m EVD.

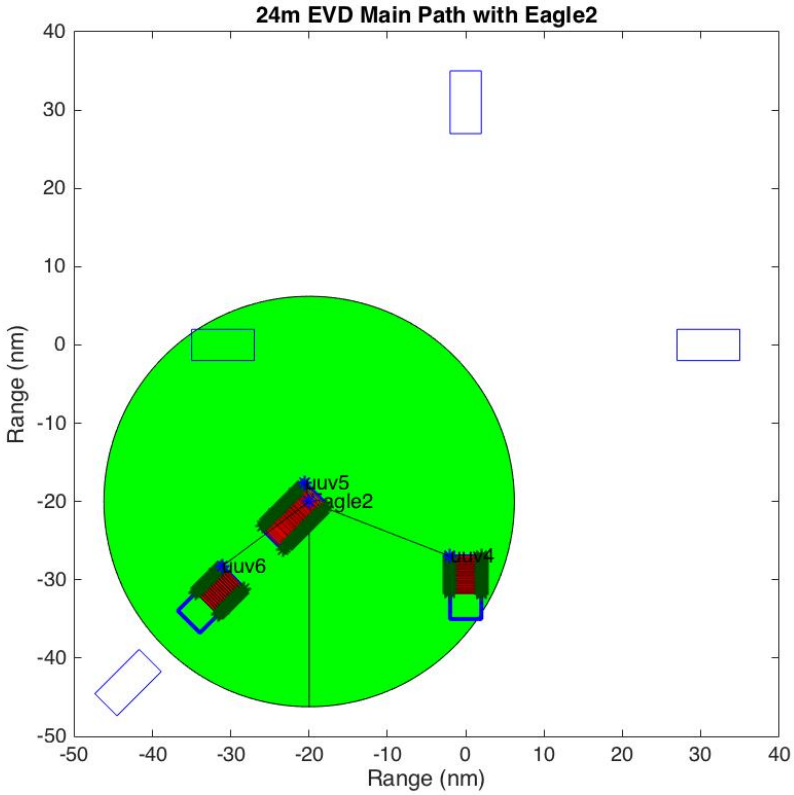


**Figure 199:** Optimal sweep distances and surface points for UUV 4, 5, and 6 under 24 m EVD.

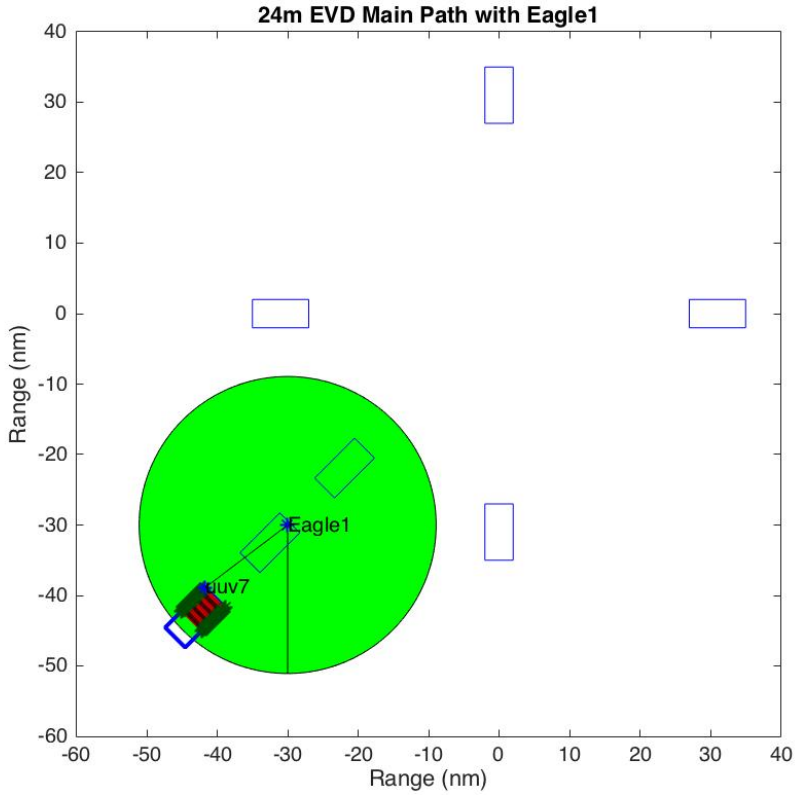


**Figure 200:** Optimal sweep distances and surface points for UUV 7 under 24 m EVD.

Note that since this is the worse environmental condition studied here, due to the signals experiencing much greater large-scale fading due to the greater multipath created by lowering the duct height, the ranges of good communication for each relay are smaller. They are big enough however to provide communication solutions that helps us maximize $IGR$ with links that are stable and robust to small scale fading mechanisms and vehicle motions.

Next we compare our optimal solution to the same two cases (evenly-spaced sweeps with acoustics communications only, and with RF communications at ranges of good communications) as in the previous two environmental conditions. Shown in Fig. 201 is the plot of case 2 for this environmental condition. In this case, neither of the

UUVs is within good range of communication, and therefore it can only communicate via acoustic communications. Therefore, case 2 is equivalent to case 1.

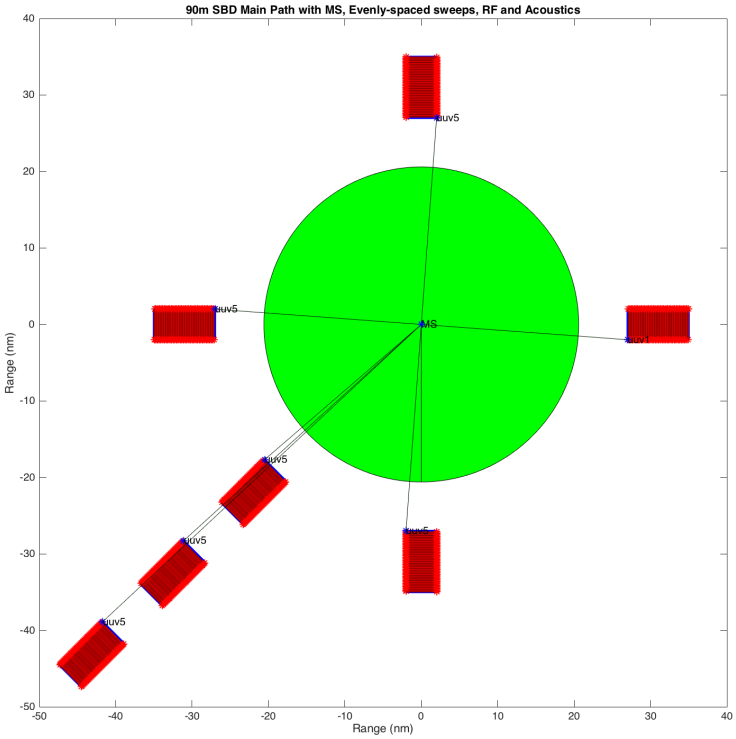


**Figure 201:** Evenly-spaced sweeps case 2 for 24m EVD.

The $IGR$ as a function of time was calculated for the two cases, and were plotted with our optimal solution for comparison in Fig. 202.

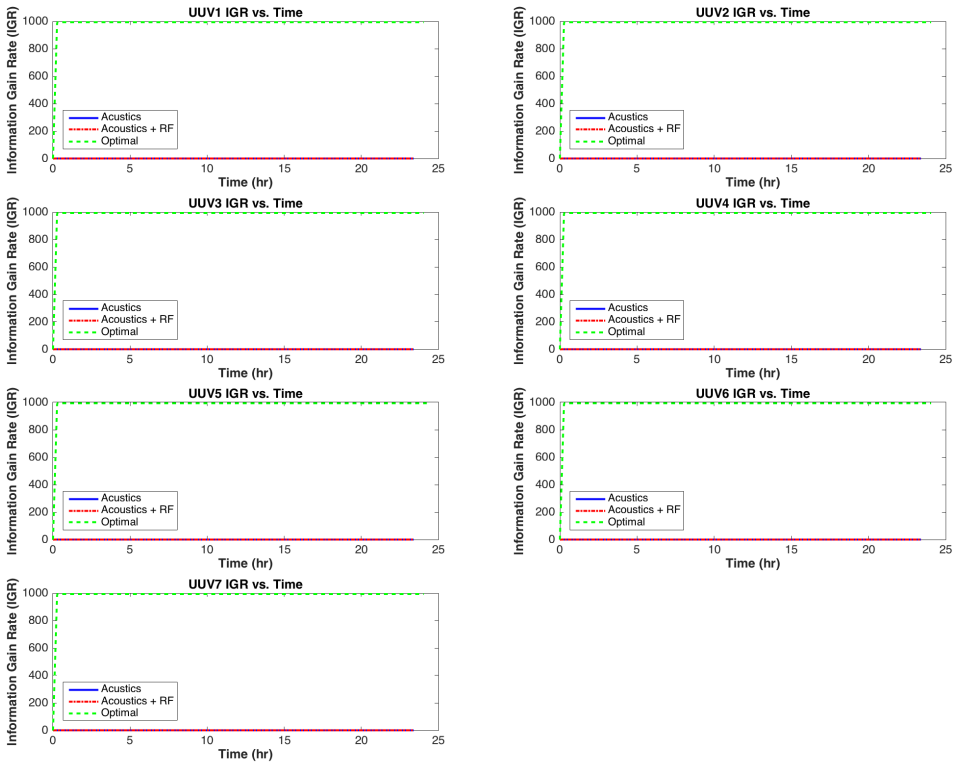


**Figure 202:** IGR vs. time for each case and our optimal solution for 24m EVD.

As can be seen from the plot, the optimal solution provides more $IGR$ over the whole duration of the mission, as expected.

## *7.9 COA Comparison and Decision*

The next step of the methodology and the NPP mission planning process, the COA Comparison and Decision shown in Fig.203, involves comparing the different COAs that were generated through the COA development and use our COA Analysis as a basis to decide which COAs are the best. This is done through further COA analysis using a simulation and visualization environment to play-out the mission and double checking our analysis. These COAs are reviewed and validated one last time before a final set of COAs is decided. The simulation of the mine-survey mission in the

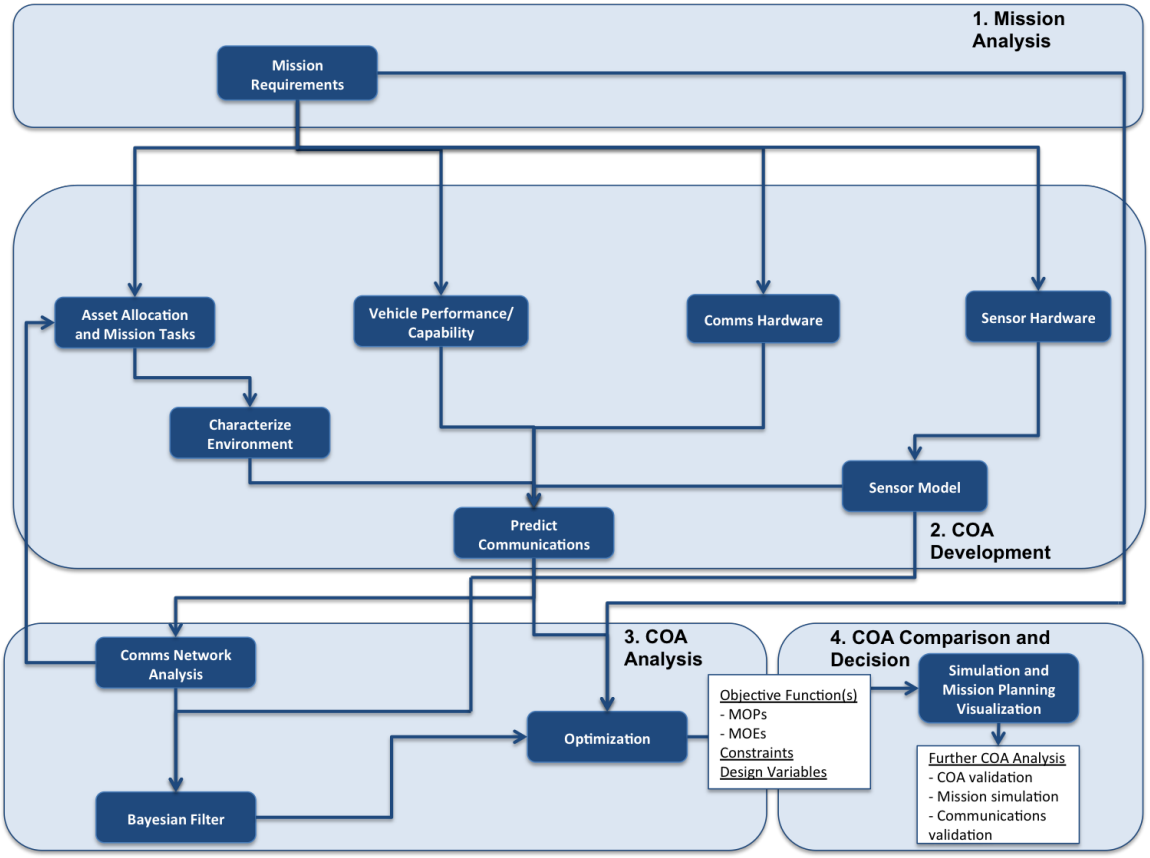


**Figure 203:** COA Comparison and Decision step of our methodology.

ACF-UV framework has not been modeled at the time of this thesis. Therefore, this step of the methodology is left for future work. Once simulations validate our proposed COAs, experimental work can be done to further validate our results by doing field testing with our vehicles. As explained during the COA Development, we chose UxV vehicle assets for this demonstration study that we can have access to in our laboratory or though collaboration with Navy SPAWAR in San Diego CA and the Naval Surface Warfare in Panama City FL. We also have access to three MPU5s that can be used as node to node and relay configurations to test our communications network topology solutions.

## *7.10 Summary of Demonstration Case Study Results and Hypothesis Validation*

The last research question RQ4 and corresponding hypothesis HP4 posed during the Proposed Methodology were the following:

**Research Question 4 (RQ4)**: *Can the proposed methodology be demonstrated on a mine survey mission scenario, providing optimal COAs that maximize a given mission level objective, while also ensuring a reliable communication network?*

**Hypothesis 4 (HP4)**: *The proposed methodology provides a useful approach towards predicting communications between UxVs, generating optimal communications-based COAs, and will be demonstrated in the mine survey mission, while ensuring communication channels are robust to environmental uncertainties, reliable to communication failures, and that optimize a given mission objective.*

In this case study we have applied the proposed methodology to the Mine Survey mission, filled the gaps with modeling and simulation using different approaches, and applied them to case scenarios that helped us appreciate the benefits and limitations of our methodology. Shown in Fig. 204 is the proposed methodology steps as it was applied to the demonstration case study. In the process of applying the methodology, we identified potential COA solutions that met part or all of the mission statement requirements, and analyzed them to quantify how good they are in meeting the mission goals. These analyses showed the possible communication tradeoffs and decisions that need to be made when deploying unmanned vehicles in the operational environment given maritime environmental conditions.

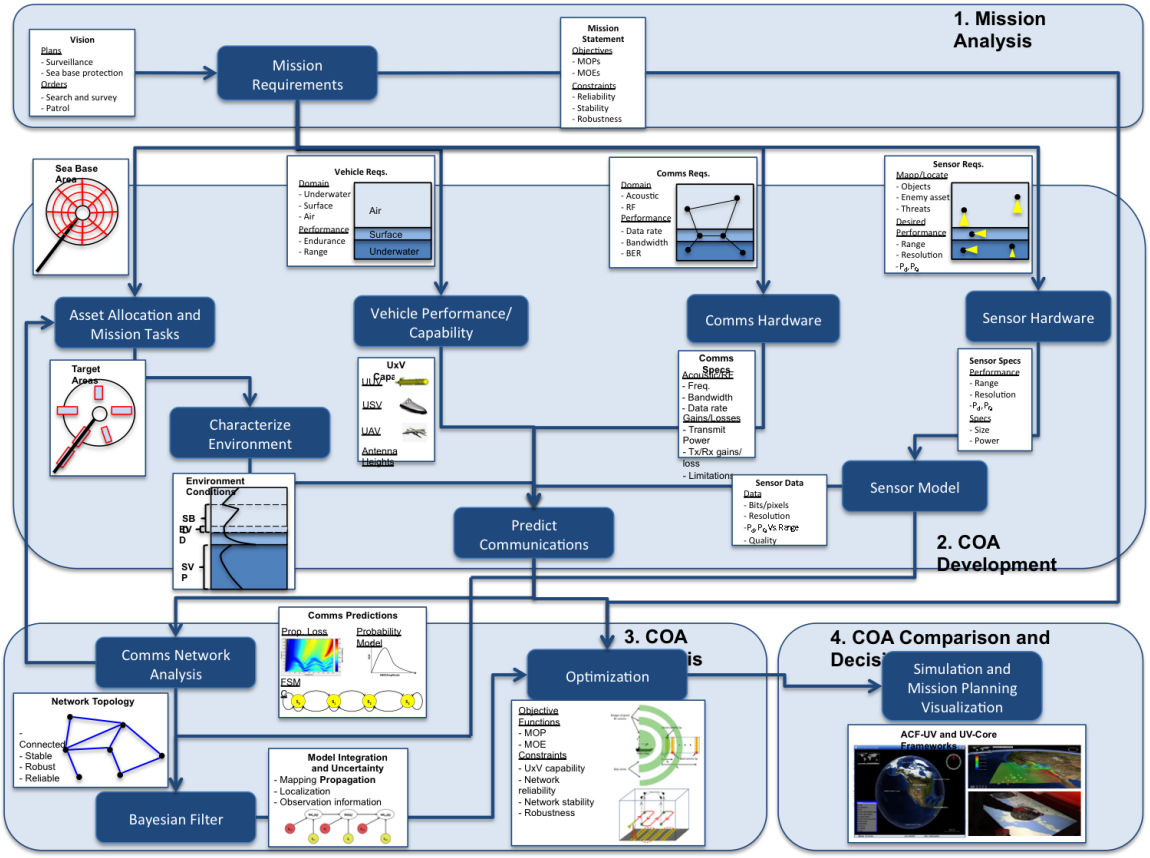


**Figure 204:** Proposed methodology applied to Mine Survey mission demonstration case study

At the end of the Demonstration Case Study we demonstrated that our network topology provides a network solution that provides the means to connect each UUV to the MS for the transmission of sensory information, and that the network is stable, robust and reliable. We used the ranges between good communications between the relays in our network topologies in some cases to relay the sensory information to the MS and determined optimal sweep distances that maximized the $IGR$. For some environmental conditions, i.e., the 24 m EVD, it was hart to meet the stability and reliability constraints with the initial set of assets. But by adding 4 more assets to the network we were able to meet the stability condition. These are the kind of trade offs this methodology was supposed to provide to the Navy Planning team while

performing the Navy Planning Process. This is not a final product, and should not be considered as "The Answer" to any communications problem, but rather should be utilized as a benchmark to consider communications between unmanned or autonomous vehicles in harsh environments such as those encountered in the maritime environment. Therefore, we have validated our hypothesis HP4.

In the next and final chapter, we provide further conclusions and discussion of the proposed methodology, and future work. A summary of each research question and corresponding hypothesis with validation or rejection based on our demonstration results is also provided at the end.

# CHAPTER VIII

# CONCLUSIONS AND DISCUSSION

As the use of unmanned and autonomous vehicles increases over the next years for different applications, communications between these vehicles need to be accounted for early during the mission planning stages. Communications is one of the major challenges between these vehicles, specially when there are many heterogeneous vehicles operating in water, surface and air. The environmental conditions that these unmanned vehicles are expected to operate are complex and can greatly affect the ability to communicate. For maritime environments, we discussed how evaporation ducts and elevated ducts can create signal multipath fading that can greatly affect the ability of different vehicles to communicate. Signal attenuation due to time-spreading and time variation of the signal as vehicles move relative to each other was also discussed. If these vehicles will be operating in these harsh environmental conditions, predicting communications is necessary and needs to be done during the mission planning phases. For the UV Sentry missions that are proposed by the concept of operations (CONOPS) of the Navy, robust and reliable UxV communications both above and below water are key for mission success.

Mission planning is a structured process for different military branches, and abiding to these doctrines will allow for a smooth concert of information flow and decision-making. The Navy Planning Process (NPP) provides a good reference of how Commanders and their planning staff perform mission planning in the matter of ours or minutes out in the operational environment to make crucial decisions on course of actions (COAs). Therefore, we proposed a methodology for assessing communications during the planning phases that follows the first four steps of the NPP process

closely to perform mission analysis, develop COAs, analyze each COA, and compare and decide on a COA. The inspiration of the proposed methodology was due to the need to account for communications between unmanned vehicles during the mission planning phases, which led to the following research objective:

**Research Objective (RO)**: ***Develop a methodology and a mission planning framework to find optimal communication COAs during the mission planning phase, which lead to high probability of mission success, and are robust to uncertainties in the environmental conditions and reliable to network failures.***

To meet this research objective, the proposed methodology was composed of different phases and steps that provided the needed analysis and investigation for each of the steps in the NPP process. In the mission analysis step, the vision of the Commander is translated into a mission statement, with specified, essential, and explicit requirements that can be quantified. In the COA Development step, we generated COAs based on our asset availability, sensor and communications hardware, and asset allocation based on required tasks for each vehicle. In the process, we characterized the environment and provided guidelines and studies for predicting communications of unmanned vehicles under different environmental conditions. In the process of building the COA Development process for generating communications based COAs, we posed two important research questions with corresponding hypotheses. The first research question dealt with asset allocation and communications network that provided a robust and reliable communications network topology. This was investigated in the Mine Survey mission demonstration study, where we modeled each communication channel link between any two vehicles, and searched for optimal ways to configure the network topology which resulted in a reliable, stable, connected, and robust communications network. The second question dealt more with the modeling

of the communications channels between mobile vehicles in maritime environments. A whole chapter was focused on characterizing the communications channel and on case studies that demonstrated our modeling approaches for large and small scale fading. In particular, probabilistic approaches were investigated to make our predictions more robust to environmental conditions and vehicle motions.

For the COA analysis step of the NPP, our methodology included procedures and guidelines to perform wargaming of our COAs. A chapter was spent on modeling communications network using graph theory, and assessing the communications network in terms of stability, quality, connectivity, and reliability. Next, the model integration and propagation of uncertainty was modeled using the Bayesian filter from Probabilistic Robotics. A separate chapter was spent on describing the different methods, and a case study allowed us to understand the effect of the measurements on the quality and quantity of the information and how it is communicated over the communication network. In the same case study, the information gain rate was optimized for a given target area using the distance between sweeps in a Mine Survey mission. The results of this study showed the benefits of our communications predictions and Bayesian filter modeling for communicating better information and faster over conventional sweeping procedures.

Communications-based optimization methods were presented in to give guidelines and recommendations on how to perform optimization based on the nature of the problem. Literature review was used to provide useful recommendations and help the planning staff pick better methods for given objective functions, design variables, and constraints.

Finally, in the demonstration case study, we applied the proposed methodology to a Mine Survey mission. Results showed the benefit of our methodology over conventional sweeping procedures for a UV Sentry operational environment. These benefits included COAs that led to stability, reliability, robustness and connectivity of our

communication networks, which provided comparable information gain rate compared to conventional methods.

The resulting methodology is intended to provide a planning framework for the mission planning staff and the Commander for finding communications based COAs that result in optimal measures of performance and measures of effectiveness of the given mission, which meeting mission level and communications constraints. With this, we have met our research objective.

## *8.1 Contributions*

The contributions of this thesis are the following:

- Prediction of the communications channel for mobile unmanned vehicles under maritime environmental conditions
- Guidelines and methods for creating communications-based COAs that lead to connected, reliable, robust, and stable communication networks
- Provided Probabilistic robotics approaches for model integration and modeling the propagation of uncertainty and quantifying information that is communicated over the network
- Optimization procedures for finding optimal COAs that lead to better measures of effectiveness and measures of performance of the mission using our communications predictions and network topology modeling
- A methodology for generating and analyzing COAs that take into account communications in harsh environmental conditions

## *8.2 Experimental Plan and Hypotheses Verification Summary*

This section summarizes for the reader the set of research questions, hypotheses, the experimental plan we used to answer each research question and verify the hypotheses. We then provide answers to each research question and validate or reject our initial hypothesis.

**Research Question 1 (RQ1)**: *What proactive communication network topology is reliable to communication link failures based on asset availability, which has the best network quality and is stable due to vehicle relative motions?*

**Hypothesis 1 (HP1)**: *A network topology that takes into account acceptable probability of communications, require the time-varying fading amplitude of the signal to be within certain thresholds, and which requires each asset to have spatial redundancy, will result in a reliable communications network.*

**Experiment 1 (Exp1)**: *For a given mission scenario (e.g. mine survey mission), determine maximum ranges (UxV to main ship and UxV to UxV ranges) based on mission requirements, and characterize the maritime environment within those ranges (e.g. unique scenarios: surface/elevated evaporation ducts). Determine propagation loss profile vs. range and height, and determine the received power at the receiver location (based on antenna height). Model the channel probabilistically using the Nakagami-m pdf to account for backscattering and different attenuation properties not accounted by propagation losses and RF link budget. The receiver sensitivity threshold value (based on communications hardware constraints) is used to determine the cumulative distribution function (cdf) representing the probability that the instantaneous received power falls below the threshold value for the given receiver sensitivity. The*

*number of degrees (number of communication links with other UxVs or main ship) of UxV nodes in the network is restricted to be at least 2 to test the reliability to link failure and capability to relay communications through other available network paths. These degrees will be based on assumed asset availability and vehicle capability (e.g. deploying UAVs from USVs).*

**Research Answer 1 (RA1)**: *In the Network Analysis Section of the Demonstration Case Study, we made assumptions about our graphs, and went further to define connectivity, stability, and reliability of the network. We broke down a set of criterions that were analyzed in order to come up with the best network topology that met all of our requirements. We first checked for connectivity through the use of the Fiedler value, and found that there can be multiple graph topologies that meet this condition. Our next criterion was to make sure the links in the graph were stable. We showed that a signal can be regarded as in good quality in terms of probability of communications, but may be unstable in terms of the relative motions with other vehicles. Stability criterion was based on discretizing the states of the transmission channels into good and bad states, and defining stability in terms of the transitions probability of transitioning from any state to the bad state. Given that neighboring state transition probabilities are higher, we defined the marginally stable state to be a bad state, and we disregarded network topologies which where in unstable or marginally stable states. The states were defined in the FSMC model in terms of the time-varying fading amplitudes of the signal near the APM large scale fading mean value $\Omega$, and we computed this state transition probabilities at each range for each APM propagation loss value. Our final criterion was to make sure the network is reliable to possible link failures. We showed that this condition is harder to meet with limited number of assets for certain environmental conditions, and therefore we proposed keep adding assets to the fleet until we were able to meet this criterion. With this, we can say that*

*we validated our hypothesis HP1.*

**Research Question 2 (RQ2)**: *How can the fading channel be modeled such that it captures multipath effects and time-variant mechanisms due to relative vehicle motion that is robust to environmental conditions uncertainty and fading fluctuations?*

**Hypothesis 2 (HP2)**: *Given communication constraints that reflect communications hardware limitations, a probability model will provide a robust fading channel model that takes into account multi-path and Doppler effects.*

**Experiment 2 (Exp2)**: *Use APM model to calculate the large scale fading characteristics of the channel, and model the small scale fading channel using an appropriate probabilistic model that captures the small scale fading due to time spreading of the signal and an FSMC model that captures the stability of the channel due to time variations of the signal. Robustness is measured as the probability of communications due to small scale fading and the stability of the channel to stay within good communication threshold states.*

**Research Answer 2 (RA2)**: *We showed during the Transmission Channel Modeling that APM can be used to model the large-scale fading mechanims due to the free-space propagation and the multipath created by the refractivity structure of the environment. We used the Rayleigh fading probability model due to the lack of empirical data to fit a more general Nakagami-m probability model, but we left the rest of the statistical modeling and analysis based on this general Nakagami model for future expansion. The time variations of the signal were simulated and validated through a modeled Rayleigh channel and assuming flat-fading non-frequency selective fading.*

*FSMC provided the probability methods to measure stability of the signal due to time-variations of the signal fading amplitude, and the model was validated and simulated through the general Nakagami-m probability model under different signal fluctuation intensities conditions. The links were deemed as robust to environmental conditions in the sense that we set a high threshold of probability of communications to take into account environmental refractivity time variations and modeling errors. Links that met this probability threshold, were more robust to fading signal intensities that could violate a threshold based solely on the receiver specifications, such as the minimum receiver power assumed for our COTS radio. We could not validate Hypothesis 2 entirely since we could not model a wide range of fluctuation intensities through the m-parameter of the Nakagami probability distribution, mainly due to the lack of empirical data. But we were able to concentrate on a special case of the Nakagami-m probability model, with* $m = 1$ *and regarded as one of the worse wireless communications conditions, to demonstrate the benefits of small-scale fading channel predictions.*

**Research Question 3 (RQ3)**: *How to model the effect of COAs on the quality and quantity of information communicated through the communications network?*

**Hypothesis 3 (HP3)**: *A sensor model can model Quality of information, and quantity of information can be modeled as the amount of state uncertainty that is communicated through the network.*

**Experiment 3 (Exp3)**: *Define the state of a target area as the occupancy of a map and determine how the probability of the state changes due to sensor measurements and vehicle motion using a histogram and binary Bayesian filter, and determine how the probability of the state affects the quality and quantity of information given a data rate and sensor model.*

**Research Answer 3 (RA3)**: *In the Bayesian Filter section of the Demonstration Case Study, we discretized the target area into a number of small cells of information that is picked up by the side-scan sonar sensor, and used our sensor model to capture the quality of information in terms of the probability of detection. The progression of sensor measurements and belief of the state of the occupancy of the cells in the target area was modeled and quantified by the Bayesian filter. The amount of information, in terms of the information entropy of each measurement, can be quantified by the information gain. Since we are concerned about getting valuable information as quick as possible during the mine-survey mission, we concentrated on the rate of the gain of information, or Information Gain Rate (IGR). We demonstrated through an example how we can find optimal sweeping distances which maximize the IGR. Our analysis was based on our modeling of the transmission channel between the UUV and the main ship at each possible surface point location. Our results showed the benefit of using the Bayesian filter to help us define the quality and quantity of information we can transmit through our RF channel, while sweeping through a given target area. Therefore, we have validated Hypothesis 3.*

**Research Question 4 (RQ4)**: *Can the proposed methodology be demonstrated on a mine survey mission scenario, providing optimal COAs that maximize a given mission level objective, while also ensuring a reliable communication network?*

**Hypothesis 4 (HP4)**: *The proposed methodology provides a useful approach towards predicting communications between UxVs, generating optimal communications-based COAs, and will be demonstrated in the mine survey mission, while ensuring communication channels are robust to environmental uncertainties, reliable to communication failures, and that optimize a given mission objective.*

**Experiment 4 (Exp4)**: *Apply proposed methodology to Mine Survey demonstration mission, and compare methodology results to baseline mission planning approaches in terms of robust, reliable, communication networks, and mission-level objectives.*

**Research Answer 4 (RA4)**: *At the end of the Demonstration Case Study we demonstrated that our network topology provides a network solution that provides the means to connect each UUV to the MS for the transmission of sensory information, and that the network is stable, robust and reliable. We used the ranges between good communications between the relays in our network topologies in some cases to relay the sensory information to the MS and determined optimal sweep distances that maximized the IGR. For some environmental conditions, i.e., the 24 m EVD, it was hart to meet the stability and reliability constraints with the initial set of assets. But by adding 4 more assets to the network we were able to meet the stability condition. These are the kind of trade offs this methodology was supposed to provide to the Navy Planning team while performing the Navy Planning Process. This is not a final product, and should not be considered as "The Answer" to any communications problem, but rather should be utilized as a benchmark to consider communications between unmanned or autonomous vehicles in harsh environments such as those encountered in the maritime environment. Therefore, we have validated our Hypothesis 4.*

Appendix A: Propagation Loss Profiles

Propagation loss profiles (PLPs) corresponding to links 9 to 13 under the three atmospheric conditions in Table are shown in Figures 205, 206, 207, 208, and 209.

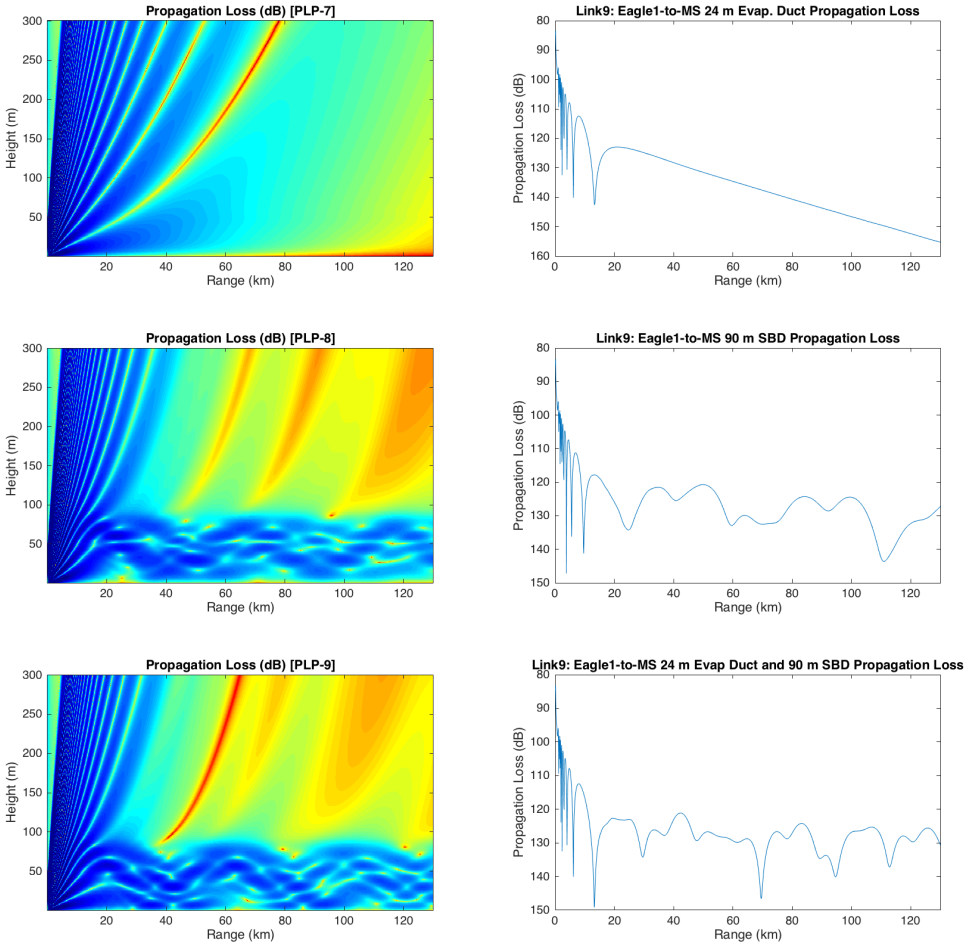


**Figure 205:** PLP-7 to PLP-9 and corresponding receiver propagation losses of link 9 under each atmospheric condition.

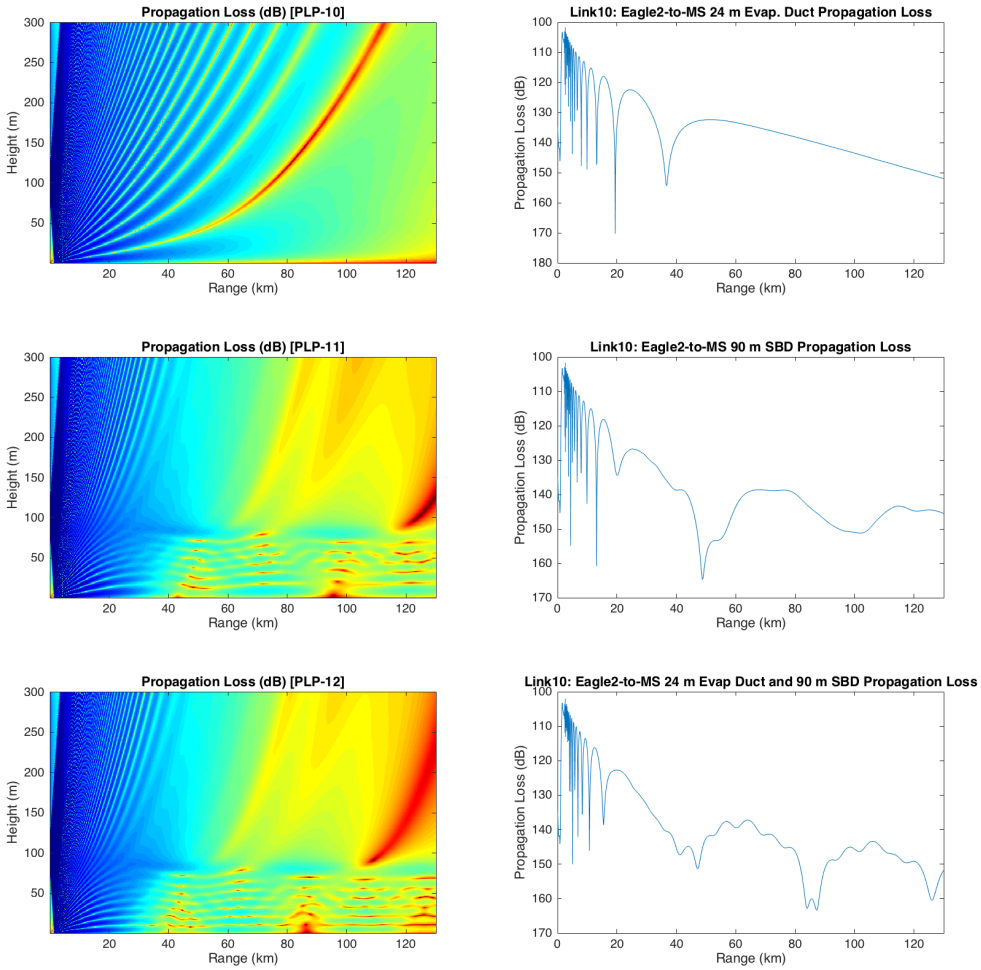


**Figure 206:** PLP-10 to PLP-12 and corresponding receiver propagation losses of link 10 under each atmospheric condition.

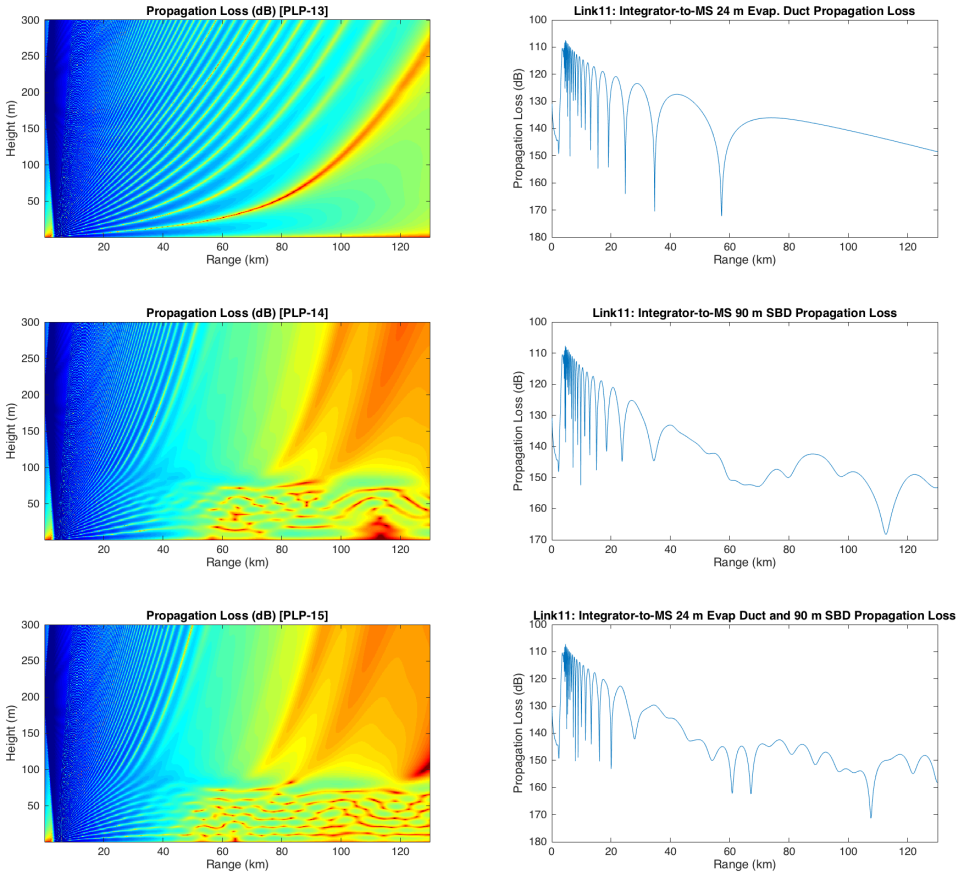


**Figure 207:** PLP-13 to PLP-15 and corresponding receiver propagation losses of link 11 under each atmospheric condition.

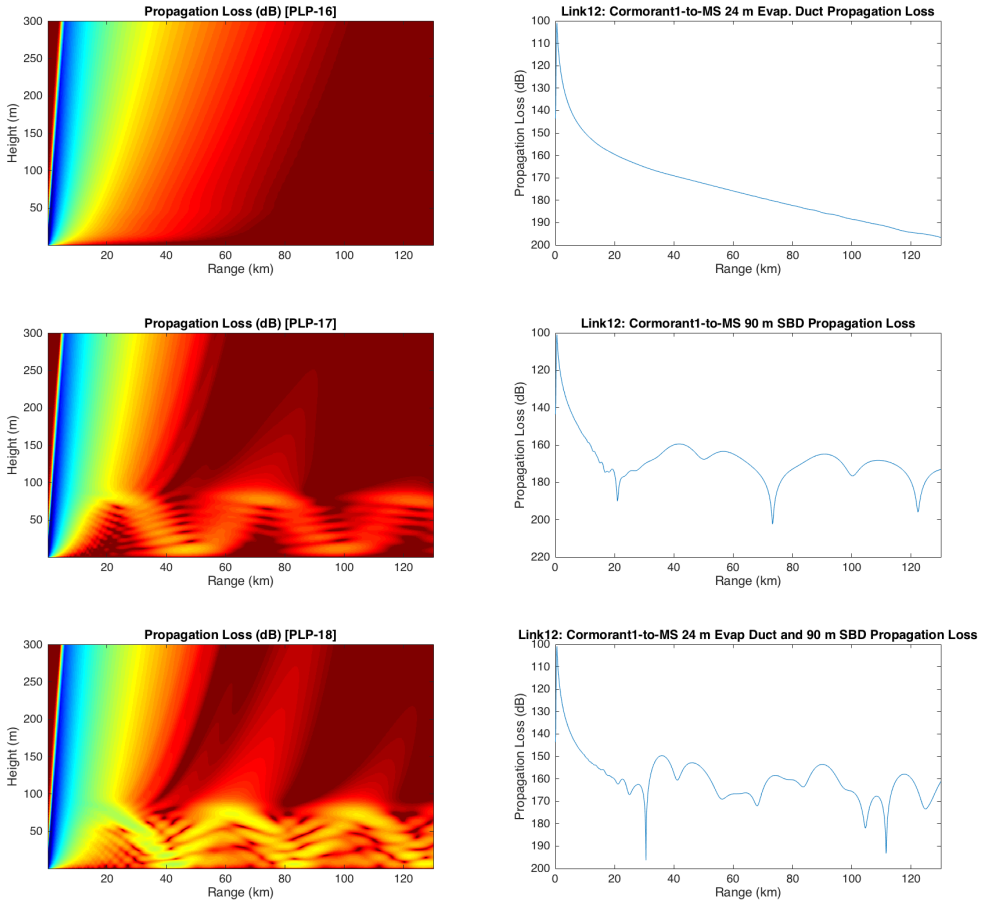


**Figure 208:** PLP-16 to PLP-18 and corresponding receiver propagation losses of link 12 under each atmospheric condition.

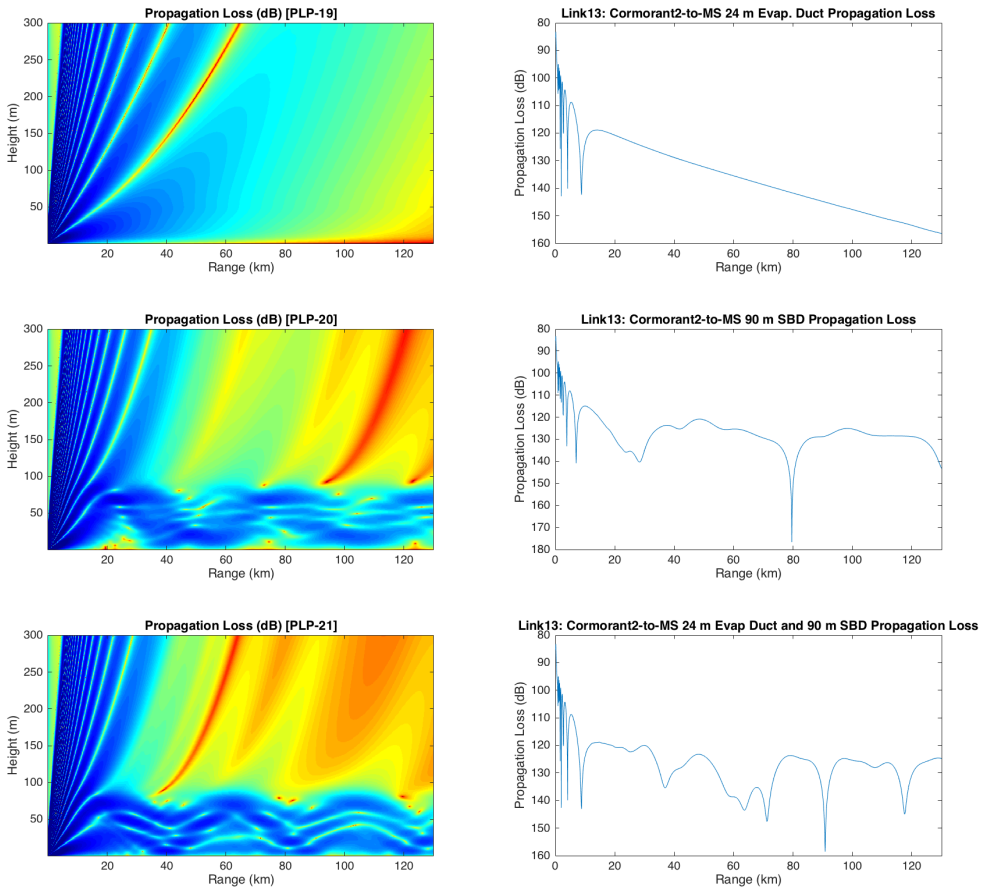


**Figure 209:** PLP-19 to PLP-21 and corresponding receiver propagation losses of link 13 under each atmospheric condition.

Appendix B: Received Power and Probability of Communications Plots The following are the received power and probability of communications for used in the demonstration case study, for all 3 atmospheric conditions: 24 m EVD, 90 m SBD, and 24 m EVD plus 90 m SBD.

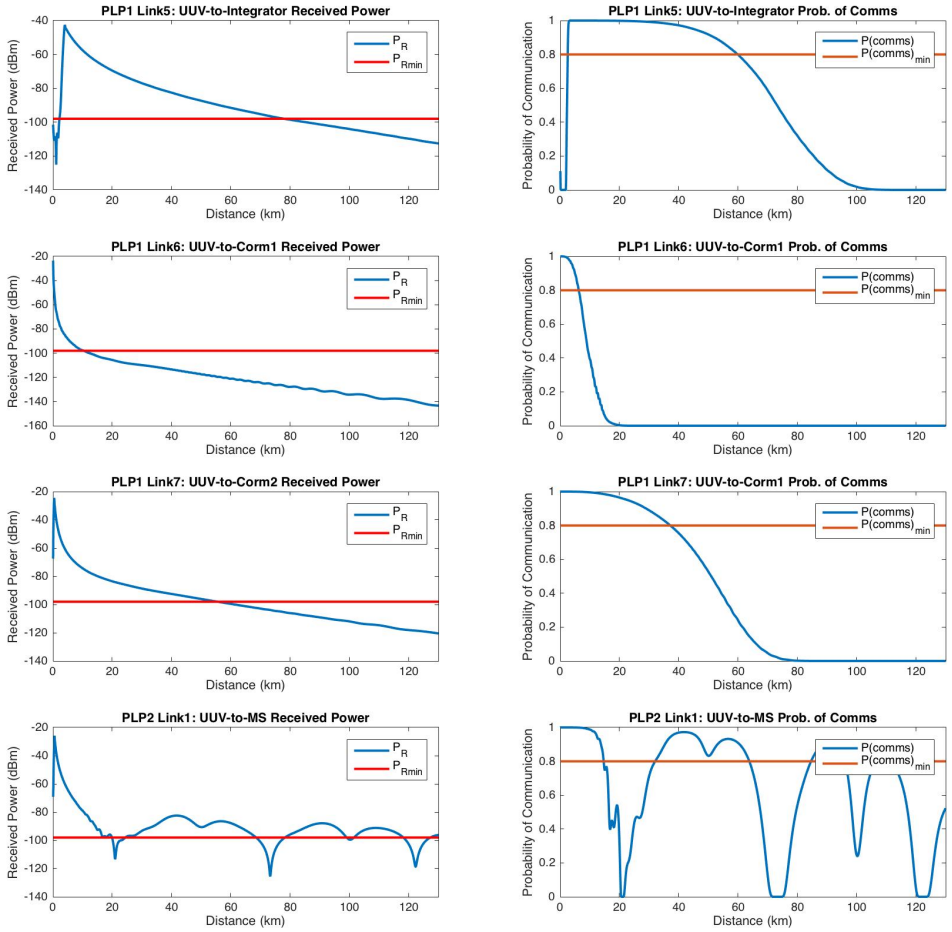


**Figure 210:** Received power and probability of communications for demonstration study.

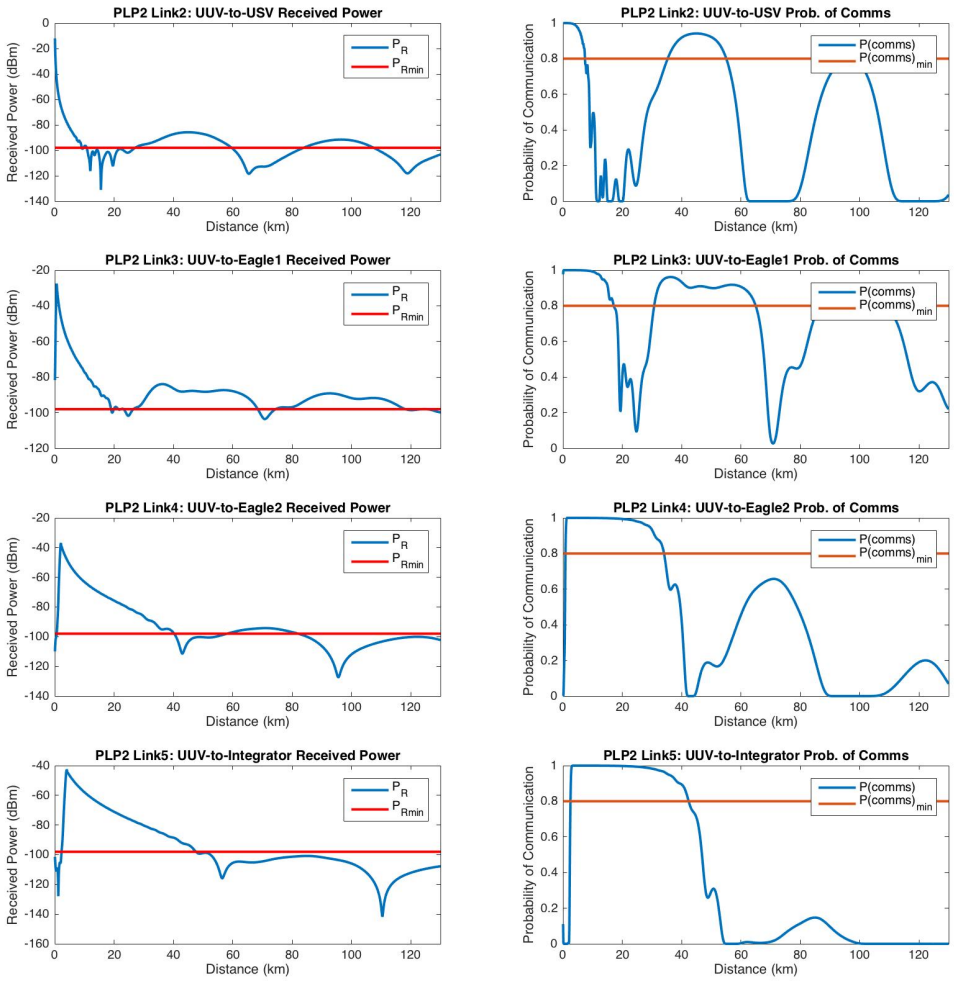


**Figure 211:** Received power and probability of communications for demonstration study.

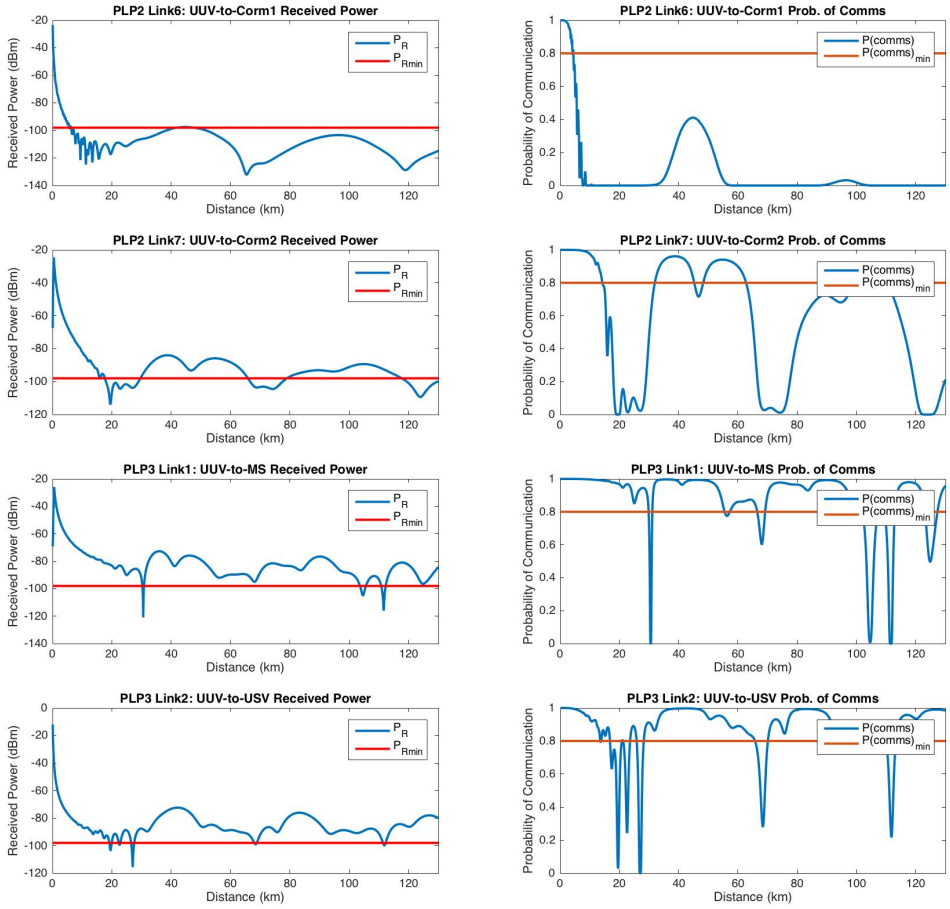


**Figure 212:** Received power and probability of communications for demonstration study.

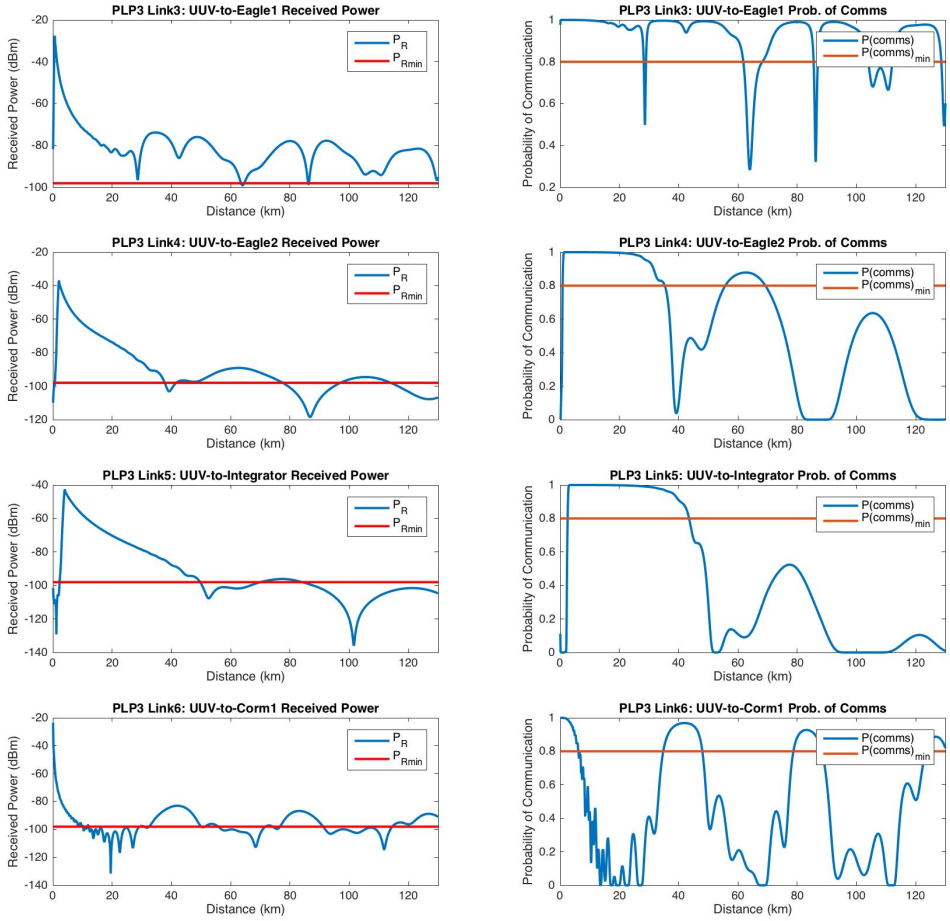


**Figure 213:** Received power and probability of communications for demonstration study.

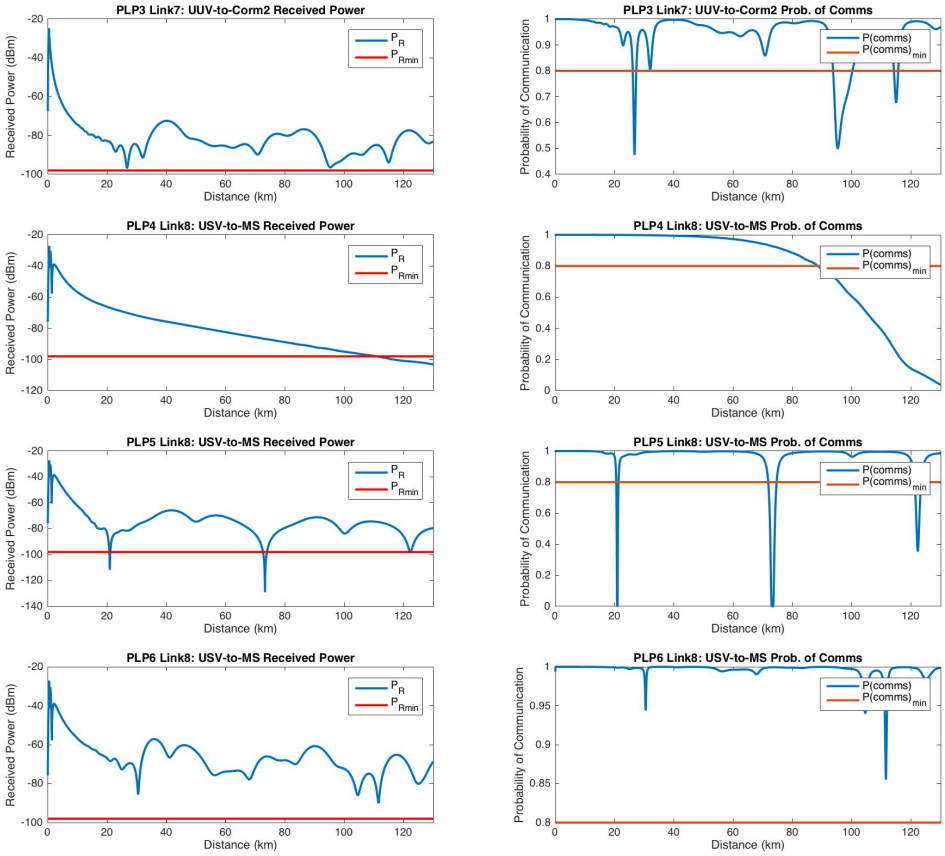


**Figure 214:** Received power and probability of communications for demonstration study.

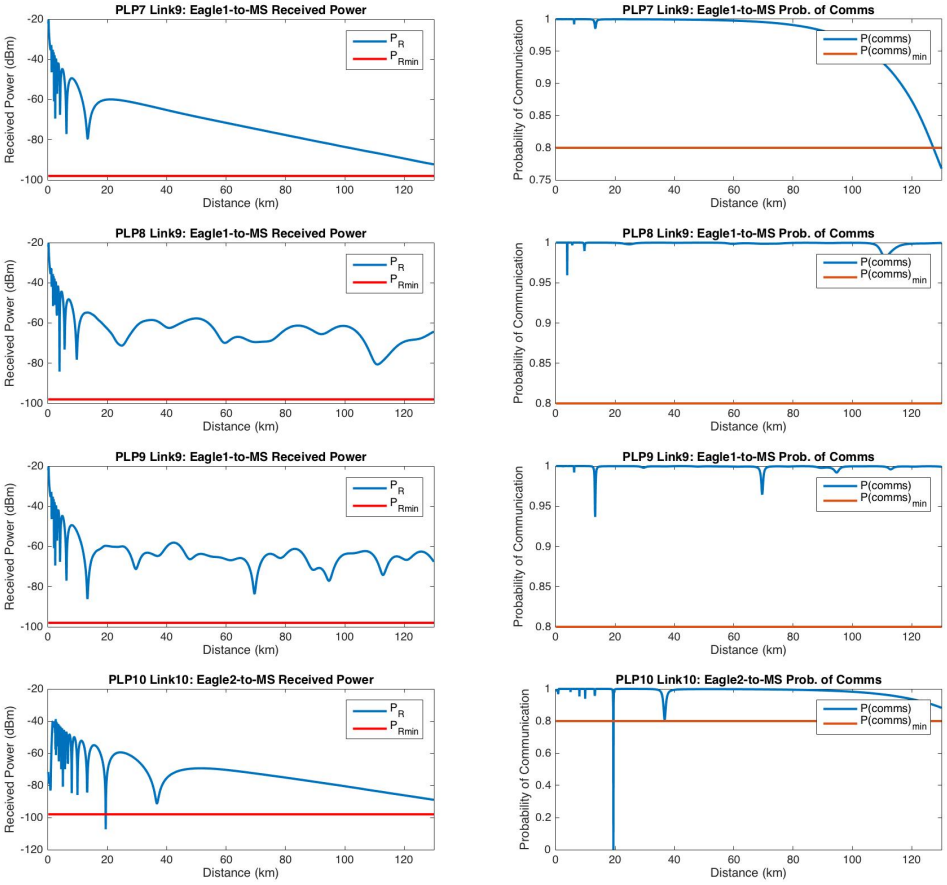


**Figure 215:** Received power and probability of communications for demonstration study.

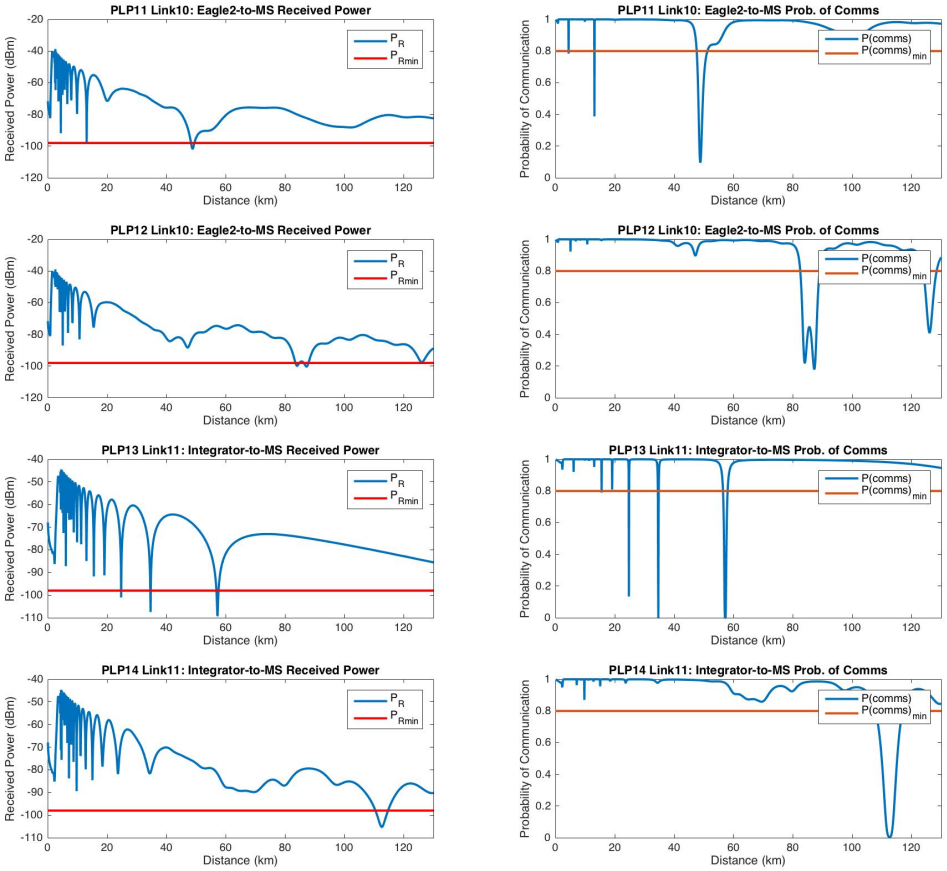


**Figure 216:** Received power and probability of communications for demonstration study.

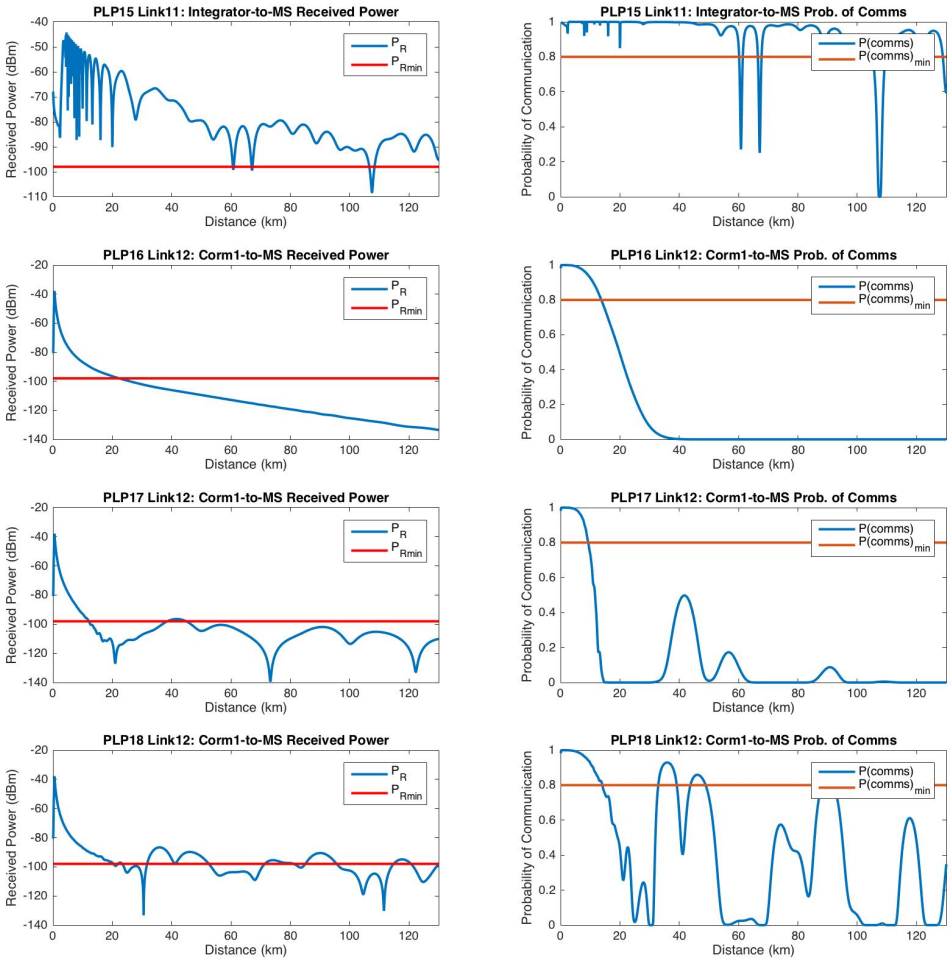


**Figure 217:** Received power and probability of communications for demonstration study.

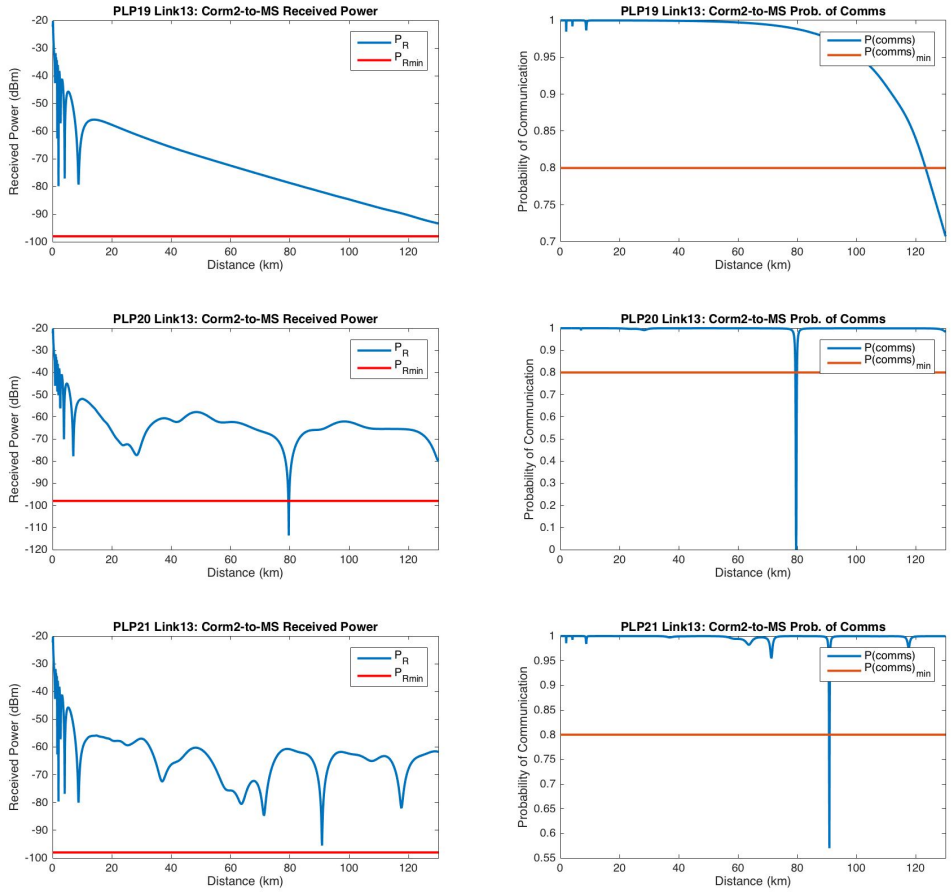


**Figure 218:** Received power and probability of communications for demonstration study.

# REFERENCES


[1] February 2013 Integrator First Maritime Flight (http://www.navaldrones.com/Integrator.html).

[2] "Irobot inc. roomba robotic floor vacuum.," December 2015 (http://www.irobot.com/For-the-Home/Vacuum-Cleaning/Roomba.aspx).

[3] Littoral Combat Ship (LCS) Independence Variant. http://www.austal.com/ships/littoral-combat-ship-lcs. October, 2016.

[4] Matlab Sensor Model, http://www.mathworks.com/help/phased/examples/detector-performance-analysis-using-roc-curves.html, February 2016.

[5] "United states frequency allocation by ntia," November 2016.

[6] October 2016 16' WAM-V USV by Marine Advance Research (http://www.wam-v.com/16-wam-v-usv).

[7] "Wave relay persistent systems mpu5 specifications," November 2016 http://www.persistentsystems.com/mpu5/.

[8] October 2016 Integrator UAV by Insitu Technologies (https://insitu.com/information-delivery/unmanned-systems/integrator).

[9] October 2016 Robot X Competition by AUVSI (http://www.robotx.org).

[10] October 2016 UAV-RF Laboratory at Aerospace Engineering Georgia Tech (http://www.uavrf.gatech.edu).

[11] Aarts, E. and Korst, J., "Simulated annealing and boltzmann machines," 1988.

[12] Abbasi, A. A., Younis, M., and Akkaya, K., "Movement-assisted connectivity restoration in wireless sensor and actor networks," *Parallel and Distributed Systems, IEEE Transactions on*, vol. 20, no. 9, pp. 1366–1379, 2009.

[13] Abbasi, A. A., Younis, M. F., and Baroudi, U. A., "Recovering from a node failure in wireless sensor-actor networks with minimal topology changes," *Vehicular Technology, IEEE Transactions on*, vol. 62, no. 1, pp. 256–271, 2013.

[14] Abdi, A. and Kaveh, M., "Performance comparison of three different estimators for the nakagami m parameter using monte carlo simulation," *Communications Letters, IEEE*, vol. 4, no. 4, pp. 119–121, 2000.

[15] Acar, E. U., Choset, H., Zhang, Y., and Schervish, M., "Path planning for robotic demining: Robust sensor-based coverage of unstructured environments and probabilistic methods," *The International Journal of Robotics Research*, vol. 22, no. 7-8, pp. 441–466, 2003.

[16] Akkaya, K., Thimmapuram, A., Senel, F., and Uludag, S., "Distributed recovery of actor failures in wireless sensor and actor networks," in *Wireless Communications and Networking Conference, 2008. WCNC 2008. IEEE*, pp. 2480–2485, IEEE, 2008.

[17] Aksaray, D., Griendling, K., and Mavris, D., "Uavs for law enforcement: A case study for connectivity and fuel management,"

[18] Aksaray, D. and Mavris, D., "Maintaining connectivity for networked mobile systems in the presence of agent loss," in *AIAA Guidance, Navigation, and Control Conference*, 2013.

[19] Alkire, B., Kallimani, J. G., Wilson, P. A., and Moore, L. R., "Applications for navy unmanned aircraft systems," tech. rep., DTIC Document, 2010.

[20] Alvarez, A., Caiti, A., and Onken, R., "Evolutionary path planning for autonomous underwater vehicles in a variable ocean," *Oceanic Engineering, IEEE Journal of*, vol. 29, no. 2, pp. 418–429, 2004.

[21] Amoroso, F., "Use of ds/ss signaling to mitigate rayleigh fading in a dense scatterer environment," *IEEE personal Communications*, vol. 3, no. 2, pp. 52–61, 1996.

[22] Andersen, J. B., Rappaport, T. S., and Yoshida, S., "Propagation measurements and models for wireless communications channels," *IEEE Communications Magazine*, vol. 33, no. 1, pp. 42–49, 1995.

[23] Arbel, T. and Ferrie, F. P., "Viewpoint selection by navigation through entropy maps," in *Computer Vision, 1999. The Proceedings of the Seventh IEEE International Conference on*, vol. 1, pp. 248–254, IEEE, 1999.

[24] Arkin, R. C., *Behavior-based robotics*. MIT press, 1998.

[25] Atanasov, N., Sankaran, B., Le Ny, J., Pappas, G. J., and Daniilidis, K., "Nonmyopic view planning for active object classification and pose estimation," *Robotics, IEEE Transactions on*, vol. 30, no. 5, pp. 1078–1090, 2014.

[26] Babich, F., Kelly, O. E., and Lombardi, G., "Generalized markov modeling for flat fading," *IEEE Transactions on Communications*, vol. 48, no. 4, pp. 547–551, 2000.

[27] Babich, F. and Lombardi, G., "A markov model for the mobile propagation channel," *IEEE Transactions on Vehicular Technology*, vol. 49, no. 1, pp. 63–73, 2000.

[28] Bajcsy, R., "Active perception," *Proceedings of the IEEE*, vol. 76, no. 8, pp. 966–1005, 1988.

[29] Barrios, A., "Parabolic equation modeling in horizontally inhomogeneous environments," *Antennas and Propagation, IEEE Transactions on*, vol. 40, no. 7, pp. 791–797, 1992.

[30] Barrios, A. E., "Considerations in the development of the advanced propagation model (APM) for US Navy applications," tech. rep., DTIC Document, 2005.

[31] Bauso, D., Giarre, L., and Pesenti, R., "Quantized dissensus in networks of agents subject to death and duplication," *Automatic Control, IEEE Transactions on*, vol. 57, no. 3, pp. 783–788, 2012.

[32] Bello, P. and Nelin, B., "The influence of fading spectrum on the binary error probabilites of incoherent and differentially coherent matched filter recievers," *IRE Transactions on Communications Systems*, vol. 10, no. 2, pp. 160–168, 1962.

[33] Benet, G., Blanes, F., Simó, J. E., and Pérez, P., "Using infrared sensors for distance measurement in mobile robots," *Robotics and autonomous systems*, vol. 40, no. 4, pp. 255–266, 2002.

[34] Benhmammouch, O., Khenchaf, A., and Caouren, N., "Modelling roughness effects on propagation of electromagnetic waves in a maritime environment: a hybrid approach," *Radar, Sonar & Navigation, IET*, vol. 5, no. 9, pp. 1018–1025, 2011.

[35] Bershadsky, D., Haviland, S., and Johnson, E. N., "Electric multirotor propulsion system sizing for performance prediction and design optimization,"

[36] Bershadsky D., Haviland, S. and N., J. E., "Electric multirotor propulsion system optimization for performance and other objectives," in *Proceedings of the AHS International 72nd Annual Forum and Technology Display*, May 2016.

[37] Biswas, A., Dasgupta, S., Das, S., and Abraham, A., "Synergy of pso and bacterial foraging optimization—a comparative study on numerical benchmarks," in *Innovations in Hybrid Intelligent Systems*, pp. 255–263, Springer, 2007.

[38] Blondel, P., *The Handbook of Sidescan Sonar*. Springer Science & Business Media, 2010.

[39] Boško, R., Petar, S., Stefan, P., Mihajlo, Č. S., and others, "Statistical characteristics of signal in the presence of two fast nakagami-m and one slow gamma fading," *Journal Name*, pp. 965–968, 2014.

[40] Boukhtouta, A., Bedrouni, A., Berger, J., Bouak, F., and Guitouni, A., "A survey of military planning systems," in *The 9th ICCRTS Int. Command and Control Research and Technology Symposium*, 2004.

[41] Bourgaul, F., Makarenko, A. A., Williams, S. B., Grocholsky, B., and Durrant-Whyte, H. F., "Information based adaptive robotic exploration," in *Intelligent Robots and Systems, 2002. IEEE/RSJ International Conference on*, vol. 1, pp. 540–545, IEEE, 2002.

[42] Branch, A. P. R., *User's Manual (UM) for Advanced Refractive Effects Prediction System*. Space and Naval Warfare Systems Center San Diego, 2006.

[43] Brayer, K., "The improvement of digital hf communication through coding: Ii-tandem interleaved cyclic coding," *IEEE Transactions on Communication Technology*, vol. 16, no. 6, pp. 779–786, 1968.

[44] Brayer, K., "Hf data transmission-lessons from the past, directions for the future," *IEEE journal on selected areas in communications*, vol. 5, pp. 90–101, 1987.

[45] Brayer, K. and Natarajan, S., "An investigation of arq and hybrid fec-arq on an experimental high latitude meteor burst channel," *IEEE Transactions on Communications*, vol. 37, no. 11, pp. 1239–1242, 1989.

[46] Brooks, R. and others, "A robust layered control system for a mobile robot," *Robotics and Automation, IEEE Journal of*, vol. 2, no. 1, pp. 14–23, 1986.

[47] Brown, G. G., Carlyle, M. W., Kelton, D., Kline, J., and Salmeron, J., "Operational planning tools for us navy maritime commanders," 2009.

[48] Button, R. W., Kamp, J., Curtin, T. B., and Dryden, J., "A survey of missions for unmanned undersea vehicles," tech. rep., DTIC Document, 2009.

[49] Cai, C. and Ferrari, S., "Information-driven sensor path planning by approximate cell decomposition," *Systems, Man, and Cybernetics, Part B: Cybernetics, IEEE Transactions on*, vol. 39, no. 3, pp. 672–689, 2009.

[50] Canny, J., *The complexity of robot motion planning*. MIT press, 1988.

[51] Cao, N., Low, K. H., and Dolan, J. M., "Multi-robot informative path planning for active sensing of environmental phenomena: A tale of two algorithms," in *Proceedings of the 2013 international conference on Autonomous agents and multi-agent systems*, pp. 7–14, International Foundation for Autonomous Agents and Multiagent Systems, 2013.

[52] Casbeer, D. W., Swindlehurst, A. L., and Beard, R., "Connectivity in a uav multi-static radar network," *American Institute of Aeronautics and Austronautics AIAA*, vol. 6209, 2006.

[53] Cavers, J. K., "The performance of phase locked transparent tone-in-band with symmetric phase detection," *IEEE transactions on communications*, vol. 39, no. 9, pp. 1389–1399, 1991.

[54] Cervenka, P. and De Moustier, C., "Sidescan sonar image processing techniques," *Oceanic Engineering, IEEE Journal of*, vol. 18, no. 2, pp. 108–122, 1993.

[55] Chen, G., Tian, Z., Shen, D., Blasch, E., and Pham, K., "A novel framework for command and control of networked sensor systems," in *Defense and Security Symposium*, pp. 65780L–65780L, International Society for Optics and Photonics, 2007.

[56] Cheng, J. and Beaulieu, N. C., "Maximum-likelihood based estimation of the nakagami m parameter," *IEEE Communications letters*, vol. 5, no. 3, pp. 101–103, 2001.

[57] Cheng, J. and Beaulieu, N. C., "Generalized moment estimators for the nakagami fading parameter," *IEEE communications letters*, vol. 6, no. 4, pp. 144–146, 2002.

[58] Chipperfield, A. and Fleming, P., "The MATLAB genetic algorithm toolbox," in *Applied control techniques using MATLAB, IEEE Colloquium on*, pp. 10–1, IET, 1995.

[59] Chu, M. J., Goeckel, D. L., and Stark, W. E., "On the design of markov models for fading channels," in *Vehicular Technology Conference, 1999. VTC 1999-Fall. IEEE VTS 50th*, vol. 4, pp. 2372–2376, IEEE, 1999.

[60] Clarke, R., "A statistical theory of mobile-radio reception," *Bell system technical journal*, vol. 47, no. 6, pp. 957–1000, 1968.

[61] Clausen, T. and Jacquet, P., "Optimized link state routing protocol (olsr)," tech. rep., 2003.

[62] Coker, A., Straatemeier, L., Rogers, T., Valdez, P., Cooksey, D., and Griendling, K., "Maritime channel modeling and simulation for efficient wideband communications between autonomous unmanned surface vehicles," in *Oceans-San Diego, 2013*, pp. 1–9, IEEE, 2013.

[63] Coker, A., Straatemeier, L., Rogers, T., Valdez, P., Griendling, K., and Cooksey, D., "Intermittent communications modeling and simulation for autonomous unmanned maritime vehicles using an integrated apm and fsmc framework," in *SPIE Defense+ Security*, pp. 908403–908403, International Society for Optics and Photonics, 2014.

[64] Corps, U. M., "Marine corps planning process," 2010.

[65] Cox, D. C., Murray, R. R., and Norris, A., "800-mhz attenuation measured in and around suburban houses," *AT&T Bell Laboratories technical journal*, vol. 63, no. 6, pp. 921–954, 1984.

[66] Cruzen, C. Braden, J. F. C. G. K. B. M. P. J. C. A. and Mavris, D., "Modeling and simulation of unmanned vehicle sentry missions to assess communications in a maritime environment," *Naval Engineer's Journal*, December 2014.

[67] Curlander, J. C. and McDonough, R. N., *Synthetic aperture radar*. John Wiley & Sons, 1991.

[68] Dai, F. and Wu, J., "An extended localized algorithm for connected dominating set formation in ad hoc wireless networks," *Parallel and Distributed Systems, IEEE Transactions on*, vol. 15, no. 10, pp. 908–920, 2004.

[69] Dantzig, G. B., "Programming in a linear structure," *Washington, DC*, 1948.

[70] DasGupta, B., Hespanha, J. P., Riehl, J., and Sontag, E., "Honeypot constrained searching with local sensory information," *Nonlinear Analysis: Theory, Methods & Applications*, vol. 65, no. 9, pp. 1773–1793, 2006.

[71] Dasgupta, D. and Michalewicz, Z., *Evolutionary algorithms in engineering applications*. Springer Science & Business Media, 2013.

[72] Davis, D. T. and Brutzman, D., "The autonomous unmanned vehicle workbench: mission planning, mission rehearsal, and mission replay tool for physics-based x3d visualization," in *Proceedings of the 14th International Symposium on Unmanned Untethered Submersible Technology*, 2005.

[73] Davis, L., "Genetic algorithms and simulated annealing," 1987.

[74] Dellaert, F., Fox, D., Burgard, W., and Thrun, S., "Monte carlo localization for mobile robots," in *Robotics and Automation, 1999. Proceedings. 1999 IEEE International Conference on*, vol. 2, pp. 1322–1328, IEEE, 1999.

[75] Denzler, J. and Brown, C. M., "Information theoretic sensor data selection for active object recognition and state estimation," *Pattern Analysis and Machine Intelligence, IEEE Transactions on*, vol. 24, no. 2, pp. 145–157, 2002.

[76] Denzler, J., Zobel, M., and Niemann, H., "Information theoretic focal length selection for real-time active 3d object tracking," in *Computer Vision, 2003. Proceedings. Ninth IEEE International Conference on*, pp. 400–407, IEEE, 2003.

[77] DiNapoli, F. and Deavenport, R., "Numerical methods of underwater acoustic propagation," *JA Desanto, ED*, vol. 40, pp. 47–55, 1977.

[78] Divsalar, D. and Simon, M., "Trellis coded modulation for 4800-9600 bits/s transmission over a fading mobile satellite channel," *IEEE Journal on Selected Areas in Communications*, vol. 5, no. 2, pp. 162–175, 1987.

[79] Dobeck, G. J., "Algorithm fusion for automated sea mine detection and classification," in *OCEANS, 2001. MTS/IEEE Conference and Exhibition*, vol. 1, pp. 130–134, IEEE, 2001.

[80] Drews, P. L., Neto, A. A., and Campos, M. F., "Hybrid unmanned aerial underwater vehicle: Modeling and simulation," in *2014 IEEE/RSJ International Conference on Intelligent Robots and Systems*, pp. 4637–4642, IEEE, 2014.

[81] Du, J., Xie, L., Sun, X., and Zheng, R., "Application-oriented fault detection and recovery algorithm for wireless sensor and actor networks," *International Journal of Distributed Sensor Networks*, vol. 2012, 2012.

[82] EdgeTech, *EdgeTech Application Note: Sidescan Sonar Range*, 4 ed., 2007.

[83] Egerstedt, M., Shamma, J. S., and others, "Decentralized degree regularization for multi-agent networks," in *Decision and Control (CDC), 2013 IEEE 52nd Annual Conference on*, pp. 7498–7503, IEEE, 2013.

[84] Elfes, A., "Using occupancy grids for mobile robot perception and navigation," *Computer*, vol. 22, no. 6, pp. 46–57, 1989.

[85] Elliott, E. O., "Estimates of error rates for codes on burst-noise channels," *The Bell System Technical Journal*, vol. 42, no. 5, pp. 1977–1997, 1963.

[86] Elmore, P. A., Avera, W. E., and Harris, M. M., "Use of the an/aqs-20a tactical mine-hunting system for on-scene bathymetry data," *Journal of Marine Systems*, vol. 78, pp. S425–S432, 2009.

[87] Emery, A. and Nenarokomov, A. V., "Optimal experiment design," *Measurement Science and Technology*, vol. 9, no. 6, p. 864, 1998.

[88] Erkan, S., Kandemir, M., and Lovell, S. D., *Energy-optimal data collection and communication using a group of UUVs*. Pennsylvania State University, Department of Computer Science and Engineering, College of Engineering, 2007.

[89] Falconer, D. D., Adachi, F., and Gudmundson, B., "Time division multiple access methods for wireless personal communications," *IEEE Communications Magazine*, vol. 33, no. 1, pp. 50–57, 1995.

[90] Feder, H. J. S., Leonard, J. J., and Smith, C. M., "Adaptive mobile robot navigation and mapping," *The International Journal of Robotics Research*, vol. 18, no. 7, pp. 650–668, 1999.

[91] Fox, D., Burgard, W., and Thrun, S., "Active markov localization for mobile robots," *Robotics and Autonomous Systems*, vol. 25, no. 3, pp. 195–207, 1998.

[92] FreeWave, "Fgr2 free wave radio specifications," 2014.

[93] Freitag, L., Grund, M., Singh, S., Partan, J., Koski, P., and Ball, K., "The WHOI micro-modem: an acoustic communications and navigation system for multiple platforms," in *OCEANS, 2005. Proceedings of MTS/IEEE*, pp. 1086–1092, IEEE, 2005.

[94] Frieden, B. R., *Science from Fisher information: a unification*. Cambridge University Press, 2004.

[95] Gelenbe, E. and Cao, Y., "Autonomous search for mines," *European Journal of Operational Research*, vol. 108, no. 2, pp. 319–333, 1998.

[96] Ghosh, A. and Boyd, S., "Growing well-connected graphs," in *Decision and Control, 2006 45th IEEE Conference on*, pp. 6605–6611, IEEE, 2006.

[97] Gilbert, E. N., "Capacity of a burst-noise channel," *Bell Labs Technical Journal*, vol. 39, no. 5, pp. 1253–1265, 1960.

[98] Gilhousen, K. S., Jacobs, I. M., Padovani, R., and Weaver, L. A., "Increased capacity using cdma for mobile satellite communication," *IEEE Journal on Selected Areas in Communications*, vol. 8, no. 4, pp. 503–514, 1990.

[99] Grocholsky, B., Keller, J., Kumar, V., and Pappas, G., "Cooperative air and ground surveillance," *Robotics & Automation Magazine, IEEE*, vol. 13, no. 3, pp. 16–25, 2006.

[100] Guan, Y. and Turner, L., "Generalised fsmc model for radio channels with correlated fading," in *Communications, IEE Proceedings-*, vol. 146, pp. 133–137, IET, 1999.

[101] Gunashekar, S., Siddle, D., and Warrington, E., "Transhorizon uhf radiowave propagation on over-sea paths in the british channel islands," *Systems Research*, vol. 1, pp. 2–5, 2005.

[102] Hager, G. and Mintz, M., "Computational methods for task-directed sensor data fusion and sensor planning," *The International Journal of Robotics Research*, vol. 10, no. 4, pp. 285–313, 1991.

[103] Han, Z., Swindlehurst, A. L., and Liu, K. R., "Smart deployment/movement of unmanned air vehicle to improve connectivity in manet," in *Wireless Communications and Networking Conference, 2006. WCNC 2006. IEEE*, vol. 1, pp. 252–257, IEEE, 2006.

[104] Hata, M., "Empirical formula for propagation loss in land mobile radio services," *IEEE transactions on Vehicular Technology*, vol. 29, no. 3, pp. 317–325, 1980.

[105] Haviland, S., Bershadsky, D., and Johnson, E. N., "Dynamic modeling and analysis of a vtol freewing concept," in *AIAA Atmospheric Flight Mechanics Conference*, p. 1289, 2016.

[106] Hess, G. C., "Land-mobile radio system engineering," *The Artech House mobile communications library*, 1993.

[107] Hoang, T. N., Low, B. K. H., Jaillet, P., and Kankanhalli, M., "Nonmyopic -bayes-optimal active learning of gaussian processes," 2014.

[108] Hollinger, G. A., Englot, B., Hover, F. S., Mitra, U., and Sukhatme, G. S., "Active planning for underwater inspection and the benefit of adaptivity," *The International Journal of Robotics Research*, p. 0278364912467485, 2012.

[109] Hollinger, G. A. and Sukhatme, G. S., "Sampling-based robotic information gathering algorithms," *The International Journal of Robotics Research*, p. 0278364914533443, 2014.

[110] Huang, W. H., "Optimal line-sweep-based decompositions for coverage algorithms," in *Robotics and Automation, 2001. Proceedings 2001 ICRA. IEEE International Conference on*, vol. 1, pp. 27–32, IEEE, 2001.

[111] Hydroid, L. and Pocasset, M., "Remus 100 autonomous underwater vehicle. brochure," *Falmouth, MA*, 2006.

[112] Hyland, J. C. and Dobeck, G. J., "Sea mine detection and classification using side-looking sonar," in *SPIE's 1995 Symposium on OE/Aerospace Sensing and Dual Use Photonics*, pp. 442–453, International Society for Optics and Photonics, 1995.

[113] Ibrahim, A. S., Seddik, K. G., and Liu, K. R., "Improving connectivity via relays deployment in wireless sensor networks," in *Global Telecommunications Conference, 2007. GLOBECOM'07. IEEE*, pp. 1159–1163, IEEE, 2007.

[114] Ji, M. and Egerstedt, M. B., "Distributed coordination control of multiagent systems while preserving connectedness.," 2007.

[115] Kaelbling, L. P. and Rosenschein, S. J., "Action and planning in embedded agents," *Robotics and autonomous systems*, vol. 6, no. 1, pp. 35–48, 1990.

[116] Kalman, R. E., "A new approach to linear filtering and prediction problems," *Journal of Fluids Engineering*, vol. 82, no. 1, pp. 35–45, 1960.

[117] Kavehrad, M. and Bodeep, G., "Design and experimental results for a direct-sequence spread-spectrum radio using differential phase-shift keying modulation for indoor, wireless communications," *IEEE journal on selected areas in communications*, vol. 5, no. 5, pp. 815–823, 1987.

[118] Kennedy, J., "Particle swarm optimization," in *Encyclopedia of Machine Learning*, pp. 760–766, Springer, 2010.

[119] Kirsch, A., Gray, P., and Hanna, D., "Field-test results of the an/gsc-10 (kathryn) digital data terminal," *IEEE Transactions on Communication Technology*, vol. 2, no. 17, pp. 118–128, 1969.

[120] Knight, W. C., Pridham, R. G., and Kay, S. M., "Digital signal processing for sonar," *Proceedings of the IEEE*, vol. 69, no. 11, pp. 1451–1506, 1981.

[121] Knorn, F., Stanojevic, R., Corless, M., and Shorten, R., "A framework for decentralised feedback connectivity control with application to sensor networks," *International Journal of Control*, vol. 82, no. 11, pp. 2095–2114, 2009.

[122] Knott, E. F., *Radar cross section measurements*. Springer Science & Business Media, 2012.

[123] Ko, Y.-C., Alouini, M.-S., and Simon, M. K., "Outage probability of diversity systems over generalized fading channels," *Communications, IEEE Transactions on*, vol. 48, no. 11, pp. 1783–1787, 2000.

[124] Kong, H. and Shwedyk, E., "Sequence detection and channel state estimation over finite state markov channels," *IEEE transactions on vehicular technology*, vol. 48, no. 3, pp. 833–839, 1999.

[125] Kongsberg, "Remus 600," June 2016.

[126] Kreucher, C., Kastella, K., and Hero Iii, A. O., "Sensor management using an active sensing approach," *Signal Processing*, vol. 85, no. 3, pp. 607–624, 2005.

[127] Kreucher, C., Wegrzyn, J., Beauvais, M., and Conti, R., "Multiplatform information-based sensor management: an inverted uav demonstration," in *Defense and Security Symposium*, pp. 65780Y–65780Y, International Society for Optics and Photonics, 2007.

[128] Kuntz, A., Schmidt-Eisenlohr, F., Graute, O., Hartenstein, H., and Zitterbart, M., "Introducing probabilistic radio propagation models in omnet++ mobility framework and cross validation check with ns-2," in *Proceedings of the 1st international conference on Simulation tools and techniques for communications, networks and systems & workshops*, p. 72, ICST (Institute for Computer Sciences, Social-Informatics and Telecommunications Engineering), 2008.

[129] Kuttler, J. R. and Dockery, G. D., "Theoretical description of the parabolic approximation/fourier split-step method of representing electromagnetic propagation in the troposphere," *Radio Science*, vol. 26, no. 2, pp. 381–393, 1991.

[130] Lebeltel, O., Bessière, P., Diard, J., and Mazer, E., "Bayesian robot programming," *Autonomous Robots*, vol. 16, no. 1, pp. 49–79, 2004.

[131] Leung, C., Huang, S., Kwok, N., and Dissanayake, G., "Planning under uncertainty using model predictive control for information gathering," *Robotics and Autonomous Systems*, vol. 54, no. 11, pp. 898–910, 2006.

[132] Li, T., Jin, X., and Collins, O. M., "Successive decoding for finite state markov modelled flat fading channels," in *Information Theory, 2006 IEEE International Symposium on*, pp. 11–15, IEEE, 2006.

[133] Li, Y. and Liu, Z., "Information entropy-based viewpoint planning for 3-d object reconstruction," *Robotics, IEEE Transactions on*, vol. 21, no. 3, pp. 324–337, 2005.

[134] Liao, X. and Carin, L., "Application of the theory of optimal experiments to adaptive electromagnetic-induction sensing of buried targets," *Pattern Analysis and Machine Intelligence, IEEE Transactions on*, vol. 26, no. 8, pp. 961–972, 2004.

[135] Lindgren, B., *Statistical theory*, vol. 22. CRC Press, 1993.

[136] Lorenz, R., "Theoretical distribution functions of multipath propagation and their parameters for mobile radio communication in quasi-smooth terrain," in *In AGARD Terrain Profiles and Contours in Electromagnetic Wave Propagation 16 p (SEE N80-19345 10-32)*, vol. 1, 1979.

[137] Low, K. H., Dolan, J. M., and Khosla, P., "Adaptive multi-robot wide-area exploration and mapping," in *Proceedings of the 7th international joint conference on Autonomous agents and multiagent systems-Volume 1*, pp. 23–30, International Foundation for Autonomous Agents and Multiagent Systems, 2008.

[138] Lu, W., Zhang, G., and Ferrari, S., "An information potential approach to integrated sensor path planning and control," *Robotics, IEEE Transactions on*, vol. 30, no. 4, pp. 919–934, 2014.

[139] Lu, W., Zhang, G., Ferrari, S., Fierro, R., and Palunko, I., "An information potential approach for tracking and surveilling multiple moving targets using mobile sensor agents," in *SPIE Defense, Security, and Sensing*, pp. 80450T–80450T, International Society for Optics and Photonics, 2011.

[140] Maia, M. M., Soni, P., and Diez, F. J., "Demonstration of an aerial and submersible vehicle capable of flight and underwater navigation with seamless air-water transition," *arXiv preprint arXiv:1507.01932*, 2015.

[141] Mailey, C., "Uv sentry: Protecting the sea base with unmanned vehicles," Space and Naval Warfare Systems Center (SPAWAR) San Diego CA.

[142] Maldague, P., Ko, A., Page, D., and Starbird, T., "Apgen: A multi-mission semi-automated planning tool," in *First International NASA Workshop on Planning and Scheduling*, pp. 363–365, 1998.

[143] Marchant, R. and Ramos, F., "Bayesian optimisation for intelligent environmental monitoring," in *Intelligent Robots and Systems (IROS), 2012 IEEE/RSJ International Conference on*, pp. 2242–2249, IEEE, 2012.

[144] Masoomzadeh-Fard, A. and Pasupathy, S., "Equalization of indoor fading channels with differentially coherent demodulation," in *Personal, Indoor and Mobile Radio Communications, 1995. PIMRC'95. Wireless: Merging onto the Information Superhighway., Sixth IEEE International Symposium on*, vol. 1, pp. 1–5, IEEE, 1995.

[145] Médard, M. and Lumetta, S. S., "Network reliability and fault tolerance," *Encyclopedia of Telecommunications*, 2003.

[146] Mi, Z., Yang, Y., and Liu, G., "Hero: A hybrid connectivity restoration framework for mobile multi-agent networks," in *Robotics and Automation (ICRA), 2011 IEEE International Conference on*, pp. 1702–1707, IEEE, 2011.

[147] Mosier, R. and Clabaugh, R., "Kineplex, a bandwidth-efficient binary transmission system," *Transactions of the American Institute of Electrical Engineers, Part I: Communication and Electronics*, vol. 76, no. 6, pp. 723–728, 1958.

[148] Motevallian, S. A., Yu, C., and Anderson, B. D., "Robustness to the loss of multiple nodes in the localizability of sensor networks," *in IFAC WC*, 2011.

[149] Nakagami, M., "The m-distribution-a general formula of intensity distribution of rapid fading," *Statistical Method of Radio Propagation*, 1960.

[150] Navy, "21st-century U.S. Navy Mine Warfare," *Program Executive Offica Littoral and Mine Warfare, Program Executive Office*, 2009.

[151] Navy, *Navy Planning Process (NPP)*. Office of the Chief of Naval Operations, Department of the Navy, December 2013.

[152] Okumura, Y., Ohmori, E., Kawano, T., and Fukuda, K., "Field strength and its variability in vhf and uhf land-mobile radio service," *Rev. Elec. Commun. Lab*, vol. 16, no. 9, pp. 825–73, 1968.

[153] Ore, J.-P., Elbaum, S., Burgin, A., and Detweiler, C., "Autonomous aerial water sampling," *Journal of Field Robotics*, vol. 32, no. 8, pp. 1095–1113, 2015.

[154] O'Rourke, R., *The United States Navy: Current Issues and Background*. Nova Publishers, 2003.

[155] Osborn, K., "Navy unveils new surface warfare strategy," 2015.

[156] Pahlavan, K., Howard, S. J., and Sexton, T. A., "Decision feedback equalization of the indoor radio channel," *IEEE transactions on communications*, vol. 41, no. 1, pp. 164–170, 1993.

[157] Pahlavan, K. and Levesque, A. H., *Wireless information networks*, vol. 93. John Wiley & Sons, 2005.

[158] Pandana, C. and Liu, K. R., "Maximum connectivity and maximum lifetime energy-aware routing for wireless sensor networks," in *Global Telecommunications Conference, 2005. GLOBECOM'05. IEEE*, vol. 2, pp. 5–pp, IEEE.

[159] Park, S., Pfenning, F., and Thrun, S., *A probabilistic language based upon sampling functions*, vol. 40. ACM, 2005.

[160] Passino, K. M., "Biomimicry of bacterial foraging for distributed optimization and control," *Control Systems, IEEE*, vol. 22, no. 3, pp. 52–67, 2002.

[161] Peled, D. A., *Software reliability methods*. Springer Science & Business Media, 2013.

[162] Pollitt, G. W., "Mine countermeasures requirements to support future operational maneuver," *Johns Hopkins APL technical digest*, vol. 21, no. 2, pp. 280–287, 2000.

[163] Ponda, S. S., Johnson, L. B., Choi, H.-L., and How, J. P., "Ensuring network connectivity for decentralized planning in dynamic environments," in *Proceedings of the AIAA Infotech@ Aerospace Conference, St. Louis, MO*, 2011.

[164] Prabhu, G. S. and Shankar, P. M., "Simulation of flat fading using matlab for classroom instruction," *IEEE Transactions on Education*, vol. 45, no. 1, pp. 19–25, 2002.

[165] Price, R. and Green, P., "A communication technique for multipath channels," *Proceedings of the IRE*, vol. 46, no. 3, pp. 555–570, 1958.

[166] Rahimi, M., Hansen, M., Kaiser, W. J., Sukhatme, G. S., and Estrin, D., "Adaptive sampling for environmental field estimation using robotic sensors," in *Intelligent Robots and Systems, 2005.(IROS 2005). 2005 IEEE/RSJ International Conference on*, pp. 3692–3698, IEEE, 2005.

[167] Rappaport, T. S. and others, *Wireless communications: principles and practice*, vol. 2. Prentice Hall PTR New Jersey, 1996.

[168] Reed, S., Petillot, Y., and Bell, J., "An automatic approach to the detection and extraction of mine features in sidescan sonar," *Oceanic Engineering, IEEE Journal of*, vol. 28, no. 1, pp. 90–105, 2003.

[169] Riediger, M. and Shwedyk, E., "Communication receivers based on markov models of the fading channel," *IEE Proceedings-Communications*, vol. 150, no. 4, pp. 275–279, 2003.

[170] Rogers, L. and Paulus, R., "Measured performance of evaporation duct models," in *Battlespace Atmospherics Conference*, pp. 3–5, 1996.

[171] Rowe, S. and Wagner, C. R., "An introduction to the joint architecture for unmanned systems (jaus)," *Ann Arbor*, vol. 1001, p. 48108, 2008.

[172] Roy, N. and Earnest, C., "Dynamic action spaces for information gain maximization in search and exploration," in *American Control Conference, 2006*, pp. 6–pp, IEEE, 2006.

[173] Ryan, A. and Hedrick, J. K., "Particle filter based information-theoretic active sensing," *Robotics and Autonomous Systems*, vol. 58, no. 5, pp. 574–584, 2010.

[174] Sabattini, L., Chopra, N., and Secchi, C., "On decentralized connectivity maintenance for mobile robotic systems," in *Decision and Control and European Control Conference (CDC-ECC), 2011 50th IEEE Conference on*, pp. 988–993, IEEE, 2011.

[175] Sabattini, L., Secchi, C., and Chopra, N., "Decentralized connectivity maintenance for networked lagrangian dynamical systems," in *Robotics and Automation (ICRA), 2012 IEEE International Conference on*, pp. 2433–2438, IEEE, 2012.

[176] Sadeghi, P., Kennedy, R., Rapajic, P. B., Shams, R., and others, "Finite-state markov modeling of fading channels-a survey of principles and applications," *Signal Processing Magazine, IEEE*, vol. 25, no. 5, pp. 57–80, 2008.

[177] Sariel, S., Balch, T., and Erdogan, N., "Naval mine countermeasure missions," *IEEE Robotics & Automation Magazine*, vol. 15, no. 1, pp. 45–52, 2008.

[178] Savitz, S., Blickstein, I., Buryk, P., Button, R. W., DeLuca, P., Dryden, J., Mastbaum, J., Osburg, J., Padilla, P., and Potter, A., "Us navy employment options for unmanned surface vehicles (usvs)," tech. rep., DTIC Document, 2013.

[179] Schilling, D. L., Milstein, L. B., Pickholtz, R. L., Bruno, F., Kanterakis, E., Kullback, M., Erceg, V., Biederman, W., Fishman, D., and Salerno, D., "Broadband cdma for personal communications systems," *IEEE Communications Magazine*, vol. 29, no. 11, pp. 86–93, 1991.

[180] Schlabach, J. L., Hayes, C. C., and Goldberg, D. E., "Fox-ga: a genetic algorithm for generating and analyzing battlefield courses of action," *Evolutionary Computation*, vol. 7, no. 1, pp. 45–68, 1999.

[181] Schmalenberger, R. M. and Edrich, M. G., "Channel modelling for wideband data communication in a maritime mobile environment," in *EUROCOMM 2000. Information Systems for Enhanced Public Safety and Security. IEEE/AFCEA*, pp. 150–154, IEEE, 2000.

[182] Schwartz, J. T., *Planning, geometry, and complexity of robot motion*. Intellect Books, 1987.

[183] Seidel, S. Y., Rappaport, T. S., Jain, S., Lord, M. L., and Singh, R., "Path loss, scattering and multipath delay statistics in four european cities for digital cellular and microcellular radiotelephone," *IEEE Transactions on Vehicular Technology*, vol. 40, no. 4, pp. 721–730, 1991.

[184] Shnidman, D. and others, "Expanded swerling target models," *Aerospace and Electronic Systems, IEEE Transactions on*, vol. 39, no. 3, pp. 1059–1069, 2003.

[185] Sim, R. and Roy, N., "Global a-optimal robot exploration in slam," in *Robotics and Automation, 2005. ICRA 2005. Proceedings of the 2005 IEEE International Conference on*, pp. 661–666, IEEE, 2005.

[186] Singh, A., Krause, A., Guestrin, C., and Kaiser, W. J., "Efficient informative sensing using multiple robots," *Journal of Artificial Intelligence Research*, pp. 707–755, 2009.

[187] Sklar, B., "Rayleigh fading channels in mobile digital communication systems. i. characterization," *IEEE Communications magazine*, vol. 35, no. 9, pp. 136–146, 1997.

[188] Sklar, B., *Digital communications*, vol. 2. Prentice Hall NJ, 2001.

[189] Smith, R. C. and Cheeseman, P., "On the representation and estimation of spatial uncertainty," *The international journal of Robotics Research*, vol. 5, no. 4, pp. 56–68, 1986.

[190] Spletzer, J. R. and Taylor, C. J., "Dynamic sensor planning and control for optimally tracking targets," *The International Journal of Robotics Research*, vol. 22, no. 1, pp. 7–20, 2003.

[191] Sprague, R., Babu, P., and others, "A new propagation prediction tool for earth-space geometries for the advanced refractive effects prediction system (areps)," in *Military Communications Conference, 2008. MILCOM 2008. IEEE*, pp. 1–6, IEEE, 2008.

[192] Stachniss, C. and Burgard, W., "Exploring unknown environments with mobile robots using coverage maps," in *IJCAI*, pp. 1127–1134, 2003.

[193] Stojanovic, M., "Underwater acoustic communications: Design considerations on the physical layer," in *Wireless on Demand Network Systems and Services, 2008. WONS 2008. Fifth Annual Conference on*, pp. 1–10, IEEE, 2008.

[194] Stojanovic, M. and Preisig, J., "Underwater acoustic communication channels: Propagation models and statistical characterization," *Communications Magazine, IEEE*, vol. 47, no. 1, pp. 84–89, 2009.

[195] Stokey, R. P., Freitag, L. E., and Grund, M. D., "A compact control language for auv acoustic communication," in *Europe Oceans 2005*, vol. 2, pp. 1133–1137, IEEE, 2005.

[196] Stokey, R. P., Roup, A., Von Alt, C., Allen, B., Forrester, N., Austin, T., Goldsborough, R., Purcell, M., Jaffre, F., Packard, G., and others, "Development of the remus 600 autonomous underwater vehicle," in *OCEANS, 2005. Proceedings of MTS/IEEE*, pp. 1301–1304, IEEE, 2005.

[197] Summers, T. H., Yu, C., and Anderson, B., "Addressing agent loss in vehicle formations and sensor networks," *International Journal of Robust and Nonlinear Control*, vol. 19, no. 15, pp. 1673–1696, 2009.

[198] Sutton, J. L., "Underwater acoustic imaging," *Proceedings of the IEEE*, vol. 67, no. 4, pp. 554–566, 1979.

[199] Sycara, K., Norman, T. J., Giampapa, J. A., Kollingbaum, M. J., Burnett, C., Masato, D., McCallum, M., and Strub, M. H., "Agent support for policy-driven collaborative mission planning," *The Computer Journal*, p. bxp061, 2009.

[200] Takeuchi, Y., Ohnishi, N., and Sugie, N., "Active vision system based on information theory," *Systems and Computers in Japan*, vol. 29, no. 11, pp. 31–39, 1998.

[201] Tan, C. C. and Beaulieu, N. C., "On first-order markov modeling for the rayleigh fading channel," *IEEE Transactions on Communications*, vol. 48, no. 12, pp. 2032–2040, 2000.

[202] Tappert, F. D., "The parabolic approximation method," in *Wave propagation and underwater acoustics*, pp. 224–287, Springer, 1977.

[203] Task Force, A., "Anti-submarine warfare concept of operations for the 21 st century," 2004.

[204] Tenenbaum, S., Stouch, D., McGraw, K., and Fichtl, T., "Multi-objective optimization to support mission planning for constellations of unmanned aerial systems," in *SPIE Defense and Security Symposium*, pp. 696215–696215, International Society for Optics and Photonics, 2008.

[205] Thrun, S., "Towards programming tools for robots that integrate probabilistic computation and learning," in *Robotics and Automation, 2000. Proceedings. ICRA'00. IEEE International Conference on*, vol. 1, pp. 306–312, IEEE, 2000.

[206] Thrun, S., Burgard, W., and Fox, D., *Probabilistic Robotics*. MIT press, 2005.

[207] Tisdale, J., Kim, Z., and Hedrick, J. K., "Autonomous uav path planning and estimation," *Robotics & Automation Magazine, IEEE*, vol. 16, no. 2, pp. 35–42, 2009.

[208] Toh, J. and Sukkarieh, S., "A bayesian formulation for the prioritized search of moving objects," in *Robotics and Automation, 2006. ICRA 2006. Proceedings 2006 IEEE International Conference on*, pp. 219–224, IEEE, 2006.

[209] Tolparev, R. and Polyakov, V., "Estimation of the nakagami probability-distribution parameters in a detector employing false-alarm probability stabilization," *TELECOMMUNICATIONS AND RADIO ENGINEERING*, vol. 43, no. 7, pp. 113–115, 1988.

[210] Traub, L. W., "Range and endurance estimates for battery-powered aircraft," *Journal of Aircraft*, vol. 48, no. 2, pp. 703–707, 2011.

[211] Uciński, D. and Korbicz, J., "Path planning for moving sensors in parameter estimation of distributed systems," in *Robot Motion and Control, 1999. RoMoCo'99. Proceedings of the First Workshop on*, pp. 273–278, IEEE, 1999.

[212] Ucinski, D., "Optimal sensor location for parameter estimation of distributed processes," *International Journal of Control*, vol. 73, no. 13, pp. 1235–1248, 2000.

[213] Urick, R. J., *Principles of underwater sound for engineers*. Tata McGraw-Hill Education, 1967.

[214] Valdez, P., S. M. C. A. and Griendling, K., "Adaptive communications framework for unmanned vehicles," *Naval Engineer's Journal*, December 2014.

[215] Vander Hook, J., Tokekar, P., and Isler, V., "Cautious greedy strategy for bearing-based active localization: Experiments and theoretical analysis," in *Robotics and Automation (ICRA), 2012 IEEE International Conference on*, pp. 1787–1792, IEEE, 2012.

[216] Vanderplaats, G. N., "Multidiscipline design optimization," *Applied Mechanics Reviews*, vol. 41, no. 6, pp. 257–262, 1988.

[217] Vázquez, P.-P., Feixas, M., Sbert, M., and Heidrich, W., "Viewpoint selection using viewpoint entropy.," in *VMV*, vol. 1, pp. 273–280, 2001.

[218] Vucetic, B., "An adaptive coding scheme for time-varying channels," *IEEE Transactions on Communications*, vol. 39, no. 5, pp. 653–663, 1991.

[219] Wang, H. S. and Moayeri, N., "Finite-state markov channel-a useful model for radio communication channels," *IEEE transactions on vehicular technology*, vol. 44, no. 1, pp. 163–171, 1995.

[220] Whitfield, C., "Development of modular mission packages providing focused warfighting capability for the littoral combat ship," in *ASNE Engineering the Total Ship Conference*, July 2010.

[221] Wong, E.-M., Bourgault, F., and Furukawa, T., "Multi-vehicle bayesian search for multiple lost targets," in *Robotics and Automation, 2005. ICRA 2005. Proceedings of the 2005 IEEE International Conference on*, pp. 3169–3174, IEEE, 2005.

[222] Yan, Y. and Mostofi, Y., "Communication and path planning strategies of a robotic coverage operation," in *American Control Conference (ACC), 2013*, pp. 860–866, IEEE, 2013.

[223] Yang, X., Liang, J., Wang, T., Yao, G., Zhao, W., and Shen, Q., "Submersible unmanned aerial vehicle concept design study," in *2013 Aviation Technology, Integration, and Operations Conference*, p. 4422, 2013.

[224] Young, T. Z., "Design and testing of an unmanned aerial to underwater vehicle," 2014.

[225] Zavlanos, B. M. M., Egerstedt, M. B., and Pappas, G. J., "Graph-theoretic connectivity control of mobile robot networks," *Proceedings of the IEEE*, vol. 99, no. 9, pp. 1525–1540, 2011.

[226] Zavlanos, M. M., Jadbabaie, A., and Pappas, G. J., "Flocking while preserving network connectivity," in *Decision and Control, 2007 46th IEEE Conference on*, pp. 2919–2924, IEEE, 2007.

[227] Zhang, G. and Ferrari, S., "An adaptive artificial potential function approach for geometric sensing," in *Decision and Control, 2009 held jointly with the 2009 28th Chinese Control Conference. CDC/CCC 2009. Proceedings of the 48th IEEE Conference on*, pp. 7903–7910, IEEE, 2009.

[228] Zhang, G., Ferrari, S., and Qian, M., "An information roadmap method for robotic sensor path planning," *Journal of Intelligent and Robotic Systems*, vol. 56, no. 1-2, pp. 69–98, 2009.